THE UNIVERSITY
of EDINBURGH

THE DEVELOPMENT OF ACOUSTIC TISSUE MIMICKING MATERIALS FOR PRECLINICAL ULTRASOUND IMAGING APPLICATIONS

Adela Rabell Montiel

A THESIS SUBMITTED FOR THE DEGREE OF

DOCTOR OF PHILOSOPHY IN CARDIOVASCULAR SCIENCE

THE UNIVERSITY OF EDINBURGH

2018

I hereby declare that this thesis is my own composition and that the work contained here is my own except where indicated in the text. The research included in this thesis was performed at the University of Edinburgh, Centre for Cardiovascular Science. No part of this thesis has been submitted elsewhere for any other degree or qualification.

To me

To my mom

To my sister

ACKNOWLEDGMENTS

I appreciate the critical constructivism, encouragement, teaching, motivation, patience and time of Dr. Carmel M. Moran, Dr. Steve Pye, and Mr. Tom Anderson. I would like to thank Mr. Adrian Thomson for all of his help, his teaching and guidance when using the Vevo 770® scanner and for always having a pleasant talk when spending long hours in the laboratory. To Dr. Jacinta Brown at the Dublin Institute of Technology for providing the opportunity to experience working in another foreign laboratory. To Irene Craig for always helping in the administrative paperwork. I thank Dr. David Kenwright for helping me understand the Matlab codes needed for analysis and for his open-minded talk when I was setting down in Edinburgh. To Dr. Noel Colinsk for always providing terrible advices at lunch time. Thanks to Christopher McLeod and Kirsty McNeill for their patience, help, and guidance when manufacturing the TMM at the Medical Physics department of the NHS Lothian.

Thanks to all my Mexican and non-Mexican friends, because without their support, motivation, and distraction, this work would not have been finished, Toño, Atenea, Oscar, Eduardo, Liss, Daniel, Manuel, Anja, Edgar, Bolthar, Emilio, Alex, Chio, Barbara, Jessica, Paola, Mariana, Val, Francesca, Sarah, Daniel, Nikki, Suzie, Leslie, Sara, Noel, David, Magda, Kamil, Annia, Matt, Pearlyn, Mark, Mariola, Paweł, Lara, Patrizia, Andrea, Adri, Silvia, Talia, Yessica, Roxana, Andrea, Marco, Martin, Callum, Alice, Julius, Juan, Anabel, Vanesa, Gaby, Ulises, Erick, David and Scott. To those who help me when I had just arrived to Edinburgh Mary, Vanessa, Rafa and Silvia. Thanks to all my, now, colleagues in DCI, Leon, Mexico for always keeping me in their mind.

Special thanks to Alejandra Sanchez, for staying with me, motivate me, distract me and support me during these 3 years of living together. To Mikołaj for dealing with me in the most stressful times, for his care and for always make me laugh.

Big special thanks to my mom and my sister for always scold at me when I most needed to keep going but above all, thanks for all their love and support.

Finally, I would like to thank the Mexican National Council of Science and Technology (CONACYT) for the scholarship provided for this PhD.

LAY ABSTRACT

Commercially available ultrasound quality assurance (QA) phantoms are generally manufactured from tissue mimicking material (TMM). The purpose of these QA phantoms is to assess the performance of ultrasound scanners. The acoustic properties of this TMM closely match those of soft tissue over the range of frequencies most often used in clinical ultrasound scanning (2 – 15 MHz). However, with increasing applications of ultrasound above 15 MHz knowledge of the acoustic properties of soft tissue at these higher frequencies is required to manufacture a QA phantom suitable for the assessment of higher frequency ultrasound scanners. There is no commercially available QA phantoms for the performance assessment of ultrasound scanners above 15 MHz.

The aim of this work was to develop a tissue-mimicking-material (TMM) that closely matches the acoustic properties of small animal soft tissues at high frequencies. Such a material would, therefore, be suitable for ultrasound QA phantoms for applications with high frequency ultrasound scanners (15 MHz to 50 MHz).

In order to develop a TMM suitable for high frequencies, a sequence of steps was followed. Firstly, the longitudinal stability of the acoustic properties of a material often used in QA phantoms, IEC agar-TMM, was assessed across the frequency range of 4.5 – 50 MHz. Secondly, the acoustic properties of the IEC agar-TMM component ingredients and the acoustic properties of small animal soft tissue were also assessed at frequencies above 15 MHz.

Using the acoustic properties of the IEC agar-TMM component ingredients and those of the small animal soft tissue, a TMM suitable for high frequencies can be developed. This TMM, based on the IEC agar-TMM, can be used to manufacture a QA phantom to assess the performance of high frequency ultrasound scanners.

ABSTRACT

Many applications of ultrasound test phantoms require that the acoustical properties of the phantom should closely match those of soft tissue. Numerous commercial test phantoms of this type are available for use with clinical ultrasound scanners, which use frequencies up to 20 MHz. However, scanners designed for imaging small animals in preclinical studies, typically operate at much higher frequencies. No commercially available test phantoms exist for use at frequencies above 20 MHz. The aim of this work was to develop a tissue-mimicking-material (TMM) that closely matches the acoustic properties of small animal tissues at high frequencies (HF). Such a material would, therefore, be suitable for ultrasound test phantoms for application with HF ultrasound scanners (20 MHz to 50 MHz).

A three-step approach was adopted to address this lack of a suitable HF-TMM. Firstly, verify the acoustic characteristics of the existing IEC agar-based TMM. Secondly, establish the acoustic properties (speed of sound and attenuation coefficient) of small animal tissue at high frequencies. Thirdly, develop a TMM which exhibits, as closely as possible, these small animal tissue acoustic characteristics.

A pulse-echo substitution method was used throughout to characterise the materials and the tissue samples.

The speed of sound and attenuation coefficient of an IEC agar-based TMM were measured using two different techniques. Initially, a widely used method was tried, where samples are wrapped in film and placed in degassed, deionised water for assessment. The second technique was developed and validated for use in this work. In this method, TMM samples were uncovered (without film) and were both stored and assessed in a TMM preserving fluid. The second method provided up to four times more consistent results.

The acoustical properties of the individual components of the IEC agar-based TMM were then measured in order to determine whether the overall attenuation coefficient of the agar TMM was a linear sum of the attenuation coefficients of its component parts. Within experimental uncertainties, this was found to be the case. This is a key

observation from which the formulation of an agar TMM, matching the acoustic properties of small animal tissue, can be facilitated.

The acoustical properties (speed of sound and attenuation coefficient) of mouse brain, liver, and kidney were measured using a preclinical ultrasound scanner.

CONTENT

LIST OF FIGURES

LIST OF TABLES

LIST OF ACRONYMS

In order of appearance

TMM	Tissue mimicking material
SoS	Speed of sound
QA	Quality assurance
SAM	Scanning acoustic macroscope
ρ	Density
k	Compressibility
Z	Acoustic impedance
V	Speed of sound
f	Frequency
λ	Wavelength
θ_i	Angle of incidence
θ_r	Reflected angle
θ_t	Transmitted angle
p_r	Reflected pressure
p_t	Transmitted pressure
I_r	Reflected intensity
I_t	Transmitted intensity
T_p	Transmitted pressure coefficient value
R_p	Reflected pressure coefficient value
T_I	Transmitted intensity coefficient value
R_I	Reflected intensity coefficient value
α	Attenuation coefficient
I_0	Original intensity
I_d	Decreased intensity
d	Distance

α_a	Amplitude absorption coefficient
α_s	Amplitude scattering coefficient
a	Disc aperture
R	Resolution integral
L_R	Depth of field
D_R	Characteristic resolution
T	Temperature
SAM	Scanning Acoustic Macroscope
IEC	International Electrotechnical Commission
RF	Radio-Frequency
ROI	Region of interest
Al_2O_3	Aluminium oxide
SiC	Silicon carbide
UTMM	Un-wrapped TMM slice
FTMM	Film-wrapped TMM slice
A	Amplitude
I	Intensity
t	Time
dB	Decibels
M	Molarity
P_{sol}	Solute weight
n	Number of moles
V	Volume
m	Mass
PM	Molecular weight of the solute

CHAPTER 1

INTRODUCTION AND BACKGROUND

1.1 INTRODUCTION

The number of medical and preclinical ultrasound imaging applications using high frequency ultrasound (above 20 MHz) has increased in recent years (Schmitt et al., 2010; Xu et al., 2012) due to technological advances, cost-effective, non-invasive and non-ionising properties of ultrasound imaging.

Ultrasound phantoms developed to date, attempt to replicate the acoustic properties of human body tissues at clinical frequencies (below 20 MHz). Commercially available quality assurance (QA) test objects are widely used to test the performance of clinical ultrasound scanners and for training purposes (BBS Medical AB, Sverige, Sweden; CIRS Tissue Simulation & Phantom Technology, Norfolk, Virginia; Kyoto Kagaku Co., LTD Kyoto, Japan; ATS Laboratories Inc. Bridgeport, CT, USA; Gamex, Inc. Middleton, WI). These phantoms, are mostly manufactured from tissue-mimicking-material (TMM) which is designed to closely match the acoustical properties of tissue; the properties being, the speed of sound (SoS), scattering and attenuation coefficient, and for some laboratory manufactured phantoms, the elastic and non-linear acoustic properties (Cabrelli et al., 2017; Pavan et al., 2013). The acoustic properties of soft tissue must be thoroughly investigated, e.g. variations of SoS, attenuation, and scattering of the ultrasound beam, in order to match the TMM acoustic properties with those of soft tissue (humans and mammals). At lower frequencies, soft tissue acoustical properties have been shown to vary with frequency and amplitude (Hill, 1986) but there have been limited studies of the properties of animal and human soft tissue at high frequencies. With increasing clinical and preclinical ultrasound imaging applications above 20 MHz, there is a need to develop and to acoustically characterise TMMs suitable for high-frequency ultrasound phantoms. To the best of my knowledge, there are no commercially available test phantoms for assessing the performance of high frequency ultrasound scanners.

1.1.1 Aim of PhD project

This PhD project assessed the suitability of an existing IEC agar-based TMM for the manufacture of QA phantoms for use at high frequencies. A three-step approach was adopted; firstly the acoustic characteristics of the existing and widely used IEC agar-based TMM were verified over the frequency range 4.5 – 50 MHz. Secondly, the acoustic properties (SoS and attenuation coefficient) of small animal soft tissue was measured at high frequencies. Thirdly, the effect of altering the constituent ingredients of the TMM on its acoustic properties were investigated to explore whether it would be possible to alter the TMM properties in order to mimic the acoustic characteristics of small animal soft tissue. Throughout this study a preclinical ultrasound scanner (Vevo 770, Visualsonics, Inc., Canada) and a Scanning Acoustic Macroscope (SAM) system were used. In this chapter, details of medical ultrasound imaging technology are introduced. This is followed by a literature review on different types of TMM and soft tissue characterisation.

1.1.2 Imaging modalities comparison

The advantages of ultrasound in comparison to other diagnostic imaging techniques such as X-ray, magnetic resonance imaging (MRI), computed tomography (CT) and positron emission tomography (PET) are its portability, cost-effectiveness, non-ionising nature (except MRI), non-invasiveness and real time imaging capability (Kips et al., 2008) as summarized in Table 1-1.

Advantages of ultrasound	Other imaging techniques
Non-ionising	X-ray, CT, PET results in a radiation dose MRI, approx. 10% of patients cannot be scanned due to claustrophobia. MRI does not use ionising radiation.
Inexpensive	MRI, CT, PET equipment costs approx. £1– £2 million Ultrasound equipment costs approx. £5k – £150k
Cost per scan	PET £1000 MRI £500 Ultrasound £50 – £100
Used for	Longitudinal studies Tissues that are radiosensitive Initial image estimate for background/control data
Real time	Real time imaging of blood flow, needle aspiration, drug injections and tissue motion.

Table 1-1. *Summary of the ultrasound advantages when compared with other medical imaging techniques. (Sun, 2012).*

Ultrasound imaging is classified into clinical (below 20 MHz) and preclinical (above 20 MHz).

1.1.3 Medical applications of ultrasound

Ultrasound imaging is widely used in cardiology, obstetrics, gynaecology, vascular applications, upper abdominal imaging, ophthalmology, dermatology, musculoskeletal and small parts imaging (Ali et al., 2008; Foster et al., 2000). Ultrasound is also used in a therapeutic mode using high-intensity focused ultrasound (HIFU) (Zderic et al., 2004). Furthermore, ultrasound is used to assist in interventional procedures such as in anaesthesiology, for needle guidance (Kuang et al., 2016; Menace et al., 2016; Raju & Grant, 2016), for implantation of catheters (Beigi et al., 2017; Fabiani et al., 2017; Menace et al., 2016) and needle biopsy (Giuliani et al., 2017; Ishii et al., 2017; Ophuis et al., 2017). Ultrasound often provides the means to visualize the location of catheters and needles in tissue. Above 40 million ultrasound scans are performed by the NHS in the UK per year (Dixon, 2015).

1.1.3.1 *High frequency ultrasound applications*

High frequency ultrasound can also be used in the assessment of skin (Machet et al., 2009), to measure vascular structures (Rhee, 2007) and retinal imaging (Rohrbach et al., 2016). In recent years, high (20 – 40 MHz) and very high ultrasound frequency (>40 MHz) have become the mainstream technology for the imaging of superficial structures mainly due to improvements in transducer design and software technology (Banchhor et al., 2016; Schmitt et al., 2010; Sundholm et al., 2015; Xu et al., 2012). More recently, these improvements allow the inclusion of high frequency transducer arrays for a needle biopsy (Wodnicki et al., 2016), the measurement in 3D of the intra-cardiac vector flow *in vivo* in humans (Wigen & Løvstakken, 2016), the measurement of erythrocyte aggregation in blood (Garcia-Duitama et al., 2016) and the measurement of the correlation between acoustic parameters and cell death index (Franceschini et al., 2016).

Recently, some research groups have undertaken research in the miniaturisation of ultrasound transducers aiming to create an ultrasound-pill that can be swallowed as an alternative to endoscopy using frequencies up to 30 MHz (Al-Rawhani et al., 2013; Ferguson, 2012; Lay et al., 2016; Memon et al., 2015, 2016; Schiavone et al., 2015).

Preclinical ultrasound is also used to size tumours, to diagnose glaucoma and to find cysts in small animals (Foster et al., 2011; Kagadis et al., 2010; Moran et al., 2011). The use of high frequency ultrasound is commonly use to scan small animals such as mice and zebrafish (Sun et al., 2008) (Figure 1-1). This project focusses on tissue characterisation of the mice.

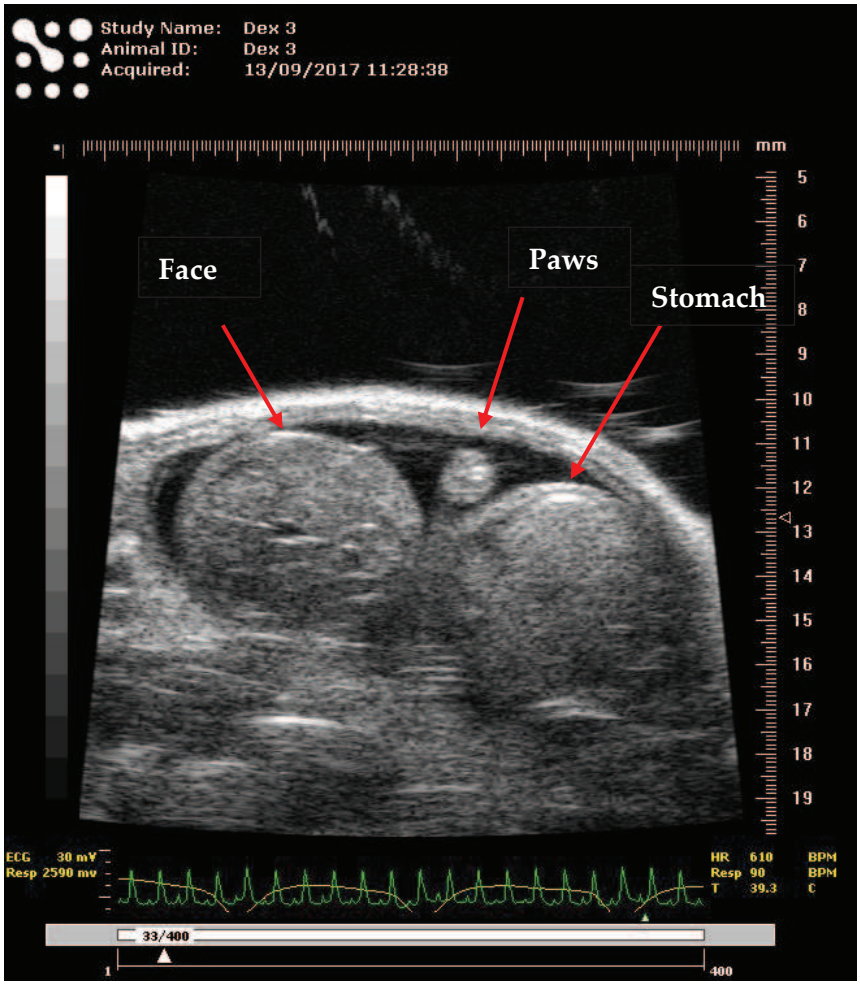

Figure 1-1. *B-scan front image of a mouse embryo. Images taken by Mr. Adrian Thomson at the Edinburgh Preclinical Imaging facilities, using a 55 MHz ultrasound probe.*

1.2 Principles of Ultrasound Imaging

An *ultrasound wave* is defined as a compressional sound wave with a frequency above that of human hearing range (20 KHz) (American National Standards Institute, 2013).

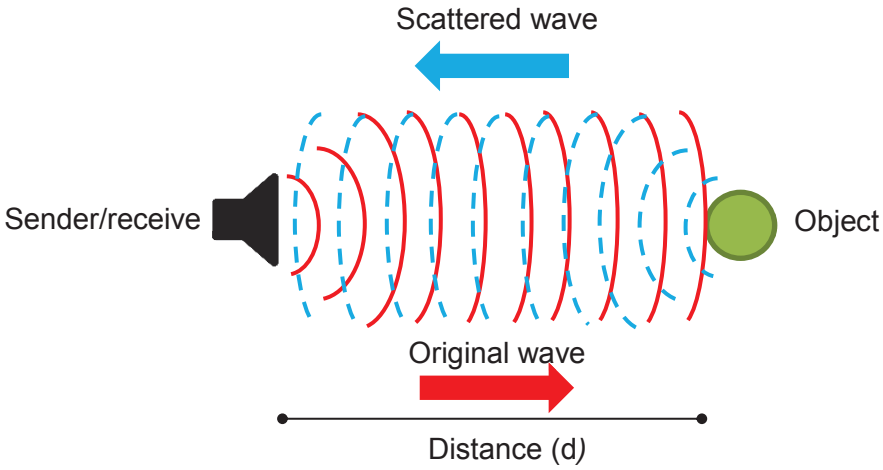

Figure 1-2. *Schematic illustrating the principle of echolocation.*

In medical applications ultrasound is used to form images of internal organs (Hoskins et al., 2003). The simplest form of ultrasound imaging is based on the principle of echolocation. A piezoelectric transducer emits pulses of ultrasound, which travels through a medium, becoming reflected by boundaries between materials, and scattered by sub-resolution scatterers within the tissue (Figure 1-2). By assuming an average speed of sound for soft tissue of 1540 ms^{-1} it is possible to construct an image of internal organs by measuring the time delay of these echoes. Echoes that are not received by the transducer will not be used to form an image. Pulses repeat over a specified unit of time, termed the pulse repetition frequency (PRF). In general, the time between one transmission pulse and the next pulse should be sufficient to allow the first pulse to reach the object and to be scattered/reflected back as an echo before the next pulse is generated (Figure 1-3).

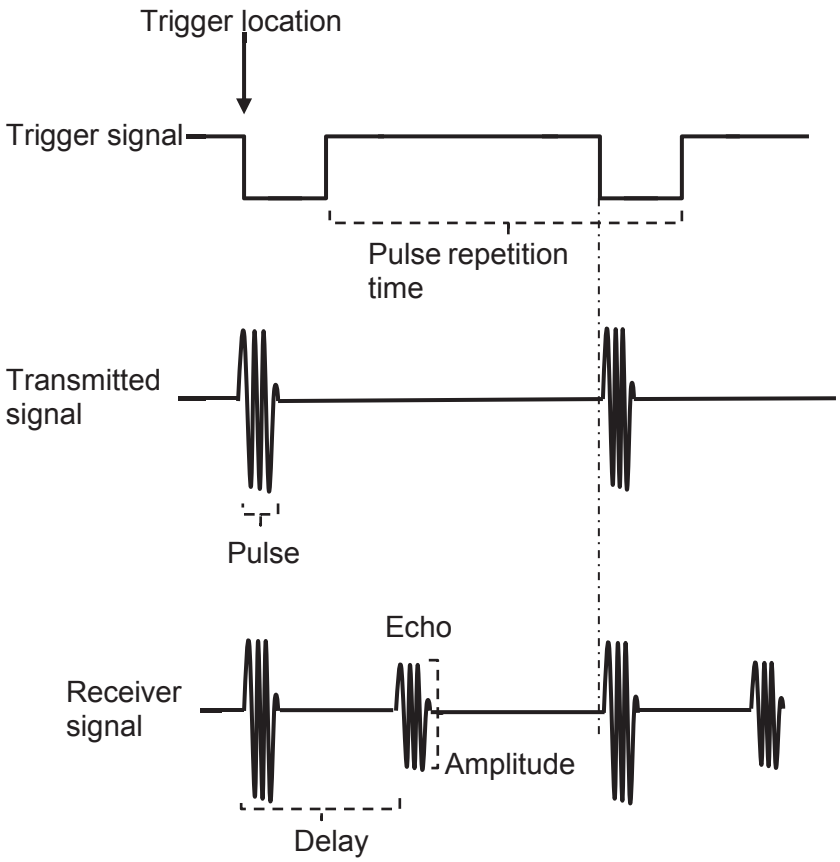

Figure 1-3. *Diagrammatic representation of ultrasound pulse generation.*

1.2.1 Definitions of ultrasound parameters in medical imaging

The *speed of sound* (SoS) of a wave is defined as *"the rate at which an acoustic wave propagates through a medium"* (AIUM, 2014). The SoS is measured in ms^{-1} (meters per second). For the purpose of ultrasound imaging, it is fortunate that the SoS in soft tissue are relatively similar. This allows the scanner to assure an average SoS value of 1540 ms^{-1} for the purpose of the image construction. In fact, SoS values will vary slightly between different tissues and organs.

When ultrasound reaches a scattering object, part of it is reflected back to the transducer. The rest is either transmitted or reflected/scattered 'out of the beam'. The magnitude and direction of the scattered ultrasound depends on the size of the scatter and acoustic impedance mismatch between the object and its surroundings.

The ultrasonic speed vibrations when travel through a medium depends on the density (ρ) and compressibility (k) of the medium (McDicken, 1991):

$$c = \sqrt{\frac{k}{\rho}} \quad 1\text{-}1$$

The compressibility (k) is also known as the Young-modulus or stiffness parameter. It is a measure of resistance of the material when pressure is applied. Equation 1-1 shows that the more rigid the tissue, the higher the SoS (Barrie Smith & Webb, 2011). The *acoustic impedance* (Z) can be expressed as the product of the density (ρ) and the SoS (V) of the tissue. Since $c = f\lambda$, where f is the frequency and λ is the wavelength, substituting Equation 1-3, then:

$$Z = \sqrt{\rho k} \quad 1\text{-}2$$

$$Z = \rho c \quad 1\text{-}3$$

When an ultrasound wave reaches a soft tissue junction that is much larger than the wavelength of the incident ultrasound (Figure 1-4), a fraction of the signal will be reflected, and a fraction will be absorbed by the soft tissue and refracted/transmitted. If the junction is formed by mediums with different values of impedance, a fraction of the wave is reflected back to the transducer (backscattered) and the other part of the wave will be transmitted deeper into the material. If the incident wave strikes the boundary between two media of different acoustic impedance at an angle of θ_i, θ_t.

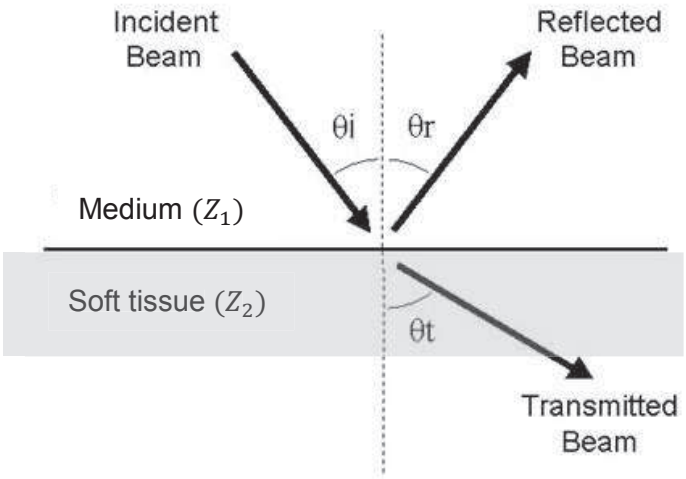

Figure 1-4. *Diagram showing the effects of an ultrasound wave incident on the junction of two different tissues types or mediums.*

The following equations relate the angles of incidence (θ_i) and reflection (θ_r), and transmission (θ_t), and the reflected (p_r) and transmitted (p_t) pressures, and the reflected (I_r) and transmitted (I_t) intensities:

$$\theta_i = \theta_r \quad \text{1-4}$$

$$R_p = \frac{P_r}{P_i} = \frac{Z_2 \cos\theta_i - Z_1 \cos\theta_t}{Z_2 \cos\theta_i + Z_1 \cos\theta_t} \quad \text{1-5}$$

$$T_p = \frac{P_t}{P_i} = \frac{2Z_2 \cos\theta_i}{Z_2 \cos\theta_i + Z_1 \cos\theta_t} \quad \text{1-6}$$

$$R_I = \frac{I_t}{I_i} = \frac{(Z_2 \cos\theta_i - Z_1 \cos\theta_t)^2}{(Z_2 \cos\theta_i + Z_1 \cos\theta_t)^2} \quad \text{1-7}$$

$$T_I = \frac{I_t}{I_i} = \frac{4Z_2 Z_1 \cos^2\theta_i}{(Z_2 \cos\theta_i + Z_1 \cos\theta_t)^2} \quad \text{1-8}$$

The relationship between the coefficients for the values of reflection and transmission pressures are:

$$T_p = R_p + 1 \quad \text{1-9}$$

The coefficients for the values of intensity reflections are:

$$T_I = 1 - |R_I|^2 \quad \text{1-10}$$

If the reflected signal is received at an angle of 90° at the boundary, then Equations 1-5 to 1-8 reduce to:

$$R_p = \frac{P_r}{P_i} = \frac{Z_2 - Z_1}{Z_2 + Z_1} \quad \text{1-11}$$

$$T_p = \frac{P_t}{P_i} = \frac{2Z_2}{Z_2 + Z_1} \quad \text{1-12}$$

$$R_I = \frac{I_t}{I_i} = \frac{(Z_2 - Z_1)^2}{(Z_2 + Z_1)^2} \quad \text{1-13}$$

$$T_I = \frac{I_t}{I_i} = \frac{4Z_2 Z_1}{(Z_2 + Z_1)^2} \quad \text{1-14}$$

When a sound wave reaches small interfaces (i.e. small reflectors with larger interfaces), the reflected wave will be *scattered* isotropically (over a large range of angles) (Hoskins et al., 2003) as shown in Figure 1-5 E. There are different types of scattering depending on the relative scatterer size within the tissue and the

wavelength of the ultrasound beam (Stirman, 2013). *Rayleigh scattering* occurs when the wavelength of the ultrasound beam is very much larger than the particle size, such scattering occurs from tissue substructure or red blood cells (Wells, 1993). In this type of scattering, the resulting pattern is a combination of constructive and destructive interference, which is commonly referred to speckle (Barrie Smith & Webb, 2011). The speckle effect is the result of the interference of waves (different phases and amplitudes) but at the same frequency. The scattering by sub-resolution scatterers is one source of attenuation. In general, more echogenic tissue will attenuate more than echolucent tissue.

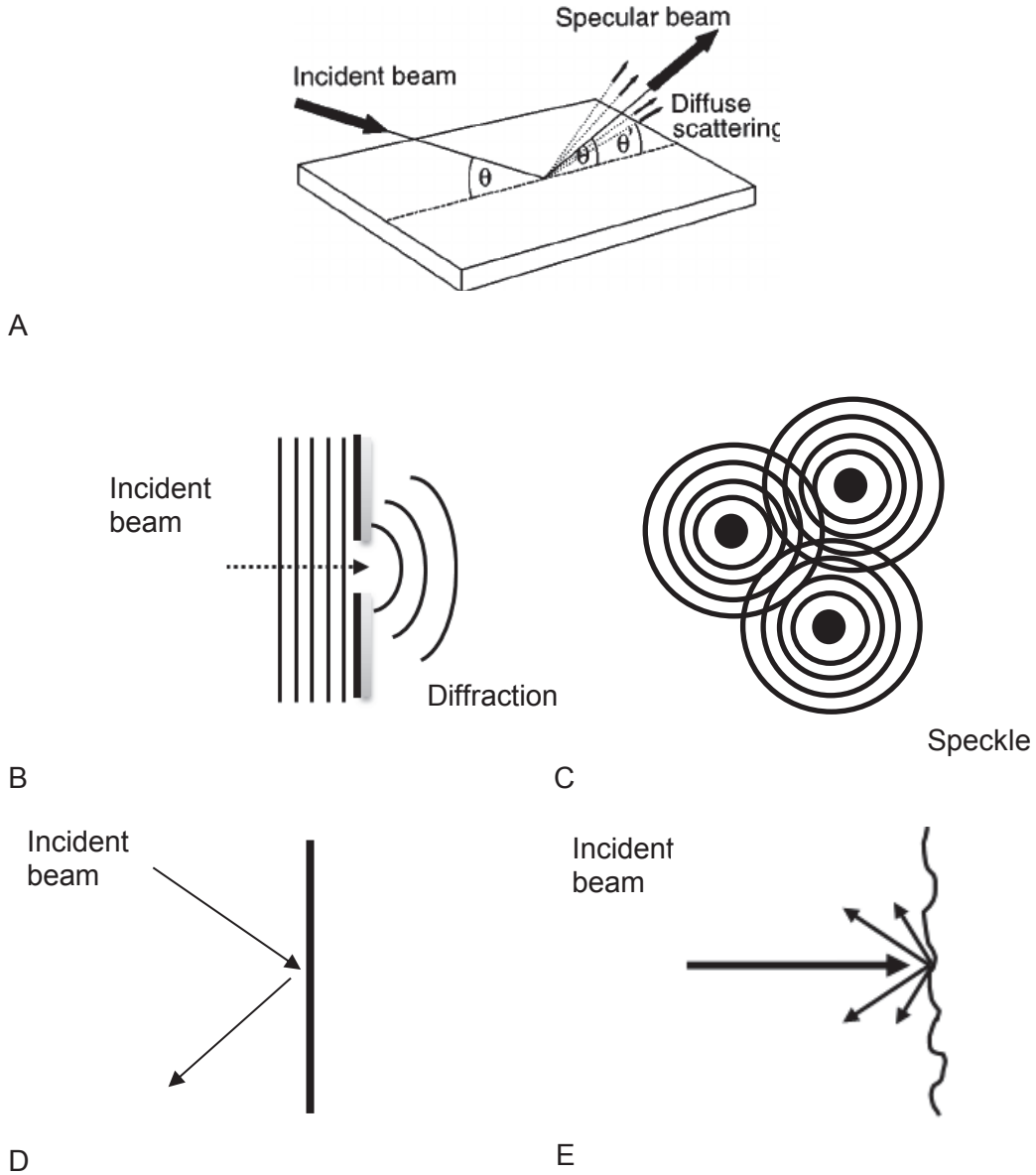

Figure 1-5. A) Diffuse scattering B) Diffraction through an aperture leading to point scattering leading to (C) speckle. Reflection from D) diffuse and E) specular boundering of the ultrasound incident beam.

The *attenuation* caused by tissue is defined in terms of the reduction in amplitude and intensity of the sound wave. When the beam travels through soft tissue, the particles vibrate producing elastic kinetic energy and heat (*absorption*). The beam is also attenuated by reflection and scattering from tissue structures.

1.2.1.1 *Calculation of ultrasound parameters*

In this PhD, the SoS and the attenuation coefficient were quantified for TMM and small animal soft tissue.

1.2.1.2 *Measurement of the speed of sound*

To measure the SoS in tissue, there are different methods. One is the transmission method using an emitter transducer and a detector placed on each side of the sample. This method is widely used by the National Physical Laboratory (NPL). The other method is called the reflection method. This method compares the time between the transmitted signal and the received pulse-echo, over a known separation using a emitter and a detector in the same transducer (Duck, 2012). The method used in this thesis was the reflection method.

1.2.1.3 *Measurement of attenuation*

To calculate the *attenuation* (α) of a plane wave at a given frequency: The intensity of ultrasound is measured in the presence and absence of a sample with thickness d.

$$\alpha\ (dB) = \frac{1}{2d}\log_{10}\frac{I_0}{I_d} \qquad 1\text{-}15$$

where I_0 is the original intensity and I_d is the decreased intensity as the wave passes through and back from a sample. The attenuation coefficient can be expressed dB per unit length. The decibel (dB) is the ratio of a value to a physical property (reference value), in acoustics is the unit of sound pressure level. It is calculated using the logarithm of the power of the signal divided by the reference power of the signal. The intensity reduction is due to a combination of the absorption, diffraction, scattering, and reflection, all of which change with ultrasound frequency.

The attenuation coefficient of tissue results from the combined losses due to absorption and scattering. Thus

$$\alpha_0 = \alpha_a + \alpha_s \quad 1\text{-}16$$

where α_a is the amplitude absorption coefficient and α_s is the amplitude scattering coefficient.

Attenuation variations with frequency can also be expressed as a power law:

$$\alpha(f) = \alpha_0 f^n \quad 1\text{-}17$$

where a_0 and n are the parameters of the material being scanned, based on acoustic data. In the case of the human brain, it was observed that these parameters were $1.08 \leq n \geq 1.2$ (Bamber, 1981; Kremkau et al., 1981), for human liver $n \approx 1$ (Tervola et al., 1985), whereas for human fat, for example, $0.4 \leq n \geq 1.4$ (Bamber, 1981). However, there is some evidence that this equation may not be appropriate over a wider frequency range (Duck, 2012).

1.2.2 Ultrasound transducers

An ultrasound transducer is a device that converts electrical pulses into an ultrasound pulse and vice-versa using a piezoelectric material (Welkowitz et al., 1992). These piezoelectric materials emit sound waves and can be organised as 'arrays' for various medical purposes as shown in Figure 1-6. These arrays enable the adjustment of focal length and temporal resolution (Hoskins et al., 2003).

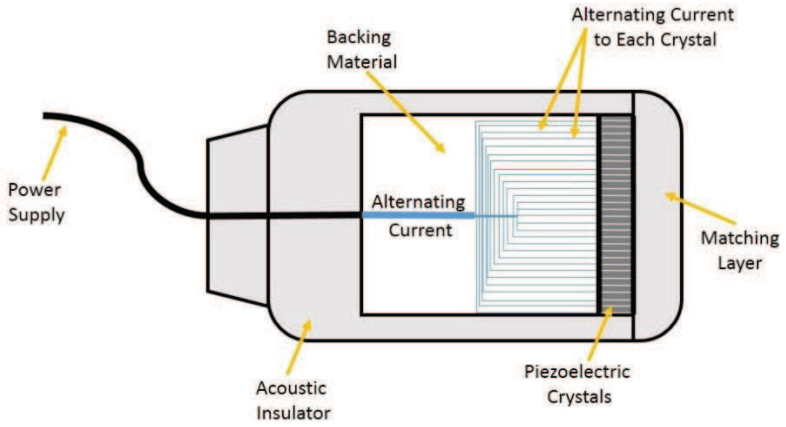

Figure 1-6. *Diagram of the internal construction of an ultrasound transducer array. Image taken from imgarchade.com (free copyright).*

Figure 1-7 shows the differences of the field of view formed from different piezoelectric arrays. These arrays are linear (Figure 1-7 A), curvilinear (Figure 1-7 B) and phased array transducers (Figure 1-7 C) and are used to scan different parts of the human body. Linear array transducers are suitable for necks and limbs. Curvilinear array transducers are suitable for abdominal and obstetrics where a wide field of view is required. Phased array transducers are predominantly used for in-body cavities, widely and almost exclusively used in cardiology (Hoskins et al., 2003).

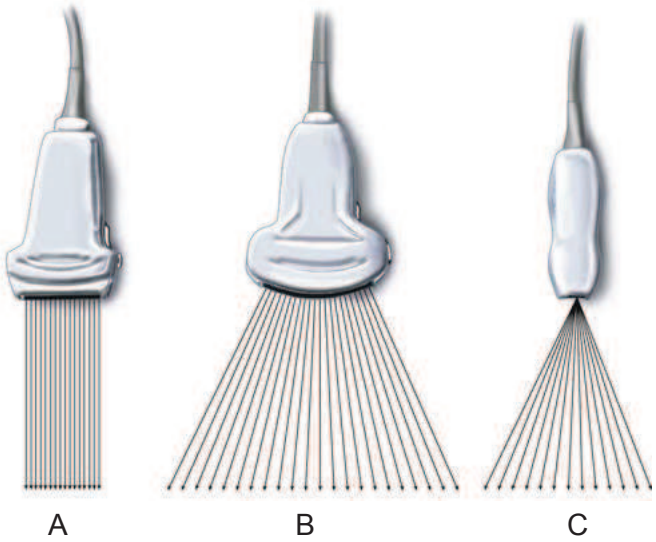

Figure 1-7. *Beam forming from A) linear transducer, B) curvilinear transducer and C) phased array transducer. Image taken from Karmakar & Kwok, (2015).*

In ultrasound imaging, a narrow ultrasound beam is preferred as this increases the lateral resolution of the image. The axial resolution depends on pulse lenghts (Figure 1-3). To produce a narrow ultrasound beam a large aperture disc is needed (Hoskins et al., 2003). A wide disc ($a >> \lambda$) will provide a well-collimated beam (Figure 1-8 A) with good lateral resolution.

Single-element transducers improve the lateral resolution (Brien, 1992; Wells, 1993; Zhou et al., 2014) by creating a focused beam using a single crystal with aperture larger than the ultrasound wavelength ($a >> \lambda$) disc (Figure 1-8 B).

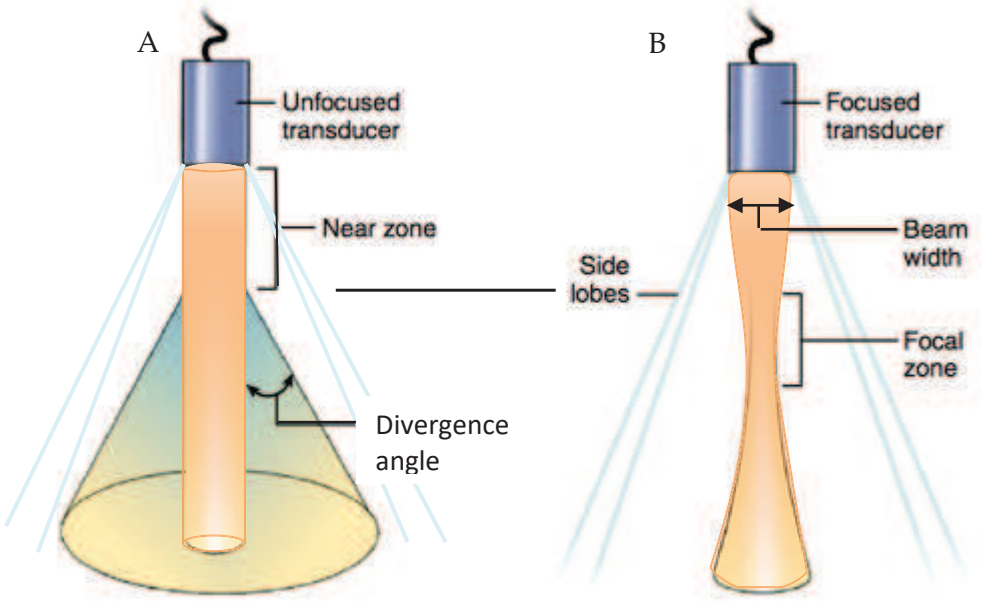

Figure 1-8. *Comparison between A) an unfocused and B) focused ultrasound beam. Image based in Otto, 2013.*

1.2.2.1 *Building an ultrasound image*

The ultrasound image in linear array transducers is generated line by line by each pulse-echo transmitted and received by the transducer (Figure 1-9). To generate a well collimated beam several piezoelectric elements are fixed in groups so that the aperture is always bigger than the wavelength. As shown in Figure 1-10 the image is generated progressively - the first line is generated, then the second and subsequently until the full image is created.

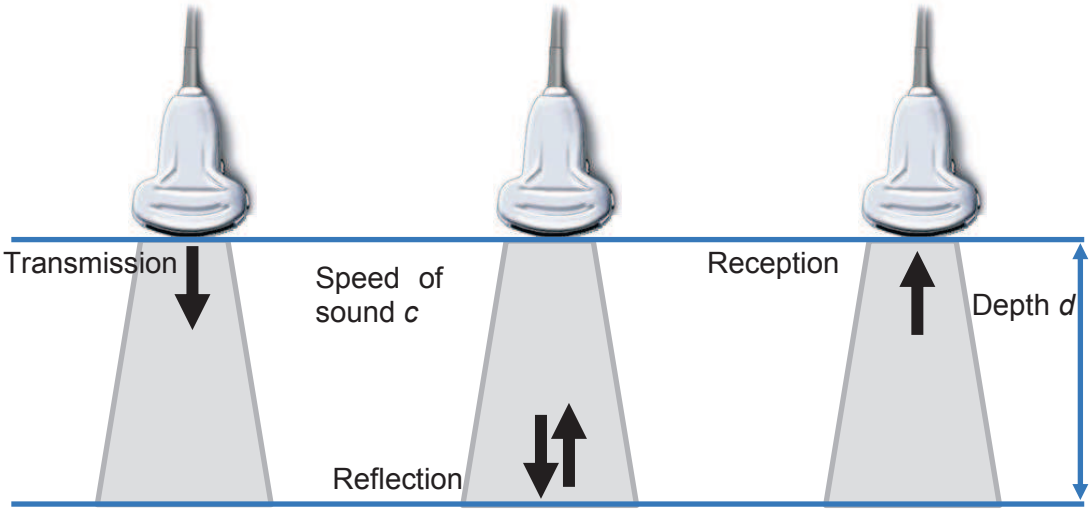

Figure 1-9*. Diagram of the pulse-echo technique.*

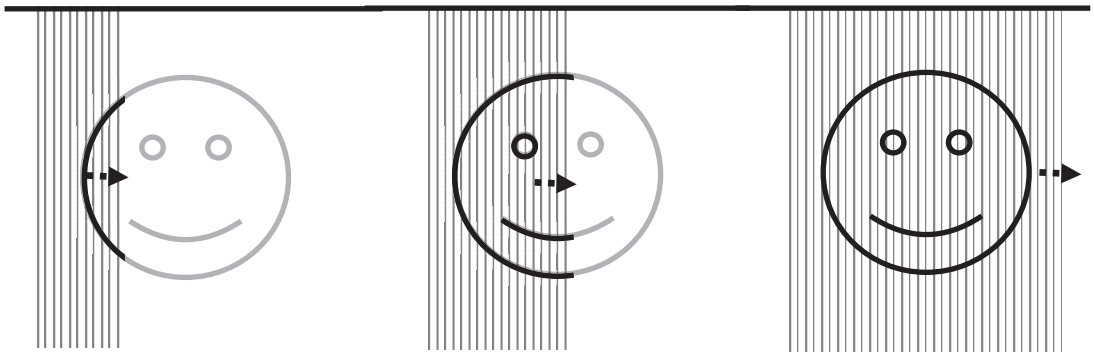

***Figure 1-10**. Forming a 2D image. The image is being built line by line as the beam is stepped along the transducer array (Hoskins et al., 2003).*

1.2.2.2 *Basic principles of imaging modes and imaging techniques*

The amplitude of the reflected echo determines the brightness of the tissue as seen on the scanner. The scanner calculates the distance to the tissue by measuring the time of the arrival of the echoes. The ultrasound scanner makes different technical assumptions (Gibbs et al., 2011) such as: that the SoS is the same in all tissues (1540 ms^{-1}), the ultrasound beam travels in straight lines, and that the echoes reflected back come from the central axis of the ultrasound beam. Any deviations from these approximations may cause distortion or artefacts in the ultrasound image.

The pulse-echo technique is used to generate an ultrasound image of tissue structure and motion: B-mode and M-mode. There are also other imaging techniques such as Spectral Doppler, Colour Doppler and Elastography. This PhD utilised a particular type of ultrasound image format known as 'B-mode'.

B-mode (Brightness mode) transmits pulse-echoes line by line to form a 2D greyscale image (Abu-Zidan et al., 2011). Each line is produced by a single transmit-receive pulse (Figure 1-10). The brightness of each spot depends on the intensity of the echoes after a time-gain correction has been applied to compensate for greater attenuation at depth. A complete B-mode image is typically made of 100 B-mode lines (Hoskins et al., 2003).

1.2.3 Image quality criteria

In ultrasound, the quality of the image depends on the temporal and the spatial resolution achievable by the scanner (Figure 1-11).

A scanner's *spatial resolution* is assessed in terms of its ability to differentiate between two closely spaced objects. In other words, spatial resolution describes how close two objects can be placed before they appear as a single echo.

The spatial resolution is expressed as the axial resolution (longitudinal resolution) and the lateral resolution. The slice thickness plane is achieved by a lens and generally cannot be modified by the operator. Figure 1-11 shows the differences of spatial, lateral and elevational resolution.

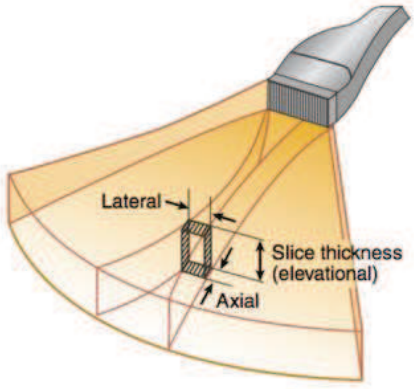

Figure 1-11. *Description of the terms, axial and lateral resolution image when using an ultrasound probe. Image taken from Otto, 2013.*

1.2.3.1 *Generating a high resolution image*

The resolution of the ultrasound images is ultimately limited by the wavelength of the ultrasound pulse. The spatial resolution of an image increases as the wavelength, λ, of the ultrasound beam gets smaller. Low-resolution imaging uses long wavelength transmitted pulses whereas a high-resolution imaging uses short wavelengths. The use of short wavelength pulses provides the ability to generate an image with higher axial resolution, thus improving the quality of the image in the axial direction.

For medical imaging, if the frequency of the ultrasound increases, the spatial intrinsic resolution of the image will increase but the penetration depth of the ultrasound within the tissue will be reduce.

1.3 TISSUE MIMICKING MATERIAL (TMM)

1.3.1 Background

US phantom development was first reported in 1978. In this first publication, the development of a material that would mimic the acoustic properties of soft tissue was described. The first tissue-mimicking-material (TMM) was made of water-based gel that contained graphite powder and alcohol (Madsen et al., 1978). Since then, different research studies have developed and tested a variety of ingredients for use as TMM with the objective of creating a more, stable and cost-effective materials that closely mimic the acoustic properties of tissue.

1.3.2 Different types of TMM

Currently, a variety of TMMs are used both commercially and within laboratories (Table 1-2).

TMM material	Speed of sound (m/s)	Attenuation coefficient* (dB $cm^{-1}MHz^{-1}$)	Reference source
	1540 ± 15	0.5 ± 0.05	IEC, (2001)
Agar-based	1498 - 600	0.04-1.40	Brewin et al., (2008); Browne et al., (2003); Cannon et al., (2011); Culjat et al., (2010); Inglis et al., (2006); Rajagopal et al., (2014); Sun et al., (2012); Teirlinck et al., (1998); Yang et al., (2013)
	1540	0.5	IEC, (2001)
Condensed-milk-based	1540	0.5	Madsen et al., (1998)
Gelatin-based	1520 -1650	0.12-1.5	Culjat et al., (2010)
Konjak-carrageenan-based	1550	0.56	Kenwright et al., (2014; Meagher et al., (2007)
Poly (vinyl alcohol) Cryo-gel (PVA-C)	1520 -1610	0.07-0.35	Cournane et al., (2010); Culjat et al., (2010); King et al., (2011)
Urethane rubber	1460	0.5-0.7	Browne et al., (2003); Cannon et al., (2011); Culjat et al., (2010)
Zerdine™	1540	0.5-0.7	Browne et al., (2003)

***Table 1-2**. SoS and attenuation of different tissue-mimicking-materials (TMM). *assuming a linear relationship between attenuation and frequency (<10 MHz).*

The IEC 2001 document "Ultrasonics –flow measurement systems –flow test objects" recommends that for frequencies between 2 – 10 MHz, a TMM should have a speed of sound of 1540 ± 15 ms^{-1} and attenuation of 0.5 ± 0.05 dB cm^{-1}. The IEC agar-based TMM has become widely used for both clinical and preclinical test objects (Brewin et al., 2008; Browne et al., 2003; Cannon et al., 2011; Culjat et al., 2010; Inglis et al., 2006; Moran et al., 2011; Rajagopal et al., 2014; Sun et al., 2012; Yang et al., 2013). The acoustical properties of this agar-based TMM are designed to comply with the ultrasound parameters provided by the IEC, hence this is often referred to as 'IEC agar-TMM'. Recently, the IEC agar-based TMM has been studied extensively at high frequencies (up to 47 MHz and 60 MHz) by Sun et al., (2011, 2012) and Rajagopal et al., (2014). No other TMM has been studied at these high frequencies.

1.3.3 TMM phantoms

There is currently a wide range of TMM phantoms in the medical industry. These can be roughly divided into two groups: clinical training phantoms, and quality assurance (QA) test objects including flow phantoms for Doppler assessment. Clinical and QA phantoms are made both commercially and within US laboratories. Some examples are outlined in this section.

1.3.3.1 *Clinical and training TMM phantoms*

Commercially available clinical training phantoms simulate the structure of human body, such as female and male pelvis, scrotal, prostate, thyroid, breast, foetal, abdominal, lumbar and transverse sections of the human torso (CIRS Tissue Simulation & Phantom Technology, Norfolk, Virginia; Kyoto Kagaku Co., Ltd Kyoto, Japan). These phantoms have been tested up to 15 MHz and are usually made of Zerdine™ (an ultrasound tissue equivalent epoxy resin), PVC-TMM, and Urethane TMM.

A range of different anatomical phantoms have been developed in-house for clinical purposes such as breast phantoms to facilitate the training of detection of lesions and for needle biopsy (Cannon et al., 2011; Vieira et al., 2013), oesophagus phantoms for endoscopy (Inglis et al., 2006), polyacrylamide hydrogel phantoms for assessing thermal lesions in response to high intensity ultrasound (Min Joo et al., 2013) and a gel phantom (agarose with canine RBCs in 0.9% isotonic saline) for assessing

ultrasound-induced cavitation damage (Maxwell et al., 2010). These phantoms were developed to target specific clinical applications at lower frequencies and have not been tested at frequencies above 12 MHz.

1.3.3.2 *Quality Assurance TMM phantoms*

The quality of an ultrasound image can be assessed by the measurement of a number of factors. These include the spatial resolution (axial, lateral and slice thickness), maximum penetration (low and high contrast, echo and noise), echo amplitude and accuracy (contrast resolution, greyscale, and sensitivity) of an ultrasound scanner. The purpose of QA testing is to characterise different performance parameters in an controlled way (Kofler, 2001).

Any test object designed to evaluate the performance of an ultrasound system, must have well-defined parameters to be of any real value. Test objects can be manufactured from a variety of TMMs and objects. Geometric objects intended for size and volume standards are often made of acrylic materials (Tofts, 2003). Commercially available QA test phantoms are manufactured by a number of different companies and are designed for frequencies up to 20 MHz (CIRS Tissue Simulation & Phantom Technology, Norfolk, Virginia; Kyoto Kagaku Co., LTD Kyoto, Japan; ATS Laboratories Inc. Bridgeport, CT, USA; Gammex, Inc Middleton, WI; BBS Medical AB, Sverige, Sweden). Table 1-3 shows some of the commercially available QA phantoms for clinical ultrasound scanners.

Company	Picture of the phantom	Details of the phantom
ATS		• Model 539 Multipurpose phantom. • Grey scale, vertical and horizontal calibration measurements, axial-lateral resolution and dead zone. • Urethane rubber-based TMM (SoS of 1450 ms^{-1} ± 1% and an attenuation of 0.5 dB cm^{-1} ± 5%)
Kyoto Kagaku		• Model N-365 Multipurpose phantom. • Measurements of grey scale, close range resolution, axial and lateral resolution. • Urethane elastomer, acryl nylon TMM (SoS of 1440 ms^{-1} and an attenuation of 0.57 dB cm^{-1} at 25°C). • The phantom consist of nylon strings and cyst targets.
CIRS	 	• Model 040GSE Multipurpose phantom. • Nine performance measurements including grey scale, axial and lateral resolution, anechoic speed masses and elasticity targets • Zerdine-based TMM (SoS of 1540 ± 10 ms^{-1} and 0.5 ± 0.05 dB cm^{-1} MHz^{-1} and 0.75 ± 0.05 dB cm^{-1} MHz^{-1}). • The phantom consist of different Nylon monofilament targets located at specific distance and sizes.
Gammex		• Model SONO408™ Phantom. • Axial, lateral and elevational resolution can be measured. • Gel-based TMM (SoS of 1540 ms^{-1} and an attenuation of 0.5 dB cm^{-1} MHz^{-1}). • The phantom consist of different anechoic spherical lesions of 2 mm and 4 mm diameter.

Table 1-3. *Shows some of the QA commercially available ultrasound phantoms.*

Additionally, ultrasound phantoms have been developed to test the performance of high frequency scanners. One such phantom is based on the design of the Edinburgh Pipe Phantom, which was developed to test the performance of clinical ultrasound scanners and has been adapted to characterise high frequency scanners (Moran et al., 2011).

1.3.3.3 *The Edinburgh Pipe Phantom*

During the course of my PhD, I have had the opportunity to use the Edinburgh Pipe Phantom to measure the performance of a high frequency ultrasound scanner. To measure the performance of clinical ultrasound scanner, Pye et al., (2004) developed the Edinburgh Pipe Phantom (Moran et al., 2011a, 2011b, 2009; Pye et al., 2004). This phantom consists of a Perspex box filled with agar-based TMM that includes anechoic pipes of different diameters, which allows the grey scale imaging performance of ultrasound scanners to be measured, using the concept of the resolution integral (MacGillivray et al., 2010; Pye et al., 2011). This resolution integral characterises the ultrasound image in terms of the ratio of penetration to the width of the ultrasound beam. The resolution integral has been shown to provide measurements that allows comparison between the performance of different systems when using different types of transducers (Filoux et al., 2012). Recently, Inglis et al., (2014) showed that the resolution integral can assess the imaging capabilities of radial mechanical and electronic echo-endoscopes using the Edinburgh Pipe Phantom.

The advantage of the Edinburgh Pipe Phantom is that it can provide an overall performance measurement (the resolution integral R). R is defined as the ratio between the depth of field (L_R) and the characteristic resolution (D_R (x-axis) (Figure 1-12). Measurements can be carried out in all transducers, allowing their characteristics and performance to be compared.

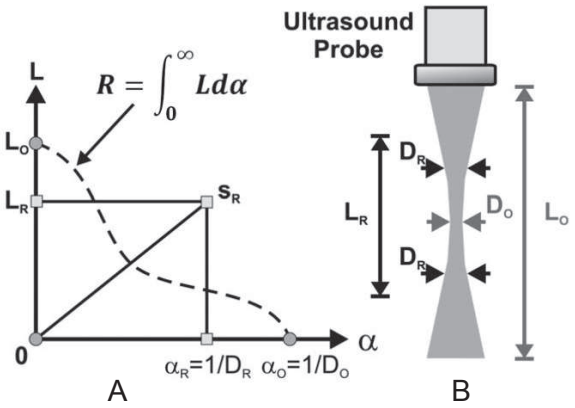

Figure 1-12. *A) A plot of L against α for a collimated beam (B) with low contrast penetration of L_0 and beam width D_0. α is the reciprocal of the effective beam width and R is the area under the curve. B) also shows the depth of field (L_R) and the characteristic resolution D_R. In A) the resolution integral is the area under the curve (Moran et al., 2014)*(MacGillivray et al., 2010)*. Image taken from Moran et al., (2014)*(MacGillivray et al., 2010)*.*

1.4 Soft Tissue

1.4.1 Background

One of the main constituents of body tissue is water, comprising approximately three-quarters of the body's total mass (Duck, 2012). Unlike water, the human body consists of a variety of tissue types and anatomical structures. Consequently, the ultrasound beam is absorbed and scattered by tissue and consequently, the acoustic properties differ from those of water.

Existing TMMs are designed to match the acoustical properties of soft tissue below 20 MHz, hence they may not accurately mimic the acoustic properties of tissue above 20 MHz. With an increasing number of high frequency ultrasound applications above 20 MHz being developed in recent years (Banchhor et al., 2016; Machet et al., 2009; Rhee, 2007; Schmitt et al., 2010; Sundholm et al., 2015; Xu et al., 2012) there is a need to develop new TMMs suitable for use above 20 MHz. Therefore, there is a requirement to measure the acoustic properties of soft tissue at higher ultrasound frequencies in order to develop a more relevant TMMs. Moreover, the measurement of the acoustic properties of different organs at these higher frequencies provides valuable knowledge that may be useful for diagnosis (Kumagai et al., 2014).

The development of phantoms that incorporate TMM to realistically mimic the properties of small animal soft tissue at high frequencies will enable a reduction in the use of small animals to optimise ultrasound imaging techniques. The reduction in the use of small animals is in line with the principles embodied in the 2012 amendment to the UK Animals (Scientific Procedures) Act 1986.

1.4.2 Acoustic properties of soft tissue

The first reported acoustic characterisation of soft tissue was obtained from animal and human soft tissue at frequencies of 1 – 2.5 MHz (Goldman & Richards, 1954; Ludwig, 1950). Duck (1990) published a literature survey where he described the physical properties of animal and human soft tissues available at that time.

This PhD work focuses on the measurement of the SoS and attenuation coefficient of small animal soft tissue above 20 MHz. The organs of interest were brain, liver, heart and kidney. Based on personal experience in the preclinical laboratory research facility of the University of Edinburgh, these were the organs scanned most often during preclinical studies. In addition, these organs also the ones for which information was available in the literature though predominantly at frequencies below 9 MHz. Measurement of the acoustic properties of these organs will be presented in this thesis.

The acoustic properties of brain, liver, and kidney, among other organs, have previously been measured from small animals at low frequencies (Frizzel et al., 1981; Goss et al., 1979; Tervola et al., 1985; Foster et al., 2000; Gray et al., 2013; Szabo, 2014), humans (Bamber et al., 1979, 1980; Kremkau et al., 1981; Ludwig, 1950; Parker, 1983; Rajagopalan et al., 1979; Sehgal et al., 1986), chickens (Martínez-Valdez et al., 2015) and mammals (Bamber et al., 1977; Ghoshal et al., 2011; Goss et al., 1979; López-Haro et al., 2009; Martial et al., 2007). These studies measured the acoustic properties up to 9 MHz at either room temperature (22 – 26°C) or at a normal human temperature (37°C). Recently, Wirtzfeld et al., (2015) measured the attenuation of murine liver and kidney across the frequency range 15 – 35 MHz, where a decellularized method was utilised and the acoustic properties measured from the extra-cellular matrix (ECM) left from the organs was analysed. This study found that the ECM of the organ contributes to the ultrasonic properties. Additionally, Frizzel & Gindorf, (1981),

O'Brien, (1988) and Tervola et al., (1985) have performed acoustical measurements up to 100 MHz using a Scanning Laser Acoustic Microscope (SLAM). Measurements performed at 100 MHz were undertaken at room temperature.

It has been shown that the SoS and attenuation of soft tissues increases with temperature (Bamber et al., 1979; Ghoshal et al., 2011; López-Haro et al., 2009; Rajagopalan et al., 1979; Suomi et al., 2016). However, there is no further increase in the SoS in soft tissue above 50°C (Duck, 1990). The attenuation of all tissues is dependent upon temperature and insonation frequency. At 7 MHz it has been shown that the minimum attenuation value, from a variety of soft tissue, was between 20°C and 40°C (Bamber & Hill, 1979; Kremkau et al., 1981). Furthermore, an increase in either water or fat content results in a decrease in the velocity of ultrasound in soft tissue (Bamber, 1981; Duck, 2012; O'Brien, 1988).

Moreover, *ex vivo* soft tissue samples decay with time after excision due to gas bubbles forming within the tissue, thus affecting the acoustic properties (Bamber, 1981; Duck, 2012). To delay this decay process, the soft tissue samples must be contained in a physiological solution such as saline, PBS, Krebs solution or should be embedded in an ultrasound compatible acoustic material such as TMM (Fraser et al., 2006). The preserving nature of saline on tissue is due to the fact of similar osmolarity and isotonic properties of blood (Barbosa et al., 2014; Wiegman, 2010).

The main cause of alteration in *post-mortem* acoustic characteristic changes in tissues is the result of the formation of 'gas bubbles' within the tissue. This reduces the accuracy of attenuation measurements. Bamber had reported a significant reduction in attenuation during a 120 hour period following death in bovine tissues (Bamber, 1981; Bamber & Hill, 1979). These changes were larger at frequencies above 1 MHz.

The acoustic properties of soft tissue have been acoustically measured *in vitro* with samples embedded in TMM (Bamber et al., 1977; Bamber & Hill, 1979; Gross et al., 1980; Martínez-Valdez et al., 2015; Muleki-Seya et al., 2016; Sundholm et al., 2015; Suomi et al., 2016), but only rarely *ex vivo* (Kumagai et al., 2014) or as *in vivo* tissue (Kagadis et al., 2010; Maklad et al., 1984; Parker et al., 1988; Zderic et al., 2004).

Table 1-4 shows a summary of the acoustic information found in the literature from brain, liver, and kidney at normal human body temperature and at room temperature. Recent studies compare their results with papers from 1980's at frequencies up to 9 MHz. Therefore, there is a necessity to update the acoustical parameters from these organs to include higher ultrasound frequencies.

Tissue	T (°C)	Frequency (MHz)	SoS (m/s)	Attenuation (dB/cm) $\alpha = af^b$	Reference
Brain, human		2.5 – 6		0.94 ± 0.13 MHz^{-1}	Strowitzki et al., 2007
				White 1.2 MHz^{-1} Grey 0.5-1 MHz^{-1}	Cook et al., 2011
	37	1	1510	0.11	Welkowitz et al., 1992
	37	1 – 5	1562 ± 1.2	0.87 at 1MHz	Kremkau et al., 1981
		1 – 6		1.1	Bamber et al., 1981
Brain, cat	37	0.5 – 7		0.27 - 5.55	Goss et al.,1979
Brain, bovine		1 – 5		0.1 – 9	Bamber & Hill 1979
	room	4 – 6		3.8 - 5.9 ± 0.05	Bamber et al., 1977
Liver, mouse	room	15 – 35		0.35 ± 0.34	Wirtzfeld et al., 2015
Liver, rat	36.3	7	1596 ± 4.5		Kumagai et al., 2014
	22	100	1570 ± 10	1.3 ± 0.09	O'Brien et al., 1988
	room	100	1550		Tervola et al 1985
Liver, human	37	3		1.66 ± 0.21	Lu et al., 1999
		2	1510	0.19	Welkowitz et al., 1992
	37	2.5		0.47 ± 0.07 MHz^{-1}	Parker et al., 1988
	37	3.5		0.55 ± 0.05 MHz^{-1}	Itoh et al., 1988
	37	3	1578.3 ± 5.4		Chen et al., 1987
	37	1.2 – 8		0.52	Lin et al., 1987
	37.2	2.25	1578 ± 2.9		Sehgal et al., 1986
	37	3.2		0.62 ± 0.12 MHz^{-1}	Garra et al., 1984
	37	2 – 8		0.52 ± 0.03 MHz^{-1}	Ophir et al., 1984

	37	3		0.52 ± 0.03 MHz^{-1}	Maklad et al., 1984
	20	1 – 6	1577 ± 11		Bamber et al., 1980 Baber et al., 1981
	37	1 – 7	1607		Bamber et al., 1979
	37	0.5 – 6		0.7 ± 0.2	Foster et al., 1979
	37	1.5 – 9		1.5 – 15.5	Gammell et al., 1979
Liver, hog	37	1.5 – 9		2 – 12	Gammell et al., 1979
Liver, bovine	37	0.5 – 7		0.33 – 6.51	Goss et al.,1979
	37	3.75		0.59 ± 0.10 MHz^{-1}	Fujii et al., 2002
	37	3		0.52 ± 0.10 MHz^{-1}	Taylor et al., 1986
	20	1 – 6		0.4 ± 0.09	Parker et al., 1983
	37	1 – 7	1597-1639		Bamber & Hill 1979
	room	4 – 6		4.4 – 6.2	Bamber et al., 1977
Liver, porcine	room	1 – 5		0.04f^0.84 (Np)	Zderic et al., 2004
	room	4 – 6		4.7 – 7.9	Bamber et al., 1977
Liver (sheep and cat)	23-26	100	1565 ± 7.8 and 1567 ± 13.2		Frizzel & Gindorf 1981
Liver, chicken	21.8	5	1588.2		Martínez-Valdez et al., 2011
	46	5	1609.8		
Kidney mouse	room	15 – 35		0.46 ± 0.011	Wirtzfeld et al., 2015
	23 – 26	100	1586 ±10.7		Frizzel & Gindorf 1981
Kidney, human		2	1560	0.27	Welkowitz et al., 1992
	37.2	100	1560 ± 1.8		Rajagopalan et al., 1979
Kidney bovine	37	0.5 – 7		0.42 – 7.55	Goss et al., 1979
Kidney porcine	37	3.5 – 7	1571	0.42 at 45°C	Worthington et al., 2001
Kidney, hog	37	1.5 – 9		2 – 9	Gammell et al., 1979

Table 1-4. *Compendium of the acoustical properties of soft tissue, focused on those studies involving brain, liver and kidney at mostly 37°C. The blank spaces represent the absence of information.*

1.4.2.1 *Additional ultrasound parameters needed from soft tissue*

Few studies have measured the nonlinear acoustic parameters of soft tissue. Table 1-5 shows a summary of additional ultrasound parameters measured from brain, liver, and kidney available in the literature. In this table, no distinction was made regarding source of the tissue (i.e. animal or human), or the frequency or temperature used in the study. The purpose of Table 1-5 is to show those published values for B/A parameter, backscatter, shear modulus (a measure of elasticity) and acoustic impedance from soft tissue. These studies measured the acoustic properties from either humans, chickens or ruminants at room or body temperature, up to 28 MHz. To the best of my knowledge no other ultrasound parameters have been published for human or animal brain, liver or kidney tissue.

Tissue	Nonlinear (B/A) parameter	Backscatter [1/Sr mm]	Elasticity (shear module) [kPa]	Acoustic impedance [(kg $m^{-1}s^{-2}$)] x 10^6
Brain	5 – 7.6		1.44 – 1.78 ± 0.20	1.38 – 1.95
Liver	1.5 – 7.2	1.7 x 10^{-4} – 3.03 x 10^{-3}	1.5 – 2.5 ± 0.46	1.65 – 1.78
Kidney	7.4	9 x10^{-4}	15.4 – 10.8 6.6 – 8.7 ± 2.5 medulla	1.62 – 1.65

Table 1-5. *Summary of the B/A parameter, backscatter, elasticity and acoustic impedance. The blank spaces represent a lack of information. References for brain (Gunawan et al., 2015; Kaster et al., 2011; Law et al., 1985; Liu et al., 2017; Ludwig, 1950; Morin et al., 2017; Pinton et al., 2011) for liver (Bamber et al., 1977; Civale et al., 2013; Degos et al., 2010; Freese & Lyons, 1977; Ghoshal et al, 2011; Ito et al., 2017; Law et al., 1985; Liu et al., 2006; Lu et al., 1999; Ludwig, 1950; Palabiyik et al., 2017; Sehgal et al., 1986; Suomi et al., 2016; Tzschatzsch et al., 2016; Wear et al., 1995) and for kidney (Gennisson et al., 2012; Grenier, Gennisson et al., 2013; Insana et al., 1992; Ludwig, 1950; Palabiyik et al., 2017).*

1.4.2.2 *Brain*

Intraoperative ultrasonography is used to locate tumours and gliomas using neuro-navigation (Dunne et al., 2017; Lee et al., 2016; Mahboob et al., 2016; Tirakotai et al., 2006; Unsgaard et al., 2002). The differing acoustic properties of healthy and

pathological brain tissue can provide additional information about the brain. This organ is one of the most delicate organs due to its gel-like tissue composition, and its tendency to disintegrate when it is fresh and handled without sufficient care.

From Table 1-4, the SoS of the brain varies between 1510 – 1562 ms^{-1} (Kremkau et al., 1981; Welkowitz et al., 1992) and the attenuation (Figure 1-13) varies between 0.87 – 1.1 dB cm^{-1} MHz^{-1} (Bamber, 1981; Bamber et al., 1977; Cook et al., 2011; Goss et al., 1979; Kremkau et al., 1981; Strowitzki et al., 2007; Welkowitz et al., 1992). Those studies were performed at room temperature and at 37°C and up to 7 MHz.

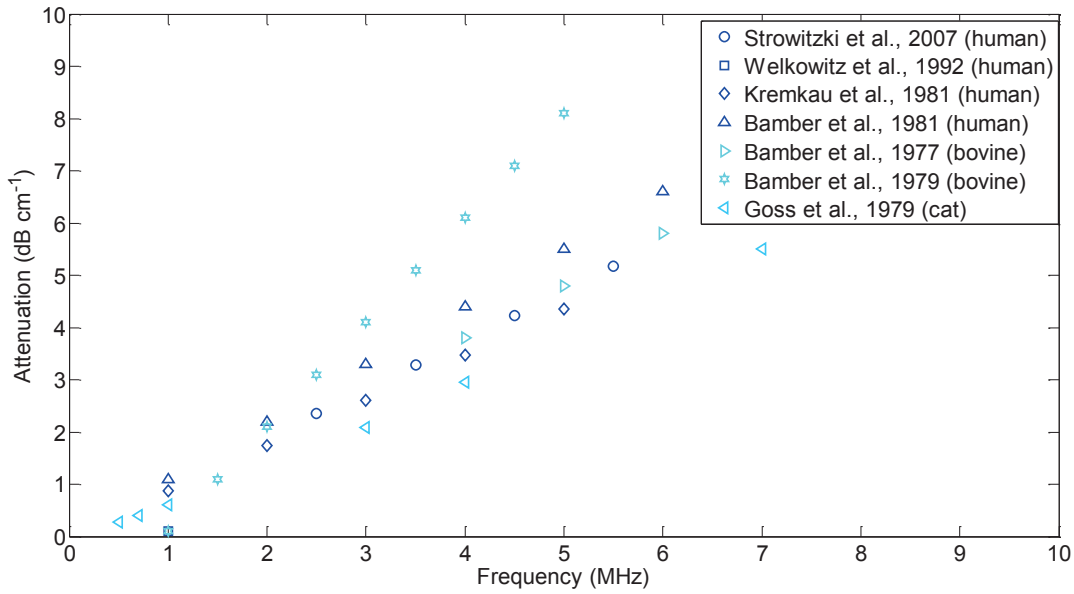

***Figure 1-13**. Attenuation versus frequency from those studies published involving brain tissue at 37°C. Bamber et al., (1977, 1979) used bovine brain samples were measured at room temperature.*

1.4.2.3 *Liver*

Liver disease mortality has increased in the UK population by 25% according to the NHS over the last decade (NHS Choices, 2012). Ultrasound is currently used as a non-invasive technique for diagnosis (Bamber et al., 1980; Fujii et al., 2002; Itoh et al., 1988).

The acoustical properties of the liver have been published extensively at low frequencies, yielding a wide range of SoS and attenuation coefficient values (Table 1-4). Based on studies published for humans and mammalian livers, from 1 to 9 MHz

ultrasound frequency at different temperatures (22°C and 37°C), the SoS varied between 1545 – 1639 ms^{-1} (Bamber & Hill, 1979, 1980; Chen et al., 1987; Frizzel & Gindorf, 1981; Kumagai et al., 2014; Martínez-Valdez et al., 2015; Welkowitz et al., 1992). The attenuation coefficient from those published studies (Figure 1-14) varied between 0.35 – 1.3 dB cm^{-1} MHz^{-1} (Bamber et al., 1977; Fujii et al., 2002; Garra et al., 1984; Goss et al., 1979; Itoh et al., 1988; Lu et al., 1999; O'Brien, 1988; Ophir et al., 1984; Parker et al., 1988, 1983; Taylor et al., 1986; Welkowitz et al., 1992; Zderic et al., 2004).

The SoS of sheep and cat liver have also been measured at 100 MHz, at room temperature by Frizzel & Gindorf, (1981), O'Brien, (1988) and Tervola et al., (1985) and have been found to be in good agreement with previous studies. Wirtzfeld et al., (2015) have measured the acoustic properties of the liver at high frequencies (15 – 35 MHz) by removing the cells from the organ in an attempt to decrease the variability found in measured ultrasound parameters.

It is known that gas is more likely to be introduced into the liver during excision than any other organ due to its highly vascular structure and its tendency to produce gas through autolytic (cells self-digestion) decay. The presence of gas in specimens is probably the greatest problem in the preparation of soft tissue samples for acoustical measurements (Bamber, 1981). A pressurization method has been advised since 1985 to prevent the production of gas in the organ (Bamber et al., 1985) especially for those studies involving extended periods of time (over 1 hr).

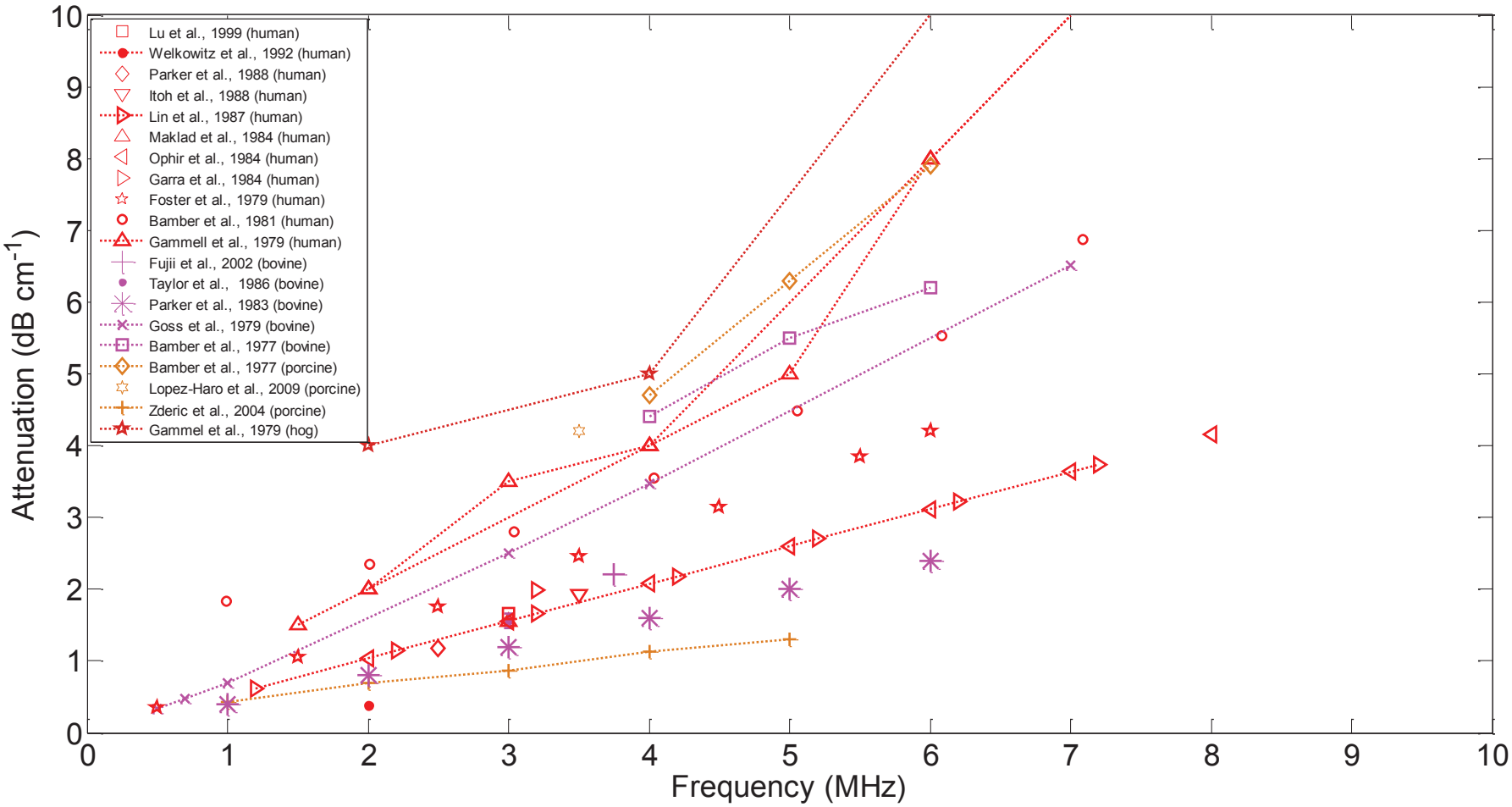

***Figure 1-14**. Attenuation versus frequency from published studies involving the liver at 37°C. Parker et al (1983), Bamber et al., (1977) and Zderic et al., (2004) measured the attenuation in mammalian liver tissue at room temperature.*

1.4.2.4 *Kidney*

According to the British Association of Urological Surgeons, kidney stones can be found in almost 3% of the population as it is one of the most prevalent diseases in the UK with 12,000 admissions in hospitals per year. Unfortunately, there is limited information in the literature about the acoustic properties of the kidney, regardless of temperature, or type of sample (humans or ruminants). The kidney is recognised to have 3 general segments, *medulla*, *cortex* and *renal pelvis*. The total thickness of the kidney *cortex* in mice is 1.3 mm (Zhai et al., 2003) and the thickness of the medulla is 3 mm approximately. Previous work has shown a variation in the acoustic properties of the kidney to be associated with five longitudinal cross-sectional regions in dog's kidney anatomy, from the *cortex* through the *capillary veins* (Sarvazyan & Klemin, 1983). In that study, the SoS showed a difference of 5 ms^{-1} and a difference of 0.5 dB cm^{-1} at 8.8 MHz in a cross-sectional dog kidney.

Based on the limited information found in the literature the mean SoS varies between 1560 – 1586 ms^{-1} (Frizzel & Gindorf, 1981; Rajagopalan et al., 1979; Welkowitz et al., 1992; Worthington et al., 2001). In these studies, kidney was measured from different animals at 37°C. Figure 1-15 shows the attenuation that has been reported in the frequency range from 0.5 to 9 MHz. The attenuation varied from 0.27 dB cm^{-1} to 9 dB cm^{-1} (Gammell et al., 1979; Goss et al., 1979; Welkowitz et al., 1992; Worthington et al., 2001). Wirtzfeld et al., (2015) studied the kidney in the frequency range of 15 – 35 MHz with the acoustic properties in good agreement with previous results. Likewise, the SoS of the kidney from mouse and human has been studied at 100 MHz by Frizzel et al., (1981) and Rajagopalan et al., (1979).

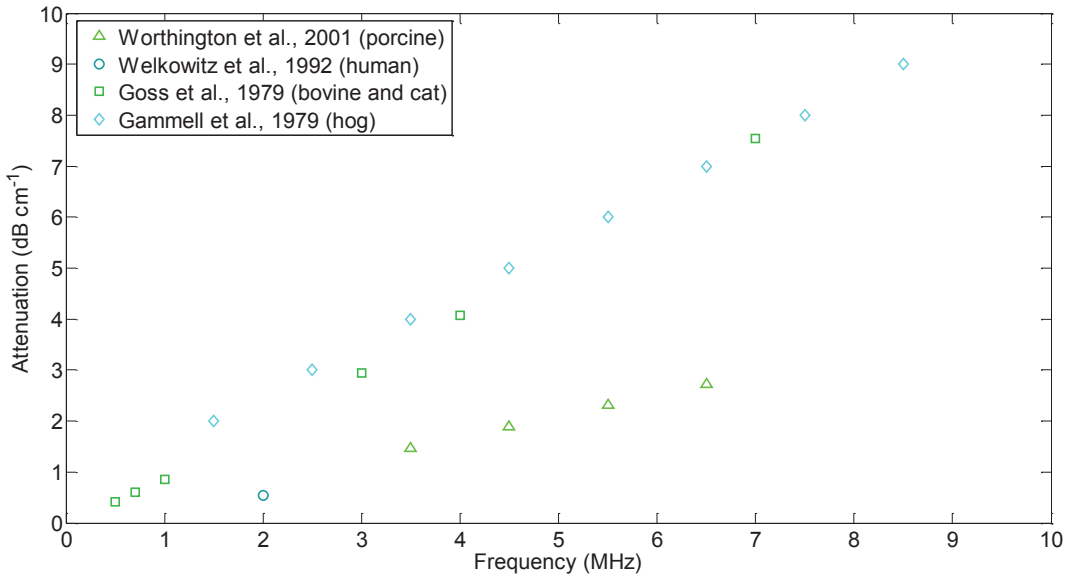

Figure 1-15. *Attenuation versus frequency from studies published involving the kidney at 37°C.*

1.5 THESIS OUTLINE

Below the structure of the rest of this thesis is explained.

In Chapter 2 the equipment used in this thesis is described, including the preclinical ultrasound scanner Vevo 770®, and the SAM system. This chapter also describes the Matlab script used in this study and the modifications from those originally developed as part of Chao Sun PhD thesis (Sun, 2012). Modification of the script was necessary for data analysis as the script was originally developed for a different measurement technique than the one use in this thesis. Measurements of the 3 dB frequency bandwidth of the Vevo 770® preclinical scanner are presented in this chapter.

In Chapter 3, the development of an additional and alternative method to characterise the acoustic properties of the IEC agar-TMM is described. This alternative method differs from the commonly used method used to characterise the acoustic properties of the IEC agar-TMM. The acoustic properties using these two techniques were assessed every 3 months for up to 1 year in the low and high frequency range (4.5 – 50 MHz). The acoustic properties are compared with the IEC guideline for TMM in

the frequency range of 2 – 10 MHz (IEC, 2001). This study has been published in *Ultrasound in Medicine and Biology* journal as Rabell-Montiel et al., (2017).

In Chapter 4 the IEC agar-TMM individual ingredients affect on SoS and attenuation are systematically investigated, where each of the ingredients was acoustically characterised in the frequency range of 12 – 50 MHz. The percentage concentrations were not modified from the IEC agar-TMM recipe. These individual formulations of ingredients were studied by production and measurement of the acoustic properties of different batches of TMM.

In Chapter 5 the acoustic properties of small animal brain, liver and kidney are assessed in the frequency range of 12 – 32 MHz. Furthermore, a comparison of the acoustic properties between perfused and non-perfused brain and liver is also included. The SoS and attenuation coefficient measured from mouse brain, liver and kidney were compared with the acoustic properties from the IEC agar-TMM and its individual component ingredients (Chapter 3 and 4). This comparison is a required first step in order to develop a TMM suitable for a high frequency QA phantom. This study has been published in *Ultrasound in Medicine and Biology* journal as Rabell-Montiel et al., (2017).

In Chapter 6 a summary of this thesis and the future work needed to develop a new TMM whose acoustical properties mimic those of soft tissue is described.

CHAPTER 2

MATERIALS AND METHODS

2.1 CHAPTER DESCRIPTION

In this chapter the high frequency ultrasound scanner, Vevo 770®, and the Scanning Acoustic Macroscope (SAM) system are described. The Vevo 770® ultrasound scanner was located within the Biological Research Facility (BRF) on the Little France Campus of the University of Edinburgh, whereas the SAM system was located at the Facility for Optical Characterisation and Spectroscopy (FOCAS) of the Dublin Institute of Technology (Dublin, Ireland).

Both systems are described in detail, including acquisition protocols, procedure for acquiring raw data and subsequent analysis. Similarly, the IEC agar-TMM sample manufacture process is described, alongside techniques developed for preparation of soft tissue samples. Acoustic characterisation of two reference fluids used in this PhD research, including the Matlab script used to analyse acoustic data, are also presented in this chapter.

2.2 HIGH FREQUENCY ULTRASOUND SCANNER VEVO 770®

The Vevo 770® (VisualSonics, Inc. Toronto, Canada) is a high- frequency ultrasound scanner (Figure 2-1) with transducers that operate between 25 and 55 MHz, actual centre frequency, depending on the transducer model used. The scanner can be operated in seven different imaging modes: B-mode, M-mode, 3D-Mode, Pulse Wave (PW) Doppler Mode, Tissue Doppler Mode, Power Doppler Mode and Digital Radio Frequency (RF) Mode (VisualSonics, 2006). The Vevo 770® software allows post imaging analysis, remote access to files and measurements, and allows the user to export data in a variety of different formats.

2.2.1 Vevo 770® Transducers

Transducers available for use with the Vevo 770® scanner include the RMV 700-Series (Real-time Microvisualisation, VisualSonics, Inc. Toronto, Canada). These transducers were developed specifically for small animal ultrasound imaging research (preclinical). The system is able to provide frame rates of up to 200 frames per second, depending on the RMV probe used (Figure 2-2). The probes are designed as single-element transducers, working as both the transmitter and receiver of the ultrasound beam. This single-element transducer is contained in a 'capsule' comprising an acoustic window filled with deionised degassed water. This fluid facilitates acoustic coupling between the single-element and tissue being scanned. Once the probe is in operation, the single-element mechanically oscillates, sweeping the ultrasound beam back and forth across the surface of interest.

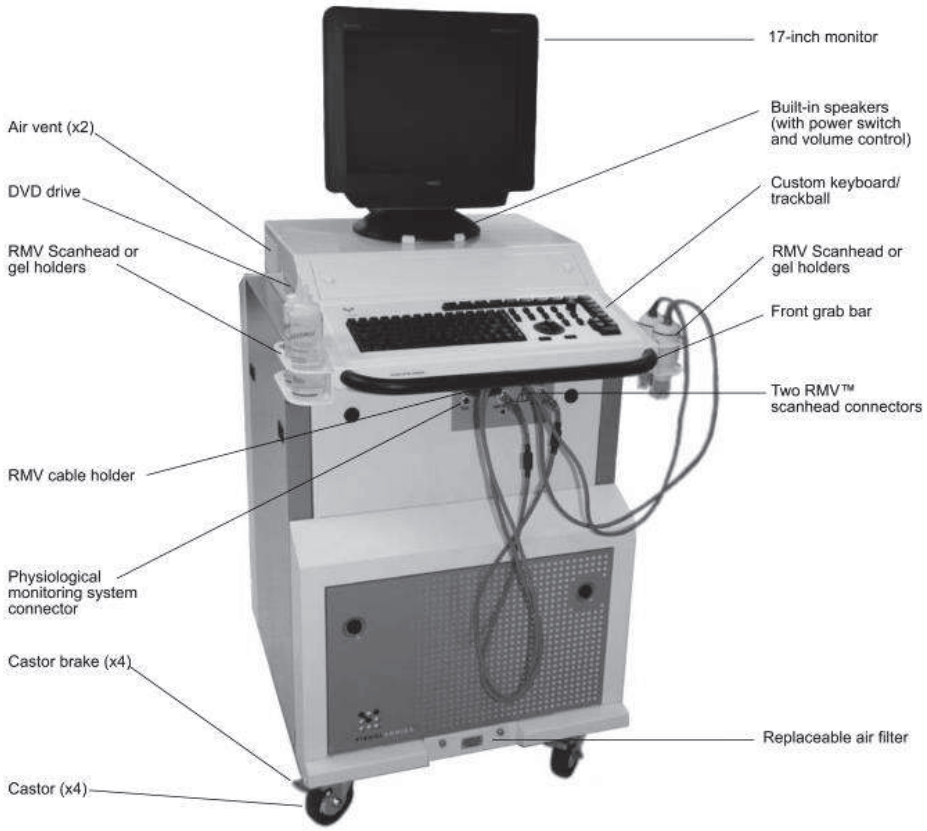

Figure 2-1. *Front view of the preclinical ultrasound Vevo 770® scanner. Image taken from the manufacturer brochure (VisualSonics, 2006).*

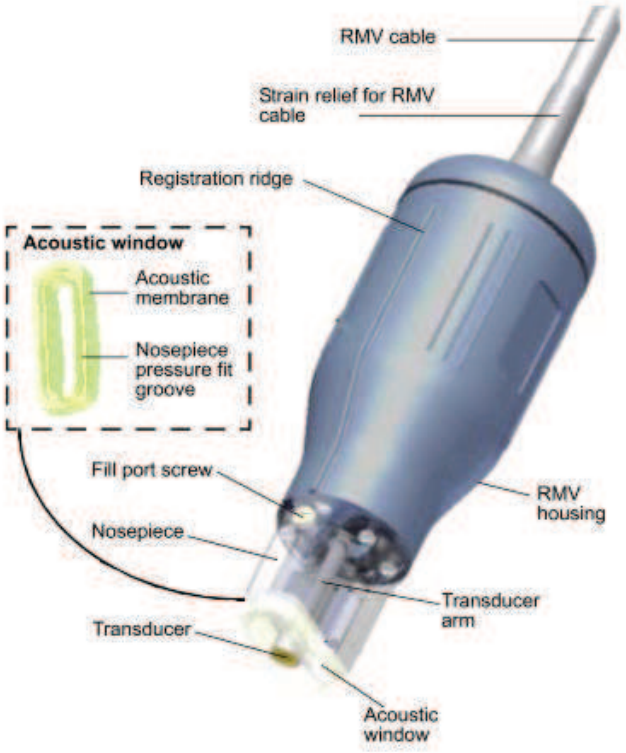

Figure 2-2. *RMV transducer diagram. Image taken from the manufacturer brochure (VisualSonics, 2006).*

The transducer models used in this work were the RMV704, RMV707B, RMV710B and RMV711, listed in Table 2-1. Table 2-1 lists the central frequency range from 25 MHz to 55 MHz; information provided by the manufacturer (VisualSonics, 2006), and the measured physical size of the acoustic window, which increases with decreasing frequency.

Model RMV	Central Frequency (MHz)	Focal Length (mm)	Axial Resolution (μm)	Lateral Resolution (μm)	Field of View (mm)	Acoustic window size (cm)
704	40	6	40	80	14.6	2.5 x 1
707B	30	12.7	55	115	20	3 x 1.5
710B	25	15	70	140	20	3 x 1.5
711	55	6	30	90	8.5	2 x 1

Table 2-1. *Parameters of the four transducers used in this work obtained from manufacturers brochure (VisualSonics, 2006).The acoustic window shown (length x width) was measured using a ruler.*

2.2.2 Radio Frequency (RF) mode

The Vevo 770® software includes a Digital Radio-Frequency data (RF) mode. RF data has been used to measure the acoustical properties of biological tissue (Insana & Hall, 1990; Lizzi et al., 1983) and is now a widely used method (Inglis et al., 2006; Martial & Cachard, 2007; Sun et al., 2011, 2012; Szabo, 2014). The RF signal refers to the pulse-echo sent and received by the ultrasound probe. This mode is typically employed to acquire, digitalise, and to export RF data for spectral analysis from user defined regions of interest (ROI). RF data are signal comprises the raw data. Processing of this raw acoustic data allows study of the frequency content by Fourier decomposition of the returning ultrasound echo. Figure 2-3 provides an example of a typical screen capture of the RF mode using the Vevo 770® scanner.

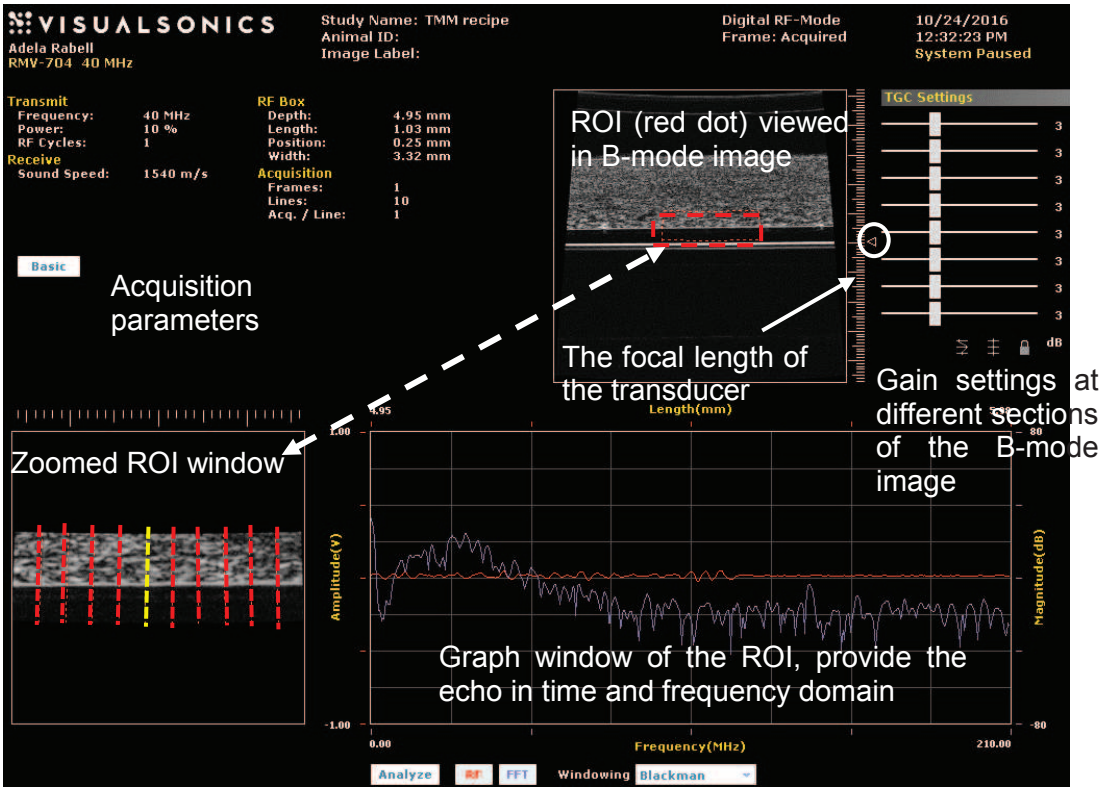

Figure 2-3. *Example of the typical screen capture of the RF data from a sample of tissue-mimicking-material (TMM) using the RMV704.*

When scanning, the single-element transducer oscillates mechanically, sweeping back and forth to produce a B-mode image. This B-mode image is shown in the right

upper corner of Figure 2-3. After the location of the ROI, the zoomed version of the image inside the ROI is shown in the bottom left corner of the screen. From the region where the zoomed ROI window is located, the raw RF data can be collected. The red lines inside the ROI window are individual lines of acquisition, in this example, 10 lines have been equally distributed along the ROI. The marked line in the zoomed ROI window (yellow) is displayed in the bottom right corner in the time domain (red line) and in the frequency domain (blue line).

Different parameters can be set when scanning with the Vevo770® Visualsonics software these are: the transmit power (%), the number of cycles in the transmitted signal, the dimensions of the ROI, the overall and individual gain values (TGC) and the format of the output saved data. When saving the data, the output content includes the number of lines inside the ROI (1 – 100), the frame number (1 – 1000) and the number of acquisitions per line (1 – 20). Only the RF data pre-selected by the ROI will be saved for later analysis.

The RF data saving formats are: *.rdb, which contains the raw RF data and the processed B-mode data from the ROI and *.rdi, which contains a description of the study and the image with the values set at the time of acquisition (e.g. the number of lines, frames, etc). Screen captures were saved in *tif format for visual reference purposes. In this PhD, the RF data were saved and analysed offline using a Matlab script (Matlab 2013a, MathWorks, Inc).

2.3 Scanning Acoustic Macroscope (SAM) system

The Scanning Acoustic Macroscope (SAM) system operates by the same principles as a scanning acoustic microscope (Foster et al., 1984). It is called macroscope as it is capable of measuring the acoustic properties of tissue *in vitro* with a similar field size to that provided by a B-mode scanner (Foster et al., 1984). The SAM system used in this study was developed in-house at the FOCAS, Dublin Institute of Technology (Dublin, Ireland) (Cannon et al., 2011) and was employed to measure the acoustic properties of the IEC agar-TMM in Chapter 3. The SAM system includes a tank filled with a reference or coupling fluid (e.g. degassed deionised water), and immersion

broadband transducers with different frequencies (Figure 2-4), a pulse-receiver (Model 5052PR; Panametrics, Waltham, MA, USA) was used to transmit and receive the pulses. The received reflected pulses were digitised and captured using a data acquisition card (PCI-5144: National Instruments, Austin, TX, USA). This data acquisition card was controlled by a LabView program (National Instruments Corporation, TX, USA), which was configured to operate the SAM system in the pulse-echo configuration.

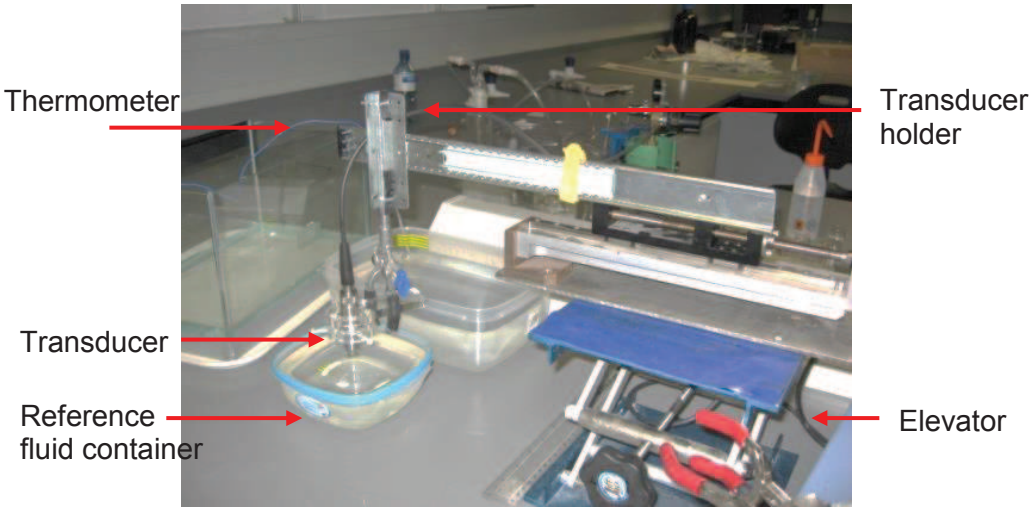

***Figure 2-4**. Diagonal view of the SAM system, developed in-house at the Dublin Institute of Technology (Dublin, Ireland).*

2.3.1 SAM system transducers

The SAM system employs a variety of broadband transducers functioning as both transmitter and receiver. The transducers used in this PhD were single-element significant low pressure immersion transducers**Error! Reference source not found.**. Three broadband immersion transducers (Table 2-2) with central frequencies of 7.5 MHz (V320-SU, Olympus NDT Inc., Waltham, MA, USA), 20 MHz (V317, Olympus NDT Inc., Waltham, MA, USA) and 50 MHz (V390-SU; Olympus NDT Inc., Waltham, MA, USA) were employed in the measurements performed in Chapter 3. Table 2-2 shows the central frequency, the focal length and the depth of view for each transducer as specified by the manufacturer (Olympus, NDT Inc.).

Transducer number (V-series)	Central frequency (MHz)	Focal length (cm)	Depth of view (cm)
V320	7.5	9.54	1.27
V317	20	6.55	0.635
V390	44.65	1.27	0.635

Table 2-2. *Parameters of the three transducers used in this work provided as provided by the manufacturer (Olympus NDT Inc.).*

2.4 SAMPLE MANUFACTURING PROCESS

In Chapter 3 two different measurement methods are described to determine the acoustic properties of the IEC agar-TMM. The first method, which is commonly used, consisted of preserving thin IEC agar-TMM samples using thin plastic film (Saran Wrap®) (FTMM). The acoustic properties were then measured in degassed deionised water (as a reference fluid). The second simpler technique, developed in this thesis, used uncovered thin slices of IEC agar-TMM samples (UTMM) immersed in a TMM preserving fluid as the reference medium. The TMM preserving fluid was specifically designed to preserve the IEC agar-TMM characteristics without the requirement of wrapping in film.

Chapter 4 presents the acoustic properties of the individual constituents of IEC agar-TMM, measured with the Vevo 770® scanner (extension of Chapter 3). These samples will be referred to as 'agar-TMM samples' and the difference in their composition ingredients is tracked by the batch number.

In Chapter 5, the acoustic properties of small animal soft tissues from brain, liver, and kidney were measured while the sample was immersed in PBS maintained at 37°C (reference fluid).

The sample manufacturing process for the IEC agar-TMM, the agar-TMM, and the small animal soft tissue samples is explained in this section.

2.4.1 IEC agar-TMM samples

A batch of the IEC agar-based TMM (Table 2-3) was manufactured following a standard method (Brewin et al., 2008; Browne et al., 2003; Cannon et al., 2001; Ramnarine et al., 2001; Teirlinck et al., 1998). Once prepared as a liquid at 90°C, the TMM mixture was cooled to 42°C and poured onto a pre-warmed metal plate. The plate was pre-warmed to ensure that the mixture spread evenly. In order to produce the samples, two methods of pouring the TMM mixture were employed. The first approach relied on the inherent viscosity of the TMM mixture to produce samples with the required sample thickness. For the second method, the TMM mixture was poured onto the pre-warmed metal plate on which were placed PVC rings. These PVC rings had the desired thickness. After the TMM mixture was poured, a ruler was employed to wipe excess TMM mixture away using the PVC rings for guidance. The TMM mixture was then left to gel and cool to room temperature. No difference was found between the two methods used to produce the TMM samples. From this batch of TMM, 22 discs of TMM with a diameter of 5.5 cm were cut using a thin-walled plastic tube. Due to the short focal lengths associated with high frequency transducers (Table 2-1 and Table 2-2), the thickness of the TMM slices was limited to less than 3.2 mm and ranged in value from 1.8 – 3.2 mm.

Ingredients	% Weight	Manufacturer
Water	78.83%	
Glycerol 99% (pure)	11.21%	Sigma-Aldrich company Ltd
Agar	3%	Merck Technical Ltd/ VWR International Ltd.
3µm Al_2O_3 power	0.95%	Logitech Ltd.
0.3µm Al_2O_3 power	0.88%	Logitech Ltd.
400 grain SiC power	0.53%	Logitech Ltd.
10% solution of Benzalkonium chloride ($C_6H_5CH_2N(CH_3)_2RCl$)	4.6%	(50% solution, diluted in-house to 10%) Sigma-Aldrich Company Ltd.

Table 2-3. *Ingredients of IEC agar-based tissue mimicking material (TMM).*

2.4.1.1 *Details of the manufacture of UTMM and FTMM samples*

After being cut, eleven of the cylindrical TMM samples were placed in a sealed container filled with TMM preserving fluid. This TMM preserving fluid was manufactured in-house (Brewin et al., 2008; Cannon et al., 2011; Inglis et al., 2006). The manufacture, acoustic properties and the reason why a TMM preserving fluid was used will be explained later. These samples are referred to as uncovered-TMM (UTMM) samples (Figure 2-5 A).

The remaining eleven TMM samples were covered with clear film in the following manner. Initially, a layer (0.015 mm thick) of Saran Wrap® film (SC Johnson Inc., Racine, USA) was stretched over an embroidery ring, of 10 cm diameter. A fast-hardening epoxy resin (Araldite Rapid; Huntsman Advanced Materials, Basel, Switzerland) was then applied to one side of a PVC ring (2 mm thick, 5.8 mm outer diameter) and the stretched Saran Wrap® was lowered onto the PVC ring. This was left to set overnight. The eleven samples were placed into the PVC rings. Five drops of TMM preserving fluid were added to the surface of the TMM to ensure good acoustic coupling between the film and the TMM. A second layer of Saran Wrap® was glued to the other side of the PVC ring, as described above, such that the TMM slices were sandwiched between the two films. These film-wrapped TMM samples (FTMM) were left to set overnight. Finally, epoxy was used to seal the edges of the film–ring–film to ensure the FTMMs did not leak. This seal was re-enforced with insulating tape to ensure that the film would not peel off over the 1-year period of investigation (Figure 2-5 B). The FTMMs were preserved in a closed box containing tissue paper moistened with TMM preserving fluid to create a saturated environment. In a similar manner, a water test cell was manufactured whereby the TMM was replaced by degassed deionised water.

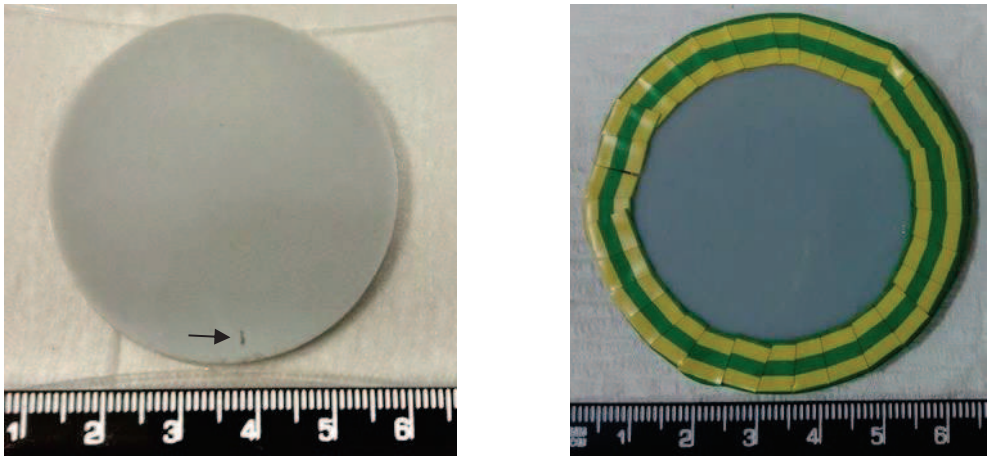

A B

Figure 2-5. *a) Un-wrapped TMM slice (UTMM), arrow indicates the identification mark on the sample and b) film-wrapped TMM slice (FTMM).*

2.4.1.2 *Details of the manufacture process of the agar-based material samples*

Different samples based on the IEC agar-TMM recipe (Table 2-3) were manufactured by varying the constituent ingredients as shown in Table 2-4. The acoustic properties of these samples are described in Chapter 4.

Using a base of agar and glycerol in the same proportions as in the IEC agar-TMM recipe (Teirlinck et al., 1998), eight batches, each yielding ten samples each of agar-based samples were manufactured by the inclusion or exclusion of the ingredients between batches (Table 2-4). These ingredients include silicon carbide (SiC), and two particles sizes of aluminium oxide (0.3µm Al_2O_3 and 3µm Al_2O_3). The percentage of each ingredient and volumes of the liquid ingredients in each of the agar-based batches was not modified from the existing IEC agar-TMM recipe (Table 2-3). These samples were manufactured in a similar manner as the UTMMs described in Section 2.4.1.1. The samples ranged in diameter from 4.5 to 5.5 cm. The thickness of the samples was between 1.78 and 3.32 mm. After being cut, these samples were placed in a sealed container filled with TMM preserving fluid.

Batch number	Composition ingredients	Agar	SiC	0.3µm Al_2O_3	3µm Al_2O_3
$B_{control}$	Control (IEC agar-TMM)	✓	✓	✓	✓
B_{SiC}	SiC	✓	✓		
B_{VWR}	Agar (VWR International)	✓			
B_{Merck}	Agar (Merck Chemicals)	✓			
$B_{SiC+0.3 Al2O3}$	SiC + 0.3µm Al_2O_3	✓	✓	✓	
$B_{SiC+3 Al2O3}$	SiC + 3 µm Al_2O_3	✓	✓		✓
B_{Al2O3}	0.3µm Al_2O_3+ 3µm Al_2O_3	✓		✓	✓
$B_{0.3 Al2O3}$	0.3µm Al_2O_3	✓		✓	
$B_{3 Al2O3}$	3µm Al_2O_3	✓			✓

Table 2-4. *Components included in each of the TMM batches. SiC = silicon carbide and Al_2O_3 = aluminium oxide.*

The agar ingredient was not removed from any batch of agar-TMM samples (Table 2-4), as this is needed to gel the samples. Specifications for the component ingredients for each agar-TMM batch was tracked by the batch name.

2.4.2 Small animal soft tissue preparation

Twenty brains, 20 livers, and 20 kidneys were analysed from 50 recently euthanized mice. Healthy male C57BL/6 were euthanized by cervical dislocation under the auspices of the Animals (Scientific Procedure) Act 1986 (Schedule 1) approved by the University of Edinburgh Animal Welfare and Ethical Review Board (AWERB). C57BL/6 mice are a common inbred strain of laboratory mouse. Within 6 minutes of euthanasia, the organs were extracted, sliced in either the coronal or transverse plane (Figure 2-6) and their SoS and attenuation measured. Excised mouse organs were sliced using a 1 mm adult rat brain acrylic slicer matrix (Zivic Instruments, Pittsburgh, PA).

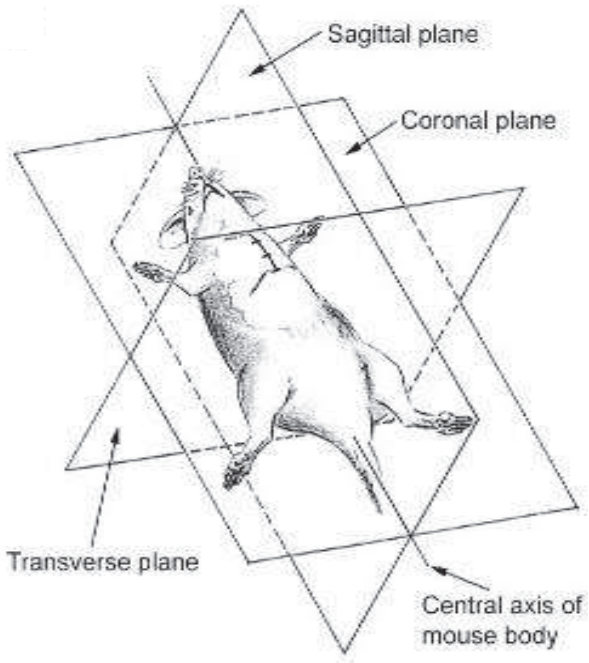

Figure 2-6. *Shows the different 3D anatomical planes. Image taken from muvag.info (date accessed 18 of January 2018).*

For brain tissue, the sample thickness was increased to 3 mm, as thinner samples tended to disintegrate during handling. Twenty brains were excised and sliced in the coronal plane at the *superior colliculus* which included the cerebral cortex (Figure 2-7 A). Measurements were made at the centre of each sample, within the grey matter. Twenty murine left lateral liver lobes were excised and sliced in the coronal plane, to a thickness of 2 mm (Figure 2-7 B). Twenty kidneys from 10 mice were excised and sliced as follows: the right kidney was sliced in the coronal plane (Figure 2-7 C) and the left kidney was sliced in the transverse plane (Figure 2-7 D). Kidney samples were sliced in the centre of the organ at 2 mm of thickness. Measurements were made from the centre of each kidney sample, aiming at the kidney *medulla*. Only one tissue sample was collected from each organ.

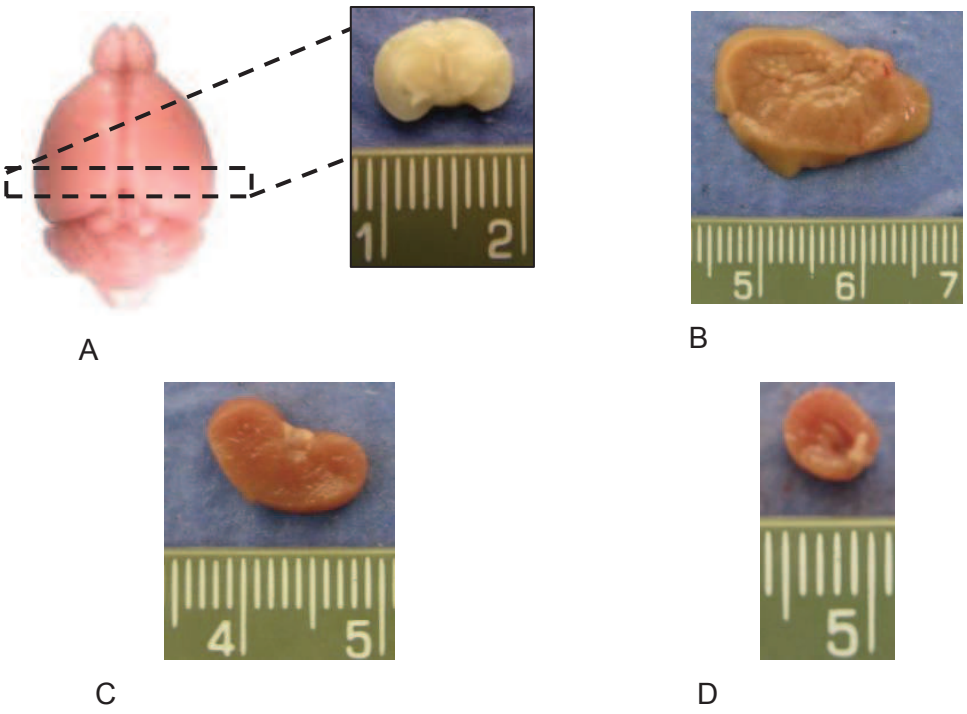

Figure 2-7. *Examples demonstrating the dissection planes of brain (A), liver (B) and kidney (C and D).*

2.5 EXPERIMENTAL SET-UP USING THE VEVO 770® SCANNER AND THE SAM SYSTEM

RF data were collected using the Vevo 770® preclinical ultrasound scanner and the SAM system. The Vevo 770® scanner was used to measure the acoustic properties of IEC agar-TMM (Chapter 3), its individual components (Chapter 4) and mouse soft tissue samples (Chapter 5). The SAM system was only used to measure the acoustic properties of the IEC agar-TMM samples described in Chapter 3. The SAM system was employed to extend the frequency range of the ultrasound measurements to lower frequencies.

Measurements were performed in a tank filled with either TMM preserving fluid, PBS, or degassed deionised water as the reference fluid. Selection of the reference fluid depended on the experiment and the type of sample being analysed (Chapters 3, 4 and 5). Acoustic and physical details of each fluid will be described in Section 2.6. The Vevo 770® scanner and the SAM system were operated in the pulse-echo

configuration (RF mode). The SAM system used a data acquisition card controlled by a LabVIEW program.

Figure 2-8 shows a schematic diagram of the experimental set-up used for the Vevo 770® and the SAM system. The sample of interest was placed and scanned in a tank filled with the appropriate reference fluid. The sample was placed above an acoustic reflector. For all the experiments using the Vevo 770® scanner, the acoustic reflector was a polymethylpentene (TPX, Boedeker Plastics, Texas, USA) cylinder of 2.5 cm diameter and 5 mm thickness. When using the SAM system, the reflector employed was a glass slide (50 x 20 x 1 mm of thick). Both the TPX reflector and the glass slide were fixed at the focal point for each transducer, using modelling clay (Plasticine, Flair, UK). To adjust the position of the transducer and the object of interest for scanning, a 3D positioning system (Visualsonics Inc., Canada) with a step size of 0.1 mm was used. This 3D positioning system contained a bench-mounted 2D (x and y axis) rail system and a z positioning system, where the transducer was mounted. For the SAM system, the transducer was fixed in a circular "transducer mount" (Figure 2-9). Three plastic screws were located on the circumference of the transducer mount, which allowed 2D movement (x and y axis). The z axis of the transducer was facilitated by a height adjustable stage, which supported the transducer mount (Figure 2-4).

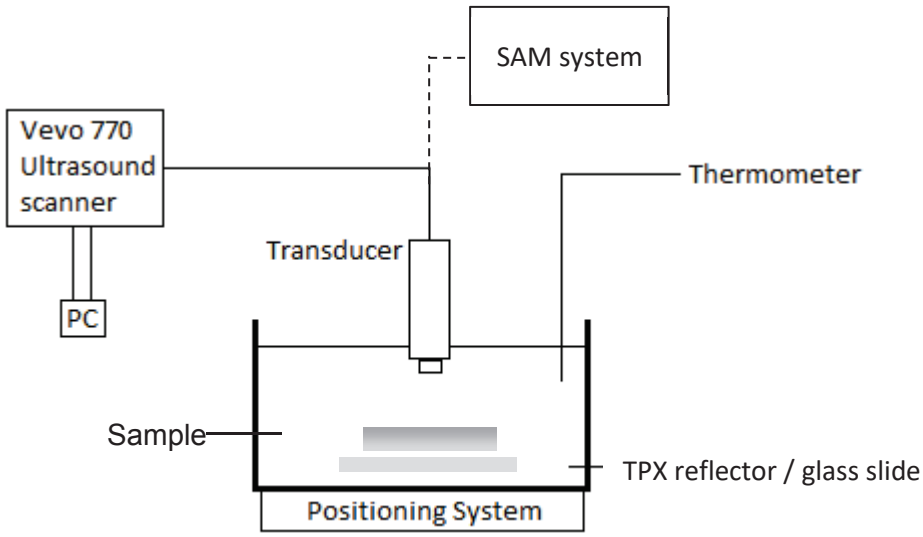

Figure 2-8. *Experimental set-up using the preclinical ultrasound scanner Vevo 770® and/or the SAM system.*

The VisualSonics software allows setting of the acoustic output power of the transducer in increments from 3% to 100%. Measurements were made using the 4 transducers mentioned earlier (Table 2-1) at 10% output power. This power was considered to provide sufficient signal magnitude to obtain a good signal-to-noise ratio without the generation of significant nonlinear effects (Sun et al., 2012). The SAM system was used at 100% output power.

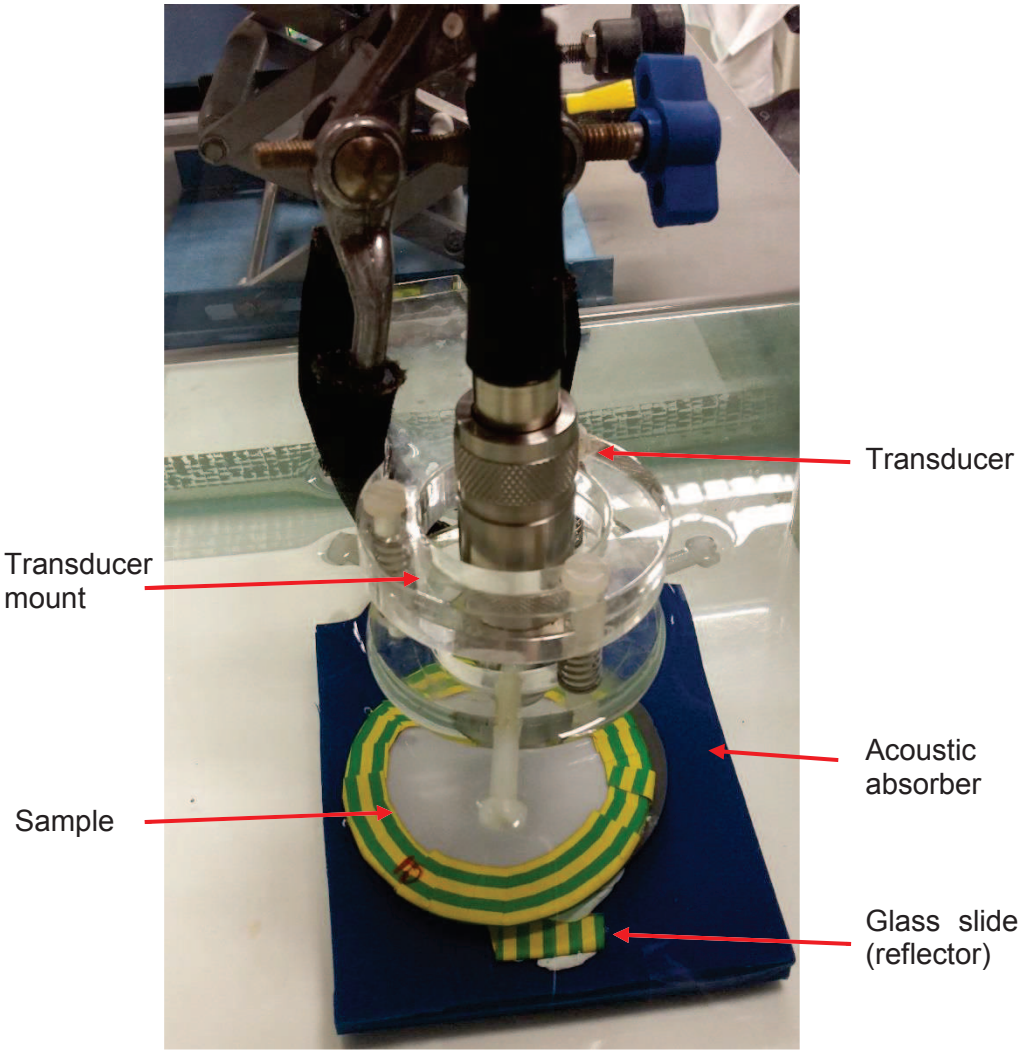

Figure 2-9. *Top view of the transducer and the transducer mount used with the SAM system at the DIT (Dublin, Ireland).*

To collect RF data, the ROIs were located at the upper surface of the reflector, with and without the sample in place, and from the front and rear surfaces of each sample.

The size of the ROIs was consistent across samples, but not across transducers. For each measurement, the RF data was collected from 10 evenly spaced scan-lines within these preselected ROIs. The calculated angular change between the RF acquisition lines was 0.15°, therefore the lines were considered essentially parallel and perpendicular to the TPX reflector.

2.5.1 Analysis of speed of sound, thickness and attenuation of samples using the Vevo 770® ultrasound scanner

A broadband reflection substitution technique (AIUM, 2014) was employed in the analysis of RF data. This technique employs the pulse-echo return times from the front and rear surfaces of the sample, to determine the thickness, and from the front surface of the reflector, with and without the sample in place. The magnitude of pulse-echoes from the front surface of the reflector, with and without the sample in place, are used to calculate the attenuation of the sample. The analysis of these echo pulses was performed using a Matlab script (Section 2.5.3).

Two methods were employed to acoustically characterise the IEC agar-TMM samples, and these are described in Chapter 3. The difference between these methods results from the presence of the film layer in the manufacturing process of the FTMM samples and UTMM samples (see earlier Section 2.4.1.1). Because of the inclusion of the film in the FTMM samples, analysis of data from the FTMM and the UTMM samples were slightly different. The method to acoustically characterise the un-covered (UTMM) samples was also used to acoustically characterise the component ingredients of the agar-TMM samples (Chapter 4) and the small animal soft tissue (Chapter 5), as none of these samples were covered in film.

2.5.1.1 *Analysis of the soft tissue and TMM uncovered samples (UTMM)*

Figure 2-10 illustrates the relevant measurements obtained for uncovered samples. Table 2-5 shows the definition of the symbols used in Figure 2-10. This method pf calculation was used for the UTMMs (Chapter 3), the agar-TMM samples (Chapter 4) and the small animal soft tissue samples (Chapter 5). The preparation process of each of these samples has been explained in Section 2.4.1 and 2.4.2, respectively.

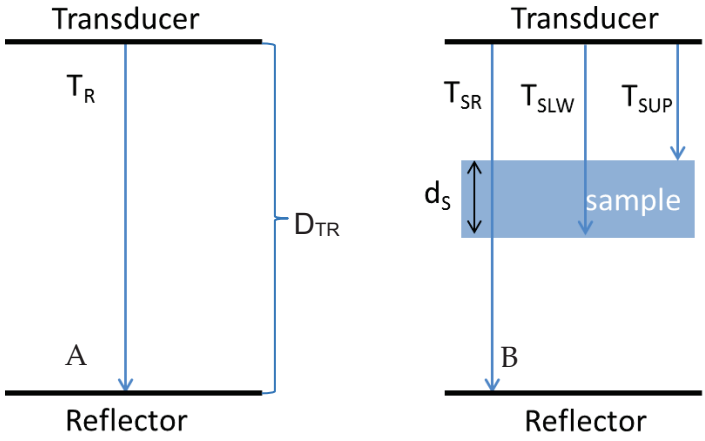

Figure 2-10. *Diagram summarising pulse-echoes intervals involved in the calculations of the acoustic properties of TMM samples. A) with reference fluid only and B) with the sample of interest. Definitions of the symbols can be found in Table 2-5.*

Symbol	Definition
D_{TR}	Distance from the transducer to the reflector
T_R	Return time interval between the surface of the reflector and the transducer, through the fluid reference.
T_{SR}	Return time interval between the surface of the reflector and the transducer through the sample.
T_{SLW}	Return time interval of the ultrasound wave from the transducer to the rear surface of the sample.
T_{SUP}	Return time interval of the ultrasound wave from the transducer to the front surface of the sample.
d_S	Thickness of the sample.
c	Speed of sound of the reference medium
c_{Sample}	Speed of sound in the sample

Table 2-5. *Definition of the symbols referenced in Figure 2-10 and involved in Equations 2-1, 2-2, 2-3 and 2-4.*

Using the Vevo 770®, the distance between the transducer and the reflector is fixed (D_{TR}). Equations 2-1 and 2-2 calculate the distance D_{TR}, with and without the sample in place. The equations below were used to calculate the speed of sound (SoS) (Equation 2-3) and thickness of the sample (Equation 2-4).

The distance between the transducer and the reflector can be calculated as:

$$D_{TR} = \frac{T_R}{2} \times c \qquad 2\text{-}1$$

The distance from the transducer to the reflector, when the sample is in place, can be calculated as:

$$D_{TR} = \left(\frac{T_{SUP}}{2} + \frac{T_{SR}}{2} - \frac{T_{SLw}}{2}\right) c + \left[\frac{T_{SLw}}{2} - \frac{T_{SUP}}{2}\right] c_{Sample} \qquad 2\text{-}2$$

Equations 2-1 and 2-2, were re-arranged and the factor of 2 gets divided out in order to calculate the speed of sound in the sample (V_{Sample}):

$$c_{Sample} = \left[1 + \frac{(T_R - T_{SR})}{T_{SLw} - T_{SUP}}\right] c \qquad 2\text{-}3$$

To calculate the thickness, and because of $V = {}^{d}/_{t}$ (V=velocity, d=distance and t=time), Equation 2-3 provides the speed of sound of the sample in terms of the return time intervals from the sample and reflector. Therefore, the thickness of the sample is given by:

$$d_S = c_{Sample}[T_{SLw} - T_{SUP}] \qquad 2\text{-}4$$

The magnitude of pulse-echoes from the reflector, with and without the sample in place, were used to calculate the attenuation of the sample. Using the echo intensities of these RF signals, and since $I = A^2$(where I stand for intensity and A for amplitude), the attenuation in dB cm^{-1} was calculated, using Equation 2-5:

$$\alpha(x, y, f) = -\frac{20}{2d_s}\left[log_{10}\frac{A_{SR}(x, y, f)}{A_R(x, y, f)}\right] \qquad 2\text{-}5$$

2.5.1.2 *Analysis of the film-wrapped samples (FTMM)*

Figure 2-11 illustrates the relevant time intervals for the samples wrapped in film. The definition of the symbols used in Figure 2-11 can be found in Table 2-6. Film-wrapped samples were only used for the IEC agar-TMM (FTMM) as explained in Section 2.4.1.1. In order to acoustically account for the film and for the water displaced by the sample, a water test cell was manufactured and included in the analysis.

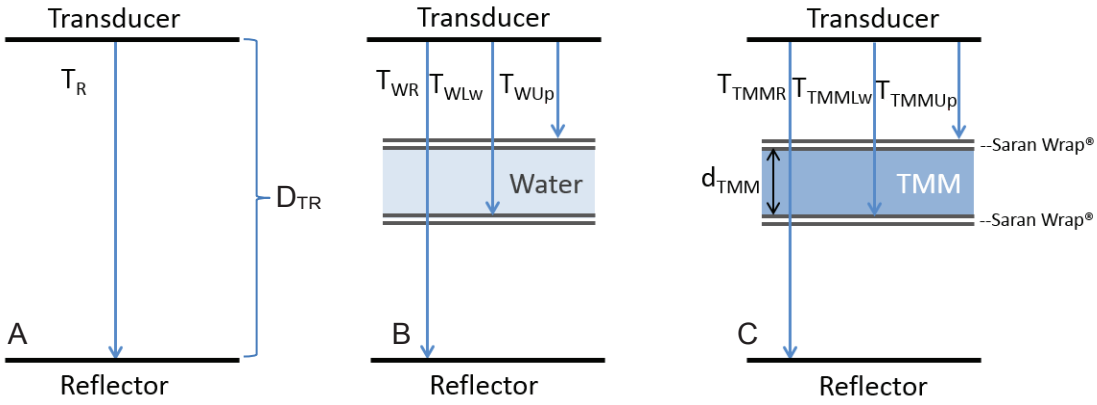

Figure 2-11. *Diagram of the pulse echoes intervals involved in the calculations of the acoustic properties a) with reference fluid only, b) with the water test cell and c) with the FTMM. The definitions of the symbols can be found in Table 2-6.*

Symbol	Definition
D_{TR}	Distance from the transducer to the reflector
T_R	Return time interval between the surface of the reflector and the transducer, through the fluid reference.
T_{WR}	Return time interval between the surface of the reflector and the transducer, through the water test cell.
T_{WLw}	Return time interval of the ultrasound wave from the transducer to the rear surface of the water test cell.
T_{WUp}	Return time interval of the ultrasound wave from the transducer to the front surface of the water test cell.
T_{TMMR}	Return time interval between the surface of the reflector and the transducer through the FTMM.
T_{TMMLw}	Return time interval of the ultrasound wave from the transducer to the rear surface of the FTMM.
T_{TMMUp}	Return time interval of the ultrasound wave from the transducer to the front surface of the FTMM.
d_{TMM}	Thickness of the FTMM.
c_W	Speed of sound of the degassed, deionised water.
c_S	Speed of sound in film.
c_{TMM}	Speed of sound in the FTMM sample.

Table 2-6*. Definition of symbols referenced in Figure 2-11 and involved in Equations 2-6, 2-7, 2-8, and 2-9.*

Using the Vevo 770®, the distance between the transducer and the reflector is fixed (D_{TR}). Equations 2-6, 2-7 and 2-8 calculate the distance D_{TR} with and without the

sample in place. The equations below were used to calculate the speed of sound (Equation 2-9) and thickness of the sample (Equation 2-10).

The distance between the transducer and the reflector can be calculated as:

$$D_{TR} = \frac{T_R}{2} \times c_W \qquad 2\text{-}6$$

The distance from the transducer to the reflector, with the water filled sampled in place, can be calculated as:

$$D_{TR} = \left(\frac{T_{WUP}}{2} + \frac{T_{WR}}{2} - \frac{T_{WL}}{2}\right) c_W + \left[\frac{T_{WL}}{2} - \frac{T_{WUP}}{2} - \left(\frac{T_R}{2} - \frac{T_{WR}}{2}\right)\right] c_W + \left(\frac{T_R}{2} - \frac{T_{WR}}{2}\right) c_S \qquad 2\text{-}7$$

The distance from the transducer to the reflector, with the FTMM sample in place, can be calculated as:

$$D_{TR} = \left(\frac{T_{TMMUP}}{2} + \frac{T_{TMMR}}{2} - \frac{T_{TMMLw}}{2}\right) c_W + \left[\frac{T_{TMMLw}}{2} - \frac{T_{TMMUP}}{2} - \left(\frac{T_R}{2} - \frac{T_{WR}}{2}\right)\right] c_{TMM} + \left(\frac{T_R}{2} - \frac{T_{WR}}{2}\right) c_S \qquad 2\text{-}8$$

Equations 2-6, 2-7 and 2-8 were re-arranged and the factor of 2 gets divided out in order to calculate the speed of sound in the sample (V_{TMM}):

$$c_{TMM} = \left[1 + \frac{(T_{WR} - TMM_R)}{T_{TMMLw} - T_{TMMUP} - (T_R - T_{WR})}\right] c_W \qquad 2\text{-}9$$

To calculate the thickness, and because $c = {}^{d}/_{t}$ (c=velocity, d=distance and t=time), Equation 2-9 provides the speed of sound in terms of the return time intervals from the sample. Therefore, the thickness can be mathematically expressed as:

$$d_{TMM} = c_{TMM}[TMM_L - TMM_{UP} - (T_R - T_{WR})] \qquad 2\text{-}10$$

The magnitude of pulse-echoes from the reflector were used to calculate the attenuation. Using the echoes amplitudes of the RF signals from the reflector, with

the water filled sample and the FTMM sample, the attenuation in terms of dB cm^{-1} was calculated, using Equation 2-11:

$$\alpha(x,y,f) = -\frac{20}{2d_{TMM}}\left[log_{10}\frac{A_{TMMR}(x,y,f)}{A_{WR}(x,y,f)}\right] \quad 2\text{-}11$$

The acoustic properties of degassed deionized water have previously been measured and found to have an attenuation coefficient (α_w) proportional to f^2 over the range of 7.5 – 67.5 MHz (Duck, 2012; Pinkerton, 1949). Furthermore, the SoS of degassed deionized water varies with temperature (Bilaniuk & Wong, 1992; Del Grosso & Mader, 1972). At 20°C the attenuation of degassed deionised water is 2.17 x 10^{-3} dB cm^{-1} MHz^2 (Duck, 2012). The attenuation of the IEC agar-TMM has been found to increase with increasing frequency. Consequently, the attenuation in this study was expressed as second degree polynomial, based on the form of the attenuation of degassed deionised water.

$$\alpha_{TMM} = \alpha(x,y,f) + \alpha_w(x,y,f) = af + bf^2 \quad 2\text{-}12$$

α_{TMM} represents the absolute attenuation of the IEC agar-TMM, f is the frequency (MHz) and a and b are the coefficients of the second degree polynomial function.

When the FTMM samples were acoustically characterised the temperature of the degassed deionised water was 22.2 ± 0.5°C corresponding to a SoS of 1488.88 ms^{-1}.

2.5.2 Analysis of the acoustic data of TMM samples using the SAM system

The SAM system displayed the RF data in real time during the measurements. For each sample, 10 consecutive pulses, equivalent to 10 lines at each position were recorded for later analysis.

In the case of the SAM system, the thickness of the sample is required to calculate the SoS of the sample (c_{TMM}). To calculate the speed of sound of the sample Equation 2-13 was used, using the same notation as in the previous section.

$$c_{TMM} = \frac{c_W}{1 + \Delta_t \frac{c_W}{2d_{TMM}}} \quad 2\text{-}13$$

where Δ_t is the time difference between T_R and, T_{TMMR} or T_{RS} (see Figure 2-10 and Figure 2-11) depending on whether the sample was covered in film or not. d_{TMM} is the known thickness of the sample. When using the SAM system, the thickness of the sample was input to the calculation from the measurements taken previously using the Vevo 770® scanner.

The attenuation measured using the SAM system was calculated in a similar manner as that for the Vevo 770® scanner.

2.5.3 Matlab script used for analysis.

To calculate the acoustic properties of the samples, RF data were analysed offline using a Matlab script. The Matlab script was developed by Dr. Chao Sun and modified by Dr. David Kenwright. Figure 2-12 shows a diagram of the Matlab script from Dr. Chao Sun and Dr. David Kenwright. This script was developed for samples wrapped in film (similar to the FTMM samples described previously) (Kenwright et al., 2014; Sun et al., 2012). This code was used to perform the acoustic characterisation of FTMM samples and the water test cell based on the reflection substitution technique described in Section 2.5.1, also used for analysis in Chapter 3. The description of the symbols used in Figure 2-12 can be found in Table 2-6.

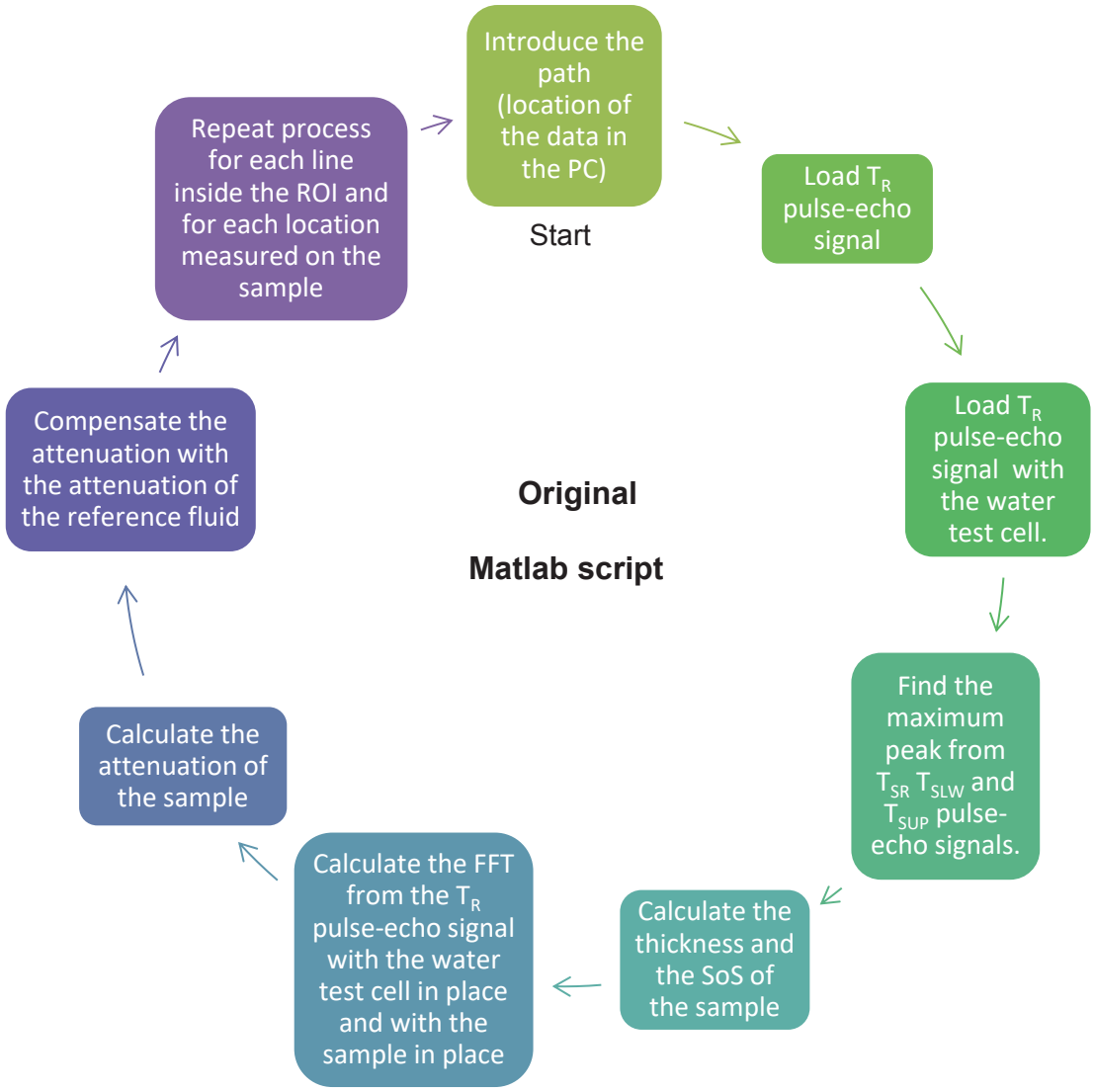

Figure 2-12. *Diagram of the original Matlab script developed by Dr. Chao Sun and improved by Dr. David Kenwright.*

In this PhD, most of the samples used (UTMM, agar-TMM and soft tissue) were not wrapped in film. It was therefore necessary to modify the script to accommodate this change. The script was modified as follows. Based on the calculations described in Section 2.5.1.1, the pulse-echo from the reflector with the water test cell was not necessary, hence the formulas included in the script to calculate the thickness and the SoS of the samples were replaced by Equations 2-3 and 2-4. A subroutine to save the acoustic properties of the sample in an Excel sheet was introduced with the help of Dr. Arjan Geers. This Excel sheet was created automatically based on the total number of samples and on the number of locations measured on each sample. The Excel sheet

was used for the later statistical analysis. Also, a script was developed to automatically plot the mean attenuation versus frequency data measured from the different locations in the sample.

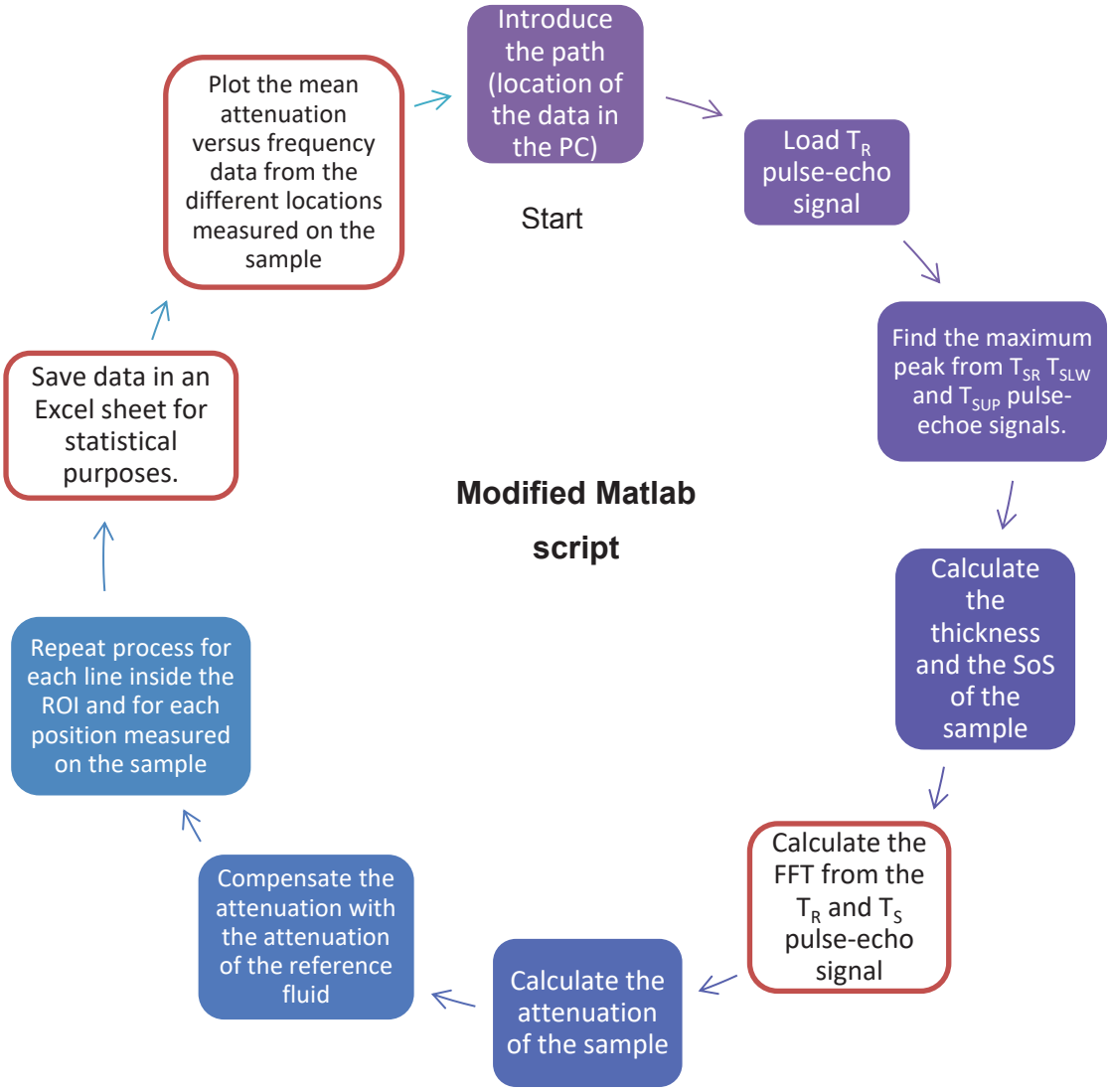

Figure 2-13. *Diagram of the Matlab script used in this PhD report. The red rectangles highlight the main modifications made to the original Matlab script (Figure 2-12).*

The red squares in Figure 2-13 highlights the modifications made based on the original Matlab script (Figure 2-12). It is important to note that compensation of the sample attenuation with the reference fluid was modified based on the acoustic

properties of the particular reference fluids (i.e. TMM preservation fluid, PBS at 37°C, and degassed deionised water).

2.5.3.1 *Matlab script used for the SAM system.*

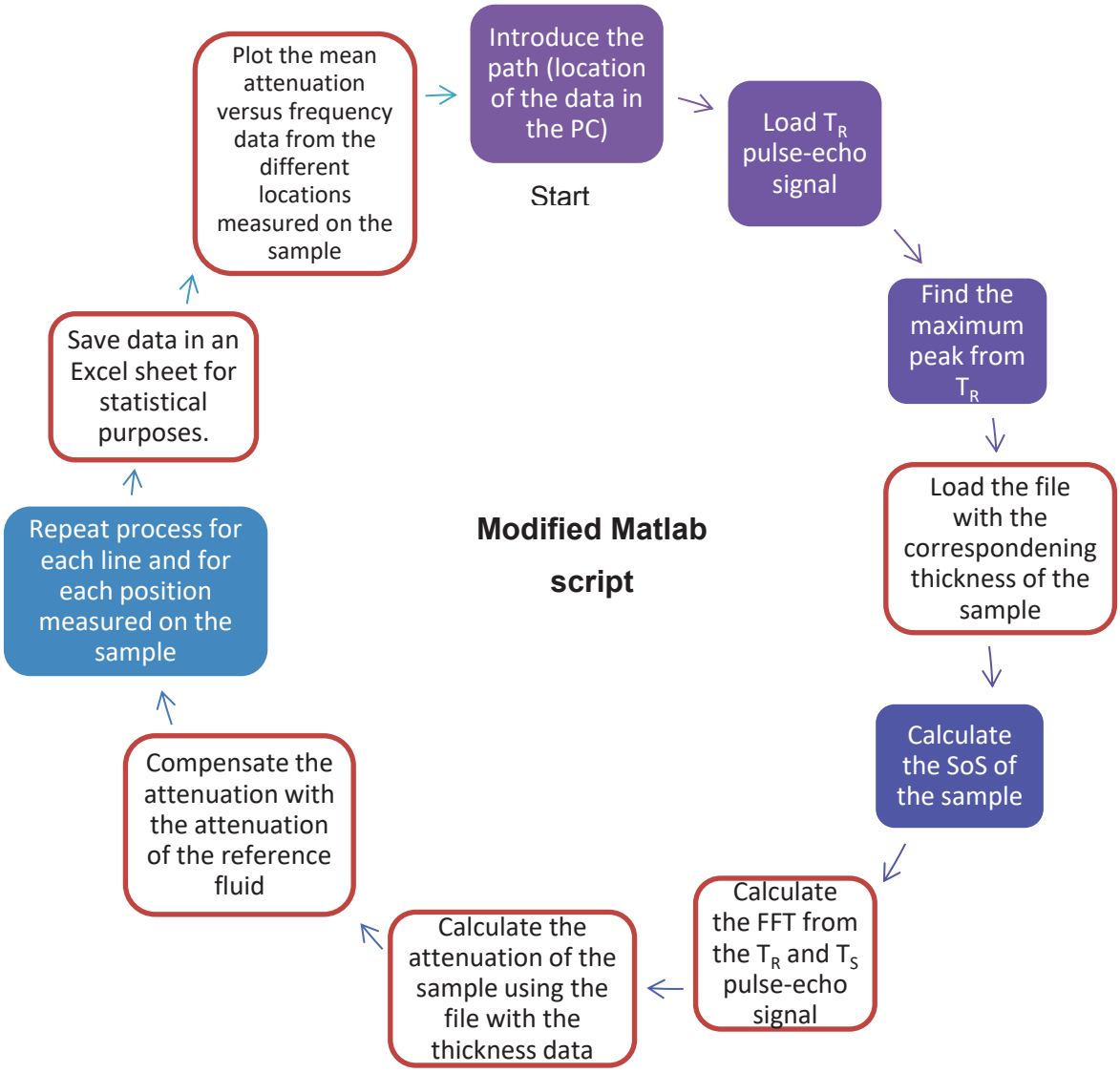

Figure 2-14. *Diagram of the Matlab script used in this PhD work. The red rectangles highlight the main modifications to the original Matlab script developed by Dr. Bakary Diarra at the Dublin Institute of Technology.*

As mentioned in Section 2.5.2, when using the SAM system, the thickness of the sample must be known in advance. This thickness value needed to be introduced in the analysis. The Matlab script used to analyse the acoustic data collected using the

SAM system was based on that from Dr. Bakary Diarra at the FOCAS of the Dublin Institute of Technology. A file with the thickness of the sample measured previously by the Vevo 770® was created. Figure 2-14 shows the diagram of the Matlab script used to analyse the data collected by the SAM system, the red squares highlighted the modifications made for this study. These modifications were based on the original script developed by Dr. Bakary Diarra.

2.5.3.2 *Manual selection of the boundaries between the sample and the medium*

To calculate the acoustic properties of the different type of samples used (with no film covering), the positions of the sample interfaces had to be selected manually from the raw RF signal. This was due to the reduced magnitude of the echoes from the boundaries of these samples compared to the film-wrap samples (FTMM). For the FTMM interfaces were detected automatically by the Matlab script. Figure 2-15 shows the difference in RF data between a UTMM sample and a FTMM sample.

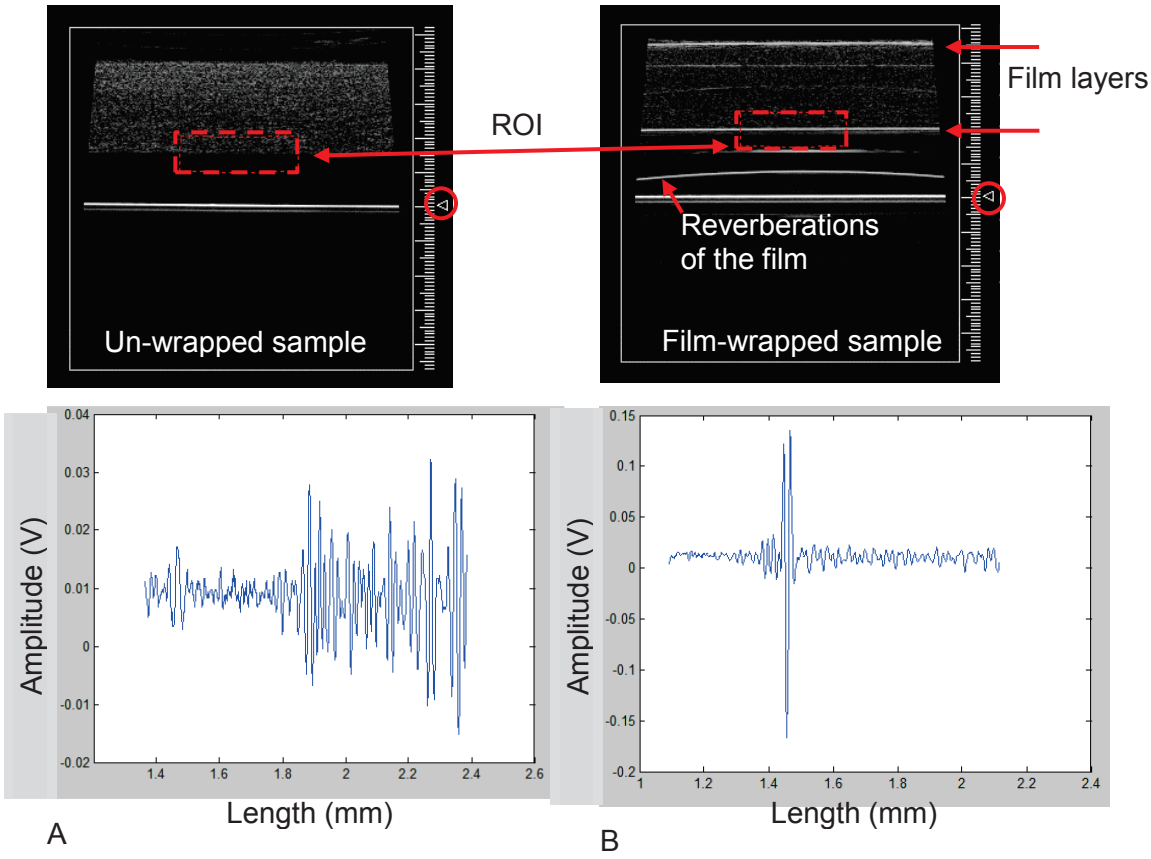

Figure 2-15. *Difference in the upper RF signal using a TMM sample between A) an un-covered sample (UTMM) and B) a film-wrapped (FTMM) sample using the RMV704 probe with the Vevo 770® ultrasound scanner. The difference in the TGC was 2 for the FTMM and 0 for the UTMM. The red circles in both upper images indicate the nominal focus of the transducer.*

Manual selection of the boundaries between the sample and the medium was performed by selecting the largest pulse-echo at each interface of the sample (Figure 2-16). The criteria for this was that the peak selected (positive or negative) should be at least 100% greater than the magnitudes of all echoes in the previous 0.2 mm time-window (as shown in Figure 2-16 below). This 0.2 mm time-window was considered sufficient for the user to visualise the boundary between the sample and the reference medium. This process was carried out for each of the 10 lines of the raw RF signal inside the ROI; the mean value from 10 lines enables the thickness of the sample to be determined each measurement.

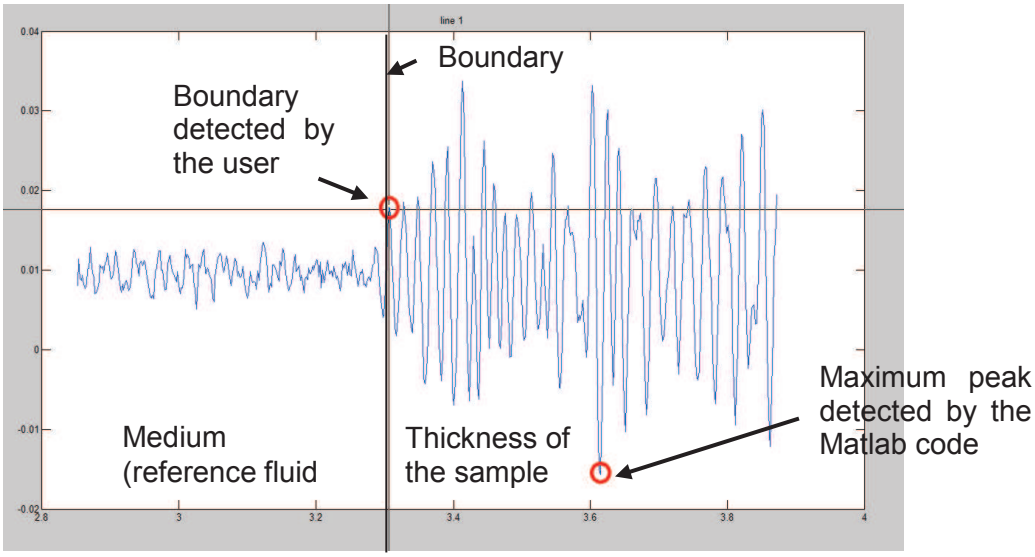

Figure 2-16. *Example of the peak detected automatically by the Matlab script and the peak detected using manual selection from the raw RF data measured with the RMV704 (18 – 40 MHz) probe.*

2.5.4 The 3dB bandwidth measurement of the Vevo 770® and the SAM system transducers

To understand the energy distribution in the frequency domain, the frequency bandwidth of each transducer signal was assessed. Figure 2-17 shows an example of the pulse-echo reflected from the TPX reflector using the RMV710B probe for the A) time domain and B) frequency domain. The frequency domain shown has not been normalized to the spectrum peak. The width of the ultrasound spectrum is commonly measured in terms of the -3 dB bandwidth. This is calculate by subtracting 3 dB either side of the peak maximum and taking the peak width between those peaks, see Figure 2-17 B) (Hoskins et al., 2003).

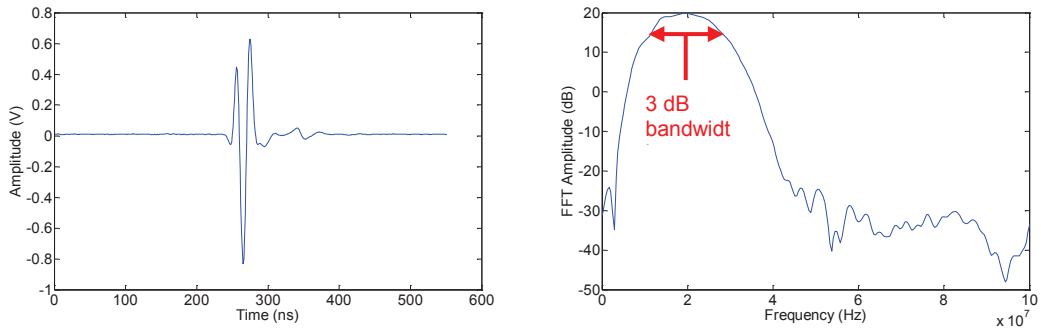

A B

Figure 2-17. *RF signal reflected from the TPX in water using the RMV710B probe at 10% power in A) time domain and B) frequency domain.*

The 3 dB bandwidth was measured for the four RMV probes of the Vevo770® scanner and for the three V-series probes of the SAM system. The 3 dB bandwidth measurements for the Vevo770® probes were made with the transmitter power at 10% of its maximum power, 1 pulse cycle. The 3 dB bandwidth measured with the SAM system was at 100% output power. The peak negative pressure value shown in Table 2-7 was obtained from Sun, (2012) and for the SAM system, the peak negative pressure was provided by Dr. Jacinta Brown who performed equivalent measurements at the Dublin Institute of Technology.

Transducer model and measurement system		Measured 3 dB bandwidth (MHz)	Peak negative pressure (MPa)
RMV 704	**Vevo 770®**	18 – 40	0.52
RMV 707B		12 – 32	1.05
RMV 710B		12 – 28	1.06
RMV 711		25 – 50	0.23
V320	**SAM system**	4.5 – 9	0.05
V317		14 – 25	0.021
V390		20 – 40	0.022

Table 2-7. *Characteristics of the Vevo 770® and the SAM system transducers. The 3 dB bandwidth value was taken from measurements. The spatial peak temporal peak negative pressure (P-) in degassed deionised water values were taken from Sun, (2012) and for the SAM system the values were provided by Dr. Jacinta E. Brown (FOCAS, DIT, Dublin, Ireland).*

The 3 dB bandwidth values shown in Table 2-7 summarise the frequency range used in the acoustic characterisation of TMM (Chapters 3 and 4) and soft tissue acoustic characterisation (Chapter 5).

2.6 ACOUSTIC CHARACTERISATION OF REFERENCE FLUIDS

During this project, different reference fluids were used to measure the acoustic properties of the different samples (Section 2.4). A TMM preservation fluid was used to facilitate measurement of the acoustic properties of the UTMM manufactured from IEC agar-TMM (Chapter 3) and the acoustic properties of its individual components (agar-TMM samples in Chapter 4). Degassed deionised water was used as the reference fluid for the measurement of the acoustic properties of the FTMM manufactured from IEC agar-TMM (Chapter 3). Phosphate-buffer saline (PBS) fluid at 37°C was used to acoustically characterise soft tissue excised from small animals (Chapter 5). The acoustic properties of the degassed deionised water have been discussed in Section 2.5.1.2.

The SoS and the attenuation coefficient of these two reference fluids (TMM preserving fluid and PBS at 37°C) were required in order to calculate the acoustic properties of the sample of interest (i.e. IEC agar-TMM, agar-TMM or soft tissue) as mentioned in Section 2.5.1 using Equations 2-1, 2-2 and 2-3.

2.6.1 TMM preserving fluid acoustic properties

During this PhD, an alternative method to measure the acoustic properties of the IEC agar TMM was established when thin slices of IEC agar-TMM were uncovered by film (UTMM). This method involved the use of a TMM preserving fluid, both as a preservation fluid and as the reference fluid. A more commonly used procedure employs degassed deionised water as the reference fluid. However, it is widely acknowledged (Brewin et al., 2008; Browne et al., 2003) that use of a TMM preservation fluid prevents drying of the TMM and also prevents glycerol leaching, which occurs when the TMM is simply immersed in water. Drying and glycerol leaching cause changes in the acoustical properties of TMM. Further details of

different method for acoustic characterisation of IEC agar-TMM samples are provided in Chapter 3.

The use of this alternative method required the acoustic characterisation of the TMM preserving fluid. This TMM preserving fluid was manufactured in-house according to a previously published article (Brewin et al., 2008; Cannon et al., 2011; Inglis et al., 2006). Table 2-8 shows the ingredients of the TMM preserving fluid.

TMM preserving fluid	
Volume (ml)	**Ingredient**
143.9 ml	99% Glycerol
58.71 ml	10% Benzalkonium chloride
1000 ml	Degassed deionized water

Table 2-8. *Ingredients of the TMM preserving fluid (Inglis et al., 2006).*

The acoustic characterisation of the TMM preserving fluid was performed by the National Physical Laboratory (NPL, Teddington, UK), using a transit time approach employing 2 transducers (pulser and receiver) (Rajagopal et al., 2014). This approach measured the time taken for the ultrasound pulse to travel through the sample. Two TMM preservation fluid test cells were manufactured by the NPL using Mylar film (12 μm thick). These cells were created by 'sandwiching' TMM preservation fluid in film, using 2 Perspex frames. Further details on the experimental set-up used by the NPL can be found elsewhere (Rajagopal et al., 2014). The SoS values of the TMM preservation fluid measurements were made over the frequency range 1 – 60 MHz, whereas to calculate the attenuation coefficient, the frequency range was from 10 – 60 MHz (with an uncertainty of 95% and an SD mean of 0.18 dB cm^{-1}). The NPL measured the SoS of the TMM preserving fluid at 19.3 ± 0.1°C to be 1538.15 ± 0.22 ms^{-1}.

Based on the data provided by the NPL a second degree polynomial function was fitted to the attenuation data (α [dB cm^{-1}]) as a function of frequency (f (MHz)), as $\alpha_{TMMfluid} = 0.00309f^2 - 0.004996f$ (R^2=0.99) over the frequency range 1 – 60 MHz.. The R^2 value is the coefficient of determination indicating the amount of variation in

response to the variable y explained by the independent variable x in the linear regression model. The larger the R^2 value is, the better the model fits the data. Figure 2-18 shows the attenuation versus frequency data as measured by the NPL and the second degree polynomial function extended to 1 MHz.

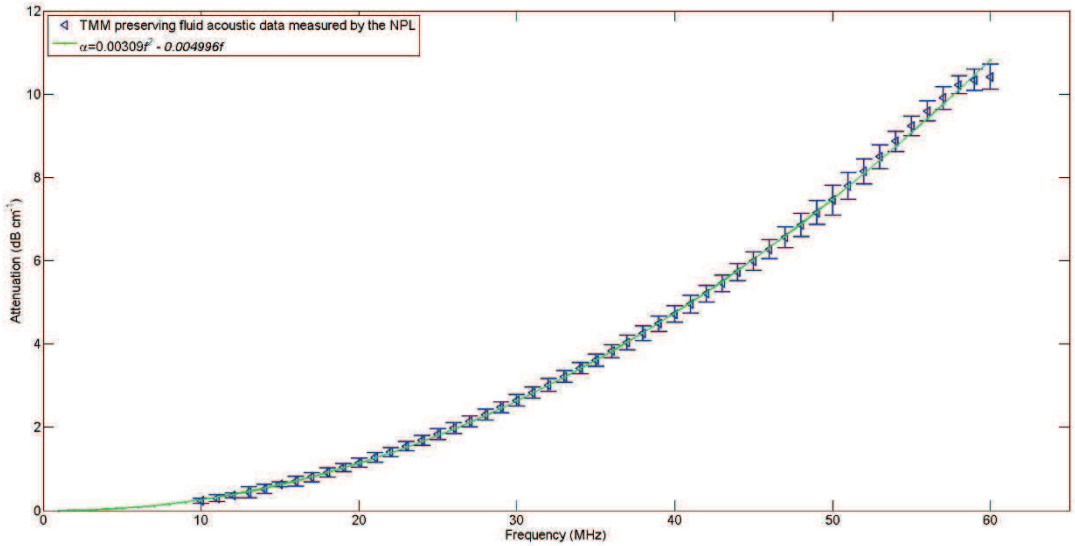

Figure 2-18. *Attenuation versus frequency data measured by the NPL together with the second degree polynomial fit.*

2.6.2 Acoustic properties of Phosphate Buffered Saline (PBS) at 37°C

It is important that the excised soft tissue acoustic characteristics be measured in a physiologically relevant environment. To achieve this, and to prevent degradation of the tissue, the samples where preserved in phosphate buffer saline (PBS) at 37°C (Edgeworth et al., 2009; Muleki-Seya et al., 2016; Wirtzfeld et al., 2015). Therefore, it was important to quantify the acoustic properties of PBS. Soft tissues were preserved at body temperature (37°C), and so the PBS fluid was characterized at the same temperature. The PBS was manufactured in-house using the recipe provided by the manufacturer (SIGMA, Life Science).

The SoS of the PBS was calculated based on the salt concentration (S) in g/100 cm^3 of water and the temperature $t = T(°C)/10$ of the fluid (Coppens, 1981):

$$C_{saline} = 1449.05 + 45.7t - 5.21t^2 + 0.23t^3 + (1.333 - 0.126t + 0.009t^2)(10S - 35) \quad \text{2-14}$$

To calculate the percentage of salinity in PBS, the formula used was:

$$\%\frac{P}{V} = \frac{M * P_{sol}}{10} \quad \text{2-15}$$

Where, *M* is the molarity, *Psol* is the solute weight or mass. To obtain the weight from the molarity we need:

$$N = \frac{n}{V} \quad \text{where} \quad n = \frac{m}{PM} \quad \text{2-16}$$

Where n number of moles, V is the volume in litres, m is the mass and PM is the molecular weight of the solute.

Because the PBS contains potassium chloride and sodium chloride, Equations 2-15 and 2-16 were used twice, each time for each compound. The salinity for the KCl was found to be 0.010 g/100 ml and 0.4 g/100 ml for NaCl (i.e. 4.1 g per litre or 0.41%). Using Equation 2-14, the SoS for the PBS at 37°C used here was 1527.9 ms^{-1}. This SoS value was confirmed experimentally when using an immersion V307 probe with 5 MHz central frequency (Olympus NDT Inc., Waltham, MA, USA). The maximum variation in the SoS of the PBS measured experimentally was found to be ± 3.9% when compared with the theory value, within a temperature range of 37.0 ± 0.4 °C.

The attenuation of PBS was assessed based on a pulse-echo substitution technique and using degassed deionised water as the reference fluid. The SoS and attenuation of distilled water are well documented over the frequency of 1 – 67.5 MHz (Bilaniuk & Wong, 1992; Coppens, 1981; Del Grosso & Mader, 1972; Pinkerton, 1949; Rajagopal et al., 2014).

2.6.2.1 *Experimental set-up for the PBS attenuation coefficient measurement*

To measure the attenuation of PBS at 37°C, the following experimental set-up was used. A temperature controlled water-filled reservoir (Grant Instruments, Cambridge, UK) with dimensions of 15 x 33 x 19 cm was used to heat the PBS to 37.2

± 0.2°C. A smaller glass container (10 x 8 x 7.5 and 1 cm thick) was placed inside the water reservoir (Figure 2-19). A 1 cm layer of an acoustic absorber (Aptflex F28, Precision Acoustics, Dorset, UK) was placed at the bottom of the glass container. A cylindrical acoustic reflector made from polymethylpentene (TPX, Boedeker Plastics, Texas, USA) with 2.5 cm diameter and 5 mm thick was glued to the absorber. The set temperature of the water-filled reservoir was regulated and maintained between 38.5 – 40 °C, so the temperature of the PBS inside the glass container could be maintained at 37°C.

Firstly, the glass tank was filled with degassed deionised water at 37°C (for the collection of the reference acoustic signal). Later, the degassed deionised water was removed from the glass container using a syringe and replaced with previously warmed PBS at 37°C. The exact temperature was recorded for each measurement with an available rectal probe for mice RET-3 (Physitemp Instruments, Inc., New Jersey, USA). This rectal probe has a tip of 0.065in and a time constant temperature record of 0.5 sec, controlled with a TM 50 mouse maintenance system (Inclus Instrument).

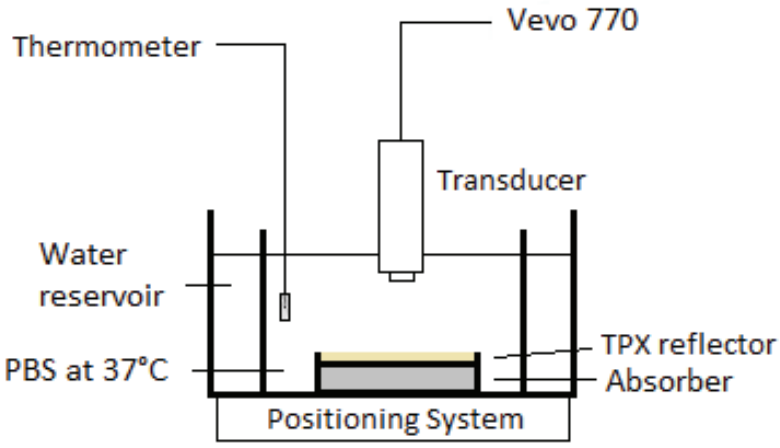

Figure 2-19. *Experimental set-up used to characterise the PBS at 37°C.*

The position and the amplitude of the TPX reflector of the pulse return time located in the glass container filled with PBS solution (Figure 2-20) were measured with 3 different transducers (RMV707B, RMV710B, and RMV711) at 10% output power

covering the frequency range from 12 – 50 MHz (Table 2-7) using the Vevo 770® scanner. The TPX reflector was located at the focal depth of each transducer. A total of 100 measurements from 10 lines all within the pre-positioned ROIs located at the surface of the TPX reflector, the raw RF data was collected and analysed offline using a Matlab script.

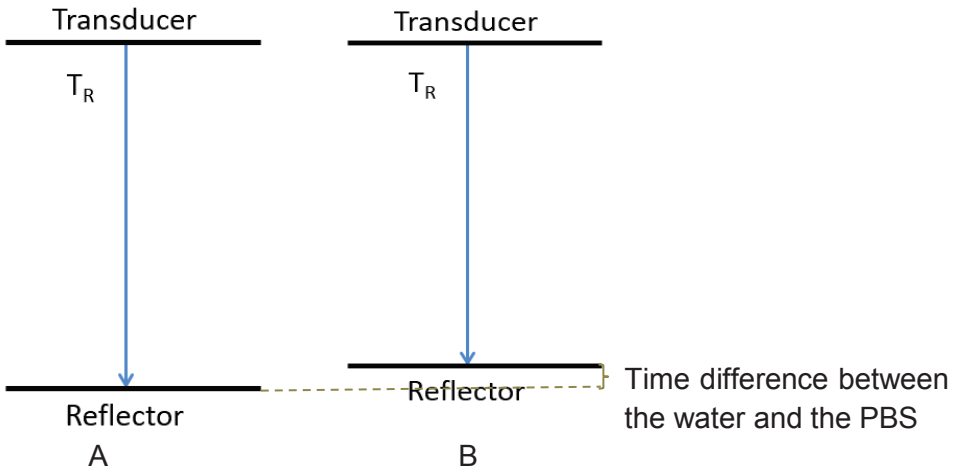

Figure 2-20. *Diagram of the pulse-echo time interval difference from the TPX reflector with the different fluids as measured by the 4 probes of the Vevo 770® ultrasound scanner. A)Time measured using degassed deionised water at 37°C and B)Time measured using PBS at 37°C.*

2.6.2.2 *Analysis of the PBS attenuation*

The attenuation of PBS was estimated based on a pulse-echo substitution technique (AIUM, 2014) using the experimental set-up shown in Figure 2-20. Using D_F as the distance between the transducer and the TPX reflector (focal point, Equation 2-1) the attenuation [α in (dB cm^{-1})] can be calculated (Equation 2-17):

$$\alpha(f) = -\frac{20}{2D_F} log_{10} \frac{A(f)_{water}}{A_0(f)_{PBS}} \qquad 2\text{-}17$$

Where $A(f)_{water}$ and $A_0(f)_{PBS}$ are the amplitude of the signal spectrum from the TPX measured in degassed deionised water and in PBS fluid respectively and, D_F is the distance calculated by the return time intervals of the pulse echoes from TPX ($D_{PBS} - D_{water}$) within the different fluids. This enabled the attenuation of PBS to be

calculated from the difference in the pulse-echoes between the degassed, deionised water as the reference fluid and the PBS both at 37°C (Figure 2-21 and Figure 2-22).

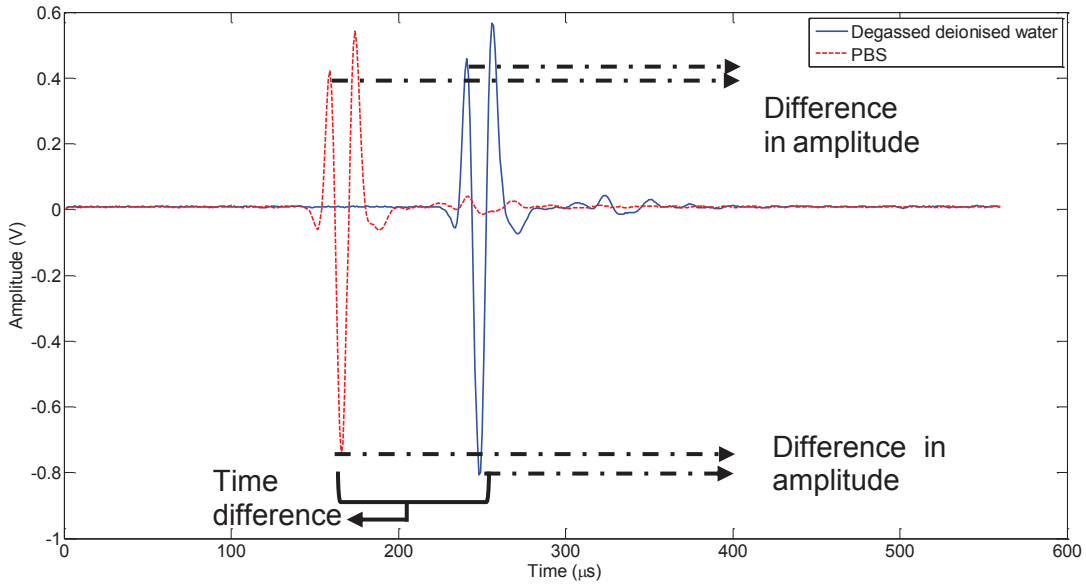

Figure 2-21. *Comparison of the RF data from degassed deionised water and PBS both at 37°C.*

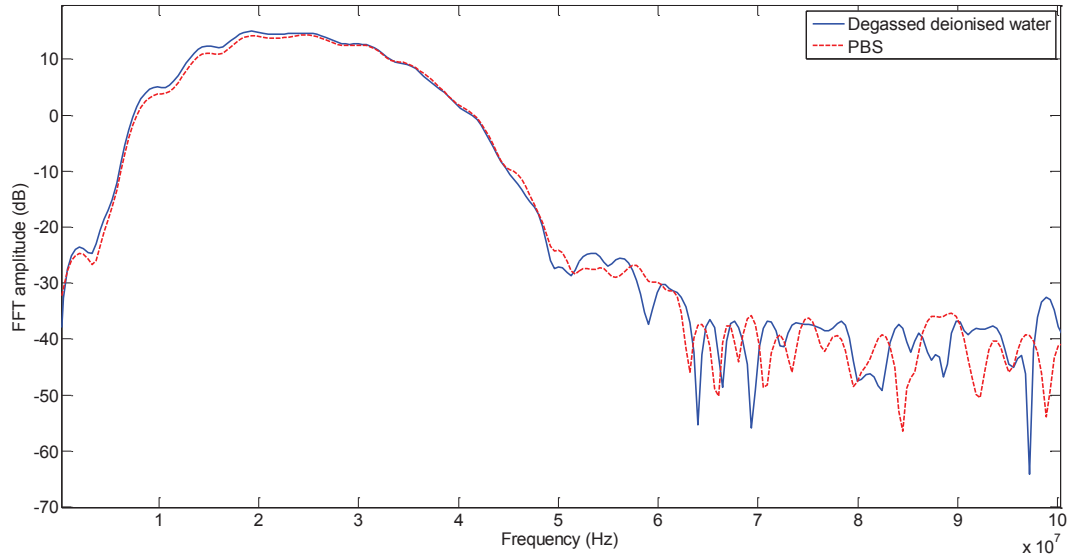

Figure 2-22. *Fast Fourier Transform (FFT) calculated from the RF data measured from degassed deionised water and PBS, both at 37°C.*

2.6.2.3 *Results of PBS attenuation measurement*

The attenuation of the PBS was measured using the RMV707B, RMV710B, and RMV711 of the Vevo 770® ultrasound scanner. Measurements were performed 5 times with each transducer. The absolute attenuation of the PBS was compensated using the attenuation of the degassed deionised water at 20°C (Duck, 2012; Pinkerton, 1949). Figure 2-23 shows the averaged attenuation versus frequency data, including the attenuation of pure water at 20°C, 30°C and 40°C (Duck, 2012). A second polynomial fit was calculated based on data at 37°C, as $\alpha = 0.002127f^2 + 0.02076f$ (R^2=0.99).

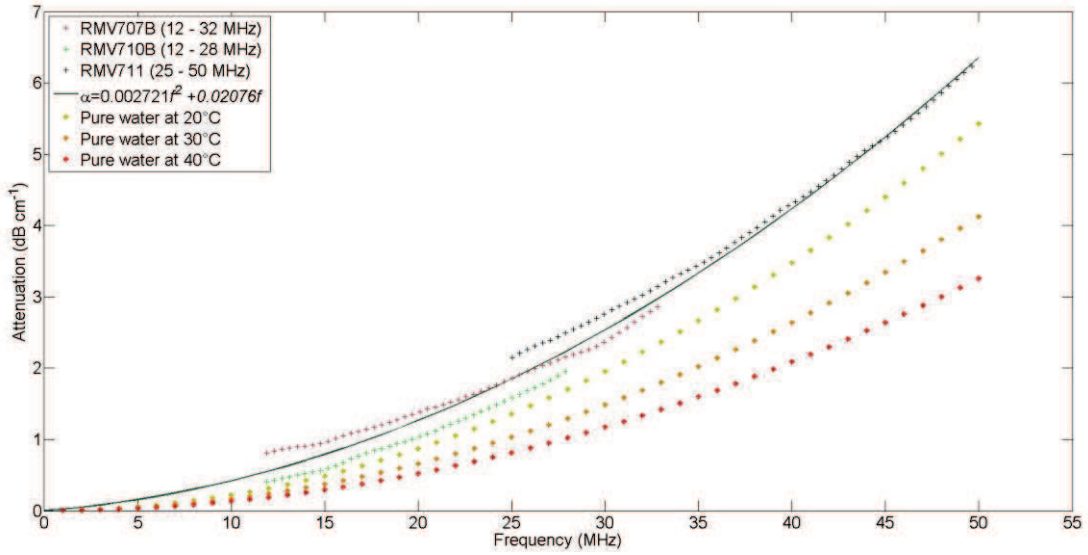

Figure 2-23. *Attenuation versus frequency data measured from PBS at 37°C with a second degree polynomial fit. The attenuation of pure water is also added at 20°C, 30°C, and 40°C (Duck, 2012).*

2.7 DISCUSSION

This chapter has presented the equipment and methodology used in this project. Specifically, the preclinical ultrasound scanner Vevo 770® and the SAM system (Dublin Institute of Technology, Dublin, Ireland) and their corresponding probes. This chapter also described the collection and the analysis of the acoustic data, and the acoustic properties of two reference fluids used in this project. The results from the acoustic characterisation of the fluids will be discussed in later chapters. The 3 dB

bandwidth measured from the Vevo 770® transducers and from the SAM system transducers corresponds to the frequency range used for the measurements described in Chapters 3, 4 and 5. The following discussion describes the impact of these settings on the assessment of the uncertainties in the measurement.

2.7.1 Sample thickness measurement

The thickness of the various samples was quantified based on a pulse-reflection substitution technique (AIUM, 2014) described in Section 2.5.1.1, using the Vevo 770® scanner. For the un-covered samples used in this project, the thickness of the sample was affected by the manual selection of the echo peaks between the boundaries firstly from the reference fluid – sample boundary, and secondly, from the sample – reference fluid boundary (Section 2.5.3.2). The manual selection method for determining the thickness of the uncovered samples was compared with the measurement of the thickness using a screen captures image saved from the Vevo 770® scanner (Figure 2-3).

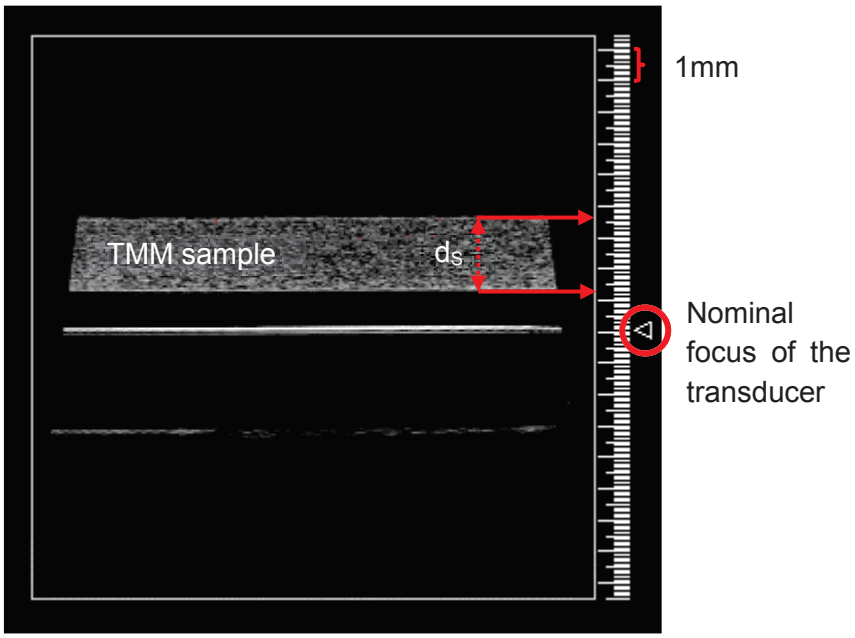

Figure 2-24. *Example of the thickness measured using a TMM sample from the screen capture of the RMV710B probe with the Vevo 770® scanner.*

The thickness of the samples was also measured from 'zoomed' screen capture images. Differences in the calculation of the thickness between the screen capture method and from the raw data using manual selection of the peak were 2%. Typical differences were found to be approximately ±0.07 mm. It was therefore concluded that the manual selection of the peak in the raw data (Section 2.5.3.2) was a sufficiently accurate method to determine the thickness of the sample. Selection of the peak was also chosen, as its inclusion in the Matlab algorithm was a straightforward process. Whereas using the thickness as determined by analysis of the screen capture image would have required development of additional code or would have been time consuming to perform manually.

2.7.2 The 3 dB bandwidth measurement of the transducers

The 3 dB bandwidth measured from the Vevo 770® transducers and from the SAM system described in Section 2.5.4, represents the sensitive frequency range of the transducers used. The 3 dB bandwidth across all 7 transducers enabled an almost complete frequency bandwidth of 4.5 – 50 MHz to be explored, with a small gap between 9 and 12 MHz.

2.7.3 PBS at 37°C

Previous studies have assumed the acoustic properties of PBS to be similar to those of degassed deionised water at the same temperature (Muleki-Seya et al., 2016). Some previous studies have used saline fluid (9% salinity) as the reference fluid (Kumagai et al., 2014; Gunawan et al., 2015). However, saline has a higher salinity concentration than PBS, which was calculated as 4%. The SoS value using Equation 2-14 (Coppens, 1981) was compared to pure water and to saline at the same temperature to calculate the SoS of PBS (4% salinity) at 37°C.

When introducing a salinity of 0% (pure water) into Equation 2-14 the SoS was calculated as 1523.9 ms^{-1} at 37°C. The acoustic properties of pure water have been previously measured using an ultrasonic interferometer and experimentally (Bilaniuk et al., 1992; Del Grosso et al., 1972). In those studies, the SoS for pure water at 37°C was found to be 1523.4 ms^{-1} (Bilaniuk et al., 1992; Del Grosso et al., 1972). The difference between the SoS calculated using Equation 2-14 and data found in the

literature was 0.5 ms^{-1}, indicating that Equation 2-14 is in good agreement with information found in the literature for pure water.

When assuming a salinity of 9% (saline fluid) using Equation 2-14, the SoS was calculated as 1531 ms^{-1} at 36°C. Previous studies report a SoS for saline fluid to be 1536 at 36°C (Hachiya, in Japanese, with English abstract) (Kumagai et al., 2014). The difference between the SoS calculated using Equation 2-14 and previous studies was found to be 5 ms^{-1}. The difference in the SoS may be attributable to the different types of salt used between sodium and/or potassium chloride.

The SoS for PBS at 37°C used in this study was 1527.8 ms^{-1}. This SoS value was found to be 8.14 ms^{-1} lower than the SoS for saline fluid (Hachiya) and up to 4.5 ms^{-1} higher than the SoS for pure water (Bilaniuk et al., 1992; Del Grosso et al., 1972). Additionally Worthington & Sherar, (2001) measured a SoS for PBS at 37°C to be 1541 ms^{-1}, with a salinity of 0.9% using the same formula as Equation 2-14. This SoS value is 13.1 ms^{-1} higher than the SoS value used in this study. The difference in these SoS values is likely to be due to the different salinities. Therefore, it is not appropriate to assume that the SoS for PBS is the same as that of pure water, as doing so, could result in higher experimental uncertainty.

The attenuation data measured from PBS using the experimental set-up shown in Figure 2-20 was fitted to a second degree polynomial. The variability of the attenuation measured across the 3 transducers (Figure 2-23) could be due to the repeatability of measurements performed using the same transducer which was ±1 dB cm^{-1}. The attenuation data for PBS at 37°C calculated in this study was found to be similar to that of degassed deionised water at 20°C and was, proportional to f^2 over the frequency range 12 – 32 MHz. Previously published studies that used PBS as a reference fluid (Gunawan et al., 2015; Muleki-Seya et al., 2016; Worthington & Sherar, 2001) assumed the attenuation coefficient to be the same as water (2.17×10^{-3} dB cm^{-1} MHz^{-2} at 20°C)(Duck, 2012). At 32 MHz the attenuation difference in between pure water at 20°C and the attenuation calculated for PBS at 37°C was found to be 0.67 dB cm^{-1}. To the best of my knowledge, there are no other studies where the attenuation of PBS has been measured.

Figure 2-25 shows the attenuation versus frequency data for degassed deionised water at 20°C (Bilaniuk & Wong, 1992; Coppens, 1981; Del Grosso & Mader, 1972; Rajagopal et al., 2014) for TMM preservation fluid measured by the NPL at 19.3 ± 0.1 °C, and for PBS measured at 37°C using the 3 transducers of the Vevo 770® ultrasound scanner. It can be seen that the difference in attenuation between degassed, deionised water and the TMM preservation fluid at 50 MHz was up to 2 dB cm^{-1}. Whereas the difference in attenuation between the PBS and degassed deionised water or TMM preservation fluid at 37°C was ±1 dB cm^{-1}.

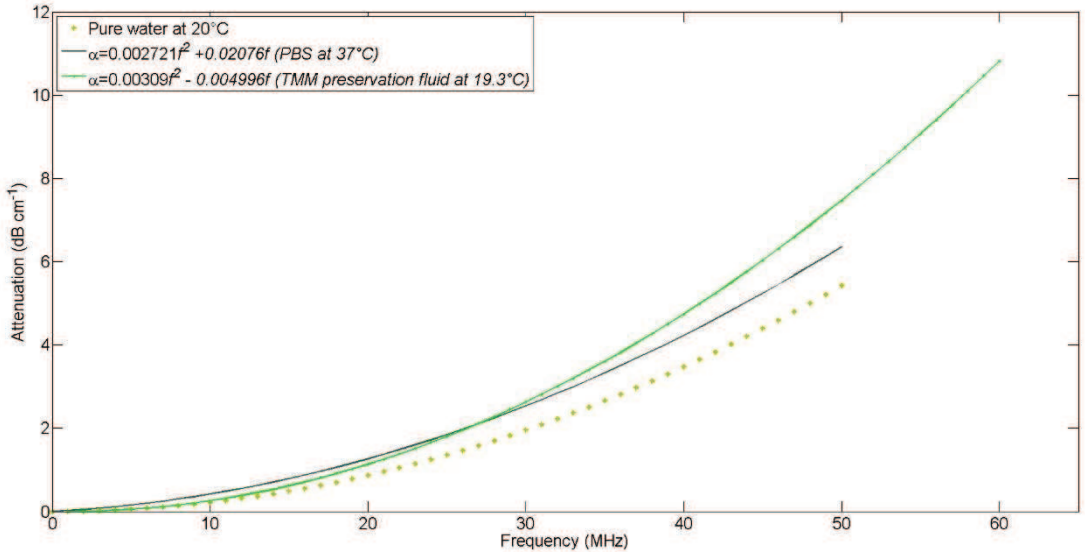

Figure 2-25. *Attenuation versus frequency data for the reference fluids used in this project.*

2.8 CONCLUSIONS

This chapter describes the Vevo 770® preclinical ultrasound scanner using 4 transducers to cover the frequency range 12 – 50 MHz and the SAM system using 3 transducers covering the frequency range 4.5 – 40 MHz, with a gap between (9 – 14 MHz). This chapter also describes:

1. The collection of RF data and the analysis using a broadband reflection substitution technique.
2. The preparation of the TMM samples and small animal tissue samples. These TMM samples consisted of IEC agar-TMM manufactured using two different

techniques, film-covered samples (FTMM) and un-covered samples (UTMM). The preparation of the agar-TMM samples with the inclusion of the varying constituent ingredients was also described.

3. Flow diagrams of the Matlab scripts used for the acoustic analysis are described.
4. The 3 dB bandwidth at 10% power for the Vevo 770® transducers and at 100% power for the SAM system transducers is described.
5. The acoustic characterisation of two different reference fluids; Phosphate Buffered Saline (PBS) at 37°C and the TMM preserving fluid at 19.3°C was performed.

The 3 dB bandwidth data, and the acoustic properties of the two reference fluids provide the reference acoustic information relating to the frequency range covered in the following Results chapters.

CHAPTER 3

THE ACOUSTICAL PROPERTIES OF THE IEC AGAR-TMM: A LONGITUDINAL STUDY USING TWO MEASUREMENT TECHNIQUES

3.1 AIM OF CHAPTER

Quality assurance (QA) phantoms manufactured from TMM are often used repeatedly over extended periods of time. This chapter examines the acoustical properties of IEC agar-TMM in the frequency range from 4.5 – 50 MHz over a one year period. Equipment used for the measurements were the Vevo 770® ultrasound scanner and the SAM system, both previously described in Chapter 2. The long term acoustical properties of TMM are likely to be affected by the method of storage and measurement procedure. The most commonly used measurement technique to acoustically characterise the IEC agar-TMM is compared and contrasted with an alternative approach developed in this project. This alternative technique was developed with the objective of examining the long term acoustic stability of the TMM material and to provide more accurate and precise acoustic values. The results from this Chapter have been published as Rabell-Montiel et al., (2017) (Appendix 1), and some of the acoustic data generated from the uncover TMM samples as a function of time, were published as Rabell-Montiel et al., (2017).

3.2 INTRODUCTION

With increasing of high-frequency ultrasound imaging applications, there is a need to develop and to acoustically characterise TMMs suitable for high-frequency ultrasound QA and training test objects. It has been shown that above 10 MHz the attenuation of TMMs in existing commercial test phantoms exhibit a nonlinear response with increasing frequency (Browne et al., 2003). The IEC guideline for TMM properties recommends a linear relationship between attenuation and frequency up to 10 MHz based on published studies for soft tissue.

The IEC agar-TMM has previously been found to have a non-linear response when acoustically investigated at frequencies up to 60 MHz (Brewin et al., 2008; Sun et al., 2012 and Rajagopal et al., 2014). In these studies, the use of test cells or TMM samples wrapped with plastic film material (Saran Wrap® or Mylar®) was employed to preserve the samples during acoustic characterisation. In these studies, degassed, deionised water was used as a coupling and reference medium. Slices of TMM ranging in thickness from 2.5 – 30 mm were employed, enabling higher ultrasound frequencies to propagate fully through the TMM slices (Brewin et al., 2008; Rajagopal et al., 2014; Sun et al., 2012). Encasing the TMM in film is important, as without the film the TMM degrades rapidly. This degradation is due to leaching of the glycerol from the TMM into the water reference medium, thus altering the acoustic properties of the TMM (Brewin et al., 2008). In these studies, a reference water test cell, also encapsulated in Saran Wrap® or Mylar® film, was used in the reference measurement in order to investigate the effect of the film on measurements (Rajagopal et al., 2014; Sun et al., 2012). The production of both the TMM slices wrapped in film and water test cells is time-consuming and technically challenging, especially for thin TMM samples.

In addition to being technically difficult to fabricate, the film-wrap method is also prone to failure as it relies on a perfect seal of the TMM by the plastic film. Therefore, this well used technique for the measurement and preservation of IEC agar-TMM materials was compared to an alternative technique. In this alternative technique the TMM is both characterised and stored in a preserving fluid. This approach aims to avoid the use of the plastic film, to provide a robust and easy-to-use alternative to using film. Furthermore, this method was evaluated over a 1 year period, to determine the longitudinal stability of the acoustic properties. This chapter compares the longitudinal acoustic stability between these two measurements techniques. Chapter 4, presents the acoustic properties of the individual ingredients composition of the IEC agar-TMM.

3.3 METHODOLOGY

As before, data were captured using two different acoustical systems. Firstly, the Vevo 770® preclinical ultrasound scanner described in the Section 2.2 and secondly, a SAM system was used, located at the FOCAS centre of the Dublin Institute of Technology (Dublin, Ireland) described in Section 2.3. The SAM system was used to provide additional acoustic data and to extend the bandwidth lower limit to 4.5 MHz.

3.3.1 Manufacture of the FTMM and the UTMM samples

In order to compare the two measurement and preservation techniques, two batches of TMM were created. The first batch consisted of un-covered IEC agar-TMM samples, stored and measured in TMM preserving fluid. The second batch consisted of film-wrapped IEC agar-TMM samples preserved in a sealed box, together with tissue moistened with TMM preservation fluid, and measured in degassed deionised water. The manufacturing process from both batches has been described in Section 2.4.1.1.

3.3.2 Experimental set-up

In this study, radio frequency (RF) data were collected and analysed from 11 film-wrapped TMM samples (FTMMs) and 11 un-covered TMM samples (UTMMs). To measure the acoustic properties, the FTMM samples were submerged in a tank filled with degassed, deionised water as the reference medium, while for the UTMM measurements, the tank was filled with TMM preserving fluid. Measurement of the TMM thickness, SoS, and attenuation of the FTMM and UTMM samples was performed using the Vevo 770® scanner. The SoS and the attenuation of the FTMM and UTMM samples were also performed by the SAM system.

Details of the experimental set-up used for both systems can be found in Section 2.5. Measurements were made using 7 transducers in total, Table 2-7 lists the bandwidth of each transducer and its peak negative pressure.

3.3.3 Acquisition of the acoustical data

For each measurement, RF data was collected from 10 adjacent scan-lines within a pre-selected ROI at 4 different positions on the FTMM or UTMM slices. Data were

analysed off-line using a Matlab script (Figure 2-13) based on a broadband pulse-echo substitution technique (Section 2.5.1.1 and 2.5.1.2).

The characteristics of both FTMM and UTMM samples were assessed over a period of 1 year at approximately 0, 3, 6, 9 and 12 month time points. At each time point, measurements taken with the Vevo 770® were performed before measurements with the SAM system.

3.3.4 Acoustic analysis of samples

The calculation of the SoS, thickness, and attenuation from UTMM (Section 2.5.1.1) and FTTM (Section 2.5.1.2) have been previously described for both the Vevo 770® ultrasound scanner (Section 2.5.1) and the SAM system (Section 2.5.2). The thickness used to calculate the acoustic properties using the SAM system, was the thickness measured the first time by the Vevo 770®.

The acoustic properties of the TMM preservation fluid and degassed deionised water used in this study have also been described previously in Section 2.6.1.

3.3.5 Unpreserved samples, batch to batch variation and measurement repeatability of the UTMMs

The acoustic properties of an additional two unpreserved UTMM samples were measured in an identical manner to that described previously but using only the RMV704 transducer (centre frequency 40 MHz, Table 2-1 and Table 2-7). Measurements were performed every 24 hours over a 96 hour period. The unpreserved samples were left exposed to the air between measurements.

An indication of TMM batch-to-batch variability was assessed by measuring the acoustical properties of 6 UTMMs manufactured from a second batch of TMM. These samples will be referred to as UTMM2. These samples had a mean thickness of 2.01 ± 0.05 mm as measured using the Vevo 770® scanner. The acoustical properties were measured with the Vevo 770® and with the SAM system at 6 and 12 months.

Data analysis was performed in the same way as for the 11 UTMM samples described in Section 2.5.1.1.

To assess the repeatability of the measurement system, the acoustic properties of the 11 UTMM samples were measured with one transducer RMV710B at 5 different times over a 1 month period. The reference medium for these repeatability tests was the TMM preserving fluid.

3.4 RESULTS

3.4.1 Speed of sound and thickness of FTMMs and UTMMs

The mean thickness of the FTMM and UTMM samples calculated using the RF ultrasound signals from the Vevo 770® over all time points (0, 3, 6, 9 and 12 months) showed a maximum variation of 0.25 mm and 0.08 mm for the FTMM and UTMM respectively, indicating less variation over time in the UTMM. The thicknesses, measured by digital calliper, from 11 UTMMs showed a maximum variation of 0.03 mm (Table 3-1).

Number of the sample	FTMM thickness (mm +SD)	UTMM thickness (mm + SD)	
	Vevo 770®		Micrometre
1	2.61 (0.04)	2.63 (0.04)	2.54 (0.02)
2	2.60 (0.05)	2.82 (0.04)	2.76 (0.02)
3	3.08 (0.13)	3.17 (0.06)	3.08 (0.00)
4	2.08 (0.25)	2.77 (0.04)	2.68 (0.01)
5	2.26 (0.08)	3.03 (0.04)	2.93 (0.01)
6	2.67 (0.11)	2.70 (0.04)	2.63 (0.01)
7	2.08 (0.15)	2.99 (0.05)	2.89 (0.03)
8	2.16 (0.10)	2.74 (0.06)	2.63 (0.01)
9	2.79 (0.19)	3.28 (0.08)	3.02 (0.01)
10	2.56 (0.05)	3.13 (0.06)	3.21 (0.01)
11	2.71 (0.05)	2.93 (0.04)	2.86 (0.03)

Table 3-1. *The mean and SD of the thickness of 11 FTMM and 11 UTMM samples measured by the Vevo 770® at all-time points. The thickness of the UTMMs were measured with micrometre at the start of each experiment.*

Table 3-2 shows the mean SoS of FTMM and UTMM samples at each time point. It can be seen that the SoS of the FTMMs exhibited larger variability than the SoS of the UTMMs. Using a Student's t-test (unpaired) it was shown that the mean SoS value of

FTMMs and UTMMs samples were not statistically different ($p > 0.5$) at the start of the experiment, but displayed a significant difference ($p < 0.05$) for the remainder of the time points. The results after 1 year showed that the SoS of the FTMM samples decreased by 22.1 ms^{-1} compared with the first measurement at 0 months, whereas the SoS of the UTMMs samples decreased 4.1 ms^{-1} over the same 12 month period. The SoS of UTMM2 samples calculated over a 6 month time period showed a decrease from 1558.1 ± 5.3 ms^{-1} to 1544.8 ± 3.3 ms^{-1}, with a difference of 13.3 ms^{-1}.

SoS ± SD (ms^{-1})	0 months	3 months	6 months	9 months	12 months
FTMM	1547.4 ± 19.2	1530.3 ± 33.5	1547.2 ± 21.5	1518.0 ± 20.3	1525.5 ± 16.5
UTMM	1545.9 ± 10.4	1543.9 ± 15.8	1544.2 ± 11.0	1544.2 ± 6.8	1541.8 ± 1.6

Table 3-2. *The mean and SD of the SoS (ms^{-1}) measured with the Vevo 770® and SAM system at each time point for the FTMMs and UTMMs samples.*

Table 3-3 shows the mean SoS averaged over all time-points for each of the measurement systems. It was found that the SoS measurements using the SAM system exhibit less variability than the SoS measurements using the Vevo 770® for the FTMM and UTMM samples.

SoS ± SD (ms^{-1})	Vevo 770®	SAM system
FTMM	1536.3 ± 13.6	1533.1 ± 12.1
UTMM	1544.1 ± 5.1	1544.1 ± 2.7

Table 3-3. *The mean and SD of the SoS (ms^{-1}) over all time points for the 11 FTMMs and 11 UTMMs measured by the four transducers of the Vevo 770® and by the three transducers of the SAM system (Table 2-7).*

The mean SoS values of the samples over all time points, using both measurement systems, were found to be 1534.7 ± 13.7 ms^{-1} for the FTMM and 1544.1 ± 3.9 ms^{-1} for the UTMM (Table 3-4). The mean SoS for the UTMM2 was found to be 1551.4 ± 6.2 ms^{-1}. Table 3-4 also shows the SoS results in comparison with those values published for IEC agar TMM (Brewin et al., 2008; Browne et al., 2003; IEC, 2001; Rajagopal et al.,

2014; Sun et al., 2012). The mean SoS of FTMMs and UTMMs are within the values specified by the IEC (IEC, 2001).

Sources	Type of samples (covered with film or uncovered)	Mean SoS ± SD (ms^{-1})	Frequency range (MHz)
IEC, 2001		1540 ± 15	2 – 10
Browne et al., 2003	UTMM measured in degassed water	1546.5 ± 3	2.25 – 15
Brewin et al., 2008	UTMM measured in degassed water	1537 ± 2.6	17 – 23
	FTMM	1540.9 ± 8.7	
Sun et al., 2012	FTMM	1547.8 ± 3.7	10 – 47
Rajagopal et al., 2014	FTMM	1544 ± 3.1	1 – 60
This study	FTMM	1534.7 ± 13.7	4.5 – 50
	UTMM measured in TMM fluid	1544.1 ± 3.9	

Table 3-4. *Values of SoS (ms^{-1} ± SD) measured in this study using two different methods, compared with published data.*

3.4.2 Attenuation as a function of frequency for FTMM and UTMM samples

Figure 3-1 and Figure 3-2 show the mean attenuation as a function of frequency for the FTMM and for the UTMM samples respectively at 0, 6 and at 12 month time points measured using the 7 different transducers. It can be seen that the variation in the mean attenuation values for UTMM samples is small in comparison to the variation observed in the mean attenuation values for FTMM samples.

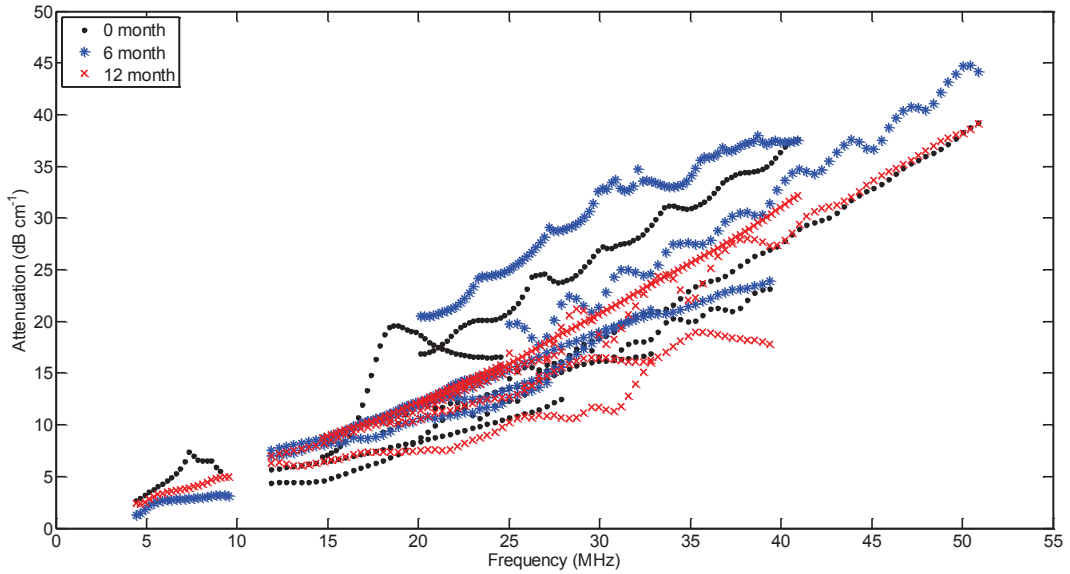

Figure 3-1. *Mean attenuation versus frequency measured with the Vevo 770® and the SAM system of 11 FTMMs at 0 month, 6 month and at 12 month time-point using 7 transducers.*

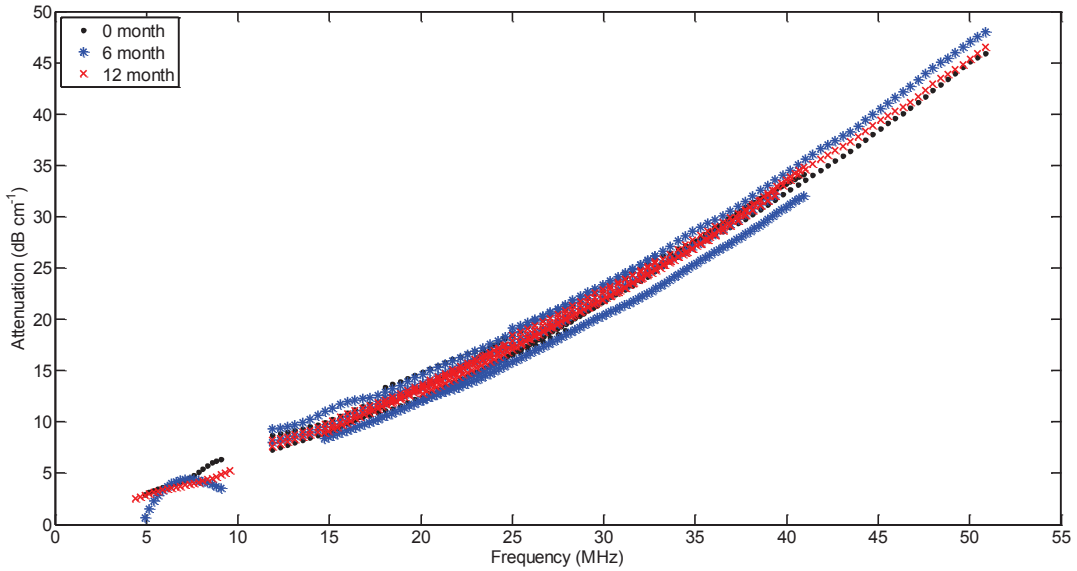

Figure 3-2. *Mean attenuation versus frequency measured with the Vevo 770® and the SAM system of 11 UTMMs at 0 month, 6 month and at 12 month time-point using 7 transducers.*

Figure 3-3 and Figure 3-4 shows the mean attenuation data over the frequency range 4.5 – 50 MHz, averaged over all 11 FTMMs and over all 11 UTMMs and time points, respectively.

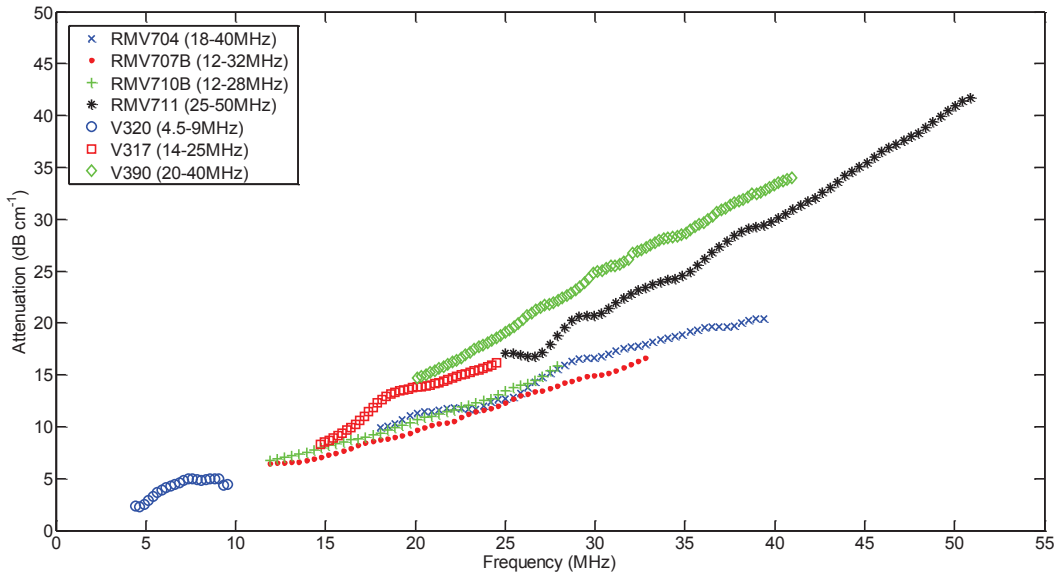

***Figure 3-3**. Attenuation data as a function of frequency averaged over all time points (data set: 11 FTMM samples measured in degassed deionised water by the Vevo 770® and SAM system in the frequency range 4.5 – 50MHz).*

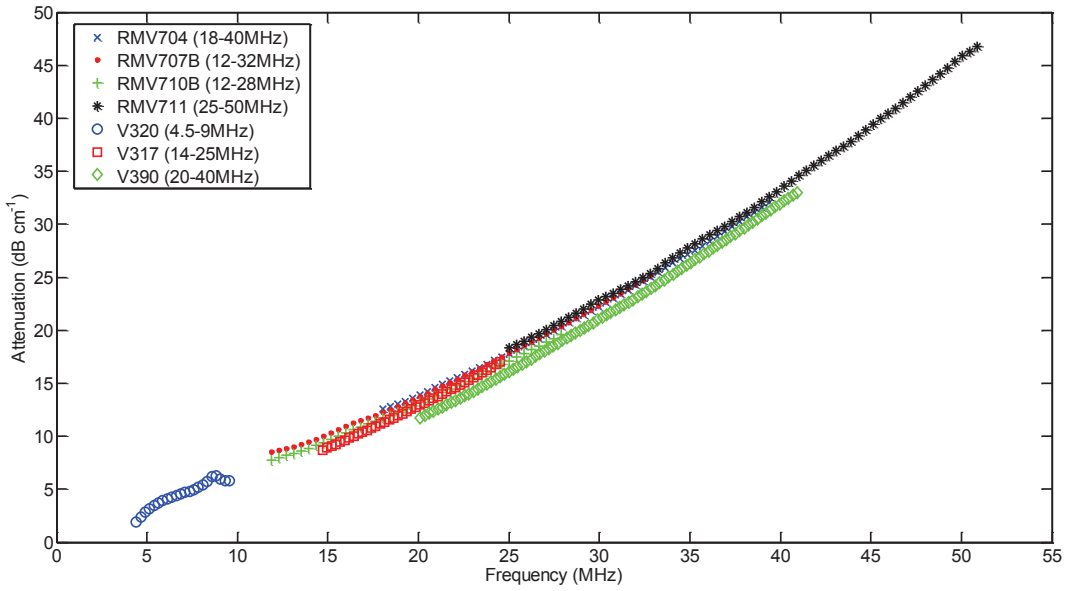

***Figure 3-4.** Attenuation data as a function of frequency averaged over all time points (data set: 11 UTMM samples measured in TMM preserving fluid by the Vevo 770® and SAM system in the frequency range 4.5 – 50MHz).*

Polynomial functions were calculated for the attenuation as a function of frequency at each time point for the FTMM and UTMM samples (Table 3-5). The best fit polynomial function was determined over all the attenuation versus frequency data

in the range 4.5 – 50 MHz as a combination of Vevo 770® and SAM system data over all time points. The polynomial fit found for FTMM was $0.4649f + 0.007363f^2$ (R^2=0.80) and $0.4897f + 0.008366f^2$ (R^2=0.99) for UTMM (Figure 3-5). The quality of fit (R^2) of the five polynomial fits at each of the five time points for the FTMMs ranged between 0.78 – 0.92 whereas for the UTMMs this value ranged between of 0.96 – 0.99. In addition, in Figure 3-5, for comparison, the attenuation data of the IEC agar TMM from studies already published is included and the attenuation from those reference fluids used (degassed deionised water and TMM preserving fluid).

	0 months	3 months	6 months	9 months	12 months
FTMMs	$0.5032f + 0.0060f^2$	$0.3608f + 0.0092f^2$	$0.5128f + 0.0082f^2$	$0.4093f + 0.0081f^2$	$0.3788f + 0.0079f^2$
UTMMs	$0.5072f + 0.0078f^2$	$0.4891f + 0.0079f^2$	$0.4643f + 0.0090f^2$	$0.4615f + 0.0089f^2$	$0.4976f + 0.0082f^2$

Table 3-5. *Polynomial fit-curve ($\alpha = af + bf^2$) of the attenuation versus frequency calculated from 11 FTMMs and 11UTMMs of the mean attenuation measured using the Vevo 770® and the SAM system over the frequency range 4.5 – 50MHz.*

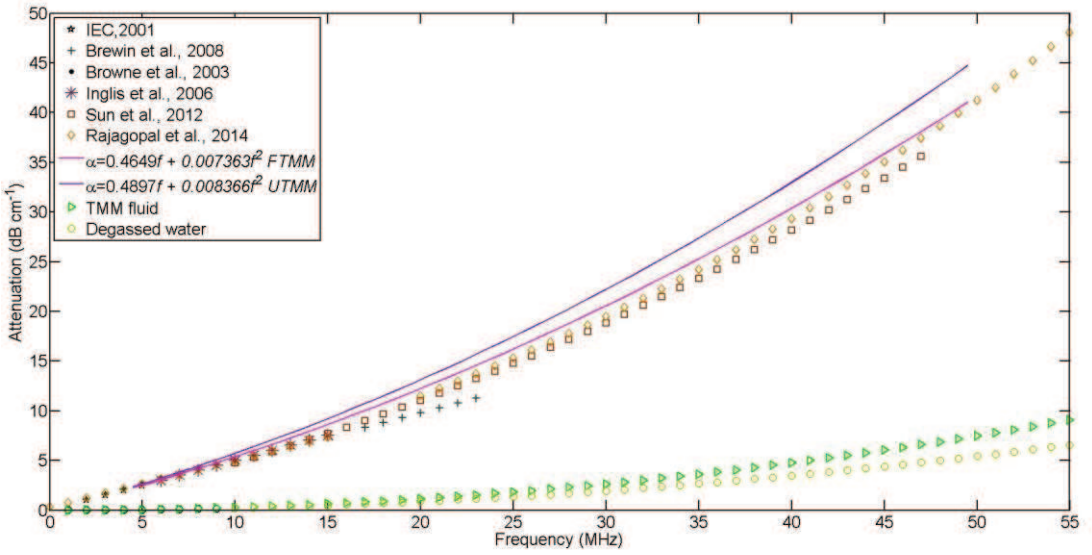

Figure 3-5. *Polynomial curve-fit of all the attenuation data as a function of frequency and the absolute attenuation of TMM in 2 – 10MHz (IEC., 2001), 17 – 23MHz (Brewin et al., 2008), 2.25 – 15MHz (Browne et al., 2003), 6 – 15MHz (Inglis et al., 2006), 10 – 47MHz* (C. Sun et al., 2012) *and 1 – 60MHz (Rajagopal et al., 2014). Also, the attenuation as a function of frequency for the TMM preserving fluid and degassed deionised water is shown.*

3.4.2.1 *Batch to batch variation of the UTMMs*

The batch to batch variation of TMM was assessed by the UTMM2 samples (2.01 ± 0.05 mm thickness). These samples were measured with both the Vevo 770® and the SAM system at 6 and 12 month time points. The mean SoS of UTMM2s was found to be 0.44% higher (7.4 ms^{-1}) than the mean SoS of the 11 UTMMs. For the attenuation, the second degree polynomial fit calculated for the UTMM2s was $0.5221f + 0.007326f^2$ (R^2=0.99). Figure 3-6 shows the second degree polynomial fit found for UTMM and UTMM2 samples. The maximum difference was found to be of ± 0.63 dB cm^{-1} in mean attenuation across the frequency range.

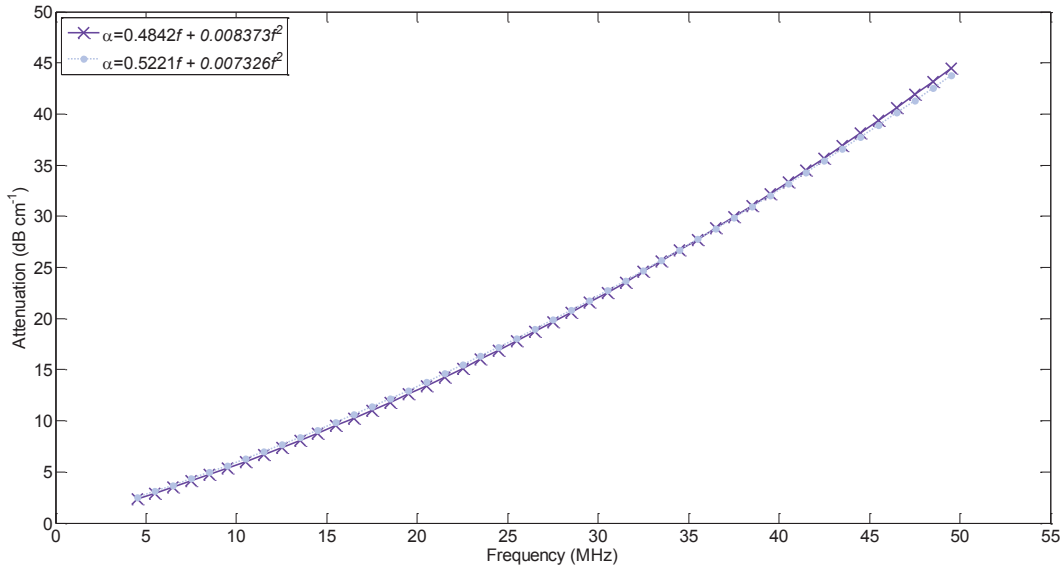

Figure 3-6. *Comparison of the polynomial fit calculated from the mean attenuation data as a function of frequency averaged over all time points from the 6 UTMM2 versus the attenuation from the 11 UTMM samples.*

3.4.3 Acoustics measurements from unpreserved samples and repeatability of the UTMMs

For the unpreserved samples, after 96 hours of exposure to air, the samples were visibly dehydrated (Figure 3-7). The mean thickness of the two samples had decreased by 1.22 mm and the diameter was decreased by 1.5 cm. Moreover, the SoS was shown to increase by 140 ms^{-1} for sample 1 and 180 ms^{-1} for sample 2 over the

total period of time. The attenuation was found to increase by approximately 10 dB cm^{-1} per day (Figure 3-8).

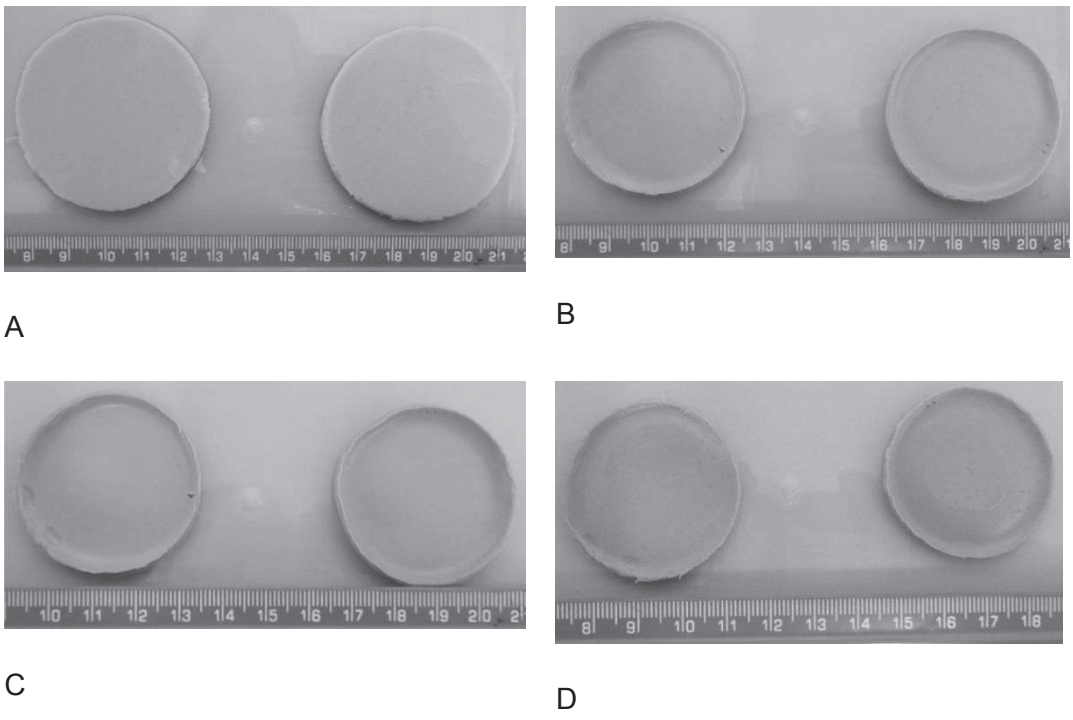

***Figure 3-7**. Show the two unpreserved samples UTMMs at A) first time measurement, B) 24hrs later, C) 72hrs later and D) 96hrs later. The samples were left open to air between measurements.*

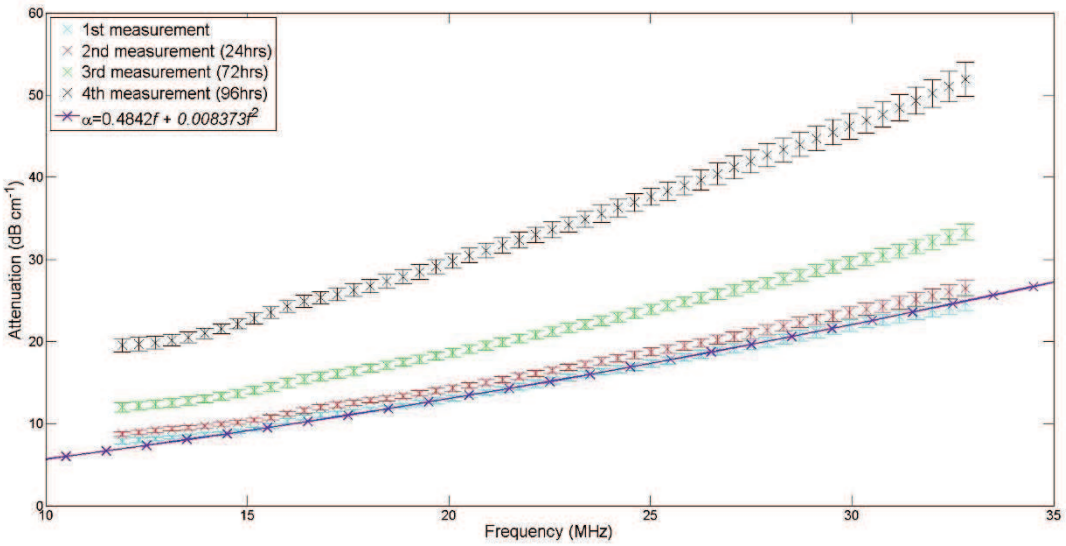

***Figure 3-8.** Attenuation versus frequency of the unpreserved TMM samples using the RMV704 with the Vevo 770®. The polynomial fit calculated from the 11 UTMMs was added for reference purposes.*

In the assessment of repeatability, the mean SoS over the five measurements taken from the 11 UTMMs was calculated to be 1543.0 ms^{-1} with a range in SoS of ± 11.0

ms^{-1}. The mean SoS was found to be smaller by 1 ms^{-1} when compared to the mean SoS calculated using all the transducers at all time points (Table 3-4) of the UTMMs. The variation in attenuation as a function of frequency was ±1 dB cm^{-1} over the frequency range of the Vevo770® RMV710B probe (Figure 3-9).

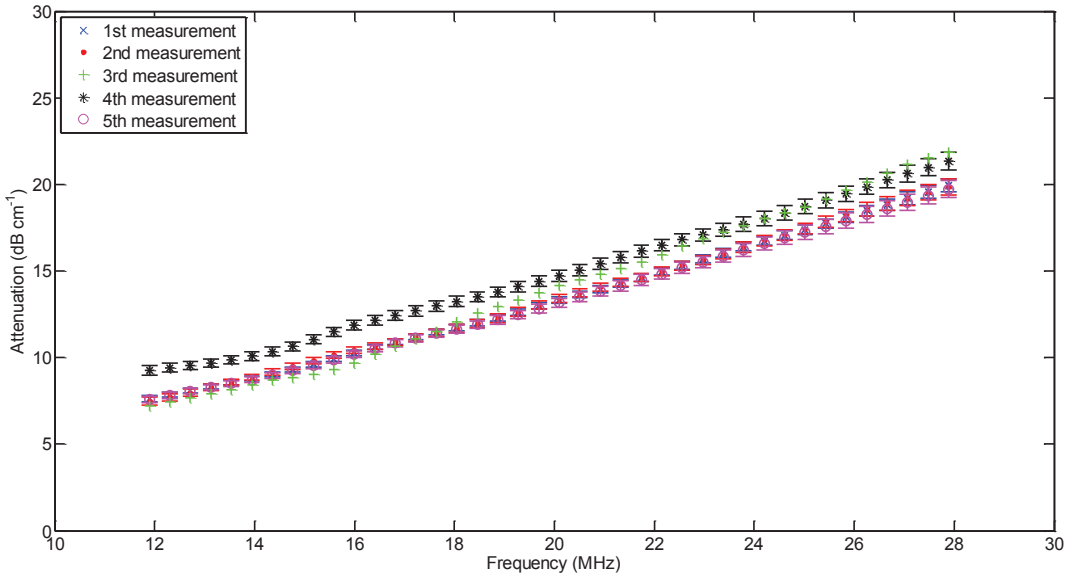

Figure 3-9. *Attenuation versus frequency of the 11 UTMMs measured with the RMV 710B to assess the repeatability of the measurement and the preservation technique.*

3.5 Discussion

This chapter describes the development of a robust and easy-to-use technique for the characterisation and preservation of the IEC agar-TMM. The results obtained were compared with the standard technique over a period of one year. This is the first time TMM samples have been studied using a reference fluid other than degassed deionised water and over a wide range of ultrasound frequencies (4.5 – 50 MHz).

3.5.1 Uncertainties and sources of error

This section discusses the different sources of error that could affect the measurement of the thickness, the SoS, and the attenuation from the FTMM and UTMM samples. The justification for the use of a water test cell for the acoustic characterisation of the FTMMs was explained earlier in Section 2.5.1.2. A variation in the thickness of the

sample would affect both the SoS and the attenuation of the sample (Equation 2-3, Equation 2-4 and Equation 2-5) when using the Vevo 770® ultrasound scanner and the SAM system (Equation 2-13).

3.5.1.1 *Thickness of the FTMM and UTMM samples*

The sample thickness values used in the calculation of SoS with the SAM system were the mean thickness calculated using the Vevo 770® scanner. Thickness values were measured from eight different locations on the UTMMs (10 lines at each point) and averaged. Ultrasound thickness of UTMM samples were also compared to micrometre measurements. Although mean thickness values were used, the SD of the SoS values from the SAM system were smaller than the SoS SD variation calculated using the Vevo 770® (Table 3-4) which would suggest that the use of this mean thickness value in the SAM system measurements did not contribute significantly to the experimental error.

3.5.1.2 *Temperature*

The acoustic properties of the UTMM samples were measured in TMM preserving fluid whose acoustical properties were assessed by the NPL at a temperature of 19.3 ± 0.1°C, whereas the UTMMs in this study were measured at 22.2 ± 0.5°C. The TMM preserving fluid is composed of the same fluids as used in the TMM manufacturing process and Brewin et al (2008) has previously shown a TMM SoS temperature dependence of 2.1 ms^{-1} $°C^{-1}$. Consequently, there is likely to be a variation of 6 ms^{-1} in the SoS of the TMM preserving fluid due to the temperature difference. Such a change would result in a potential error of less than 7ms^{-1} in the measured SoS of the UTMM samples. Nevertheless, the SoS values of the UTMM were found to be in good agreement with Rajagopal et al., (2014); Sun et al., (2012) and Brewin et al., (2008). Furthermore, the SoS of the UTMMs was found to decrease by 4.1 ms^{-1} over a 12 month period compared with FTMMs which showed a decrease in the mean SoS of 22.1ms^{-1} over the same period of time. Additionally, the standard deviation of the mean SoS values for FTMM samples was larger than that for UTMM samples at all time-points. This increased variation in SoS values for the FTMMs in comparison to UTMMs may be attributed to a number of reasons. Firstly, although a visual inspection was performed on each of the FTMMs before each acoustic measurement

and no evidence of leakage was observed, nevertheless, in several of the samples, the epoxy securing the film to the rings showed signs of ageing as the Saran Wrap® film appeared to become less taut over the 1 year period. This could have potentially have allowed glycerol from the TMM to leach into the water medium resulting in a decrease in the measured SoS properties of the FTMM. However, although a decrease in SoS in FTMMs was measured between 0 and 12 months, this did not decrease continuously over the 1-year period which would suggest that the measured variation is not likely to be attributable to glycerol leakage. Secondly, for the FTMMs, the position of the water-film interfaces was selected using Matlab code based on the identification of the position of the maximum rectified RF signal and it was assumed that this signal also marked the TMM interface. Although this is a reasonable assumption, if any of the FTMM samples were subject to shrinkage (by drying out) over the 1-year period, this would represent a potential source of error.

3.5.1.3 *Speed of sound in FTMM and UTMM samples*

The SoS results of both FTMM and UTMM samples in this study were compared with previously published work (Table 3-4). It can be seen that the UTMM mean SoS values are in agreement with those in the literature, whereas the mean SoS of FTMM was found to be 11.3 ms^{-1} less when compared with Rajagopal et al., (2014) and up to 14.5 ms^{-1} less when compared with Sun et al., (2012). In Rajagopal et al., (2014) the manufacture of FTMM was achieved by sandwiching the TMM slice between 2 sheets of Mylar® (~12μm thickness) affixed into Perspex frames, whereas in Sun et al., (2012) the manufacture process of the FTMMs was similar to the method used in this study (referred to as TMM test cells in that study). However, in Rajagopal even though the acoustic measurement was completed relatively quickly (within seconds) the edges of the TMM were not covered, which is likely to have led to some undefined glycerol leakage and potentially affect the measured acoustical properties. Furthermore, in Brewin et al., (2008) the acoustical properties of 2 different batches of TMM were measured over a 3 year period with a thickness range from 3 mm to 12.7 mm. In Brewin, the first batch consisted of TMM samples which were not protected by a film and were measured in double degassed, deionized water. The SoS was found to decrease by 2.1 ms^{-1} $°C^{-1}$ as a result of glycerol leaching from the samples in this batch. The second batch consisted of TMM samples protected by Saran Wrap® and was also

measured in water. Using this method, thinner samples (3mm) displayed the largest SoS variation of 13.4 ms^{-1}. This value is comparable to the SD found in this study for the FTMM samples (Table 3-4) but considerably higher than that measured for the UTMMs.

3.5.1.4 *Attenuation in FTMM and UTMM samples*

Figure 3-1 and Figure 3-2 show the attenuation of FTMM and UTMM samples respectively, at 0, 6 and 12 month time points. It can be observed that there is a much larger variation in the attenuation measurements obtained from the FTMM compared to the UTMM. At both the lower (4.5 – 9MHz) and the higher (40 – 50MHz) frequency ranges, the data displayed is obtained from a single transducer. Nevertheless, the attenuation versus frequency for the FTMM samples would suggest that with increasing frequency there is an increasing difference in measured mean attenuation values between the 6 month data and 0 and 12 month data. The maximum difference, 7 dB cm^{-1}, ocurring over the frequency range from 30 – 42 MHz and a minimum difference at 15 – 19 MHz. For the UTMM samples, a maximum variation of 2 dB cm^{-1} was observed across the time points, at a frequency of 47 MHz and a minimum variation from 37 to 47 MHz.

The difference in mean attenuation values between the UTMM and FTMM samples would suggest that, despite compensation for the effects of the Saran Wrap®, some additional acoustic effects are introduced which are not fully compensated for using the Saran-wrapped reference water test-cell. Furthermore, as discussed in Sun, (2012), the reflection of the Saran Wrap® in the FTMM samples contributes to the uncertainty in the attenuation measurements. Additionally, these effects are unlikely to be due to the difference in non-linear effects between water and TMM preserving fluid as it has previously been shown (Sun, 2012) that even in water, at these output powers, the second harmonic component of the ultrasound beam is at least 30 dB smaller in magnitude than the first harmonic (fundamental). Since non-linear effects are easier to generate in water than in the TMM preserving fluid, it is unlikely that nonlinearities are significantly greater than the experimental errors identified.

Figure 3-3 and Figure 3-4 show the mean attenuation of the 11 FTMMs and the 11 UTMMs across the 7 different transducers and measured 5 times during the time

period of 1 year. The FTMM samples (Figure 3-3) showed larger variability (~15dB cm^{-1}) across samples and transducers. This may be due to inadequate acoustical correction for the interface layers when using the reference water test cell, leading to increased uncertainty in the attenuation measurements in addition to the factors previously described. The UTMM samples (Figure 3-4) showed good consistency and little variability in the attenuation over the frequency range of 4.5 – 50 MHz.

Polynomial fits from FTMM and UTMMs were in good agreement with previous studies in the frequency range of 17 – 23 MHz (Brewin et al., 2008), 10 – 47 MHz (Sun et al., 2012) and 1 – 60 MHz (Rajagopal et al., 2014). The polynomial fits were also in good agreement at lower frequencies 4.5 to 10 MHz as reported by IEC (IEC, 2001) and in other studies (Browne et al., 2003; Inglis et al., 2006) as can be seen in Figure 3-5. The attenuation of the FTMM and UTMM samples does not increase linearly with frequency as shown by the quadratic terms of the polynomial fit. This quadratic term was found to be 0.0073 for FTMM and 0.0083 for UTMM which is in good agreement with 0.0076 reported by Sun et al., (2012) and with 0.0081 reported by Rajagopal et al., (2014).

3.5.1.5 *Unpreserved samples*

Finally, the unpreserved samples displayed significant visual degradation and changes in SoS and attenuation values over the 96 hours (Figure 3-7). These results are consistent with those of Brewin et al., (2008) who also reported shrinking and hardening of TMM samples which were not preserved. Furthermore, the thickness appears to be inversely related to the SoS of the samples (Figure 3-10).

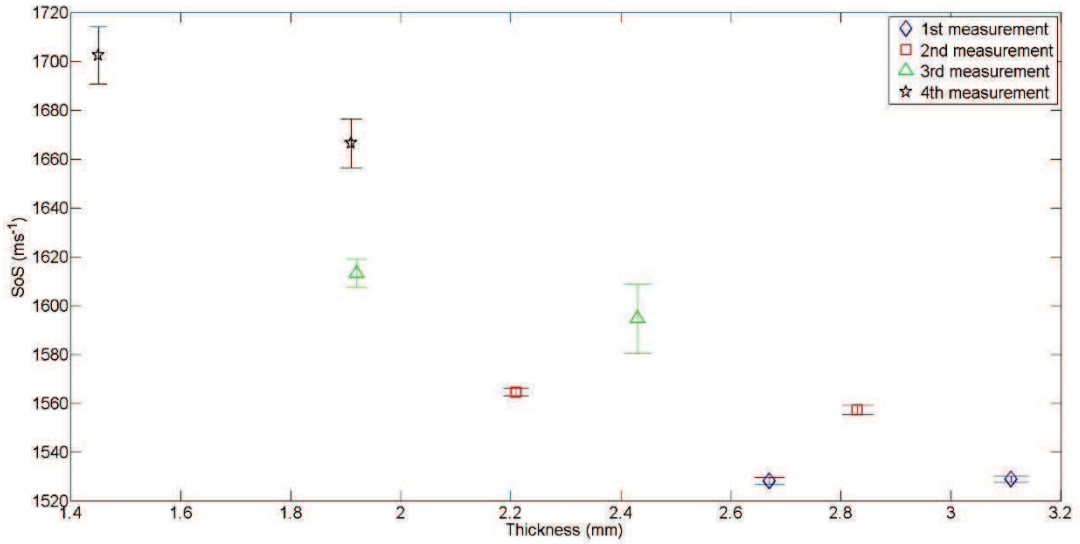

Figure 3-10. *SoS (ms^{-1}) versus thickness (mm) of each un-preserved sample at each measurement point using the RMV704 probe with the Vevo 770®.*

3.5.1.6 *Batch-to-batch variations*

The mean SoS difference between the 11 UTMM and the 6 UTMM2 samples was found to be 0.44% higher for the UTMM2 samples. The difference in the attenuation coefficient between the UTMM and the UTMM2 was found to be ±0.63 dB cm^{-1} (Figure 3-6). This indicated that the acoustical properties of the IEC agar-TMM samples, when manufactured from different batch, did have markedly different SoS or attenuation properties. These results confirmed that the technique developed in this PhD is a robust technique for measurement of the acoustic properties of TMM over periods up to 1 year.

3.5.2 IEC agar-TMM modification towards a new TMM matching the properties of soft tissue

The IEC agar-TMM samples measured in TMM preserving fluid showed good longitudinal stability and characteristics consistent with published studies at low frequency. However, increasing use of high frequency scanners, both clinical and preclinical, means that there is a need for a TMM, for which the acoustic properties are well defined at higher frequencies. Consequently, further research is required into the magnitude of SoS and attenuation values of the individual constituent ingredients

of the IEC agar-TMM. Additionally, there is a requirement for soft tissue acoustic data at high frequencies so that the individual constituent ingredients of the IEC agar-TMM can be adjusted to match these values.

3.6 CONCLUSIONS

In this study, two different measurement techniques were used to evaluate the temporal stability of the acoustic properties of the IEC agar TMM over the frequency range 4.5 – 50 MHz. In the first technique, thin slices were wrapped and stored in Saran Wrap® and assessed in degassed, deionised water. In the second technique, thin slices of TMM were stored and measured in TMM preserving fluid. Measurements were undertaken over a period of 1 year. The measured SoS of an IEC agar-TMM by the Vevo 770® and SAM system was found to be 1538.2 ± 14.5 ms^{-1} for the FTMM samples and 1544.0 ± 3.5 ms^{-1} for the UTMM samples. For FTMM the SoS values were 14.5 ms^{-1} lower when compared with those in the literature. The acoustic properties of UTMMs (SoS and attenuation values) were found to be in good agreement with results in earlier studies by Brewin et al., (2008) over the range of 17 – 23 MHz, Sun et al., (2012) over the range of 10 – 47 MHz and Rajagopal et al., (2014) over the range of 1 – 60 MHz. The results for both FTMM and UTMM samples were consistent at low frequencies (Browne et al., 2003; Inglis et al., 2006) and within the range provided by the IEC (IEC, 2001). The attenuation coefficient was shown to be nonlinear as a function of frequency. The attenuation was found to increase as $0.4649f + 0.007363f^2$ for FTMMs and as $0.4897f + 0.008366f^2$ for UTMM. The quadratic term was also found to be in good agreement with previous studies.

Finally, this study has demonstrated that using un-covered TMM slices (UTMM), results in approximately 4 times smaller SD values for the SoS and up to 5 times smaller variation for the attenuation compared to FTMMs. These UTMMs samples were maintained and measured in TMM preserving fluid. These better acoustic stability values were compared with the common method of film-wrapped TMM samples (FTMM) measured in degassed, deionised water. This suggests that, despite compensation through calculation of the attenuation effects of the Saran Wrap®, additional acoustic effects are introduced which are not fully compensated using the

standard technique of enclosing TMM samples in thin films. Moreover, this study has also brought into question the acoustic stability of encasing gel TMM QA phantoms in a sealed film-dry environment.

CHAPTER 4

ACOUSTIC CONTRIBUTION OF TMM INDIVIDUAL COMPONENTS TO OVERALL ACOUSTIC PROPERTIES OF IEC-AGAR TMM

4.1 AIM OF CHAPTER

To develop a new TMM that closely matches the acoustical properties of soft tissue at higher ultrasound frequencies, it is necessary to study the contribution of the individual components to the overall acoustic properties of the TMM. Following the longitudinal acoustic assessment of IEC agar-TMM using two measurement techniques (Chapter 3) this chapter investigates whether the overall attenuation of IEC agar-TMM is the linear sum of the attenuation of its individual components. This chapter present the measurements of the acoustical properties of individual components of IEC agar-TMM over the frequency range from 12 – 50 MHz. Studying the acoustic properties of the individual components will help to understand how the IEC agar-TMM recipe might be modified in order to match the acoustic properties of soft tissue at high frequencies (Chapter 5).

4.2 INTRODUCTION

As mentioned in Section 1.3.2, the International Electrotechnical Commission (IEC, 2001) define the acoustic parameters for TMMs up to 10 MHz (SoS 1540 ± 15 ms^{-1} and attenuation coefficient 0.5 ± 0.05 dB cm^{-1}). The IEC agar- based TMM has become widely used and has been studied for clinical and preclinical applications up to 60 MHz, as discussed in Chapter 3. In this PhD the IEC agar-TMM has been chosen as the basis for developing a new TMM to match the acoustic properties of soft tissues at high frequencies.

In order to manufacture a TMM that closely matches the acoustic properties of soft tissue at high frequency the acoustic properties of the individual component ingredients of the IEC agar-TMM need to be measured. This will help to determine if

it is possible to modify the existing IEC agar-TMM recipe in order to match attenuation properties of the TMM to those of mouse soft tissue at high ultrasonic frequencies. The main ingredients of IEC agar-TMM are shown in Table 2-3.

The acoustic properties of agar-based materials has previously been studied up to 14 MHz as a function of agar concentrations up to 6.6% in weight (Gettings et al., 1977; Madsen et al., 2005; Manickam et al., 2014a, 2014b; Ross et al., 2006; Zell et al., 2007). As can be seen from Table 2-3 the agar component in the IEC agar-TMM is 3% of the total weight (Teirlinck et al., 1998).

The SoS of the IEC agar-TMM is controlled by adjusting the ratio of water to glycerol (Brewin et al., 2008; Madsen et al., 2005; Moran et al., 2009; Rajagopal et al., 2014). The SoS increases by 4.4 ms^{-1} per 1% by weight of glycerol concentration while also increasing the attenuation coefficient by 0.02 dB cm^{-1} MHz^{-1} of the IEC agar-TMM (Madsen et al., 2005).

The attenuation of IEC agar-TMM has been shown to increase with increasing frequency above 10 MHz (Brewin et al., 2008; Rabell-Montiel et al., 2016, 2017; Rajagopal et al., 2014; Sun et al., 2011, 2012). Furthermore, it is known that the attenuation coefficient and the backscatter of the IEC agar-TMM depend on the percentage concentrations of the aluminium oxide (Al_2O_3) and the silicon carbide (SiC) (Cannon et al., 2011; Inglis et al., 2006).

The acoustic properties of the individual ingredients composition at high frequencies of the IEC agar-TMM have not been studied previously.

4.3 METHODOLOGY

RF data were acquired using each of the 4 transducers of the Vevo 770® scanner (Section 2.2) covering the frequency range 12 to 50 MHz.

4.3.1 Manufacture of samples

The manufacture of agar-based samples has previously being explained in Section 2.4.1.2. All the samples described in this chapter were stored in TMM preserving fluid similar to the UTMM samples as described in Chapter 3.

For convenience Table 2-4, has been reproduced below.

Batch number	Composition ingredients	Agar	SiC	0.3µm Al_2O_3	3µm Al_2O_3
$B_{control}$	Control (IEC agar-TMM)	✓	✓	✓	✓
B_{SiC}	SiC	✓	✓		
B_{VWR}	Agar (VWR International)	✓			
B_{Merck}	Agar (Merck Chemicals)	✓			
$B_{SiC+0.3\ Al2O3}$	SiC + 0.3µm Al_2O_3	✓	✓	✓	
$B_{SiC+3\ Al2O3}$	SiC + 3 µm Al_2O_3	✓	✓		✓
B_{Al2O3}	0.3µm Al_2O_3+ 3µm Al_2O_3	✓		✓	✓
$B_{0.3\ Al2O3}$	0.3µm Al_2O_3	✓		✓	
$B_{3\ Al2O3}$	3µm Al_2O_3	✓			✓

Table 2-4. *The component ingredients included in each of the TMM batches manufactured. SiC = silicon carbide and Al_2O_3 = aluminium oxide.*

4.3.2 Experimental set-up and acquisition of acoustic data

For each combination of ingredients, a batch of ten samples was manufactured giving a total of eighty samples to be assessed. The acoustic properties were measured in a reservoir filled with TMM preserving fluid at room temperature using the same method as for UTMM samples described in Chapter 3. The schematic diagram of the experimental set-up used with the Vevo 770® scanner is shown in Figure 2-8.

4.3.3 Acoustic analysis of the batches

A broadband reflection substitution technique (AIUM, 2014) was employed to calculate the SoS, the thickness and the attenuation coefficient of the different agar-TMM batches, details of the analysis method can be found in Section 2.5.1.1.

4.3.4 Acoustic difference in agar suppliers

During the course of this study, the agar supplier changed from Merck Chemicals (Merck Chemicals Ltd, Nottingham, UK) to VWR (VWR International Ltd, Dublin, Ireland). The acoustic properties of the two agars were measured in order to

determine if they have any acoustic differences. The agar-based material samples were manufactured using the VWR agar, whereas the UTMMs in Chapter 3 were manufactured using Merck agar. If there is any difference in the acoustic properties between agar suppliers these then might be acoustically different between the UTMMs (Chapter 3) and $B_{control}$.

In order to measure the experimental error value in this study an extra batch of ten agar-based samples were manufactured from VWR agar and from a different agar supplier Merck Chemicals (Merck Chemicals Ltd, Nottingham, UK). The acoustic properties from these batches were measured in a similar manner to the other sample batches. The agar batches was named B_{VWR} and B_{VWR2} for VWR agar and B_{Merck} for the Merck agar.

The acoustic properties were measured using 4 transducers with the preclinical ultrasound Vevo 770® scanner. The acoustic analysis was carried out in a similar way to that for the agar-TMM samples.

4.4 RESULTS

4.4.1 Speed of sound of the agar-TMM samples

Table 4-1 shows the mean SoS of all agar-based material batches (Table 2-4). It can be seen that the largest difference in SoS was 13.7 ms^{-1} between B_{SiC} and B_{VWR}. B_{Merck} having the largest SD variation of 12.5 ms^{-1}. The mean SoS value measured from all the samples was 1538.8 ± 5.1 ms^{-1}.

Batch	$B_{control}$	B_{SiC}	B_{VWR}	B_{Merck}	$B_{SiC+0.3\ Al2O3}$
SoS (ms^{-1} ± SD)	1536.6 ± 2.0	1531.6 ± 6.7	1545.3 ± 1.8	1533.3 ± 12.5	1539.2 ± 8.4
Batch	$B_{SiC+3\ Al2O3}$	B_{Al2O3}	$B_{0.3\ Al2O3}$	$B_{3\ Al2O3}$	
SoS (ms^{-1} ± SD)	1542.0 ± 3.8	1536.7 ± 8.7	1537.2 ± 6.0	1546.8 ± 4.5	

Table 4-1. *The mean and the SD of the SoS (ms^{-1}) measured with the Vevo 770® across all the agar-TMM batches.*

4.4.2 Attenuation as a function of frequency for the different batches

Figure 4-1 shows the attenuation measured from each of the different batches with varying constituents over the frequency range of 12 – 50 MHz. The attenuation values for each batch, shown in Figure 4-1, were averaged across 1 MHz intervals based on the frequency bandwidth of the four transducers used. From Table 2-7, the 3 dB bandwidth of the four high frequency probes overlapped over the frequency range from 12 – 28 MHz. From 28 – 40 MHz the attenuation values corresponds to the RMV704, RMV707B, and RMV711 probes. The attenuation shown from 40 – 50 MHz correspond only to the RMV711 transducer. The SD shown in Figure 4-1 was calculated from the attenuation values measured in 1 MHz interval over the frequency range. For clarity of data visualisation, the rest of the figures in this chapter do not include the SD.

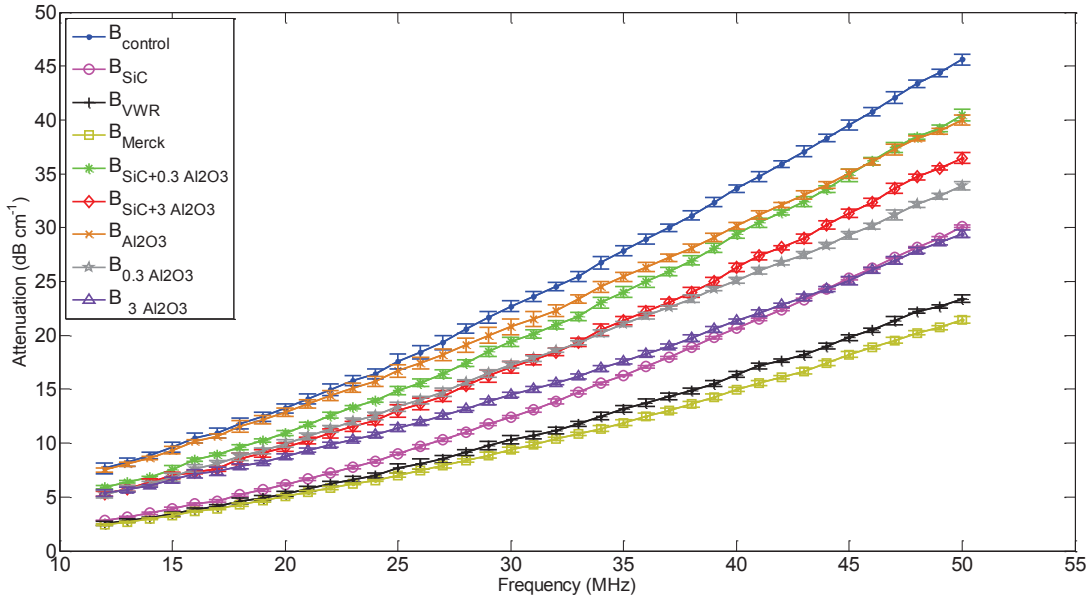

Figure 4-1. *Mean attenuation data as a function of frequency averaged over the three measurements. Each batch description can be found in Table 2-3. The SD shown has been calculated across frequency from the overlap 3 dB bandwidth of the 4 transducers used with the Vevo 770® ultrasound scanner.*

It can be seen that the attenuation increases with increasing frequency for all of the different agar-based material batches (Figure 4-1).The attenuation from the agar-

TMM batches composed of 0.3 μm + 3 μm particles of Al_2O_3 (B_{Al2O3}) overlapped with the IEC agar-TMM attenuation ($B_{control}$) between 12 – 25 MHz. The attenuation of the agar-based material batches comprising SiC + 3μ Al_2O_3, 0.3μ Al_2O_3 and 3μ Al_2O_3 ($B_{SiC+3\ Al2O3}$, $B_{0.3\ Al2O3}$ and $B_{3\ Al2O3}$, respectively) overlapped at low frequencies (12 – 18 MHz). The attenuation of the $B_{SiC+3\ Al2O3}$ and $B_{0.3\ Al2O3}$ showed a similar attenuation coefficient from 12 – 40 MHz, but at 50 MHz the difference had increased by 2.6 dB cm^{-1}. The attenuation from the SiC batch samples, and that from the two agar supplier (B_{SiC}, B_{VWR} and B_{Merck} respectively) overlapped in the frequency range of 12 – 23 MHz. The attenuation from B_{SiC} coincided with the attenuation from $B_{3\ Al2O3}$ at higher frequencies (43 – 50 MHz).

Not surprisingly, the biggest difference in attenuation was 24.1 dB cm^{-1} between the attenuation of $B_{control}$ and the attenuation of B_{Merck} at 50 MHz. Also, at higher frequencies, the attenuation from $B_{SiC+0.3\ Al2O3}$ overlapped with the attenuation of B_{Al2O3}, and B_{SiC} attenuation overlapped with the attenuation of $B_{3\ Al2O3}$.

The attenuation of the agar B_{VWR} samples was subtracted from the attenuation values of B_{SiC}, $B_{0.3\ Al2O3}$ and $B_{3\ Al2O3}$ (Figure 3) to yield the attenuation values of SiC, 0.3μm Al_2O_3 and 3μm Al_2O_3 respectively. These comprise the main ingredients of the IEC agar-TMM. The subtraction of the agar attenuation enabled the calculation of the attenuation value of each of the main IEC agar-TMM constituent components and allows direct comparison of their attenuation over frequency.

In Figure 4-2 the attenuation of $B_{SiC-VWR}$, B_{VWR}, and $B_{3\ Al2O3-VWR}$, overlapped at low frequencies (12 – 16 MHz) whereas the attenuation from $B_{SiC-VWR}$ and $B_{0.3\ Al2O3-VWR}$ overlapped at higher frequencies (44 – 50 MHz).

The attenuation values from each of the individual constituent components of the IEC agar-TMM ($B_{SiC-VWR}$, B_{VWR}, $B_{0.3\ Al2O3-VWR}$ and $B_{3\ Al2O3-VWR}$) were added together. This data is showed in Figure 4-2. The addition of the attenuation from these batches enabled a comparison between the attenuation of IEC agar-TMM ($B_{control}$) and its individual components.

The attenuation calculated from the addition of the individual components ($B_{SiC-VWR}$, B_{VWR}, $B_{0.3\ Al2O3-VWR}$ and $B_{3\ Al2O3-VWR}$) was found to be higher by +1.28 dB cm^{-1}, across the

frequency bandwidth of 12 – 50 MHz when compared with the attenuation of the control samples ($B_{control}$).

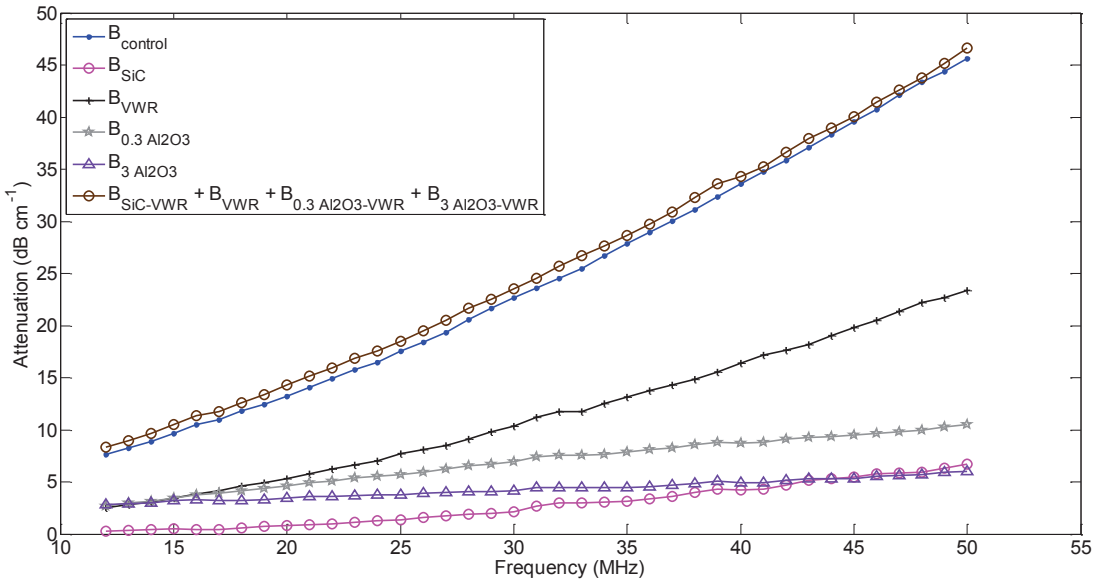

Figure 4-2. *Attenuation data as a function of frequency of the linear sum of the attenuation values from $B_{SiC\text{-}VWR}$, B_{VWR}, $B_{0.3\ Al2O3\text{-}VWR}$ and $B_{3\ Al2O3\text{-}VWR}$ in comparison with the attenuation measured from $B_{control}$.*

4.4.3 Difference in acoustic properties between agar suppliers

As shown in Table 4-1., it can be seen that the SoS varied by 12 ms^{-1} between the B_{VWR} and the B_{Merck}. The SD for B_{Merck} was 10.7 ms^{-1} higher than the SD of B_{VWR}. The SD for B_{Merck} was 10.7 ms^{-1} higher than the SD of B_{VWR}. This difference may indicate that the variation in the acoustic properties between the UTMMs in Chapter 3 are due to the TMM being made with Merck agar.

Figure 4-1 shows the attenuation of B_{VWR} and B_{Merck}. Comparing the attenuation from B_{VWR} and B_{Merck} it can be seen that, at 50 MHz the difference was up to 2.2 dB cm^{-1} whereas at 12 MHz the difference was 0.13 dB cm^{-1}.

The SoS of B_{VWR2} was found to be 1543.9 ± 6.0 ms^{-1}. The SoS difference between the B_{VWR} and B_{VWR2} was 1.4 ms^{-1}.

Figure 4-3 shows the attenuation versus frequency of the B_{VWR}, B_{Merck}, and B_{VWR2}. It can be seen that the attenuation of the B_{VWR2} falls between the attenuation of B_{VWR} and

B_{Merck}. At 50 MHz the attenuation difference of B_{VWR2} was found to be -0.64 dB cm^{-1} when compared with the attenuation of $B_{VWR,}$ was higher by 1.34 dB cm^{-1} compared with the attenuation of B_{Merck}.

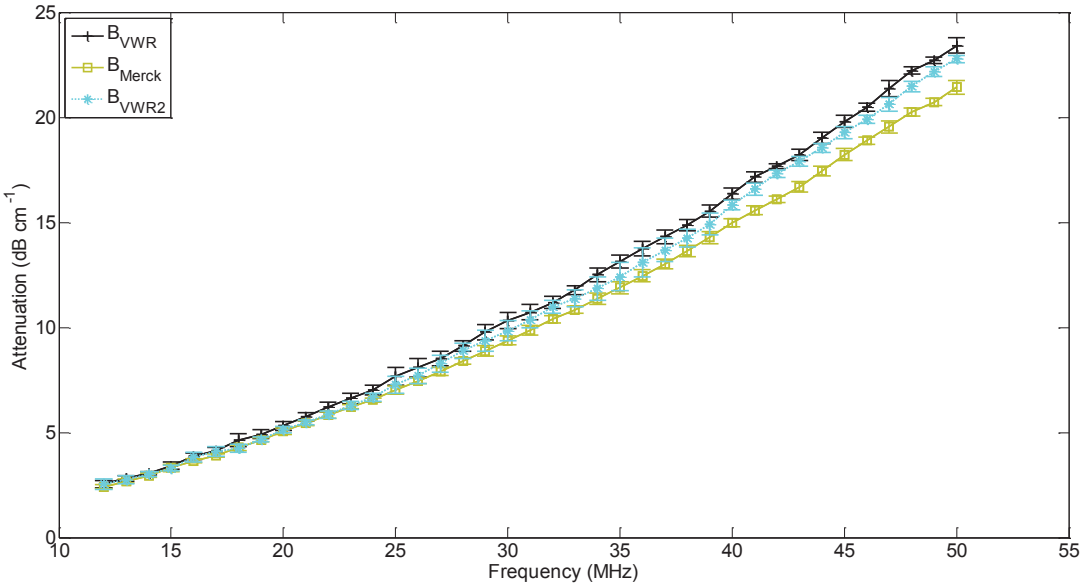

Figure 4-3. *Mean attenuation versus frequency of the different agar suppliers (B_{VWR}, B_{MERCK} and B_{VWR2}).*

4.5 Discussion

This chapter describes the results of acoustic measurements performed on the IEC agar-TMM individual composition ingredients. The aim of this study was to investigate the acoustic properties of 8 different agar-based materials (Table 2-4). The acoustic properties of two different agar suppliers (Merk agar and VWR Chemicals agar) were also measured.

4.5.1 Speed of sound in agar-TMM sample batches

The mean SoS of all the agar-based material samples was found to be 5.2 ms^{-1} less than the reported SoS for UTMMs (Rabell Montiel et al., 2017), where a similar technique to measure the acoustical properties using TMM preservation fluid was employed. The difference in the SoS values between the ingredient combination agar-TMM component samples and the UTMMs (IEC agar-TMM) indicates the SoS

dependence on the composition ingredients of the IEC agar-TMM. The SoS measured from $B_{control}$ was found to be 7.5 ms^{-1} smaller than that for the UTMM samples measured in Chapter 3 (Table 4-1.1 and Table 3-4, respectively). Both samples of Batch 1 and the UTMMs (Chapter 3) were manufactured using the IEC agar-TMM recipe. Nevertheless, the difference in SoS of 7.5 ms^{-1} was within the expected SoS range due to batch-to-batch variation, as discussed in Section 3.4.2.1. The SD value from $B_{control}$ is smaller than the SD value measured from the UTMM samples in Table 3-2 found using the Vevo 770®.

Also when comparing the SoS from B_{Merck} and the UTMM samples from Chapter 3, both manufactured with Merck agar, it can be seen that the SoS in B_{Merck} decreased by 10.8 ms^{-1}. The SD in B_{Merck} was twice as big as the SD reported for the UTMM samples. This could be due to aging of the Merck agar as there was a difference in age of 1.5 between the two batches of chemicals.

It is known that the SoS in the IEC agar-TMM is largely controlled by the portion of glycerol content (Table 2-3) (Brewin et al., 2008; Madsen et al., 2005; Moran et al., 2009; Rajagopal et al., 2014). Moreover, it is interesting to note that all the SoS values from each of the agar-TMM samples fall within the IEC recommended range for the SoS values. This was expected as the glycerol concentration was not modified in the manufacturing process of any of the agar-based material batches.

4.5.2 Attenuation of agar-TMM sample batches

4.5.2.1 *Subtraction of the agar attenuation*

Comparing Figure 4-1 and Figure 4-2 it can be seen that the attenuation from B_{SiC}, $B_{0.3\ Al2O3}$ and $B_{3\ Al2O3}$ decreased after the subtraction of the attenuation values measured from B_{VWR}. The attenuation shown for $B_{SiC\text{-}VWR}$, $B_{0.3\ Al2O3\text{-}VWR}$ and $B_{3\ Al2O3\text{-}VWR}$ do not increase with increasing frequency as fast as shown in Figure 4-1. The difference in the attenuation after the subtraction of the agar attenuation suggests that the agar does contribute to the attenuation, affecting the absorption in the overall attenuation of the IEC agar-TMM.

4.5.2.2 *Building up the IEC-agar TMM attenuation*

The summation of the attenuation of the individual IEC-agar TMM component ingredients ($B_{SiC\text{-}VWR}$, B_{VWR}, $B_{0.3\ Al2O3\text{-}VWR}$ and $B_{3\ Al2O3\text{-}VWR}$) was compared with the attenuation measured of $B_{control}$. Both attenuation curves were in good agreement across the full experimental spectral range as shown in (Figure 4-2).

Figure 4-4 show the attenuation of $B_{control}$, the summation of the attenuation ($B_{SiC\text{-}VWR}$, B_{VWR}, $B_{0.3\ Al2O3\text{-}VWR}$ and $B_{3\ Al2O3\text{-}VWR}$) and the attenuation calculated of the IEC agar-TMM (UTMM) in Chapter 3. The attenuation of $B_{control}$ was shown to be in good agreement with the IEC agar-TMM attenuation (Rabell Montiel et al., 2017) as expected. The summation of the attenuation values of $B_{SiC\text{-}VWR}$, B_{VWR}, $B_{0.3\ Al2O3\text{-}VWR}$ and $B_{3\ Al2O3\text{-}VWR}$ showed a 1.8 dB cm^{-1} higher value when compared with the attenuation of the IEC agar-TMM over the frequency range of 12 – 50 MHz. This difference falls within 1 SD reported of 2 dB cm^{-1} for the IEC agar-TMM (Rabell-Montiel et al., 2017). Moreover, the difference in these two attenuation values could also be an indication of the error in the acoustic measurement of the agar (B_{VWR}). Since the agar is the base ingredient in all the agar-TMM batches, the measurement of the attenuation of B_{VWR} would have increased the influence on the summation of the attenuation ($B_{SiC\text{-}VWR}$, B_{VWR}, $B_{0.3\ Al2O3\text{-}VWR}$ and $B_{3\ Al2O3\text{-}VWR}$) procedure.

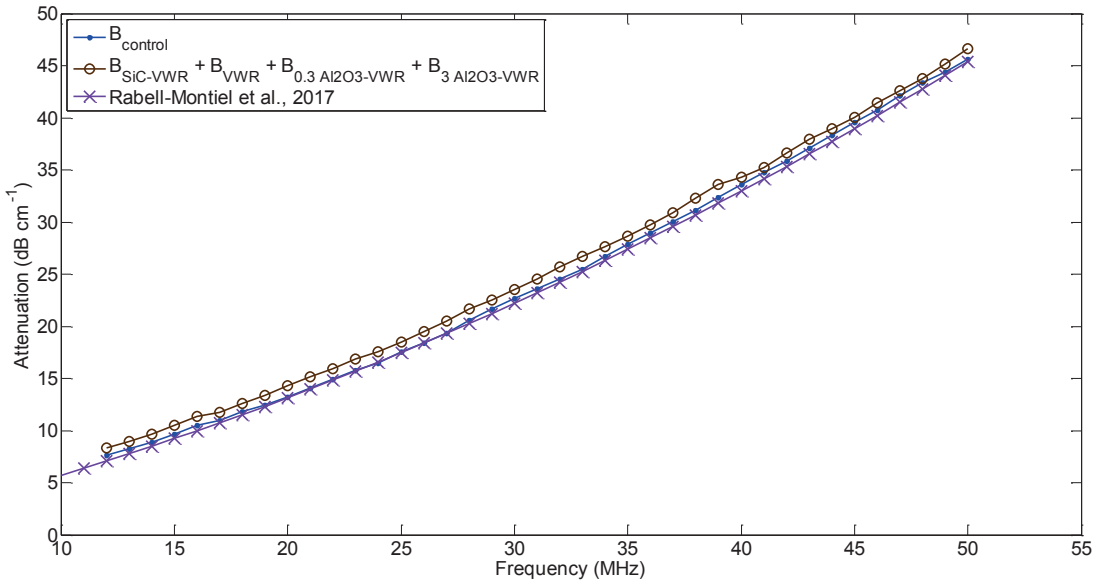

Figure 4-4. *Attenuation versus frequency of $B_{control}$, build-up attenuation from the IEC-agar TMM component ingredients ($B_{SiC\text{-}VWR}$, B_{VWR}, $B_{0.3\ Al2O3\text{-}VWR}$ and $B_{3\ Al2O3\text{-}VWR}$) in comparison with the IEC agar-TMM attenuation (Rabell Montiel et al., 2017).*

4.5.2.3 *Acoustical properties between two agar suppliers*

The acoustic properties between B_{VWR}, B_{VWR2} and B_{Merck} were found to fall within the 1 SD attenuation expected for the overall IEC agar-TMM (Rabell-Montiel et al., 2016, 2017).

The attenuation difference between the summation attenuation of $B_{SiC\text{-}VWR}$, B_{VWR}, $B_{0.3\ Al2O3\text{-}VWR}$ and $B_{3\ Al2O3\text{-}VWR}$ and the IEC agar-TMM (1.84 dB cm^{-1}, Figure 4-2) can be accounted for by the variability in the agar attenuation (B_{VWR}, B_{VWR2} and B_{Merck}).

4.6 CONCLUSIONS

In this study, the acoustic properties of IEC agar-TMM ingredient components were evaluated over the frequency range 12 – 50 MHz. The percentages of water, glycerol and benzalkonium chloride as specified in the original recipe were not modified.

The mean SoS across all the different agar-TMM batches was found to be 1538.8 ± 5.1 ms^{-1}. The SoS was found to be in good agreement with those studies published of IEC agar-TMM acoustics (Brewin et al., 2008; Browne et al., 2003; Rabell Montiel et al., 2017b; Rajagopal et al., 2014; C. Sun et al., 2012) and falls within the IEC recommended guideline (IEC, 2001).

The attenuation value of the agar was subtracted from each of the agar-based material batches enabling the calculation of the attenuation value for each of the IEC agar-TMM constituent components. By adding together the attenuation values from each of the individual constituent ingredients, the attenuation of the IEC-agar TMM was reproduced. The SD between the summation of the attenuation values and the IEC agar-TMM (UTMM) was within the expected SD value when using the same measurement technique as described for previous measurements (Chapter 3).

The difference in the acoustic properties of agar obtained from two different manufacturers was found to fall within the expected 1 SD value calculated from the measurements performed in Chapter 3.

Finally, this information forms a valuable source for the future development of TMMs with acoustic properties similar to that of soft tissue at high frequencies.

CHAPTER 5

THE ACOUSTIC PROPERTIES OF SMALL ANIMAL SOFT TISSUE OVER THE FREQUENCY RANGE 12 – 32 MHZ

5.1 AIM OF CHAPTER

The acoustic properties of tissue mimicking materials aim to mimic those of soft tissue. This chapter examines the acoustical properties of small animal soft tissue over the frequency range 12 – 32 MHz using the Vevo 770® scanner. The organs of interest were mouse brain, liver, and kidney. The mean values of the measured SoS and attenuation were compared with studies published previously up to 9 MHz (Section 1.4.2 and Table 1-4) and with SoS and attenuation of IEC-agar TMM described in Chapter 3. The intention is to use the acoustic properties of small animal soft tissue as a basis for development of a new TMM. This new TMM would be incorporated into test phantoms suited to measuring the performance of preclinical ultrasound scanners and high frequency clinical scanners. The results from this chapter have been published as Rabell-Montiel et al., (2018) (Appendix 1), and the acoustic properties of brain, liver, and kidney at the baseline were published as Rabell-Montiel et al., (2017 b).

5.2 INTRODUCTION

The purpose of ultrasonic tissue mimicking materials is to closely mimic the acoustic properties of tissue. Currently, the IEC (2001) guideline recommends standard acoustic values for soft tissue mimicking material up to 10 MHz. However, with the increasing use of high frequency ultrasound imaging applications above 15 MHz there is a need to extend the range of the IEC (2001) standard values to include those for higher frequencies. Such an extension will ensure that performance test and training phantoms can be developed that are relevant to higher frequency applications. Furthermore, the development of TMM phantoms, that realistically

mimic the properties of small animal soft tissue, will enable a reduction in the use of small animals to optimise ultrasound imaging techniques. Also, a realistic assessment of the performance of ultrasound scanners will enable future animal studies to be powered more accurately. The reduction in the use of small animals is in line with the principles embodied within the UK 2012 amendment of the Animal (Scientific Procedures) Act 1986.

The acoustic properties of human and animal soft tissue have previously been assessed using different methods and samples, including *in vivo* and *ex vivo* tissue. Soft tissue acoustic data has been reported from mammals including humans, up to 9 MHz and small animals up to 15 – 35 MHz, and chickens up to 100 MHz (Table 1-4). These measurements were performed either at 22°C and at 37°C using either degassed deionised water, saline and Krebs solution, or by embedding a soft tissue sample in TMM (Fraser et al., 2006)(see Section 1.4.2).

This study aims to measure the acoustic properties from *ex vivo* brain, liver, and kidney samples extracted from surplus male mice, measurements are obtained with the tissue samples immersed in phosphate-buffer saline (PBS) at 37°C, over the frequency range 12 – 32 MHz. These results have potential to be used to inform the development of new TMMs suitable for high frequency imaging.

5.3 MATERIALS AND METHODS

5.3.1 Soft tissue samples preparation

Twenty *ex vivo* non-perfused brains, livers and kidneys (ten left and ten right) from fifty mice were analysed for their acoustic properties. Mice were surplus healthy male C57BL/6. Details on extraction and preparation of the sample have been described in Section 2.4.2.

The mean age and SD for the animals was 8.5 months (range: 5.4 – 11.6 months) for the brains, 6.8 months (range: 2 – 11.7 months) for the livers and 5.2 months (range: 2 – 8.8 months) for the kidneys. The mean body weight of the mice was 34.4 ± 6 g (minimum 22.6 g, maximum 45 g).

5.3.2 Experimental set-up using the Vevo 770® ultrasound scanner

The experimental set-up used to acquire acoustic data from small animal soft tissue samples was similar to that described in Section 2.5, with the addition of a spacer (washer) placed between the TPX reflector and the tissue sample. The washer was made of acoustic absorbing material (Aptflex F28, Precision Acoustics, Dorset, UK) which was 1 mm thick, 2.5 mm inner diameter and 2.5 cm outer diameter. This was attached to the top of the TPX reflector as shown in Figure 5-1. The circular washer acted as a tissue holder and ensured there was a space between the soft tissue sample and the TPX reflector. The aim of this separation was to allow the echoes from the tissue and from the TPX reflector to be individually identified during later analysis. To ensure the PBS reached the desired temperature of 37°C, the PBS warmed for an hour until it reached thermal equilibrium. The animals were then euthanized and organs excised for measurement of the acoustic properties of each sample.

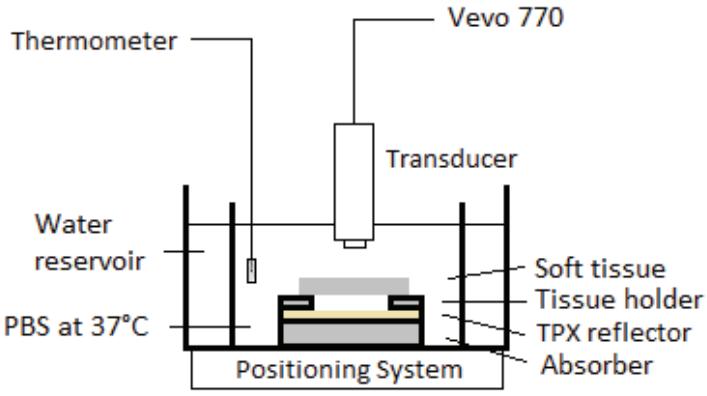

Figure 5-1. *Lateral view of the experimental set-up using the RMV707B probe from the preclinical ultrasound scanner Vevo 770® (Visualsonics, Inc., Canada). The tissue holder (spacer) was made from an acoustic absorbing material.*

5.3.3 Acquisition and analysis of the acoustic data

RF data from sixty soft tissue samples were acquired using the Vevo 770® scanner equipped with a single-element high frequency probe RMV707B (Section 2.2). The RMV707B probe has a centre frequency of 30 MHz, a focal depth of 12.7 mm, a

negative peak pressure of 1.05 MPa at 10% output power, and a 3 dB bandwidth from 12 – 32 MHz (Table 2-1 and Table 2-7).

The acoustic properties of the soft tissue were measured while immersed in PBS at 37.2 ± 0.2°C. The TPX reflector was located at 12.7 mm from the probe (focal point) (Figure 5-1). Data were analysed as explained in Section 2.5.1.1. After each set of measurements, the tissues were disposed of.

After slicing, the sample was immediately immersed and placed on the tissue holder in the PBS tank, ready for acoustic measurements to be performed. As far as possible, acoustic measurements were undertaken with each sample in the same orientation. Precise thickness measurements were obtained at each measurement site using the pulse-echo technique. Three acoustic measurements were acquired for each sample: immediately after immersion in PBS (t=0), after 5 minutes (t=5) and after 10 minutes (t=10). The PBS reference fluid was changed daily. Up to 3 organ samples were assessed on any given day.

5.3.3.1 *Development of the tissue holder*

Different methods to achieve robust acoustic measurements of soft tissue were tested. These methods included: the design of a tissue holder (spacer), the effect of film wrapping the tissue samples, the possibility of gluing the tissue sample to a tissue holder for acoustic data collection, and embedding of the tissue sample within a TMM. However, these preparation methods proved to be overly time-consuming given that our project goal was to assess the acoustic properties of small animal soft tissue within minutes of euthanasia, so that the tissue was as fresh as possible.

In developing a tissue holder, on first approach was to place the recently excised sample between two washers made of the acoustic absorbing material. However, the upper washer was found to float resulting in misalignment of the samples within the inner circles of the two spacers. Later, the washers were pinned in place using of two needles (Figure 5-2 A), however, forcing the pins through the washer-sample-washer was found to deform the tissue sample (Figure 5-2 B). Consequently, to reduce the force required to insert the pins through the washer-sample-washer combination, four holes of the same diameter as the needle were drilled around the inner circle of

the washer. This helped reduced the force required to pin the sample between the washers. However, several issues were found using this method. First, the upper washer tended to float through the pins. Secondly, the sample placed between the two washers was misaligned when the upper washer floated away. Thirdly, the whole washer-sample-washer method was difficult to locate in the acoustical path due to space limitations within the experimental set-up (Figure 5-3). Fourthly, the washer-sample-washer method increased the total thickness of the sample beyond the focal depth of the transducer. Thus, this technique of placing the sample in between two washers was abandoned.

Finally, the experimental set-up described earlier (Section 5.3.2) was found to provide the optimal method of measuring the acoustic properties of soft tissue within minutes of euthanasia. The soft tissues did not require extra weight to be provided by the washer-sample-washer method as the samples did not float in the reference medium.

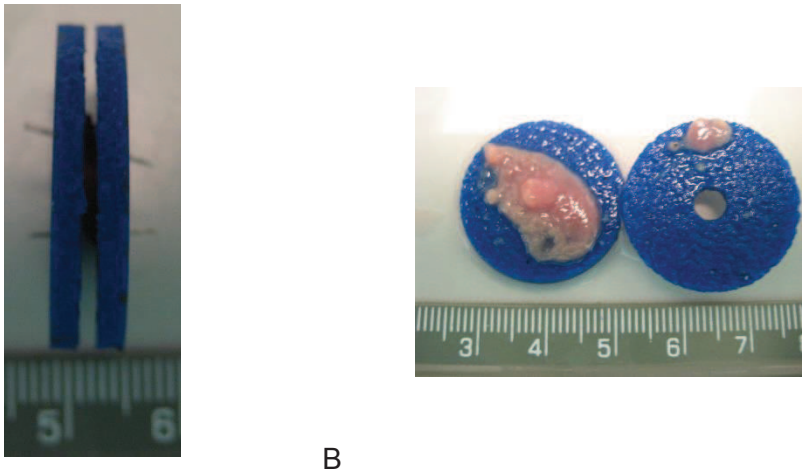

Figure 5-2. *Shows the sample placed in between 2 washers made of the acoustic absorber material. A) Lateral view of the tissue placed between 2 washers. B) Shows an example of liver tissue being deformed by pressure exerted during the insertion of the pin for the washer-sample-washer set-up.*

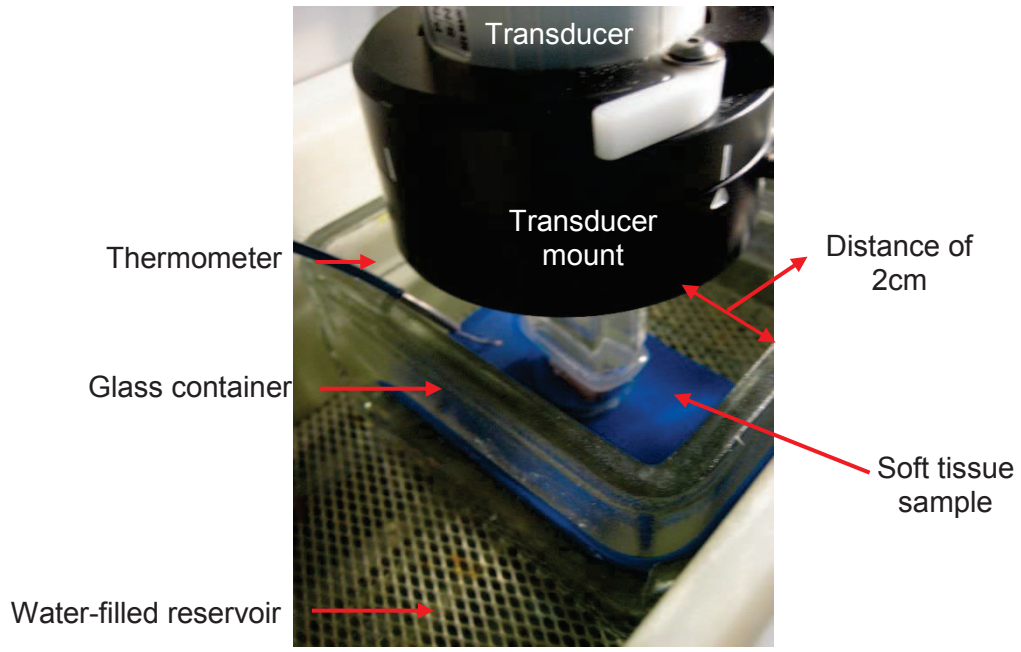

Figure 5-3. *Close-up view of the experimental set-up of the transducer and the glass box inside the water-filled tank.*

5.3.3.2 *Acoustic properties of the heart*

The heart was originally another organ of interest in addition to the brain, liver, and kidney. Few studies have measured the acoustic properties of the heart from mammals at 37°C (Bronez et al., 1985; Law et al., 1985). The SoS within the heart measured in those limited studies was found to lie between 1566 – 1570 ms^{-1} and up to 1620.2 ± 8.2 ms^{-1} in normal myocardium (Saijo et al., 1997). Nevertheless, to my knowledge, there have been no other studies published measuring the acoustic properties of either animal or human heart tissue.

The mammalian heart consists principally of 4 chambers (2 atriums and 2 ventricles, left and right). Given that, if the heart is sliced in the coronal plane, the result would be a sample with two cavities, if sliced in the transversal plane, the result would be a concave sample or a sample with a cavity in the middle. I found that slicing the heart in either the coronal or transverse plane resulted in a tissue sample with insufficient tissue for characterisation as used with the other organs. Due to the natural curvature of the cardiac tissue a method was required in order to be able to collect the acoustic data from as much tissue as possible. Initial attempts include opening the heart from the *cava vein* through the *apex*, exposing the *tricuspid valve*, the *left ventricle* and the *left*

atrium of the heart. The inner wall of the heart was found to be curved due to the muscular tissue (endocardium/myocardium). No distinction between the different layers of tissue (from pericardium to myocardium) within the heart could be made either visually or acoustically when imaged ultrasonically.

Once open, the heart tissue was held flat (Figure 5-4 A) while preparing the tissue sample. However, the heart tissue sample was found to coil back when immersed in PBS at 37°C (Figure 5-4 B). It is believed that because the PBS is a physiological fluid, it reactivated the cells of the heart, inducing the tissue to curl back to its natural form. To prevent this, the heart tissue sample was pinned to a washer made out of an acoustic absorber material using needles (Figure 5-4 C). This method of pinning the heart is similar to the method used for the samples in Section 5.3.3.1, but had to be discarded due to curling and/or shredding of tissue by the pins. Moreover, when recovering the heart tissue from the warmed PBS fluid, it was found that the sample had increased in stiffness compared to the fresh sample (Figure 5-4 D). The design of a special tissue holder for the heart was difficult due to the limited space between the glass box and the transducer holder (Figure 5-3).

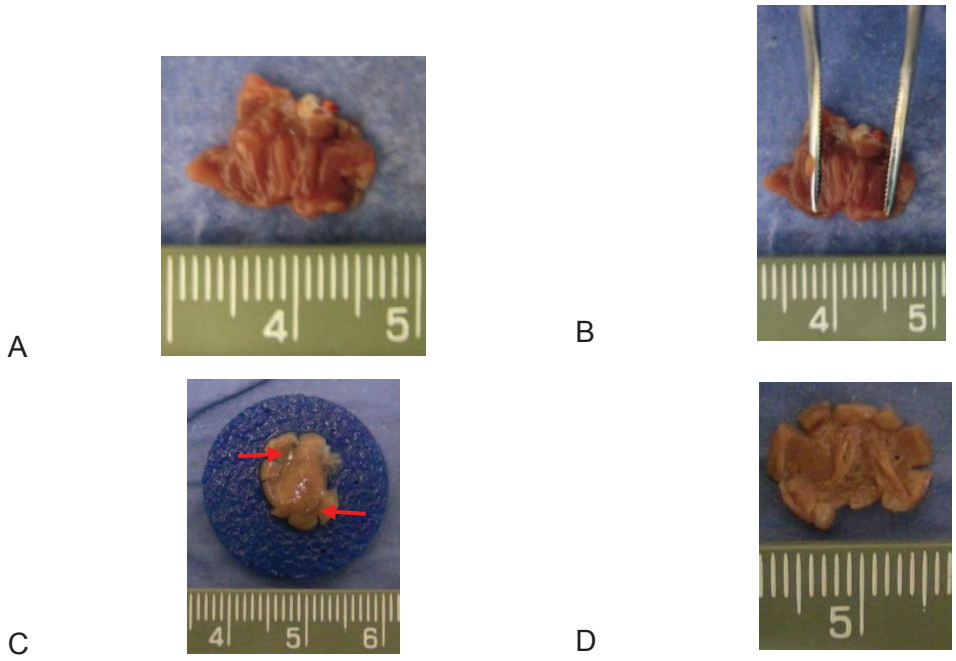

Figure 5-4. *A) Shows the heart tissue sample before being immersed and B) after immersion in PBS at 37°C. C) Shows the heart tissue attached to the circular washer tissue holder and pinned using needles (marked with red arrows). D) Shows the heart tissue after recovering the sample from the warmed PBS fluid. The sample increased in stiffness and curled after immersion in PBS at 37°C.*

5.3.4 Measurement of the acoustic properties of the PBS

The acoustic properties of the PBS at 37°C were measured and described in Section 2.6.2. The SoS of the PBS at 37°C used in this study was calculated as 1527.86 ms^{-1} using Equation 2-8. The PBS attenuation used in this study was fitted to a second degree polynomial as $\alpha(\mathrm{dBcm}^{-1}) = 0.02076f + 0.002127f^2$.

5.3.5 Acoustic measurement of *in vivo* soft tissue to investigate the impact of perfusion on acoustic properties

To assess whether blood affected the acoustic properties of *ex vivo* soft tissue in this study, the acoustic properties of one perfused brain and two perfused livers from three mice were acoustically characterised. These three mice were healthy C57BL/6 male mice. The perfusion technique involved the introduction of a fluid through the left ventricle of the heart while it was still pumping. Perfusion was performed by Julie McNairn PhD using PBS at room temperature. The acoustic measurement and analysis from perfused samples were carried out in a similar manner to the soft tissue samples mentioned in Section 5.3.2. Measurements were performed at t=0 and t=5 minutes. The first measurement was performed after perfusion which took approximately 1.3 minutes, plus another 6 minutes to extract, slice and scan the perfused sample. After perfusion the tissue samples were visibly pale and had a lack of colour when compared with non-perfused samples, as expected.

5.4 RESULTS

5.4.1 Speed of sound measurements

Table 5-1 shows the mean SoS of all samples at t=0 and then at t=5 and t=10 minute intervals for brain, liver and kidney tissue. The SD shown is the value calculated across all the 20 samples from the same organ. It can be seen that the variation in the mean SoS as a function of time were less than 1.5 ms^{-1} across the soft tissue samples. Although the SD of the mean SoS values increased for the brain and the liver samples, for the final measurement (approximately 16 minutes after euthanasia), a Student's t-

test (paired) suggest any statistically significant difference ($p > 0.5$) t=0, t=5 or t=10 between the baseline and subsequent time points.

Organs	Mean SoS ± SD (ms^{-1})		
	t=0 (6 minutes post euthanasia)	t=5	t=10
Brain	1565.9 ± 9.6	1566.1 ± 9.5	1566.9 ± 11.2
Liver	1604.4 ± 16.5	1603.8 ± 15.9	1604.7 ± 18.2
Kidney	1575.3 ± 10.8	1574.8 ± 11.9	1574.1 ± 9.5

Table 5-1. *The SoS and SD (ms^{-1}) measured immediately after excision and mounting (6 minutes) then at +5 and +10 minutes. Measurements were made using a Vevo 770® preclinical ultrasound scanner over the frequency range 12 – 32 MHz.*

The mean SoS across all time points from the twenty soft tissue samples of brain, liver, and kidney are shown in Table 5-2. The SD is based on the measurements from samples for each organ tissue. Table 1-4 shows the SoS of published studies of the acoustic properties of brain, liver, and kidney measured at room and body temperature.

Organs	Brain	Liver	Kidney
SoS ± SD (ms^{-1})	1566.3 ± 9.9	1604.7 ± 16.8	1574.9 ± 10.8

Table 5-2. *Mean SoS and SD (ms^{-1}) of small animal soft tissue samples, brain, kidney and liver measured using the Vevo 770® preclinical ultrasound scanner over the frequency range of 12 – 32MHz.*

The difference in SoS between the left and right kidney (different dissection planes, Figure 2-7 C and Figure 2-7 D) was 0.97 ± 0.69 ms^{-1}.

5.4.2 Attenuation measurements

Figure 5-5, Figure 5-6 and Figure 5-7 show the mean attenuation versus frequency at each time point for brain, liver, and kidney respectively. The SD shown was calculated from the mean attenuation data at all time points. A second degree polynomial curve was estimated to provide the best fit for mean attenuation versus

frequency data and over all time points. The goodness of fit (R^2) varied between 0.70 – 0.85 for small animal soft tissue. The best fit was found to correspond to attenuation versus frequency data of brain tissue (R^2=0.85) and kidney tissue (R^2=0.83). Figure 5-5, Figure 5-6 and Figure 5-7 also show the polynomial fit calculated from the data of twenty brains, twenty livers, and twenty kidneys, respectively averaged over all time points. The polynomial fit was found to be $0.7533f + 0.006477f^2$ (R^2=0.85) for brain tissue, $0.7252f + 0.01414f^2$ (R^2=0.70) for liver tissue and $0.5771f + 0.006322f^2$ (R^2=0.83) for kidney tissue over a frequency range of 12 – 32 MHz.

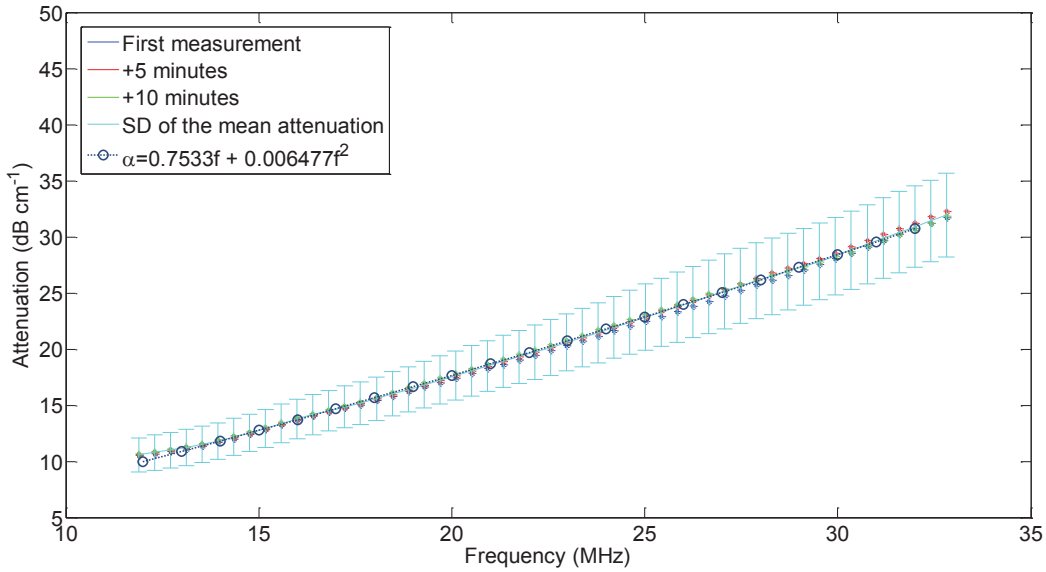

***Figure 5-5**. Attenuation as a function of frequency for brain (20 samples) measured immediately after excision and then at t=5 and t=10 minutes. The SD was estimated based on the SD of the mean attenuation across all time points. The second degree polynomial-fit calculated in this study is also shown*

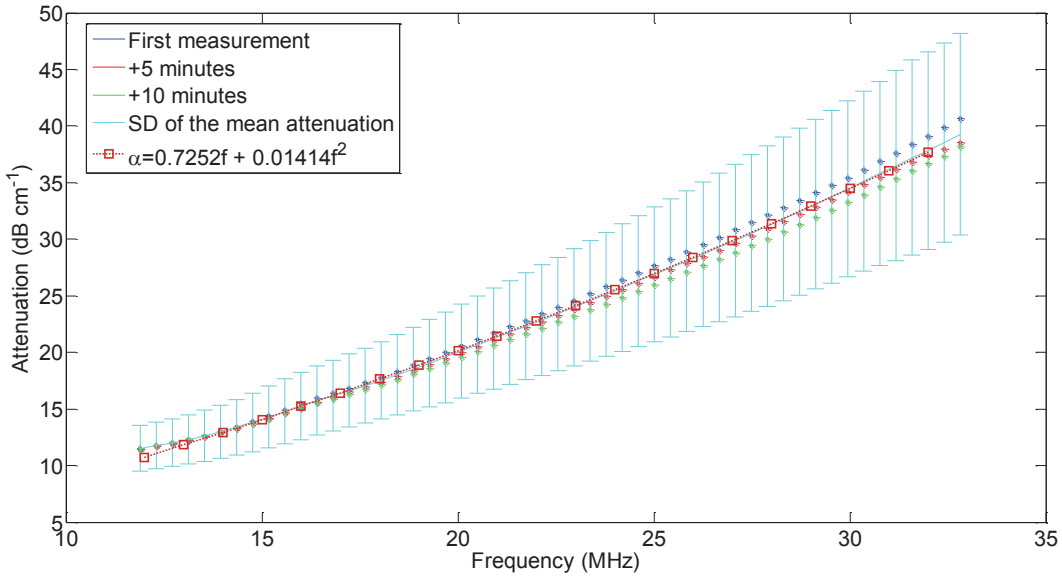

Figure 5-6. *Attenuation as a function of frequency for liver (20 samples) measured immediately after excision and then at t=5 and t=10 minutes. The SD was estimated based on the SD of the mean attenuation across all time points. The second degree polynomial-fit calculated in this study is also shown.*

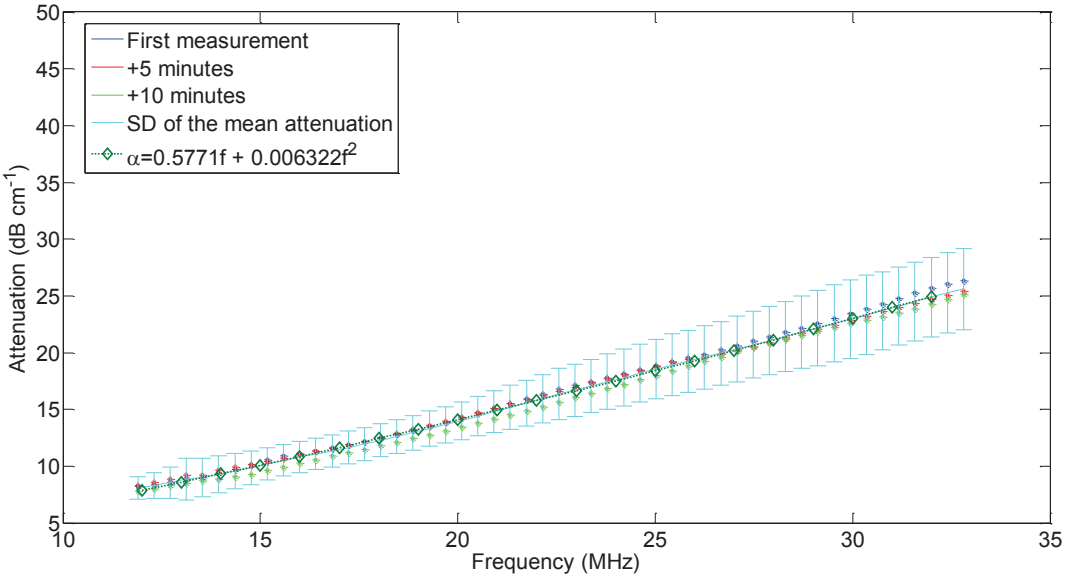

Figure 5-7. *Attenuation as a function of frequency measured for kidney (20 samples, 10 left and 10 right) immediately after excision and then at t=5 and t=10 minutes. The SD was estimated based on the SD of the mean attenuation across all time points. The second degree polynomial-fit calculated in this study is also shown.*

Figure 5-8, Figure 5-9 and Figure 5-10 show the polynomial fit calculated, with other published studies for each organ shown in Section 1.4.2. The polynomial fits were extended to lower frequencies to allow comparison with data from previous published research.

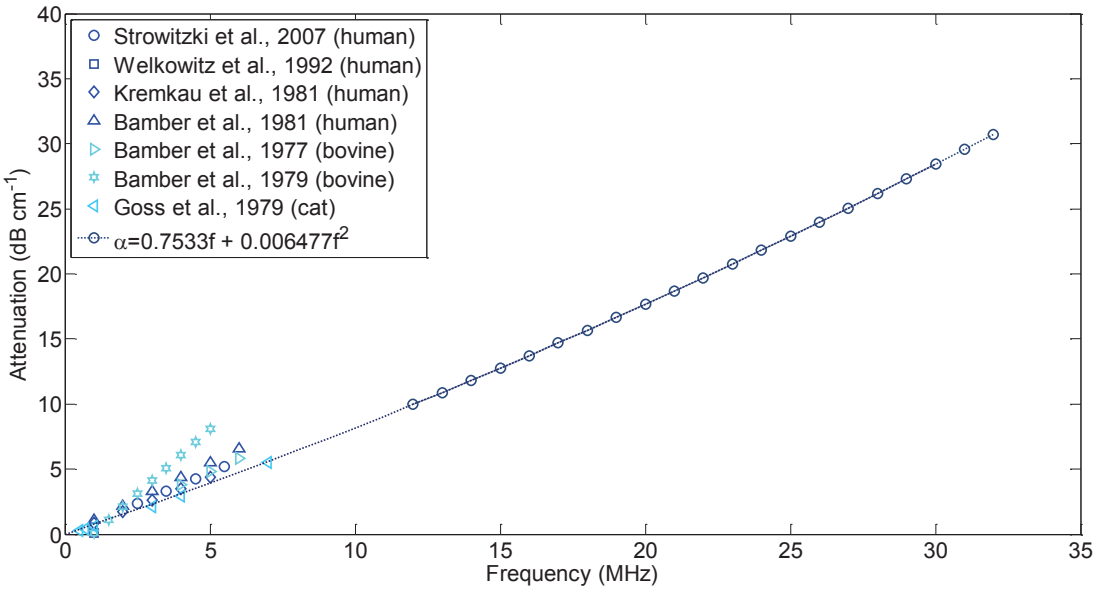

***Figure 5-8**.Attenuation versus frequency of brain tissue data as published in the literature with extrapolation of the second degree polynomial fit calculated in this study to zero.*

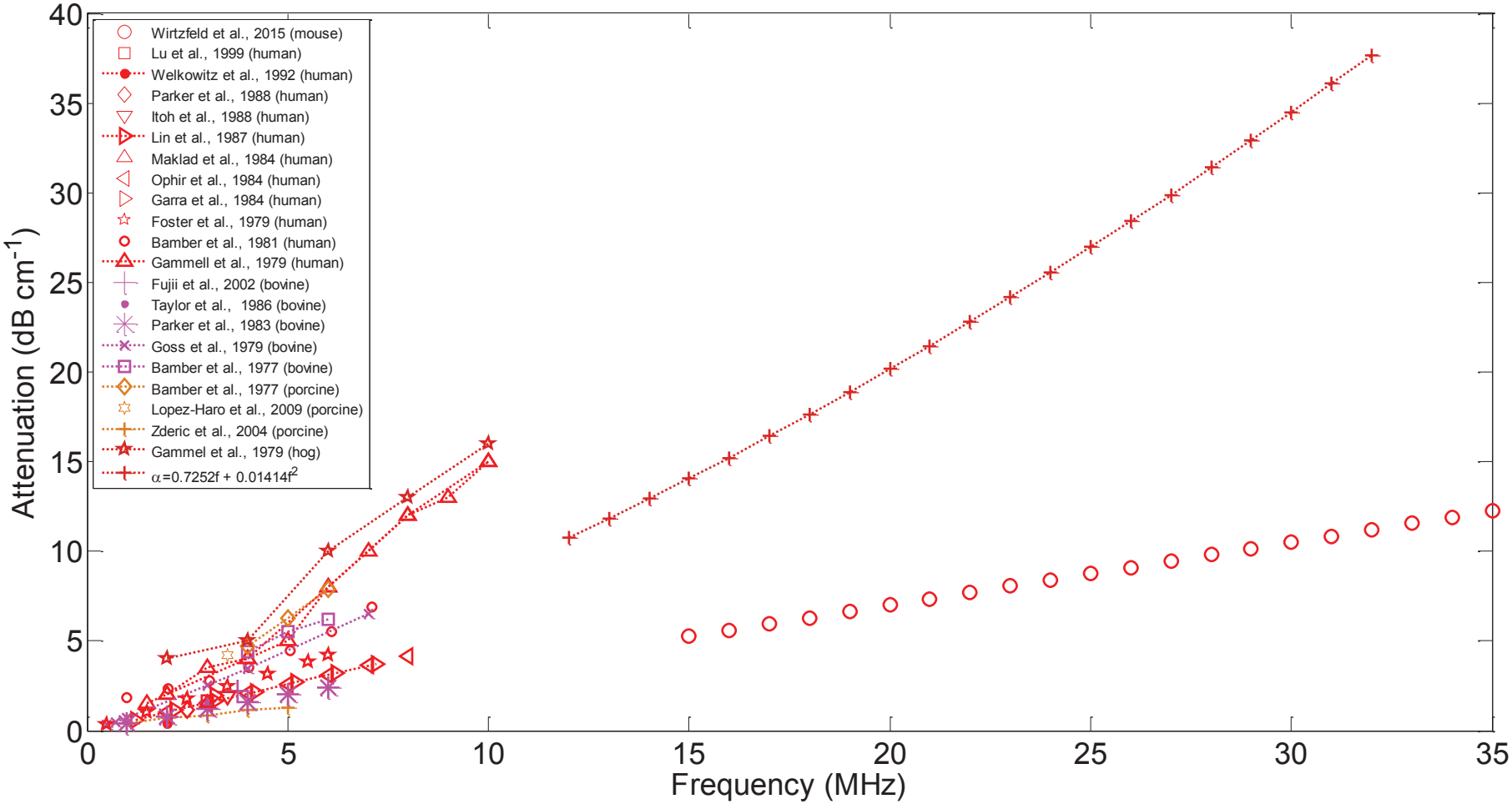

Figure 5-9. *Attenuation versus frequency of liver tissue data as published in the literature with extrapolation of the second degree polynomial fit calculated in this study to zero.*

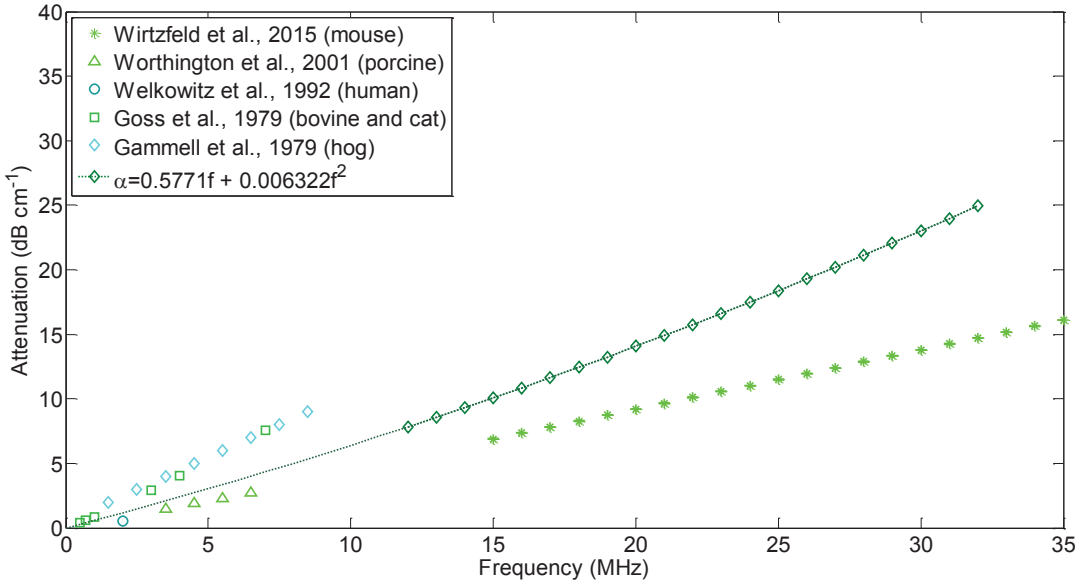

Figure 5-10. *Attenuation versus frequency of the kidney tissue data as published in the literature with extrapolation of the second degree polynomial fit calculated in this study to zero.*

Figure 5-11 shows the three polynomial-fits calculated for each organ tissue in this study as a comparison with the UTMMS (Chapter 3) IEC agar-TMM (Rabell-Montiel et al., 2017) in the frequency range 4.5 – 50 MHz and the IEC guideline (IEC, 2001).

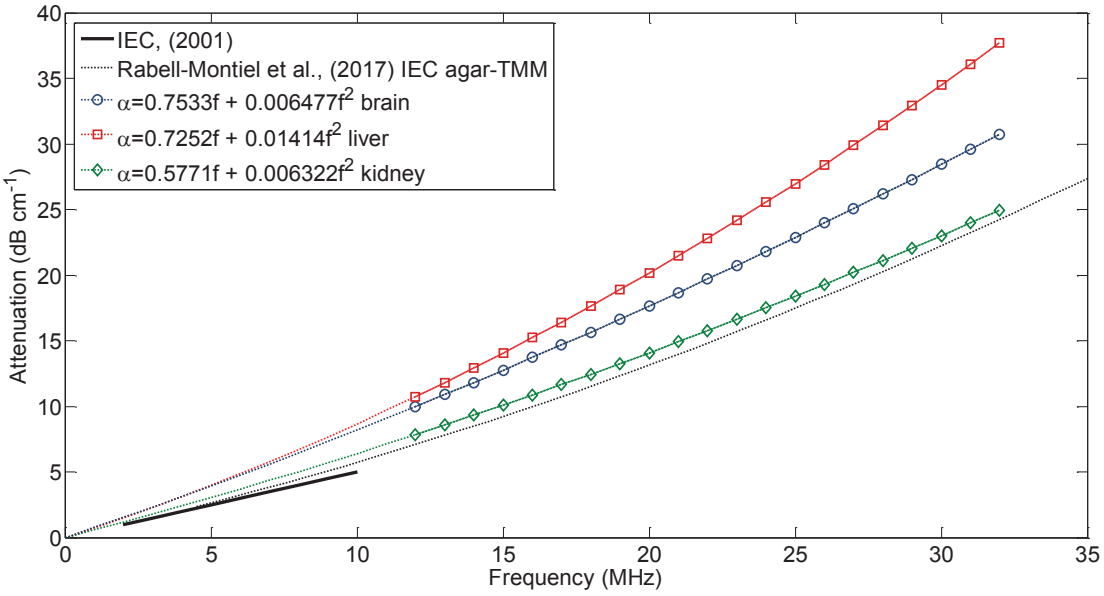

Figure 5-11. *Attenuation versus frequency graph comparing the polynomial fit found in this study and the attenuation data from the UTMMs and the IEC agar-TMM (IEC, 2001; Rabell-Montiel et al., 2017).*

5.4.3 Heart tissue acoustic measurements

Despite the issues described in Section 5.3.3.2 for the collection of the acoustic data of heart tissue, measurements were obtained from nine heart tissue samples. Measurements were undertaken twice in one location using the same experimental set-up as with brain, liver and kidney tissue. To collect the RF data, the sample was orientated to appear as flat as possible. This location varied for each heart tissue sample.

Table 5-3 show the SoS values measured from heart tissue. The SD shown is that found within the 10 lines inside the ROI of interest when the soft tissue was being scanned. The SD is higher than that obtained from the other soft tissue samples and this is most likely due to the non-flat surface of the sample. The difference between the first measurement of SoS and after 5 minutes was found to be 53.1 ms^{-1}.

Heart	SoS ± SD (ms^{-1})
First measurement	1525.6 ± 120.4
t=5	1578.7 ± 91.4

Table 5-3. *Mean SoS and SD (ms^{-1}) of nine heart tissue samples. Measurements were performed using the Vevo 770® preclinical ultrasound scanner over the frequency range of 12 – 32 MHz.*

From Table 5-3, the mean SoS of the heart tissue was calculated as 1548.9 ± 101 ms^{-1}. This value was found to be 21 ms^{-1} lower than the expected SoS reported in the literature (1570 ms^{-1}). The SD found in the mean SoS is an indication of the extent of the experimental error in the determination of the SoS for heart tissue.

A second degree polynomial was fit estimated from the attenuation versus frequency data averaged at all time points. The second degree polynomial fit for heart tissue was calculated as $0.6049f + 0.007426f^2$ (R^2=0.62). The attenuation versus frequency at each measurement point for heart tissue is presented in Figure 5-12. The SD displayed was estimated based on the SD of the mean attenuation versus frequency across nine samples over all time points. Figure 5-12 also includes the extrapolation of the attenuation coefficient published from human myocardial measured at 200 MHz (Saijo et al., 1997). In Figure 5-13 the polynomial-fit calculated for heart tissue is

compared to the polynomial fits found for brain, liver and kidney tissue, together with the IEC agar-TMM and the IEC guideline, as shown in Figure 5-11.

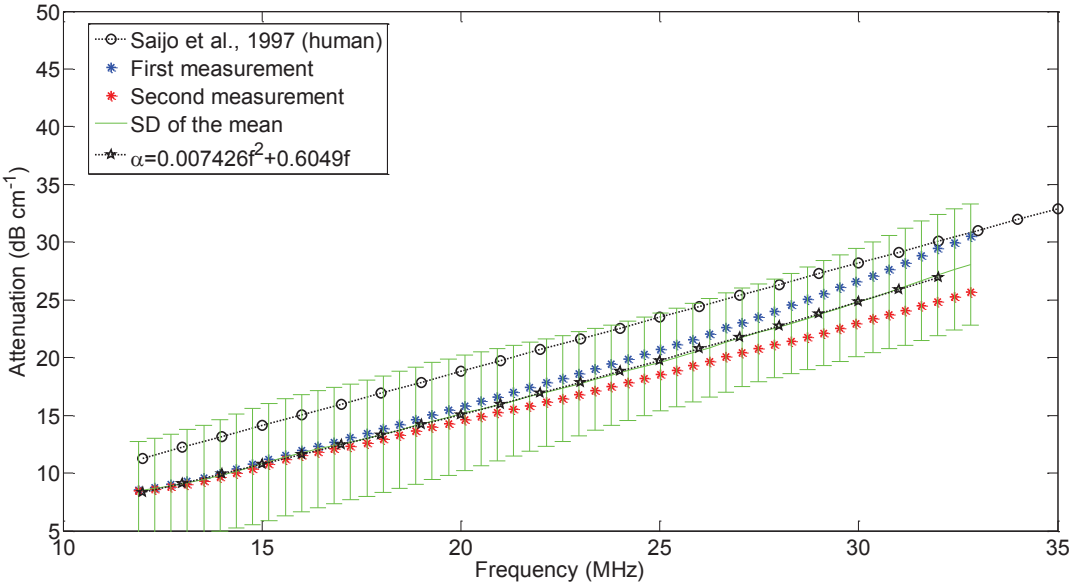

Figure 5-12. *Attenuation versus frequency of the heart (9 samples) tissue data as published in the literature with the timed measurements. The SD shown was calculated from the mean attenuation over all time points. The second degree polynomial-fit calculated in this study is also shown.*

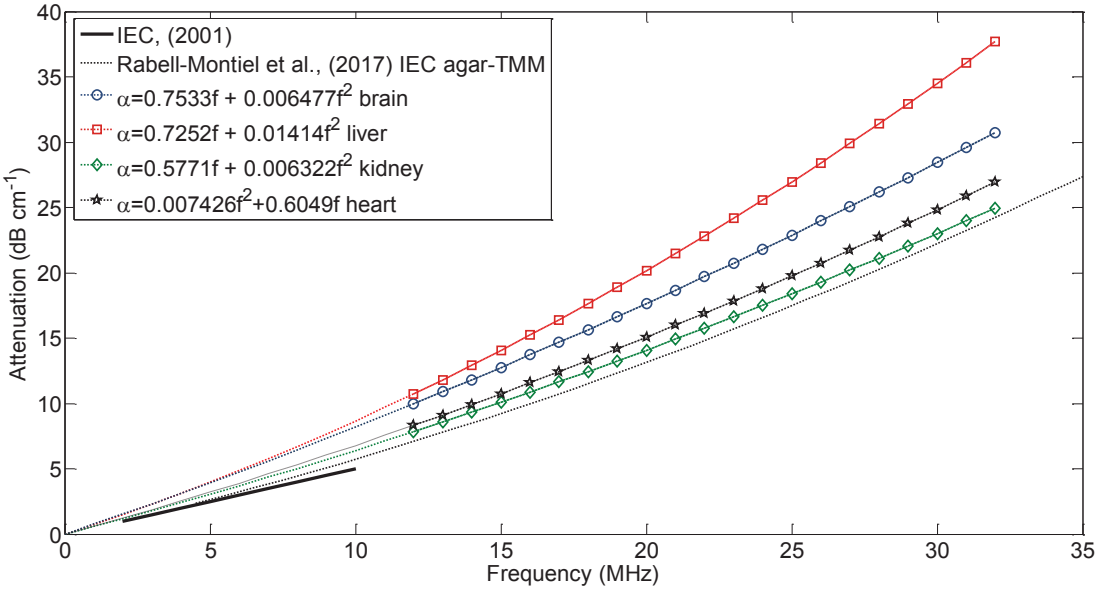

Figure 5-13. *Attenuation versus frequency of polynomial fit found in this study, compared with the attenuation data for IEC agar-TMM (IEC, 2001; Rabell-Montiel et al., 2017).*

5.4.4 Acoustic measurements from perfused tissue

Table 5-4 shows the mean SoS of the perfused brain and liver at t=0 and at t=5 minutes. The SD shown is the value calculated from 10 perpendicular scan-lines inside the ROI. It can be seen that the variation in the SoS as a function of time is less than 2.2 ms^{-1}. The SoS increased 1.4 ms^{-1} for perfused brain and 2.2 ms^{-1} for perfused liver within 5 minutes between measurements. The mean SoS was found to be 1563.1 ± 0.9 ms^{-1} for perfused brain and as 1605.7 ± 2.1 ms^{-1} for perfused liver.

Organ	Mean SoS ± SD (ms^{-1})	
	t=0	t=5
Brain	1562.4 ± 4.1	1563.8 ± 3.1
Liver	1604.9 ± 4.1	1607.1 ± 3.7

Table 5-4. *The SoS and SD (ms^{-1}) measured immediately after excision and perfusion and then at t=5 minutes. Measurements were made using a Vevo 770® preclinical ultrasound scanner over the frequency range of 12 – 32MHz.*

Figure 5-14 and Figure 5-15 shows the mean attenuation versus frequency for perfused brain and liver compared to the previously calculated polynomial-fits for non-perfused tissue (Figure 5-5 and Figure 5-6 respectively). The displayed SD was calculated from the mean attenuation data at all time points. It can be seen in Figure 5-14 that the attenuation measured from perfused brain increases more slowly with frequency than for non-perfused brain tissue. The biggest difference was found at 32 MHz with a value of 12.46 dB cm^{-1}. The smaller difference was at 12 MHz with a value of 3.4 dB cm^{-1}. In Figure 5-15 the attenuation measured from perfused liver can be to increase with increasing frequency in a similar manner as non-perfused liver; the biggest difference was found at 32 MHz with a difference of 2.87 dB cm^{-1}, the smallest difference was seen at 12 MHz with a value of 0.3 dB cm^{-1}.

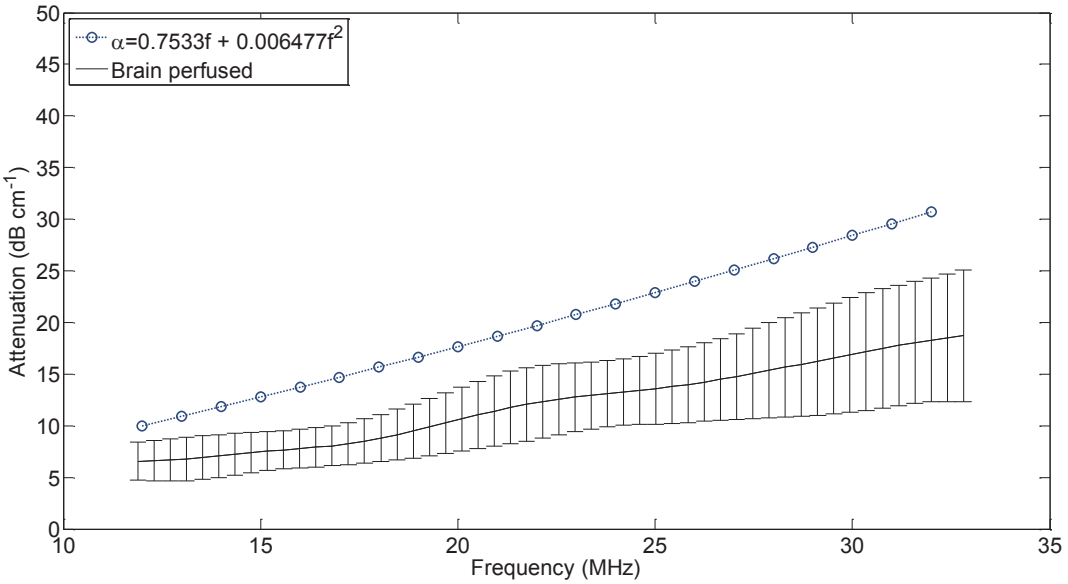

Figure 5-14. *Attenuation as a function of frequency for perfused brain (1 sample) measured after perfusion and t=5 minutes. The SD shown was calculated based on the SD of the mean of data from the two time points.*

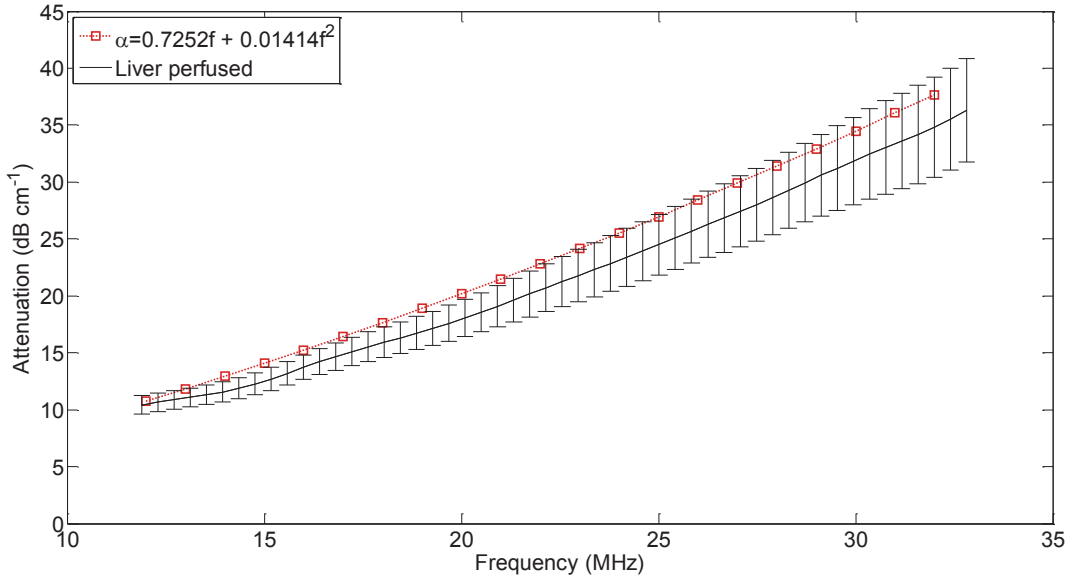

Figure 5-15. *Attenuation as a function of frequency for perfused liver (2 samples) measured after perfusion and t=5 minutes. The SD shown was calculated based on the SD of the mean of data from the two time points.*

5.5 DISCUSSION

The aim of this study was to measure the acoustic properties of *ex vivo* small animal soft tissue in order to determine if the acoustic properties of the IEC agar-TMM were comparable to those of soft tissue at high frequencies. Twenty brains, twenty livers and twenty kidneys (ten left and ten right kidneys) from fifty mice were extracted, sliced, and their acoustic properties assessed using a Vevo 770® scanner. The acoustic properties were measured in PBS at 37°C (body temperature). Initial measurements were undertaken within 6 minutes after euthanasia (t=0) and then at t=5 and t=10 minutes after the initial measurement.

An increase in either water or fat content results in a decreased velocity of ultrasound in soft tissue (Duck, 1990). For the brain and the liver samples, the SoS and the attenuation were analysed against the weight, the age of the animal and against the precise measured thickness of the sample. Also, the SoS and the attenuation of the soft tissue samples were analysed as a function of time after excision. None of these parameters appeared to significantly interfere the measured demographic parameters (age, weight, sex) acoustic properties. It is hypothesized that the SoS and the attenuation variability across small animal soft tissue samples may be due to the diverse animal models used and also due to the intrinsic structural properties of the tissue which were not investigated in this study.

5.5.1 PBS

The acoustic properties of the PBS at 37°C in comparison with those of degassed deionised water and saline fluid at the same temperature were previously discussed in Section 2.7.3.

5.5.2 Brain

The SoS measured in brain samples was in good agreement with Kremkau et al., (1981) whose measurements were taken from human brain samples over the frequency range 1 – 5 MHz and measured at 37°C. From Table 5-2 and Table 1-4, the largest variation in SoS data was with Welkowitz et al., (1992) in which the SoS of mouse brain tissue was found to be 56 ms^{-1} lower than the data from this study.

For the brain attenuation, the largest inter-sample difference of 13.2 dB cm^{-1} was found at 26 MHz (Figure 5-5). Extending the second degree polynomial fit calculated in this study to lower frequencies, it was found that the attenuation from this study agrees at 1 MHz with a 0.5 dB cm^{-1} difference with Bamber, (1981), Goss et al., (1979), Kremkau et al., (1981) and Welkowitz et al., (1992). The attenuation from human brain was found to be up to 3 dB cm^{-1} less at lower frequencies (6 MHz) when compared with Bamber et al., (1977). The attenuation versus frequency data calculated in this study agrees up to 1.8 dB cm^{-1} with those published studies in the frequency range 1 – 7 MHz (Bamber, 1981; Bamber et al., 1977; Goss et al., 1979; Kremkau et al., 1981; Strowitzki et al., 2007; Welkowitz et al., 1992). Moreover, the attenuation versus frequency measured in this study was re-expressed and extended to lower frequencies as a power-law of the form af^b, where f is the frequency (MHz) and a and b are the coefficients of the fit. The power-law fit calculated for the brain was 0.91 dB cm^{-1} MHz^{-1} (R^2=0.84). Kremkau et al., (1981) reported an attenuation of 1.08 dB cm^{-1} MHz^{-1}, Bamber et al., (1981) reported 1.1 dB cm^{-1} MHz^{-1} and Strowitzki et al., 2007 reported an attenuation of 0.94 ± 0.13 dB cm^{-1} MHz^{-1}. The maximum difference (4.2 dB cm^{-1} at 5 MHz) in the attenuation power law calculated in this study, was found with that of Bamber et al., (1979) (Figure 5-8).

5.5.3 Liver

There have been a number of previous papers published to describe the acoustic properties of liver at low frequencies, yielding a wide range of SoS and attenuation coefficient values (Table 1-4). The SoS of the liver measured in this study was shown to be in good agreement within 5 ms^{-1} with Bamber & Hill, (1979) and Martínez-Valdez et al., (2015) and was up to 33 ms^{-1} higher than Bamber et al., (1980); Chen et al., (1987); Kumagai et al., (2014); Martínez-Valdez et al., (2015); López-Haro et al., 2009; O'Brien, (1988) and Sehgal et al., (1986). The biggest SoS difference was again found to be with Welkowitz et al., (1992) who reported a SoS in mice of 1510 ms^{-1} at 2 MHz.

It is known that gas is more likely to be introduced into the liver during excision than any other organ due to its highly vascular structure and tendency to produce gas during autolytic decay. The presence of gas in specimens is reported to be the greatest

problem in the preparation of soft tissue samples for acoustic measurements (Bamber, 1981). Measurements in this study were initiated within 6 minutes post euthanasia. During the measurement sequences, the samples were kept in PBS at 37°C. Therefore, it is not believed that the attenuation variability of 10 dB cm^{-1} at 32 MHz, see Figure 5-6, observed in this study derives from the production of gas due to autolytic decay.

Previous studies found attenuation ranging from 0.44 – 0.65 dB cm^{-1} MHz^{-1} (Itoh et al. 1988; Lu et al. 1999; Parker et al. 1988; Fujii et al. 2002). Despite the extensive number of liver studies in various publications, there is an 8.8 dB cm^{-1} variation in the attenuation coefficients at 9 MHz (Garra et al. 1984; Itoh et al. 1988; Lu et al. 1999; Maklad et al. 1984; Parker et al. 1988; Taylor et al. 1986). The attenuation of the liver has also been studied over a similar frequency range to that used in this study. Wirtzfeld et al., (2015) found a difference of 26.5 dB cm^{-1} at 32 MHz when compared with the results of this study. This difference is attributed to the type of sample (extra-cellular from a decelularised process) measured used by Wirtzfeld et al., (2015) versus the *ex vivo* fresh tissue method used in this study. Furthermore, by extending the second degree polynomial fit found in this study to lower frequencies (Figure 5-9 good agreement was found with the data published of bovine and human liver at 37°C up to 9 MHz (Foster & Hunt, 1979; Fujii et al., 2002; Gammell et al., 1979; Goss et al., 1979; Lu et al., 1999). Also, the second degree polynomial fit calculated in this study was found to be within ±6 dB cm^{-1} with pig, rat and human livers measured up to 9 MHz by López-Haro et al., (2009), O'Brien et al., (1988), Lu et al., (1999) and Gammell et al., (1977).

The attenuation calculated in this study can also be expressed as a power-law as 1.08 dB cm^{-1} MHz^{-1} (R^2=0.66) and thus extended to lower frequencies. This power-law value was found to be in smaller (up to 0.42 dB cm^{-1}) from pig, rat and human livers measured by López-Haro et al., (2009), O'Brien et al., (1988), Lu et al., (1999) and Gammell et al., (1977). The power-law reported on those studies was 1.2 dB cm^{-1} MHz^{-1}, 1.3 ± 0.09 dB cm^{-1} MHz^{-1}, 1.6 ± 0.21 dB cm^{-1} MHz^{-1} and 1.5 dB cm^{-1} MHz^{-1}, respectively.

5.5.4 Kidney

The difference in SoS values between the left and right kidney, using different dissection axes, was 0.97 ms^{-1}. Based on the second polynomial fit, the difference was found to be up to 1.31 dB cm^{-1} between the diverse dissection planes (left and right kidney) across the frequency range 12 – 32 MHz. Despite measuring the acoustic properties from different dissection planes the mean attenuation values did not show a consistent variation. Previous work has shown the variation in the acoustic properties of the kidney to be associated with five sections across the longitudinal axis in canine renal anatomy (Sarvazyan & Klemin, 1983) see (Section 1.4.2.4). In that study, the SoS showed a difference of 5 ms^{-1} and a difference of 0.5 dB cm^{-1} at 8.8 MHz in dog's kidney (from the *cortex* through to the *renal veins*).

In this study, effort was made to ensure measurements were undertaken within the *medulla* in both dissection planes. The limited variation in our measurements suggests that this was achieved. The acoustic properties found for both the left and the right kidney were combined by taking the mean value for comparison with previous literature. The mean magnitude of the SoS values of the kidney were found to lie between the values obtained from studies published from human, pigs and mice at different temperatures (Table 1-4). The inter-sample attenuation as a function of frequency was found to vary up to 5 dB cm^{-1} at 30 – 32 MHz, with the smallest difference (1 dB cm^{-1}) at 3 MHz. In Figure 5-10 the polynomial fit calculated in this study is compared with published studies. The magnitude of the attenuation given by the second degree polynomial fit calculated in this study fall within the magnitude of attenuation found in the published studies. This polynomial fit was found to be smaller by 2.7 dB cm^{-1} compared with data from Gammell et al., (1979), Goss et al., (1979), Welkowitz et al., (1979) and higher by up to 1.6 dB cm^{-1} with data reported by Worthington et al., (2001) in the frequency range from 1 – 9 MHz. Moreover, the attenuation of the kidney can be re-calculated as a linear attenuation coefficient. The value obtained was 0.73 dB cm^{-1} MHz^{-1} (R^2=0.81) which is 0.33 dB cm^{-1} MHz^{-1} higher than the attenuation measured from bovine and porcine kidney at 37°C and at 45°C (Goss et al., 1979; Worthington et al., 2001). These differences could be attributable to real differences in animal kidneys or to the difference due to the temperature at which

the studies were undertaken (up to 65°C) (Worthington & Sherar, 2001). The mouse kidney has been studied up to 35 MHz by Wirtzfeld et al., (2015), the difference in attenuation compared to this study of up to 10.2 dB cm^{-1} at 32 MHz.

5.5.4.1 *Heart acoustic measurements*

In order to acoustically characterise the heart tissue, different methods to slice/open the heart with sufficient tissue in the sample were tested. Diverse methods of holding the tissue designed for the heart were also devised.

Results taken from measurements on heart tissue, while testing these different methods were presented in Section 5.3.3.2. The SoS of this organ exhibited large variability (up to 10%) within each sample. Nevertheless, the SoS measured 5 minutes after the first measurement was found to be in agreement with published studies. The analysis of RF data was performed in a similar way to that of the brain, liver, and kidney. The high SD shown for the SoS could be due to the topography and the muscular nature of heart tissue. Alternatively, very small pieces of tissue could have overlapped within background noise, introducing a large uncertainty when analysing the RF data. The value of the SoS of the heart may predict cardiac arrest (Butts, 2017).

Heart attenuation measurement (Figure 5-13) agreed closely with those measured for the kidney at low frequencies and within 2 dB cm^{-1} at 30 MHz. Attenuation of the heart tissue was found to be 10 dB cm^{-1} lower at 30 MHz with than for liver.

Because of the issues with heart tissue handling, described previously, no more measurements were performed on this organ.

5.5.4.2 *Perfused versus non-perfused tissue*

For the SoS, measurements of perfusion of the brain was not found to influence our measurements of SoS. The difference between non-perfused and perfused tissue was less than 3.2 ms^{-1}. Similarly, SoS for perfused liver was found to be +1 ms^{-1} when compared with non-perfused liver. Both differences in the SoS values fall within the SD reported for normal tissue in Table 5-2.

The difference in the attenuation values between non-perfused and perfused soft tissue indicates that for brain tissue, blood does result in a detectable change in

attenuation properties. The mean attenuation between perfused brain tissue was 2.2 dB cm^{-1} less than the mean attenuation measured from the non-perfused tissue. In the case of the liver, the attenuation from perfused liver tissue falls within 1 SD measured values for non-perfused tissue (Figure 5-6).

5.5.5 Comparison with TMM

The frequency range used in this study (12 – 32 MHz) falls outside of the range over which the IEC guideline give recommended values (2 – 10 MHz). The biggest difference in the SoS from recommended TMM SoS values was found in liver tissue which varied from the IEC agar-TMM by 64 ms^{-1}.

For the attenuation coefficient, the polynomial-fits calculated from the brain, liver, and kidney tissue data were compared with previously published acoustic measurements from the IEC agar-TMM (Figure 5-11) up to 50 MHz. The attenuation of the kidney matched the IEC agar-TMM with a consistent difference of 0.5 dB cm^{-1} in the frequency range 12 to 32 MHz. This difference falls within one SD of the IEC agar-TMM (±2 dB cm^{-1}). The biggest difference in the attenuation coefficient was found to be with liver tissue of 14 dB cm^{-1} at 32 MHz when compared with the IEC agar-TMM (Rabell Montiel et al., 2017).

5.5.5.1 *Matching the acoustic properties of the IEC agar-TMM to those of small animal soft tissue*

As mentioned in Section 5.4, a modification of the IEC agar-TMM recipe based on the results of soft tissue is needed for the development of a TMM for high frequency ultrasound applications. Chapter 4 presented the acoustic properties of the individual components of the IEC agar-TMM by the inclusion and exclusion of some of the ingredients, without altering the percentage concentration. The acoustic properties of an agar-based material have been studied by changing the percentage concentration of the ingredient components, based on the IEC agar-TMM recipe (Cannon et al., 2011; Inglis et al., 2006). In order to adjust the acoustic properties of the IEC agar-TMM to match those of small animal soft tissue, the results showed in Section 5.4 have been compared with previously published work where the percentage concentrations of ingredients within agar-based materials have been modified.

The acoustic properties of the agar-TMM have been measured by Cannon et al., (2011) by changing the concentration of the 4 main composition ingredients as follows: 1) glycerol concentration variation at 0% and 50 – 150% in steps of 10%, 2) SiC (size particle 17 μm), Al_2O_3 (both sizes of particles 0.3 μm and 3 μm) varied concentrations in steps of 5% from 0 – 20%, in steps of 10% from 30 – 60%, in steps of 20% from 75% and 100 – 200%. 3) Al_2O_3 (both sizes of particles 0.3 μm and 3 μm) varied concentrations in steps of 10% and 250% from 100 – 200%. 4) SiC (size particle 17 μm) concentration variation from 0 – 100% in steps of 10%. These measurements were performed using the SAM system in the frequency range from 14.8 – 24.5 MHz at 20°C by Cannon et al., (2011). Furthermore, the attenuation of the agar-TMM has also been assessed when changing the percentage concentrations of the aluminium oxide particles (both particle sizes) and the silicon carbide (400 grain) increased from 0 – 100% using the SAM system with a centre frequency probe of 7 MHz (Inglis et al., 2006).

Figure 5-16 shows the effects of the glycerol concentrations on the agar-TMM SoS measured at 20 MHz by Cannon et al., (2011) as a comparison to the soft tissue SoS measured in Section 5.4.1. It can be seen that, to achieve the SoS of mouse brain tissue, the concentration of glycerol has to increase to approximately 130%, whereas for liver the glycerol concentration will have to be increased above 150%. To match the SoS of the agar-TMM to the SoS of the kidney, the glycerol concentration should be increase of to 140%. The IEC recommends a SoS value of 1540 ± 15 ms^{-1} for TMM. The SoS reported by Cannon et al., (2011) with 100% glycerol concentration falls outside of the specifications provided by the IEC (Figure 5-16).

The concentrations of the aluminium oxide and/or silicon carbide, demonstrated no effect on the SoS of the agar-TMM. Moreover, increasing the glycerol concentrations did not affect the attenuation coefficient on the agar-TMM (Cannon et al., 2011). With a reported SoS of the glycerol of 1923 ms^{-1} and an impedance of 2.44 x 10^3 kg cm^{-3} s at 9.6 MHz (Dymling et al., 1991); the variations in the concentration of glycerol showed no significant effect on the density nor on the impedance of the agar-TMM (Cannon et al., 2011).

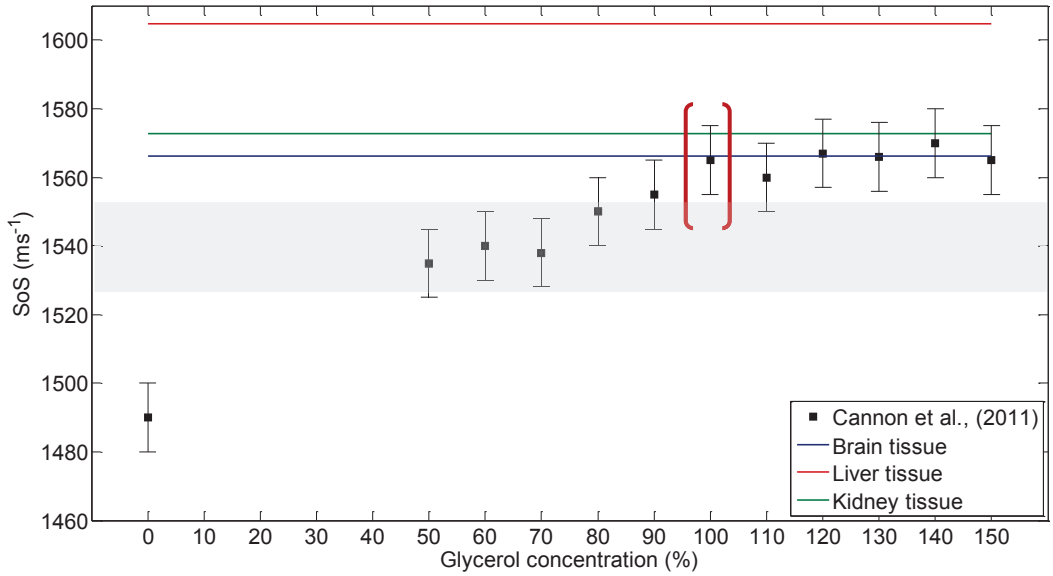

Figure 5-16. *SoS as a function of glycerol concentration. The graph also shows the SoS measured in this PhD report from brain, liver, and kidney tissue. The red double bracket indicate the IEC, (2001) guideline. The grey shadowed area indicate the actual SoS value recommended by the IEC (IEC, 2001).*

In order to match the attenuation coefficient from brain, liver or kidney tissue; the concentration of both aluminium oxide sizes particles and also silicon carbide should increase above 180% as shown in Figure 5-17.

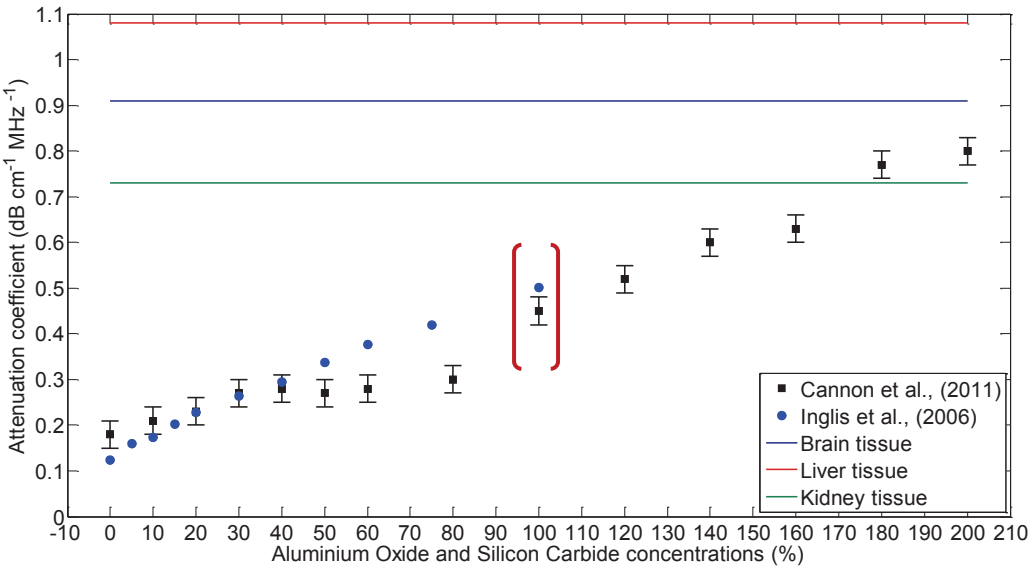

Figure 5-17. *Attenuation as a function of aluminium oxide (0.3 μm and 3 μm) and Silicon Carbide (17 μm) from Cannon et al., (2011) and 400 grain from Inglis et al., (2006) concentrations. The graph also shows the power-law of the attenuation measured in this PhD report from brain, liver and kidney tissue. The red double bracket indicate the IEC, (2001) guideline.*

Moreover, according to Figure 5-18, the attenuation from brain showed good agreement with the attenuation of the percentage of aluminium oxide (both particles sizes) at 250%. The kidney attenuation falls within the increments between 190 – 200% of Al_2O_3. Figure 5-18 also indicates that to match the attenuation of liver both sizes of aluminium oxide particles should increase to quantities above 250% with respect to the base values.

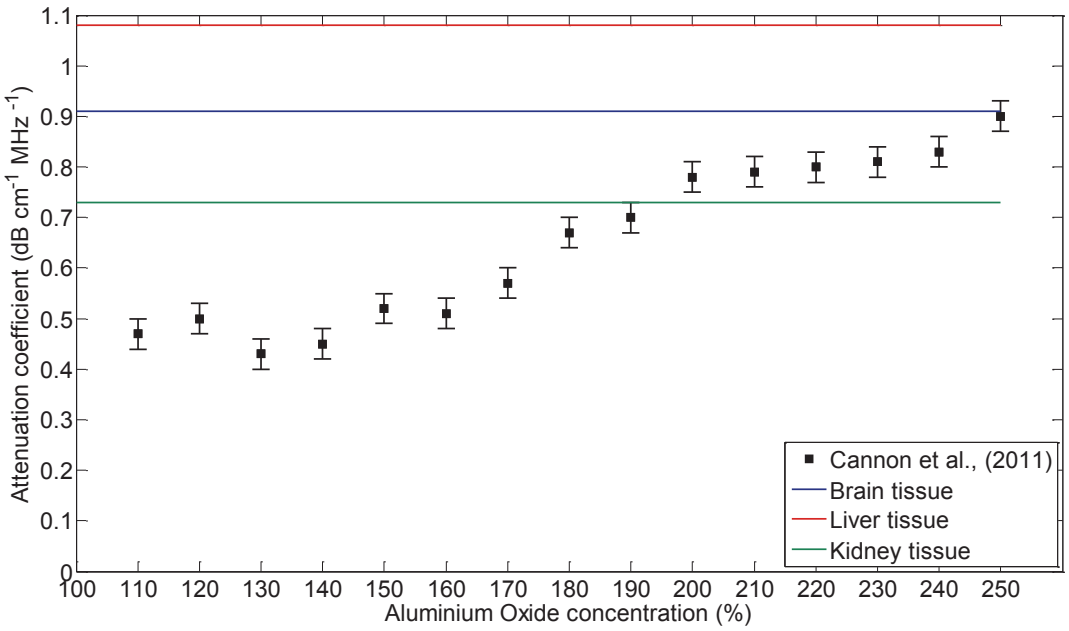

Figure 5-18. *Attenuation as a function of aluminium oxide (0.3 µm and 3 µm) concentration. The graph also shows the power-law fit of the attenuation measured in this PhD report from brain, liver and kidney tissue over the frequency range 12 – 32 MHz.*

Figure 5-19 shows that when increasing the concentration of the SiC the overall attenuation of the agar-TMM did not show a high variability (±0.1 dB cm^{-1} MHz^{-1}). The aluminium oxide has been found to mainly contribute to the overall attenuation of the agar-TMM (Cannon et al., 2011; Inglis et al., 2006). Therefore, the largest modification in the IEC agar-TMM recipe should be on the glycerol (to match the SoS) and on the Al_2O_3 particles (to match the attenuation) in order to closely match the acoustical properties to those of soft tissue.

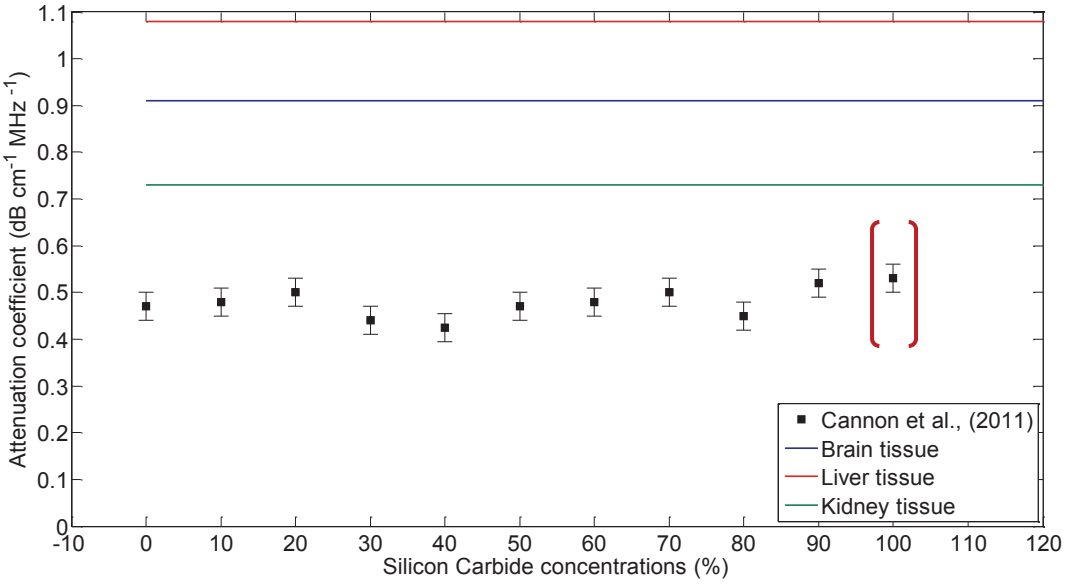

Figure 5-19. *Attenuation as a function of Silicon Carbide (17 µm) concentration. The graph also shows the power-law fit of the attenuation measured in this PhD report for brain, liver and kidney tissue measured over the frequency range 12 – 32 MHz. The red double bracket indicate the IEC, (2001) guideline.*

5.6 Conclusions

The acoustic properties of mouse soft tissue (brain, liver, and kidney) were measured over the frequency range of 12 – 32 MHz with the tissue immersed in PBS at 37°C. The samples were obtained from recently euthanized C57BL/6 healthy surplus male mice with a mean age of 6.9 ± 3.9 months. Measurements were undertaken within 6 minutes of excision and then at 5 and 10 minute time-points after the first measurement. Attempts to measure the acoustic properties from mouse heart tissue were also investigated.

The measured SoS of soft tissue was found to be 1566.3 ± 9.9 ms^{-1} for the brain, 1604.7 ± 16.8 ms^{-1} for the liver and 1574.9 ± 10.8 ms^{-1} for the kidney. For all the small animal soft tissue, the SoS results were comparable with those published for low ultrasound frequencies (1 – 9 MHz).

The attenuation of the small animal soft tissue was confirmed to increase with increasing frequency. The attenuation was shown to be nonlinear as a function of

frequency and was modelled as second degree polynomials: $0.7533f + 0.006477f^2$ (R^2=0.85) for brain, $0.7252f + 0.01414f^2$ (R^2=0.70) for liver and $0.5771f + 0.006322f^2$ (R^2=0.83) for kidney. The attenuation coefficient calculated from the data generated in this study was extended to lower frequencies for comparison with previously published work.

The attenuation from perfused liver falls within 1 SD of the attenuation measured for non-perfused liver.

In order to create a TMM suitable for use as a high frequency QA phantom and based on an IEC agar-TMM recipe, the recipe should be modified. For the SoS of the TMM to match the SoS of mouse brain and kidney, the glycerol concentration should increase by 40%. For the attenuation coefficient of the TMM to match the attenuation of mouse brain the concentration of both sizes of Al_2O_3 particles (3μm and 0.3μm) should increase by 150%.

Finally, QA phantoms are made of materials that mimic the acoustic properties of tissue. The acoustic properties of soft tissue have been previously assessed up to 9 MHz and at 15 – 35 MHz. Establishing the acoustic properties of soft tissue at high frequency is a required step in the development of a suitable TMM QA phantom. Currently, the IEC guidelines do not provide the necessary data to develop a TMM suitable for frequencies above 10 MHz. Therefore, the data provided in this chapter can be used as a basis from which a recipe for TMM, which is representative of tissue properties at high frequencies, can be based.

CHAPTER 6

CONCLUSIONS AND FUTURE WORK

6.1 CONCLUDING REMARKS

The goal of this thesis was to develop a TMM with high frequency acoustic properties matching those of small animal soft tissue. The aim of this TMM was to incorporate this material into a fit for purpose high frequency QA phantom. These high frequency QA phantoms would then be more suitable for performance assessment of high frequency ultrasound scanners than those manufactured using existing formulations. Although this new TMM was not manufactured, the work presented in this thesis provides the knowledge upon which such a TMM could be developed.

To summarize, Chapter 2 presented the methods, the equipment and the Matlab scripts used to analyse the existing IEC agar-TMM in order to develop a new TMM. The methods and the experimental setup described in Chapter 2 were the basis of the following results chapters. Chapter 3 compared the acoustic properties of the IEC agar-TMM when using 2 different measurement techniques. These are firstly, the most widely used method of film-wrapping thin samples of TMM measured in degassed, deionised water and secondly the use of un-covered thin samples of TMM measured in TMM preserving fluid. The latter method was developed as an integral part of this PhD. Using this method, the advantages of using a preserving solution for the study and storage for up to a year of TMM has been demonstrated. The acoustic properties of the individual formulation ingredients of the IEC agar-TMM were presented in Chapter 4. It has been shown that the overall attenuation of the IEC agar-TMM was accomplished by the linear summation of the attenuation values from each of the composition ingredients. Chapter 5 presents the results of the SoS and attenuation coefficient values of the small animal soft tissue (brain, liver, and kidney) at high frequencies including the comparison of the acoustic properties between perfused and non-perfused tissue. Conclusions and highlights of each chapter are described below.

In Chapter 2, the 3 dB frequency bandwidth was measured for the seven transducers used in this PhD project providing the total bandwidth over which acoustical measurements were made in this thesis. This was 4.5 – 50 MHz, using four transducers on the Vevo 770® preclinical scanner and three transducers as part of the SAM system. Also, in Chapter 2 the acoustical properties of the reference fluids used in this thesis were presented (TMM preserving fluid, phosphate buffered saline (PBS) and degassed deionised water). The TMM preserving fluid was characterised by the NPL, whereas the PBS at 37°C was characterised in this thesis using a standard substitution technique. The 3 dB frequency bandwidth of the transducers and the acoustic properties of the different reference fluids provided necessary information for the acoustic properties of the IEC agar-TMM and of the small animal soft tissue at high frequencies as derived in the following results chapters.

In Chapter 3 the acoustic measurements of IEC agar-TMM at high frequency using 2 different measurement techniques were performed. These measurement techniques were as follows, firstly, the most commonly used technique for measuring the acoustic properties of TMM. This technique involves the film-wrapping of thin slices of agar TMM samples (FTMMs) measured in degassed water. The second technique measured the acoustic properties of uncovered agar TMM slices (UTMMs) immersed in TMM preserving fluid. The second technique was developed as part of the production of this PhD. The SoS and the attenuation coefficient values from TMM samples manufactured using both different measurement techniques were compared every 3 months over a period of 1 year. To extend the measurements to lower frequencies, the SAM system was used to acquire acoustic data at the Dublin Institute of Technology. The results from this study were compared with information found in the literature and with the IEC guideline for TMM, finding good agreement. The results also found that 1) the SoS values were 1538.2 ± 14.5 ms^{-1} for FTMMs and 1544.0 ± 3.5 ms^{-1} for UTMMs. 2) the attenuation for TMM increases with increasing frequency as $0.4649f + 0.007363f^2$ for FTMMs and as $0.4897f + 0.008366f^2$ for UTMMs and 3) the TMM samples manufactured using the second technique pioneered in this PhD demonstrated a better acoustic stability with up to 4 times smaller SD for the SoS values and up to 5 times smaller variation in the attenuation coefficient values.

Chapter 4 presents the results obtained for the acoustic properties of the individual components of the IEC agar-TMM using the alternative sample preparation and experimental method developed in Chapter 3. The mean SoS for all the different batches (with varying constituent ingredients) was found to be within the IEC recommended values for SoS. This result was expected since there was no modification of the percentages of the fluids (water, benzalkonium chloride, and glycerol) included in the different component ingredient batches. The mean SoS from all the TMM batches was found to be 1538.8 ± 5.1 ms^{-1}. The overall attenuation of the IEC agar-TMM was found to be the linear sum of the attenuation coefficients of its component parts. This resulted in a key observation from which the formulation of an agar-TMM matching the acoustic properties of small animal tissue can be achieved.

In Chapter 5 the results from the measurement of the acoustic properties of mouse brain, liver, and kidney, that were obtained at higher frequencies were presented and compared to those obtained in the literature. The SoS obtained from mouse soft tissue was found to fall outside of the IEC recommended values for TMM. The IEC does not provide guidance on how to develop a TMM suitable for frequencies above 10 MHz. The results of Chapter 5 show that only the attenuation of mouse kidney was inside the 1 SD of the measured attenuation value (Chapter 3) of the IEC agar-TMM. In order to reproduce the acoustic properties of small animal soft tissue, modifications to the IEC agar-TMM recipe should be implemented to match the SoS and the attenuation of liver and brain at these higher frequencies. The data provided in this chapter can be used as a basis from which to develop a TMM suitable for high frequency imaging.

6.2 FUTURE WORK

6.2.1 Additional ultrasound parameters of IEC agar-TMM

In Chapter 5 only the SoS and the attenuation coefficient of biological tissue was quantified at high frequencies. Other ultrasound parameters such as B/A coefficient, backscatter, elasticity or impedance were not assessed during this PhD thesis. These parameters, in addition to those shown in Table 1-5, may be needed to develop a TMM whose acoustic properties match those of soft tissue at high frequencies.

The IEC recommends an impedance of $1.60 \pm 0.16 \times 10^{6}$ kg m^{-2} s^{-1} and a backscatter coefficient of $1 - 4 \times 10^{-28}$ f^{4} m^{-1} Hz^{-4} sr^{-1} but does not recommend a value for elasticity or B/A coefficient values for TMM (IEC, 2001). A few studies have reported the backscatter and the elasticity values of the IEC agar-TMM. Brewin et al, (2008) reported a backscatter power slope for the IEC agar-TMM as 1.48 dB MHz^{-1} over a frequency range of 17 – 23 MHz. Additionally, the relative backscatter of the agar-TMM has been shown to remain constant with increasing temperature (Browne et al., 2003). The shear modulus of the agar-TMM is reported to decrease with increasing temperature over a frequency range of 1 – 10 MHz (Dunmire et al., 2013).

Furthermore, the backscatter has been studied when changing the concentrations of both particle sizes of aluminium oxide (Al_2O_3) and silicon carbide (SiC) at 20 MHz by Cannon et al., (2011) and at 7.5 MHz by Inglis et al., (2006) both at 20°C. It was reported that the backscatter changed from 0 to -11.8 dB when the particle concentration decreased from 100% to 0% (Inglis et al., 2006). Cannon et al., (2011) also showed a decrease in backscatter from 0 to -20 dB when decreasing the particle concentration.

It has been shown that the backscatter is predominantly provided by the aluminium oxide particles (Inglis et al., 2006) and that the silicon carbide does not contribute to the SoS, attenuation coefficient or backscatter of the agar-TMM (Cannon et al., 2011). The backscatter and nonlinear parameters of the IEC agar-TMM have been quantified up to 20 MHz (Browne et al., 2003; Cannon et al., 2011; Madsen et al., 1999; Wear et al., 2005). Further acoustic data (backscatter and nonlinear parameters) is needed above 20 MHz from the IEC agar-TMM. Also, the backscatter and nonlinear parameters from small animal soft tissue are needed in order to develop a TMM suitable for a QA phantom that can assess the performance of high frequency elastography ultrasound scanners with a realistic image appearance and YM values. More information on the nonlinear parameter, backscatter and elasticity of the IEC agar-TMM at high frequencies are needed in order to develop a new TMM whose acoustic properties match those of mouse soft tissue.

6.2.2 Acoustic measurement of in vivo soft tissue

Since the SoS and attenuation of small animal soft tissue were assessed in this, it would be useful to measure the acoustic properties of *in vivo* soft tissue for comparison. The measurement of the acoustic properties of *in vivo* soft tissue will provide data from functioning soft tissue without the presence of coagulated blood and potential degradations of the tissue. The acoustic properties of small animal soft tissue *in vivo* have been assessed in only a few studies (Kagadis et al., 2010; Zderic et al., 2004) and pose significant technical challenges. It is known that blood pressure influences soft tissue elasticity values (Gennisson et al., 2012).

More acoustic information, including the measurement of both linear and non-linear parameters, from perfused and non-perfused soft tissue will help to quantify the influence of blood on the acoustic properties of tissue. Blood has been reported to have a SoS of 1575ms^{-1}, an attenuation coefficient of 0.15 dB MHz$^{-1.21}$ cm^{-1}, a B/A coefficient of 6 and an acoustic impedance of 1.66 x10^{6} kg m^{-2} s with a density of 1050 kg m^{-3} (Azhari, 2010; Duck, 2012). As such these acoustic properties are given by the IEC as recommended values for blood-mimicking-fluid (IEC, 2001).

6.2.3 Acoustic measurement of heart tissue

Additionally, an experimental set-up is needed to acoustically characterise mouse heart. In Section 5.4.3, the difficulties in obtaining an adequate heart sample were discussed. It was found that, due to the anatomy of the organ, the heart sample curled when immersed in PBS at 37°C.

6.2.4 3 dB bandwidth of the Vevo 770® transducers at body temperature

The 3 dB bandwidths of the Vevo 770® transducers were measured at room temperature in this thesis. Additional probe characterisation at human body temperature may be needed due to the variations in the nonlinear parameters of degassed deionised water (Van Dongen & Verweij, 2008) found at higher temperatures (Bilaniuk & Wong, 1992; Del Grosso & Mader, 1972; Pinkerton, 1949). It is known that nonlinear effects of degassed water increase with increasing temperature (Van Dongen & Verweij, 2008). Van Dongen et al., (2008) showed that

the B/A (nonlinearity) parameter of degassed water is 5 times more sensitive to temperature than SoS. The ultrasound nonlinear parameter is often expressed as a B/A coefficient value. The values of A and B are the coefficients of the first and second order terms in a Taylor series of the equation relating pressure to density. Thus further characterisation may be needed for accurate *ex vivo* and *in vivo* acoustic characterisation of soft tissue at 37°C for future clinical applications.

This variation in nonlinear parameters can lead to variations in the beam profile and a change in the focal depth of the transducer. The focal depth of the transducer used in this thesis was the one established by the manufacturer and shown (Figure 2-3) in the Vevo 770® software (Visualsonics, Inc).

6.2.5 Development of a TMM suitable for high frequency QA phantoms

The results presented in this thesis describe the acoustic properties of mouse soft tissue and individual components of an IEC agar-TMM at high frequencies, this work represents is a first step towards the development of a TMM suitable for high frequency QA test objects.

Based on the data provided in Chapters 3, 4 and 5, in order to manufacture a QA phantom which is relevant at higher frequencies; a TMM should be developed to closely match the SoS and the attenuation of small animal soft tissue at these ultrasound frequencies. In order to produce a TMM suitable for high frequency QA phantoms some extra steps need to be taken. Firstly, based on the discussion in this chapter, a TMM with the required modification of the silicon carbide and aluminium oxide particles needs to be manufactured and its acoustic properties measured in order to compare these results with the small animal soft tissue acoustic properties measured in this thesis. This will corroborate the modification of the TMM recipe in order to match its acoustic properties to those of small animal soft tissue. To measure the acoustic properties of TMM samples, the use of the alternative measurement technique developed in Chapter 3 will be beneficial, as this method shows less variable measurements and better longitudinal acoustic stability for both the SoS and the attenuation coefficient values.

In summary, the acoustical data reported in this thesis from the IEC agar-TMM and from the small animal biological tissue extends the available information and understanding of the interaction of ultrasound with tissue and TMM structures to higher ultrasound frequencies. The data reported in this thesis will allow additional developments of QA phantom design for high frequency ultrasound applications.

APPENDICES

APPENDIX 1.

PAPERS PUBLISHED IN THE ULTRASOUND IN MEDICINE AND BIOLOGY JOURNAL REFERENCED AS RABELL-MONTIEL ET AL., (2017) AND RABELL-MONTIEL ET AL., (*2018*).

LIST OF PRESENTATIONS

JOURNAL PUBLICATIONS

- **Rabell Montiel, A**., Thomson, A. J. W., Pye, S. D., Anderson, T. A., & Moran, C. M. (2018). The acoustic properties of small animal soft tissue in the frequency range 12 – 32 MHz. *Ultrasound in Medicine & Biology*. doi.org/10.1016/j.ultrasmedbio.2017.11.003.
- **Rabell Montiel, A**., Browne, J. E., Pye, S. D., Anderson, T. A., & Moran, C. M. (2017). Broadband acoustic measurement of an agar-based tissue mimicking material: A longitudinal study. *Ultrasound in Medicine & Biology*, *43*(7), 1494–1505. doi:10.1016/j.ultrasmedbio.2017.02.019.

PROCEEDING PAPERS

- **Rabell-Montiel, A**., Thomson, A. J. W., Pye, S. D., Anderson, T. A., & Moran, C. M. (2017 b). The acoustical properties of brain, liver and kidney soft tissue from small anmals over the frequency range 12 – 32 MHz. In *2017 IEEE International Ultrasonics Symposium* Proceedings (Vol. 2017-Novem) doi:10.1109/ULTSYM.2017.8092756.
- **Rabell-Montiel, A**., Browne, J. E., Pye, S. D., Anderson, T. A., & Moran, C. M. (2016). The acoustical properties of IEC agar-based tissue mimicking material over the frequency range 4.5MHz to 50MHz – a longitudinal study. In *2016 IEEE International Ultrasonics Symposium Proceedings* (Vol. 2016–Novem, pp. 8–10). doi:10.1109/ULTSYM.2016.7728862.

CONFERENCE PRESENTATIONS

- **Rabell-Montiel, A**., Pye, S. D., Anderson, T. A., Browne, J. E., & Moran, C. M. Ultrasound acosutic properties of small animal soft tissue over the frequency range 12 – 32 MHz. *2017 XV Symposium of Mexican Studies and Students* oral presentation, Durham, UK.

- **Rabell-Montiel, A**., Pye, S. D., Anderson, T. A., Browne, J. E., & Moran, C. M. Measurement of the acoustical properties of tissue mimicking samples from 4.5 – 50 MHz – a comparisong of two measurement techniques. *2017 Institute of Physics and Engineering in Medicine (IPEM)*, oral presentation, York, UK.
- **Rabell-Montiel, A**., Pye, S. D., Anderson, T. A., Browne, J. E., & Moran, C. M. Measurement of the acosutical properties of tissue mimicking samples from 4.5 – 50 MHz – a comparison of two different measurement techniques. *2017 Scottish Ultrasound Annual Meeting* poster presentation, Edinburgh, UK.
- **Rabell-Montiel, A**., Pye, S. D., Anderson, T. A., Browne, J. E., & Moran, C. M. Acoustic measurements of small animal soft tissue at high ultrasound frequency. *2016 XIV Symposium of Mexican Studies and Students* oral presentation, Edinburgh, UK.
- **Rabell-Montiel, A**., Pye, S. D., Anderson, T. A., & Moran, C. M. The development of tissue mimicking phantoms for testing the performance of high resolution ultrasound scanners. *2016 International Conference on Ultrasonic Biomedical Microscanning (UBM)*, oral presentation by Dr. Carmel M Moran, Bonaire, Netherlands.
- **Rabell-Montiel, A**., Browne, J. E., Pye, S. D., Anderson, T. A., & Moran, C. M. Acoustical characterisation of an IEC agar based tissue-mimicking longitudinal stability over 1 year and initial measurements of small animal soft tissue using high resolution ultrasound. *2016 Translational Medicine Centre for Doctoral Ttraining (CDT) Student Conference,* poster presentation, Edinburgh, UK.
- **Rabell-Montiel, A**., Browne, J. E., Pye, S. D., Anderson, T. A., & Moran, C. M. The acoustic stability of an IEC agar based TMM over 1 year and initial measurements of small animal soft tissue using high resolution ultrasound. *2016 University of Edinburgh / British Heart Foundation Centre of Cardiovascular Science Symposium Day* poster presentation, Edinburgh, UK.
- **Rabell-Montiel, A**., Browne, J. E., Pye, S. D., Anderson, T. A., & Moran, C. M. High frequency measurement of the speed of sound and attenuation of small

animal soft tissue. *2015 British Medical Ultrasound Society (BMUS) annual meeting* poster presentation by Dr. Carmel M Moran, Cardiff, UK.

- **Rabell-Montiel, A**., Browne, J. E., Pye, S. D., Anderson, T. A., & Moran, C. M. Measurement of the acosutical properties of tissue mimicking samples measured and preserved in tissue mimicking maintenance fluid. *2015 University of Edinburgh / British Heart Foundation Centre of Cardiovascular Science Symposium Day* poster presentation, Edinburgh, UK.
- **Rabell-Montiel, A**., Pye, S. D., Anderson, T. A., & Moran, C. M. Measurement of the acosutical properties of tissue mimicking samples measured and preserved in tissue mimicking maintenance fluid. *2015 Institute of Physics and Engineering in Medicine (IPEM)*, oral presentation, York, UK.

COURSES ATTENDED

- Beginners Guide to Imaging for MVM, HSS, and SCE Students, Edinburgh, UK, 2015.

REFERENCES

Abu-Zidan, F. M., Hefny, A. F., & Corr, P. (2011). Clinical Ultrasound physics. *Journal of Emergencies, Trauma and Shock*, *4*(4), 501–503. doi:10.4103/0974

AIUM. (2014). *Methods for specifying acoustic properties of Tissue-Mimicking phantoms and objects*.

Al-Rawhani, M. A., Beeley, J., Chitnis, D., Collins, S., & Cumming, D. R. S. (2013). Sensors and Actuators B : Chemical Wireless capsule for autofluorescence detection in biological systems. *Sensors & Actuators: B. Chemical*, *189*, 203–207. doi:10.1016/j.snb.2013.03.037

Ali, M., Magee, D., & Dasgupta, U. (2008). Signal Processing Overview of Ultrasound Systems for Medical Imaging, (November), 1–27.

Azhari, H. (2010). Appendix A - Typical acoustic properties of tissues. In *Basics of Biomedical Ultrasound for Engineers* (pp. 313–314). John Wiley & Sons, Inc. doi:10.1002/9780470561478

Bamber, J. C. (1981). Ultrasonic attenuation in fress human tissues. *Letter to the Editor*, 187–188.

Bamber, J. C., Fry, M. J., Hill, C. R., & Dunn, F. (1977). Ultrasonic attenuation and backscattering by mammalian organs as a function of time after excision. *Ultrasound in Medicine & Biology*, *3*(1), 15–20. doi:10.1016/0301-5629(77)90116-8

Bamber, J. C., & Hill, C. R. (1979). Ultrasonic Attenuation and Propagation Speed in Mammalian Tissues as a Function of Temperature. *Ultrasound in Medicine & Biology Biology*, *5*, 149–157.

Bamber, J. C., & Hill, C. R. (1980). Acoustic Properties of Normal and Canceroues Human Liver -I. Dependence on Pathological Condition. *Ultrasound in Medicine & Biology*, *7*, 121–133.

Bamber, J. C., & Nassiri, D. K. (1985). Effect of Gaseous Inclusions on the Frequency

Dependence of Ultrasonic Attenuation in Liver. *Ultrasound in Medicine & Biology*, *11*(2), 293–298.

Banchhor, S. K., Araki, T., Londhe, N. D., Ikeda, N., Radeva, P., Elbaz, A., … Suri, J. S. (2016). Five multiresolution-based calcium volume measurement techniques from coronary IVUS videos: A comparative approach. *Computer Methods and Programs in Biomedicine*, *134*, 237–258. doi:10.1016/j.cmpb.2016.07.009

Barbosa, P., Berry, D. L., & Kary, C. S. (2014). Appendix Dissecting fluids and saline solutions. In *Insect Histology : Practical Laboratory Techniques* (First Edit., pp. 325–331). Wiley & Sons, Ltd. doi:10.1002/9781118876114.app1

Barrie Smith, N., & Webb, A. (2011). *Introduction to Medical Imaging: Physics, Engineering and Clinical* (First Edit.). Cambridge, UK: Cambridge University Press.

Beigi, P., Malenfant, P., Rasoulian, A., Rohling, R., Dube, A., & Gunka, V. (2017). Three-Dimensional Ultrasound-Guided real-time midline epidural needle placement with epiguide: A propsective feasibility study. *Ultrasound in Medicine and Biology*, *43*(1), 375–379. doi:10.1016/j.ultrasmedbio.2016.08.033

Bilaniuk, N., & Wong, G. S. K. (1992). Speed of sound in pure water as a function of temperature, *93*, 1609–1612.

Brewin, M., Pike, L. C., Rowland, D. E., & Birch, M. J. (2008). The acoustic properties, centered on 20 MHZ, of an IEC agar-based tissue-mimicking material and its temperature, frequency and age dependence. *Ultrasound in Medicine & Biology*, *34*(8), 1292–306. doi:10.1016/j.ultrasmedbio.2007.12.017

Brien, W. D. O. (1992). AAPM Tutorial. Single-Element Transducers. *Radriographics*, *13*(4), 947–957.

Bronez, M. A., Shung, K. K., Heidary, H., & Hurwitz, D. (1985). Measurement of Ultrasound Velocity in Tissues Utilizing a Microcomputer-Based System. *IEEE Transactions on Biomedical Engineering*, *BME-32*(9), 723–726. doi:10.1109/TBME.1985.325592

Browne, J. E., Ramnarine, K., Watson, A. J., & Hoskins, P. R. (2003). Assessment of the

acoustic properties of common tissue-mimicking test phantoms. *Ultrasound in Medicine & Biology*, *29*(7), 1053–1060. doi:10.1016/S0301-5629(03)00053-X

Butts, C. (2017). Ultrasound Predicts Cardiac Arrest Survival. *Emergency Medicine News*, (January), 2017.

Cabrelli, L. C., Pelissari, P. I. B. G. B., Deana, A. M., Carneiro, A. A. O., & Pavan, T. Z. (2017). Stable phantom materials for ultrasound and optical imaging. *Physics in Medicine and Biology*, *62*(2), 432. doi:10.1088/1361-6560/62/2/432

Cannon, L. M., Fagan, A. J., & Browne, J. E. (2011). Novel tissue mimicking materials for high frequency breast ultrasound phantoms. *Ultrasound in Medicine & Biology*, *37*(1), 122–35. doi:10.1016/j.ultrasmedbio.2010.10.005

Chen, C. F., Robinson, D. E., Wilson, L. S., Griffiths, K. A., Manoharan, A., & Doust, B. D. (1987). Clinical Sound Speed measurement in liver and spleen in vivo. *Ultrasonic Imaging*, *9*, 221–235.

Choices, N. (2012). *Liver disease deaths "up by 25%." NHS*. Retrieved July 4, 2017, from http://www.nhs.uk/news/2012/03march/Pages/liver-disease-death-alcohol-increase.aspx

Civale, J., Rivens, I., ter Haar, G., Morris, H., Coussios, C., Friend, P., & Bamber, J. (2013). Calibration of ultrasound backscatter temperature imaging for high-intensity focused ultrasound treatment planning. *Ultrasound in Medicine and Biology*, *39*(9), 1596–1612. doi:10.1016/j.ultrasmedbio.2013.04.001

Cook, J. R., Bouchard, R. R., & Emelianov, S. Y. (2011). Tissue-mimicking phantoms for photoacoustic and ultrasonic imaging. *Biomedical Optics Express*, *2*(11), 3193–206. doi:10.1364/BOE.2.003193

Coppens, A. B. (1981). Simple equations for the speed of sound Neptunin waters. *J Acoust Soc*, *69*, 862–863.

Culjat, M. O., Goldenberg, D., Tewari, P., & Singh, R. S. (2010). A review of tissue substitutes for ultrasound imaging. *Ultrasound in Medicine & Biology*, *36*(6), 861–73. doi:10.1016/j.ultrasmedbio.2010.02.012

Degos, F., Perez, P., Roche, B., Mahmoudi, A., Asselineau, J., Voitot, H., & Bedossa, P. (2010). Diagnostic accuracy of FibroScan and comparison to liver fibrosis biomarkers in chronic viral hepatitis: A multicenter prospective study (the FIBROSTIC study). *Journal of Hepatology*, *53*(6), 1013–1021. doi:10.1016/j.jhep.2010.05.035

Del Grosso, V. A., & Mader, C. W. (1972). Speed of Sound in Pure Water. *J Acoust Soc*, *52*, 1442–1446.

Dixon, S. (2015). *Diagnostic Imaging Dataset Statistical Release*. *NHS England*. Retrieved from https://www.england.nhs.uk/statistics/wp-content/uploads/sites/2/2015/08/Provisional-Monthly-Diagnostic-Imaging-Dataset-Statistics-2016-03-17.pdf

Duck, F. A. (2012). *Physical Properties of Tissues. A Comprehensive Reference Book* (Re-publish.). Bath, England: Academic Press.

Dunmire, B., Kucewicz, J. C., Mitchell, S. B., Crum, L. A., & Sekins, K. M. (2013). Characterizing an Agar/Gelatin phantom for image guided dosing and feedback control of high-intensity focused ultrasound. *Ultrasound in Medicine and Biology*, *39*(2), 300–311. doi:10.1016/j.ultrasmedbio.2012.09.016

Dunne, R. M., O'Neill, A. C., & Tempany, C. M. (2017). Imaging Tools in Human Research : Focus on Image-Guided Intervention. In *Clinical and Translational Science* (pp. 181–190). Elsevier Inc. doi:10.1016/B978-0-12-802101-9.00010-7

Dymling, S. O., Persson, H. W., & Hertz, H. C. (1991). Measurement of Blood Perfusion in Tissue using Dopper Ultrasound. *Ultrasound in Medicine & Biology*, *17*(5), 433–444.

Edgeworth, A. L., Anderson, T., Ross, J. a., Ansell, I. F., Butler, M., Norrie, L., … Moran, C. (2009). Strength of attachment of an in-house, microbubble, ultrasound contrast agent. *Ultrasonics Symposium (IUS), 2009 IEEE International*, 1262–1265.

Fabiani, A., Dreas, L., & Sanson, G. (2017). Ultrasound-guided deep-arm veins insertion of long peripheral catheters in patients with difficult venous access

after cardiac surgery. *Heart and Lung The Journal of Acute and Critical Care*, *46*(1), 46–53. doi:10.1016/j.hrtlng.2016.09.003

Ferguson, W. (2012). Insulin by ultrasound. *NewScientist*, 20. doi:10.1016/S0262-4079(12)61610-8

Filoux, E., Mamou, J., Moran, C., Pye, S. D., & Ketterling, J. A. (2012). Correspondence-Characterization of the effective performance of a high-frequency annular-array-based imaging system using anechoic-pipe phantoms. *IEEE Transactions on Ultrasonics, Ferroelectrics, and Frequency Control*, *59*(12), 2825–2830. doi:10.1109/TUFFC.2012/2525

Foster, F. S., Hossack, J., & Adamson, S. L. (2011). Micro-ultrasound for preclinical imaging. *Interface Focus*, *1*(June), 576–601.

Foster, F. S., & Hunt, W. (1979). Transmission of Ultrasound Beams through Human Tissue - Focussing and Attenuation studies. *Ultrasound in Medicine and Biology*, *5*(1973), 257–268.

Foster, F. S., Pavlin, C. J., Harasiewicz, K. A., Christopher, D. A., & Turnbull, D. H. (2000). Advances in ultrasound biomicroscopy. *Ultrasound in Medicine and Biology*, *26*(1), 1–27. doi:10.1016/S0301-5629(99)00096-4

Foster, F. S., Strban, M., & Austin, G. (1984). The Ultrasound Macroscope: Initial studies of breast tissue. *Ultrasonic Imaging*, *6*, 243–261.

Franceschini, E., Pognonec, P., Guillet, B., Pourcher, T., Universit, A. M., & Marseille, C. (2016). Polydisperse Structure Factor Model for understanding the ultrasonic scattering from apoptotic cells. In *2016 IEEE International Ultrasonics Symposium Proceedings* (pp. 8–11).

Fraser, K. H., Poepping, T. L., McNeilly, A., Megson, I. L., & Hoskins, P. R. (2006). Acoustic speed and attenuation coefficient in sheep aorta measured at 5-9 MHz. *Ultrasound in Medicine and Biology*, *32*(6), 971–980. doi:10.1016/j.ultrasmedbio.2006.02.1417

Freese, M., & Lyons, E. A. (1977). Ultrasonic backscatter from human liver tissue: Its dependence on frequency and protein/lipid composition. *Journal of Clinical*

Ultrasound, *5*(5), 307–312. doi:10.1002/jcu.1870050504

Frizzel, L. A., & Gindorf, J. D. (1981). Measurement of Ultrasonic Velocity in Several Biological Tissues. *Ultrasound in Medicine and Biology*, *7*(4), 385–387.

Fujii, Y., Taniguchi, N., Itoh, K., Shigeta, K., Wang, Y., Tsao, J., … Itoh, T. (2002). A New Method for Attenuation Coefficient Measurement in the Liver. *Journal Ultrasound Medicine*, *21*, 783–788.

Gammell, P. M., Croissette, D. H. L. E., & Heyser, R. C. (1979). Temperature and frequency dependence of ultrasonic attenaution in selected tissues. *Ultrasound in Medicine and Biology*, *5*, 269–277.

Garcia-Duitama, J., Chayer, B., Goussard, Y., & Cloutier, G. (2016). Segmentation of blood layers with particle image velocimetry (PIV) for reproducible in vivo characterization of erythrocyte aggregation. In *2016 IEEE International Ultrasonics Symposium Proceedings* (pp. 1–4).

Garra, B. S., Shawker, T. H., Nassi, M., & Russell, M. A. (1984). Ultrasound Attenuation measurements of the Liver In Vivo using a commercial sector scanner. *Ultrasonic Imaging*, *6*, 396–407.

Gennisson, J. L., Grenier, N., Combe, C., & Tanter, M. (2012). Supersonic Shear Wave Elastography of In Vivo Pig Kidney: Influence of Blood Pressure, Urinary Pressure and Tissue Anisotropy. *Ultrasound in Medicine and Biology*, *38*(9), 1559–1567. doi:10.1016/j.ultrasmedbio.2012.04.013

Gettings, J. W., Jobling, P. L., & Wyn-Jones, E. (1977). Ultrasonic Relaxation Spectra of Agarose Sols and Gels. *Journal of Chemical Society*, (2321240), 1246–1252.

Ghoshal, G., Luchies, A. C., Blue, J. P., & Oelze, M. L. (2011). Temperature dependent ultrasonic characterization of biological media. *The Journal of the Acoustical Society of America*, *130*(4), 2203. doi:10.1121/1.3626162

Gibbs, V., Cole, D., & Sassano, A. (2011). *Ultrasound Physics and Technology E-book: How, Why and When*. Elsevier Health Sciences.

Giuliani, M., Rinaldi, P., Rella, R., Fabrizi, G., Petta, F., Carlino, G., … Bonomo, L.

(2017). The impact of needle size in US-guided Core-Needle Breast Biopsy: comparison of 14-, 16- and 18-gauge needles. *Clinical Breast Cancer*. doi:10.1016/j.clbc.2017.02.008

Goldman, D. E., & Richards, J. R. (1954). Measurement of high-frequency sound velocity in mammalian soft tissues. *The Journal of the Acoustical Society of America*, *26*(6), 981–983. doi:10.1121/1.1907465

Goss, S. A., Frizzell, L. A., & Dunn, F. (1979). Ultrasonic absorption and attenuation in mammalian tissues. *Ultrasound in Medicine and Biology*, *5*(2), 181–186. doi:10.1016/0301-5629(79)90086-3

Goss, S. A., Johnston, R. L., & Dunn, F. (1980). Compilation of emperical ultrasonic properties of mammalian tissues. II. *J. Acoust. Soc. Am.*, *68(1)*(July), 93–99?? doi:10.1121/1.384509

Gray, G. A., White, C. I., Thomson, A., Kozak, A., Moran, C., & Jansen, M. A. (2013). Imaging the healing murine myocardial infarct in vivo: ultrasound, magnetic resonance imaging and fluorescence molecular tomography. *Experimental Physiology*, *98*(3), 606–13. doi:10.1113/expphysiol.2012.064741

Grenier, N., Gennisson, J. L., Cornelis, F., Le Bras, Y., & Couzi, L. (2013). Renal ultrasound elastography. *Diagnostic and Interventional Imaging*, *94*(5), 545–550. doi:10.1016/j.diii.2013.02.003

Gunawan, A. I., Hozumi, N., Yoshida, S., Saijo, Y., Kobayashi, K., & Yamamoto, S. (2015). Numerical analysis of ultrasound propagation and reflection intensity for biological acoustic impedance microscope. *Ultrasonics*, *61*, 79–87. doi:10.1016/j.ultras.2015.03.010

Hill, C. R. (1986). *Physical Principles of Medical Ultrasonics* (1st editio.). Ellis Horwood.

Hoskins, P. R., Thrush, A., Martin, K., & Whittingham, T. A. (Eds.). (2003). *Diagnostic ultrasound. Physics and Equipment*. Greenwich Medical Media Limited.

IEC. European Standard. British Standard. (2001). Ultrasonics. Flow measurement systems. Flow test object.

Inglis, S., Janeczko, A., Ellis, W., Plevris, J. N., & Pye, S. (2014). Assessing the Imaging Capabilities of Radial Mechanical and Electronic Echo-endoscopes Using the Resolution Integral. *Ultrasound in Medicine & Biology*, *40*(8), 1896–907. doi:10.1016/j.ultrasmedbio.2014.02.009

Inglis, S., Ramnarine, K., Plevris, J. N., & McDicken, W. N. (2006). An anthropomorphic tissue-mimicking phantom of the oesophagus for endoscopic ultrasound. *Ultrasound in Medicine and Biology*, *32*(2), 249–59. doi:10.1016/j.ultrasmedbio.2005.10.005

Insana, M. F., & Hall, T. J. (1990). Characterising the microstructure of random media using ultrasound. *Physics in Medicine and Biology*, *35*(10), 1373–86. doi:10.1088/0031-9155/35/10/003

Insana, M. F., Wood, J. G., & Hall, T. J. (1992). Indentifying acoustic scattering sources in normal renal parenchyma in vivo by varying arterial and ureteral pressures. *Ultrasound in Medicine and Biology*, *17*(2), 179–185. doi:10.1016/0301-5629(91)90125-G

Ishii, M., Takeno, S., Nashida, T., Nanashima, A., Kubota, Y., Kawakami, H., … Akiyama, Y. (2017). Thoracoscopic enucleation in the left decubitus position for leiomyoma of the upper thoracic esophagus : utility of preoperative diagnosis applying endoscopic ultrasound-guided fine needle aspiration. *International Journal of Surgery Case Reports*. doi:10.1016/j.ijscr.2017.03.007

Ito, K., Yoshida, K., Maruyama, H., Mamou, J., & Yamaguchi, T. (2017). Acoustic Impedance Analysis with High-Frequency Ultrasound for Identification of Fatty Acid Species in the Liver. *Ultrasound in Medicine and Biology*, *43*(3), 700–711. doi:10.1016/j.ultrasmedbio.2016.11.011

Itoh, S. T., Jing-wen, S. T., & Konishi, S. T. (1988). Studies on Frequency-Dependent Attenuation in the Normal Liver and Spleen and in Liver Diseases, Using the Spectral-Shift Zero-Crossing Method. *Journal of Clinical Ultrasound*, *16*(October), 553–562.

Kagadis, G. C., Loudos, G., Langer, S. G., & Nikiforidis, G. C. (2010). In vivo small

animal imaging: Current status and future prospects. *Med. Phys*, *37*(12), 6421–6442. doi:10.1118/1.3515456

Karmakar, M. K., & Kwok, W. H. (2015). *Ultrasound-guided regional Anaesthesia*. *Clinical Gate. Anaesthesiology*. Retrieved June 4, 2017, from https://clinicalgate.com/ultrasound-guided-regional-anesthesia/

Kaster, T., Sack, I., & Samani, A. (2011). Measurement of the hyperelastic properties of ex vivo brain tissue slices. *Journal of Biomechanics*, *44*(6), 1158–1163. doi:10.1016/j.jbiomech.2011.01.019

Kenwright, D. A., Sadhoo, N., Rajagopal, S., Anderson, T., Moran, C. M., Hadoke, P. W., … Hoskins, P. R. (2014). Acoustic Assessment of a Konjac–Carrageenan Tissue-Mimicking Material at 5–60 MHz. *Ultrasound in Medicine & Biology*, *40*(12), 2895–2902. doi:10.1016/j.ultrasmedbio.2014.07.006

King, D. M., Moran, C., McNamara, J. D., Fagan, A. J., & Browne, J. (2011). Development of a Vessel-Mimicking Material for use in Anatomically Realistic Doppler Flow Phantoms. *Ultrasound in Medicine and Biology*, *37*(5), 813–826. doi:10.1016/j.ultrasmedbio.2011.02.012

Kips, J. G., Segers, P., & Bortel, L. M. Van. (2008). Identifying the vulnerable plaque : A review of invasive and non-invasive imaging modalities. *Artery Research*, *2*, 21–34. doi:10.1016/j.artres.2007.11.002

Kofler, J. M. (2001). Quality assurance of ultrasound imagers: procedures, expectations, and philosophies. *AAPM 43rd Annual Meeting of the American …*, 1–37. Retrieved from http://www.aapm.org/meetings/2001am/pdf/7194-74902.pdf

Kremkau, F. W., Barnes, R. W., & McGraw, C. P. (1981). Ultrasonic attenuation and propagation speed in normal human brain. *Journal of the Acoustical Society of America*, *70*(July), 29–38.

Kuang, Y., Hilgers, A., Sadiq, M., Cochran, S., Corner, G., & Huang, Z. (2016). Modelling and characterisation of a ultrasound-actuated needle for improved visibility in ultrasound-guided regional anaesthesia and tissue biopsy.

Ultrasonics, *69*, 38–46. doi:10.1016/j.ultras.2016.02.018

Kumagai, H., Yokoyama, K., Katsuyama, K., Hara, S., Yamamoto, H., Yamagata, T., … Itoh, K. (2014). A New Method for Measuring the Speed of Sound in Rat Liver ex Vivo Using an Ultrasound System: Correlation of Sound Speed with Fat Deposition. *Ultrasound in Medicine & Biology*, 1–9. doi:10.1016/j.ultrasmedbio.2014.03.019

Law, W. K., Frizzell, L. A., & Dunn, F. (1985). Determination of the nonlinearity parameter B/A of biological media. *Ultrasound in Medicine and Biology*, *11*(2), 307–318. doi:10.1016/0301-5629(85)90130-9

Lay, H., Cox, B., Sunoqrot, M., Demore, C. E. M., Näthke, I., Gomez, T., & Cochran, S. (2016). Microultrasound characterisation of ex vivo porcine tissue for ultrasound capsule endoscopy. *Journal of Physics: Conference Series*, *797*. doi:10.1088/1742-6596/755/1/011001

Lee, W., Lee, S. D., Park, M. Y., Foley, L., Purcell-Estabrook, E., Kim, H., … Yoo, S.-S. (2016). Image-Guided Focused Ultrasound-Mediated regional brain stimulation in sheep. *Ultrasound in Medicine and Biology*, *42*(2), 459–470. doi:10.1016/j.ultrasmedbio.2015.10.001

Liu, X. Z., Gong, X. F., Zhang, D., Ye, S. G., & Rui, B. (2006). Ultrasonic characterization of porcine liver tissue at frequency between 25 to 55 MHz. *World Journal of Gastroenterology*, *12*(14), 2276–2279.

Liu, Y. L., Li, G. Y., He, P., Mao, Z. Q., & Cao, Y. (2017). Temperature-dependent elastic properties of brain tissues measured with the shear wave elastography method. *Journal of the Mechanical Behavior of Biomedical Materials*, *65*(July 2016), 652–656. doi:10.1016/j.jmbbm.2016.09.026

Lizzi, F. L., Greenebaum, M., Feleppa, E. J., & Elbaum, M. (1983). Theoretical framweok for spectrum analysis in ultrasonic tissue characterisation. *Journal of the Acoustical Society of America*, *73*(4).

López-Haro, S. A., Leija, L., Favari, L., & Vera, A. (2009). Measurement of ultrasonic properties into biological tissues in the hyperthermia temperature range. In

International Congress on Ultrasonics (Vol. 3, pp. 551–558). Elsevier. doi:10.1016/j.phpro.2010.01.071

Lu, Z. F., Zagzebski, J. A., & Lee, F. T. (1999). Ultrasound Bacscatter and Attenuation in Human Liver with diffuse disease. *Ultrasound in Medicine and Biology*, *25*(7), 1047–1054.

Ludwig, G. D. (1950). The Velocity of Sound through Tissues and the Acoustic Impedance of Tissues. *Journal of the Acoustical Society of America*, *22*(6), 862–866.

MacGillivray, T. J., Ellis, W., & Pye, S. (2010). The resolution integral: visual and computational approaches to characterizing ultrasound images. *Physics in Medicine and Biology*, *55*(17), 5067–88. doi:10.1088/0031-9155/55/17/012

Machet, L., Belot, V., Naouri, M., Boka, M., Mourtada, Y., Giraudeau, B., … Vaillant, L. (2009). Preoperative Measurement of Thickness of Cutaneous Melanoma Using High-Resolution 20 MHz Ultrasound Imaging: A Monocenter Prospective Study and Systematic Review of the Literature. *Ultrasound in Medicine and Biology*, *35*(9), 1411–1420. doi:10.1016/j.ultrasmedbio.2009.03.018

Madsen, E. L., Dong, F., Frank, G. R., Garra, B. S., Wear, K. a, Wilson, T., … Miller, J. G. (1999). Interlaboratory comparison of ultrasonic backscatter, attenuation, and speed measurements. *Journal of Ultrasound in Medicine : Official Journal of the American Institute of Ultrasound in Medicine*, *18*, 615–631. doi:10478971

Madsen, E. L., Hobson, M. A., Shi, H., Varghese, T., & Frank, G. R. (2005). Tissue-mimicking agar/gelatin materials for use in heterogeneous elastography phantoms. *Physics in Medicine and Biology*, *50*(23), 5597–618. doi:10.1088/0031-9155/50/23/013

Madsen, E. L., Zagzebski, J. A., Benjavie, R. A., & Jutila, R. E. (1978). Tissue mimicking materials for ultrasound phantoms. *Med. Phys*, *5*(5), 391–394.

Mahboob, S., McPhillips, R., Qiu, Z., Jiang, Y., Meggs, C., Schiavone, G., … Eljamel, S. (2016). Intraoperative Ultrasound-Guided Resection of Gliomas: A Meta-Analysis and Review of the Literature. *World Neurosurgery*, *92*, 255–263. doi:10.1016/j.wneu.2016.05.007

Maklad, N. F., Ophir, J., & Balsara, V. (1984). Attenuation of Ultrasound in normal Liver and difusse liver disease in vivo. *Ultrasonic Imaging*, *6*, 117–125.

Manickam, K., Machireddy, R. R., & Seshadri, S. (2014a). Characterization of biomechanical properties of agar based tissue mimicking phantoms for ultrasound stiffness imaging techniques. *Journal of the Mechanical Behavior of Biomedical Materials*, *35*, 132–143. doi:10.1016/j.jmbbm.2014.03.017

Manickam, K., Machireddy, R. R., & Seshadri, S. (2014b). Study of ultrasound stiffness imaging methods using tissue mimicking phantoms. *Ultrasonics*, *54*(2), 621–631. doi:10.1016/j.ultras.2013.08.018

Martial, J., & Cachard, C. (2007). Acquire real-time RF digital ultrasound data from a commercial scanner. *Electronic Journal Technical Accoustics*, *3*, 1–16.

Martínez-Valdez, R., Contreras, M. V. H., Vera, A., & Leija, L. (2015). Sound speed measurement of chicken liver from 22°C to 60°C. In *International Congress on Ultrasonics* (Vol. 70, pp. 1260–1263). Elsevier B.V. doi:10.1016/j.phpro.2015.08.280

Maxwell, A. D., Wang, T.-Y., Yuan, L., Duryea, A. P., Xu, Z., & Cain, C. a. (2010). A tissue phantom for visualization and measurement of ultrasound-induced cavitation damage. *Ultrasound in Medicine & Biology*, *36*(12), 2132–43. doi:10.1016/j.ultrasmedbio.2010.08.023

McDicken. (1991). *Diagnostic Ultrasonics* (Third Edit.). Churchill Livingstone.

Meagher, S., Poepping, T. L., Ramnarine, K., Black, R. A., & Hoskins, P. (2007). Anatomical flow phantoms of the nonplanar carotid bifurcation, part II: experimental validation with Doppler ultrasound. *Ultrasound in Medicine & Biology*, *33*(2), 303–10. doi:10.1016/j.ultrasmedbio.2006.08.004

Memon, F., Touma, G., Wang, J., Baltsavias, S., Moini, A., Chang, C., … Khuri-yakub, B. T. (2015). Capsule Ultrasound Device. In *IEEE International Ultrasonics Symposium Proceedings*.

Memon, F., Touma, G., Wang, J., Baltsavias, S., Moini, A., Chang, C., … Khuri-yakub, B. T. (2016). Capsule Ultrasound Device: Further Developments. In *IEEE International Ultrasonics Symposium Proceedings*.

Menace, C., Choquet, O., Abbal, B., Bringuier, S., & Capdevila, X. (2016). Comparison of a GPS needle-tracking system, multiplanar imaging and 2D imaging for real-time ultrasound-guided epidural anaesthesia : A randomized , comparative , observer-blinded study on phantoms. *Societe Francaise d'Anaesthesie et de Reanimation*. doi:10.1016/j.accpm.2016.05.002

Min Joo, C., Sitaramenjaneya Reddy, G., Kang Il, L., Dong Guk, P., & Coleman, A. (2013). A Tissue Mimicking Polyacrulamide Hydrogel Phantom for Visualizing Thermal Lesions Generated by High Intensity focused Ultrasoind. *Ultrasound in Medicine and Biology*, *39*(3), 439–448.

Moran, C., Ellis, W., Janeczko, A., Bell, D., & Pye, S. (2011). The Edinburgh Pipe Phantom: characterising ultrasound scanners beyond 50 MHz. *Journal of Physics: Conference Series*, *279*, 12008. doi:10.1088/1742-6596/279/1/012008

Moran, C. M., Ellis, B., Janeczko, A., Bell, D., & Pye, S. (2009). 1406: The Edinburgh Pipe Phantom: Characterising Ultrasound Scanners up to 60MHz. *Ultrasound in Medicine & Biology*, *35*(8), S209–S210. doi:10.1016/j.ultrasmedbio.2009.06.792

Moran, C. M., Inglis, S., & Pye, S. D. (2014). The Resolution Integral - a tool for characterising the performance of diagnostic ultrasound scanners. *Ultrasound*, *22*(1), 37–43. doi:10.1177/1742271X13518202

Moran, C., Pye, S., Ellis, W., Janeczko, A., Morris, K., McNeilly, A. S., & Fraser, H. (2011). A comparison of the imaging performance of high resolution ultrasound scanners for preclinical imaging. *Ultrasound in Medicine and Biology*, *37*(3), 493–501. doi:10.1016/j.ultrasmedbio.2010.11.010

Morin, F., Courtecuisse, H., Reinertsen, I., Lann, F. Le, Palombi, O., Payan, Y., & Chabanas, M. (2017). Brain-shift compensation using intraoperative ultrasound and constraint-based biomechanical simulation. *Medical Image Analysis*, *40*. doi:https://doi.org/10.1016/j.media.2017.06.003

Muleki-Seya, P., Guillermin, R., Guglielmi, J., Chen, J., Pourcher, T., Konofagou, E., & Franceschini, E. (2016). High Frequency Quantitative Ultrasound Spectroscopy of Excised Canine Livers and Mouse Tumors using the Structure Factor Model.

In *IEEE Transactions on Ultrasonics, Ferroelectrics, and Frequency Control* (Vol. 3010, pp. 1–1). doi:10.1109/TUFFC.2016.2563169

O'Brien, W. D. (1988). Ultrasonic propagation properties (@100MHz) in excessively fatty rat liver. *Journal of the Acoustical Society of America*, *83*(3), 1159–1166.

Ophir, J., Shawker, T. H., Maklad, N. F., Miller, J. G., Flax, S. W., Narayana, P. A., & Jones, J. P. (1984). Attenuation estimation in reflection: Progress and Prospects. *Ultrasonic Imaging*, *6*, 349–395.

Ophuis, C. M. C. O., Verhoef, C., Grünhagen, D. J., Siegel, P., Shoengen, A., Röwert-Huber, J., … van Akkooi, A. C. J. (2017). Long-term results of ultrasound guided fine needle aspiration cytology in conjunction with sentinel node biopsy support step-wise approach in melanoma. *EJSO The Journal of Cancer Surgery*, 1–8. doi:10.1016/j.ejso.2017.02.009

Otto, C. M. (2013). *Textbook of Clinical Echocardiography* (5th ed.). Philadelphia: Elsevier/Saunders.

Palabiyik, F. B., Inci, E., Turkay, R., & Bas, D. (2017). Evaluation of Liver, Kidney, and Spleen Elasticity in Healthy Newborns and Infants Using Shear Wave Elastography. *Journal of Ultrasound in Medicine*. doi:10.1002/jum.14202

Parker, K. J. (1983). Ultrasonic attenuation and absorption in liver tissue. *Ultrasound in Medicine and Biology*, *9*(4), 363–369. doi:10.1016/0301-5629(83)90089-3

Parker, K. J., Asztely, M. S., Lerner, R. M., Schenk, E. A. H., & Waag, R. C. (1988). In-vivo measurements of ultrasound attenuation in normal or diseased liver. *Ultrasound in Medicine and Biology*, *14*(2), 127–136.

Pavan, T. Z., Madsen, E. L., Frank, G. R., Jiang, J., Carneiro, A. A. O., & Hall, T. J. (2013). A nonlinear elasticity phantom containing spherical inclusions. *Physics in Medicine and Biology*, *57*(15), 4787–4804. doi:10.1088/0031-9155/57/15/4787.A

Pinkerton, J. M. M. (1949). The Absorption of Ultrasonic Waves in Liquids and its Relation to Molecular Constitution. *Proceedings of the Physical Society*, *Section B*, 129–141.

Pinton, G., Aubry, J.-F., Fink, M., & Tanter, M. (2011). Effects of nonlinear ultrasound propagation on high intensity brain therapy. *Medical Physics*, *38*(3), 1207–1216. doi:10.1118/1.3531553

Pye, S., & Ellis, W. (2011). The Resolution Integral as a metric of performance for diagnostic grey-scale imaging. *Journal of Physics: Conference Series*, *279*, 12009. doi:10.1088/1742-6596/279/1/012009

Pye, S., Ellis, W., & MacGillivray, T. (2004). Medical ultrasound: a new metric of performance for grey-scale imaging. *Journal of Physics: Conference Series*, *1*, 187–192. doi:10.1088/1742-6596/1/1/041

Rabell-Montiel, A., Browne, J. E., Pye, S. D., Anderson, T. A., & Moran, C. M. (2016). The acoustical properties of IEC agar-based tissue mimicking material over the frequency range 4.5MHz to 50MHz – a longitudinal study. In *2016 IEEE International Ultrasonics Symposium Proceedings* (Vol. 2016–Novem, pp. 8–10). doi:10.1109/ULTSYM.2016.7728862

Rabell Montiel, A., Browne, J. E., Pye, S. D., Anderson, T. A., & Moran, C. M. (2017). Broadband Acoustic Measurement of an Agar-Based Tissue-Mimicking-Material: A Longitudinal Study. *Ultrasound in Medicine and Biology*, *43*(7), 1494–1505. doi:10.1016/j.ultrasmedbio.2017.02.019

Rabell-Montiel, A., Thomson A. J. W., Pye, S. D., Anderson, T. A., & Moran, C. M. (2017 b). The acoustical properties brain, liver and kidney soft tissue from small animals over the frequency range 12 - 33 MHz. In *2017 IEEE International Ultrasonics Symposium Proceedings* (Vol. 2017–Novem, pp. 1–4). doi:10.1109/ULTSYM.2017.8092756

Rabell Montiel, A., Thomson A. J. W., Pye, S. D., Anderson, T. A., & Moran, C. M. (2018). Acoustic Properties of Small Animal Soft Tissue in the Frequency Range 12–32 MHz. *Ultrasound in Medicine and Biology*, *44*(3), 708-713. doi:10.1016/j.ultrasmedbio.2017.11.003

Rajagopal, S., Sadhoo, N., & Zeqiri, B. (2014). Reference Characterisation of Sound Speed and Attenuation of the IEC Agar-Based Tissue-Mimicking Material Up to

a Frequency of 60 MHz. *Ultrasound in Medicine & Biology*, *41*(1), 317–333. doi:10.1016/j.ultrasmedbio.2014.04.018

Rajagopalan, B., Greenleaf, J. F., Thomas, P. J., Johnson, S. A., & Bahn, R. C. (1979). Variation of acoustic speed with temperature in various excised human tissues studied by ultrasound computerized tomography. *Ultrasonic Tissue Characterization II*, *525*, 227–233.

Raju, P. K. B. C., & Grant, C. R. K. (2016). Practical aspects of ultrasound-guided regional anaesthesia. *Anaesthesia and Intensive Care Medicine*, *17*(4), 171–174. doi:10.1016/j.mpaic.2015.12.010

Ramnarine, K., Anderson, T., & Hoskins, P. (2001). Construction and Geometric stability of physiological flow rate wall-less stenosis phantoms. *Ultrasound in Medicine and Biology*, *27*(2), 245–250.

Rhee, S. (2007). High frequency (IVUS) ultrasound transducer technology - applications and challenges. In *IEEE International Symposium on the Applications of Ferroelectrics* (pp. 856–857).

Rohrbach, D., Reisner, A. S., Wen, Q., Mcfadden, S. A., Silverman, R. H., Hoang, Q. V, & Mamou, J. (2016). Microstructural Assessment of the Guinea Pig Sclera Using Quantitative Acoustic Microscopy. In *2016 IEEE International Ultrasonics Symposium Proceedings*.

Ross, K. A., Pyrak-Nolte, L. J., & Campanella, O. H. (2006). The effect of mixing conditions on the material properties of an agar gel - Microstructural and macrostructural considerations. *Food Hydrocolloids*, *20*(1), 79–87. doi:10.1016/j.foodhyd.2005.01.007

Saijo, Y., Tanaka, M., Okawai, H., Sasaki, H., Nitta, S.-I., & Dunn, F. (1997). Ultrasonic tissue characterization of infarcted myocardium by scanning acoustic microscopy. *Ultrasound in Medicine & Biology*, *23*(1), 77–85. doi:10.1016/S0301-5629(96)00174-3

Sarvazyan, A. P., & Klemin, V. A. (1983). Study of Ultrasonic Topography of the Kidney. In *Ultrasound Interactions in Biology and Medicine*. Plenum Press, New

York.

Schiavone, G., Jones, T., Price, D., Mcphillips, R., Jiang, Y., Qiu, Z., … Desmulliez, M. P. Y. (2015). A highly compact packaging concept for ultrasound transducer arrays embedded in neurosurgical needles. *Microsystem Technologies*. doi:10.1007/s00542-015-2775-1

Schmitt, C., Hadj Henni, A., & Cloutier, G. (2010). Ultrasound dynamic micro-elastography applied to the viscoelastic characterization of soft tissues and arterial walls. *Ultrasound in Medicine & Biology*, *36*(9), 1492–503. doi:10.1016/j.ultrasmedbio.2010.06.007

Sehgal, C. ., Brown, G. M., Bahn, R. C., & J.F., G. (1986). Measurement and use of acoustic nonlinearity and sound speed to estimate composition of excised livers. *Ultrasound in Medicine & Biology*, *12*(11), 865–874.

Stirman, J. (2013). *Scattering in tissue*. *Labrigger*. Retrieved September 27, 2017, from http://labrigger.com/blog/2013/05/06/scattering-in-tissue/

Strowitzki, M., Brand, S., & Jenderka, K.-V. (2007). Ultrasonic radio-frequency spectrum analysis of normal brain tissue. *Ultrasound in Medicine & Biology*, *33*(4), 522–9. doi:10.1016/j.ultrasmedbio.2006.09.004

Sun, C. (2012). *Acoustic characterisation of ultrasound contrast agents at high frequency*. University of Edinburgh.

Sun, C., Pye, S., Browne, J., Janeczko, A., Ellis, B., Butler, M., … Moran, C. (2012). The Speed of Sound and Attenuation of an IEC Agar-Based Tissue-Mimicking Material for High Frequency Ultrasound Applications. *Ultrasound in Medicine and Biology*, *38*(7), 1262–1270. doi:10.1016/j.ultrasmedbio.2012.02.030

Sun, C., Pye, S., Janeczko, A., Ellis, B., Brewin, M., Butler, M., … Moran, C. (2011). The acoustic attenuation of an IEC agar-based tissue-mimicking material measured at 12-47 MHz. *2011 IEEE International Ultrasonics Symposium Proceedings*, 1376–1378.

Sun, L., Lien, C. L., Xu, X., & Shung, K. K. (2008). In Vivo Cardiac Imaging of Adult Zebrafish Using High Frequency Ultrasound (45-75 MHz). *Ultrasound in*

Medicine and Biology, *34*(1), 31–39. doi:10.1016/j.ultrasmedbio.2007.07.002

Sundholm, J. K. M., Olander, R. F. W., Ojala, T. H., Andersson, S., & Sarkola, T. (2015). Feasibility and precision of transcutaneous very-high resolution ultrasound for quantification of arterial structures in human neonates - Comparison with conventional high resolution vascular ultrasound imaging. *Atherosclerosis*, *239*(2), 523–527. doi:10.1016/j.atherosclerosis.2015.02.016

Suomi, V., Han, Y., Konofagou, E., & Cleveland, R. O. (2016). The effect of temperature dependent tissue parameters on acoustic radiation force induced displacements. *Physics in Medicine and Biology*, *61*(20), 7427–7447. doi:10.1088/0031-9155/61/20/7427

Szabo, T. L. (2014). Scattering From Tissue and Tissue Characterization. In *Diagnostic Ultrasoind Imaging: Inside Out* (2nd editio., pp. 295–363). Boston, MA, USA: Academic Press. doi:10.1016/B978-0-12-396487-8.00009-4

Taylor, K. J. W., Riely, C. A., Hammers, L., Flax, S., Garcia-Tsao, G., Conn, H. O., … Barwick, K. W. (1986). Quantitative US Attenuation in Normal Liver and in Patients with Diffuse Liver Disease: Importance of Fat. *Radiology*, *66*, 65–71.

Teirlinck, C. J., Bezemer, R. a, Kollmann, C., Lubbers, J., Hoskins, P., Ramnarine, K., … Schaarschmidt, U. G. (1998). Development of an example flow test object and comparison of five of these test objects, constructed in various laboratories. *Ultrasonics*, *36*(1–5), 653–60.

Tervola, K. M. U., Foster, S. G., & O'brien, W. D. (1985). Attenuation Coefficient Measurement Technique at 100 MHz with the Scanning Laser Acoustic Microscope. In *IEEE Transactions on Sonics and Ultrasonics* (Vol. 32, pp. 259–265). doi:10.1109/T-SU.1985.31592

Tirakotai, W., Miller, D., Heinze, S., Benes, L., Bertalanffy, H., & Sure, U. (2006). A Novel Platform for Image-Guided Ultrasound. *Neurosurgery*, *58*(4), 710–718. doi:10.1227/01.NEU.0000204454.52414.7A

Tofts, P. S. (2003). QA: Quality Assurance, Accuracy, Precision and Phantoms. In *Quantitative MRI of the Brain* (pp. 55–81). doi:10.1002/0470869526.ch3

Tzschatzsch, H., Nguyen Trong, M., Scheuermann, T., Ipek-Ugay, S., Fischer, T., Schultz, M., … Sack, I. (2016). Two-Dimensional Time-Harmonic Elastography of the Human Liver and Spleen. *Ultrasound in Medicine and Biology*, *42*(11), 2562–2571. doi:10.1016/j.ultrasmedbio.2016.07.004

Unsgaard, G., Ommedal, S., Muller, T., Gronningsaeter, A., & Nagelhus Hernes, T. A. (2002). Neuronavigation by Intraoperative Three-dimensional Ultrasound: Initial Experience during Brain Tumor Resection. *Neurosurgery*, *50*(4), 804–812.

Van Dongen, K. W., & Verweij, M. D. (2008). Sensitivity study of the acoustic nonlinearity parameter for measuring temperatures during high intensity focused ultrasound treatment. *J. Acoust. Soc. Am.*, *123* (June), 3225. doi:10.1121/1.2933437

Vieira, S. L., Pavan, T. Z., Junior, J. E., & Carneiro, A. a O. (2013). Paraffin-gel tissue-mimicking material for ultrasound-guided needle biopsy phantom. *Ultrasound in Medicine & Biology*, *39*(12), 2477–84. doi:10.1016/j.ultrasmedbio.2013.06.008

VisualSonics. (2006). VisualSonics Vevo 770 ® Digital RF Option.

Wear, K. A., Garra, B. S., & Hall, T. J. (1995). Measurements of ultrasonic backscatter coefficients in human liver and kidney in vivo. *J. Acoust. Soc. Am.*, *98*(4), 1852–1857. doi:10.1121/1.413372

Wear, K. A., Stiles, T. A., Frank, G. R., Madsen, E. L., Cheng, F., Feleppa, E. J., … Yuan, J. R. (2005). Interlaboratory comparison of ultrasonic backscatter coefficient measurements from 2 to 9 MHz. *Journal of Ultrasound in Medicine : Official Journal of the American Institute of Ultrasound in Medicine*, *24*(9), 1235–50. doi:10.7863/jum.2005.24.9.1235

Welkowitz, W., Deutsch, S., & Akay, M. (1992). *Biomedical Instruments. Theory and Design* (2nd editio.). Academic Press.

Wells, P. N. T. (Ed.). (1993). *Advances in Ultrasound Techniques and Instrumentation*. Churchill Livingstone.

Wiegman, S. (2010). *What is normal saline*. *Sharecare*. Retrieved from https://www.sharecare.com/health/nutritive-drugs/what-is-normal-saline

Wigen, M., & Løvstakken, L. (2016). In vivo three-dimensional intra-cardiac vector flow imaging using a 2D matrix array transducer. In *2016 IEEE International Ultrasonics Symposium Proceedings* (pp. 2–5).

Wirtzfeld, L. A., Berndl, E. S. L., & Kolios, M. C. (2015). Ultrasonic Characterization of Extra-Cellular Matrix in Decellularized Murine Kidney and Liver. *IEEE Ultrasonics Symposium*, 3–6.

Wodnicki, R., Cummins, T., Jung, H., & Shung, K. K. (2016). Integrated High Frequency Linear Transducer Array for Needle Biopsy Probe. In *2016 IEEE International Ultrasonics Symposium Proceedings* (pp. 2–4).

Worthington, A. E., & Sherar, M. D. (2001). Changes in ultrasound properties of porcine kidney tissue during heating. *Ultrasound in Medicine and Biology*, *27*(5), 673–682.

Xu, J., Tripathy, S., Rubin, J. M., Stidham, R. W., Johnson, L. a, Higgins, P. D. R., & Kim, K. (2012). A new nonlinear parameter in the developed strain-to-applied strain of the soft tissues and its application in ultrasound elasticity imaging. *Ultrasound in Medicine & Biology*, *38*(3), 511–523. doi:10.1016/j.ultrasmedbio.2011.12.009

Yang, X., Sun, C., Anderson, T., Moran, C., Hadoke, P. W. F., Gray, G., & Hoskins, P. (2013). Assessment of spectral doppler in preclinical ultrasound using a small-size rotating phantom. *Ultrasound in Medicine and Biology*, *39*(8), 1491–1499. doi:10.1016/j.ultrasmedbio.2013.03.013

Zderic, V., Keshavarzi, A., Andrew, M. A., Vaezy, S., & Martin, R. W. (2004). Attenuation of porcine tissues in vivo after high-intensity ultrasound treatment. *Ultrasound in Medicine and Biology*, *30*(1), 61–66. doi:10.1016/j.ultrasmedbio.2003.09.003

Zell, K., Sperl, J. I., Vogel, M. W., Niessner, R., & Haisch, C. (2007). Acoustical properties of selected tissue phantom materials for ultrasound imaging. *Physics in Medicine and Biology*, *52*(20), N475-84. doi:10.1088/0031-9155/52/20/N02

Zhai, X. Y., Birnk, H., Jensen, K. B., Thomsen, J. S., Andreasen, A., & Christensen, E.

I. (2003). Digital Three-Dimensional Reconstruction and Ultrastructure of the Mouse Proximal Tubule. *Journal of the American Society of Nephrology*, *14*(3), 611–619. doi:10.1097/01.ASN.0000051725.00406.0C

Zhou, Q., Ho, K., Zheng, H., Qiu, W., & Shung, K. K. (2014). Piezoelectric single crystals for ultrasonic transducers in biomedical applications. *Prog Mater Scie*, *66*, 1–34.

Ultrasound in Med. & Biol., Vol. 43, No. 7, pp. 1494–1505, 2017

0301-5629/$ - see front matter

http://dx.doi.org/10.1016/j.ultrasmedbio.2017.02.019

● *Original Contribution*

BROADBAND ACOUSTIC MEASUREMENT OF AN AGAR-BASED TISSUE-MIMICKING-MATERIAL: A LONGITUDINAL STUDY

Adela Rabell Montiel,* Jacinta E. Browne,† Stephen D. Pye,‡ Tom A. Anderson,* and Carmel M. Moran*

*Centre for Cardiovascular Science, University of Edinburgh, Edinburgh, UK; †School of Physics & IEO, FOCAS, Dublin Institute of Technology, Dublin, Ireland; and ‡Medical Physics, NHS Lothian, Royal Infirmary of Edinburgh, Edinburgh, UK

(*Received* 19 *September* 2016; *revised* 27 *February* 2017; *in final form* 27 *February* 2017)

Abstract—Commercially available ultrasound quality assurance test phantoms rely on the long-term acoustic stability of the tissue-mimicking-material (TMM). Measurement of the acoustic properties of the TMM can be technically challenging, and it is important to ensure its stability. The standard technique is to film-wrap samples of TMM and to measure the acoustic properties in a water bath. In this study, a modified technique was proposed whereby the samples of TMM are measured in a preserving fluid that is intended to maintain their characteristics. The acoustic properties were evaluated using a broadband pulse-echo substitution technique over the frequency range 4.5–50 MHz at 0, 6 and 12 months using both techniques. For both techniques, the measured mean values for the speed of sound and attenuation were very similar and within the International Electrotechnical Commission-recommended value. However, the results obtained using the proposed modified technique exhibited greater stability over the 1-y period compared with the results acquired using the standard technique. (E-mail: adela.rabell@ed.ac.uk) © **2017 World Federation for Ultrasound in Medicine & Biology.**

Key Words: **Ultrasound, High frequency, Tissue-mimicking material, Speed of sound, Attenuation coefficient, Long term.**

INTRODUCTION

Commercially available quality assurance (QA) test phantoms are widely used to test the performance of clinical ultrasound scanners. These phantoms are manufactured from tissue-mimicking-material (TMM) that is designed to closely match the acoustical properties of the speed of sound (SoS) and the attenuation coefficient of soft tissue. The aim in manufacturing these phantoms is to provide a reproducible method to assess the performance of ultrasound scanners. However, these phantoms are intended for use with clinical ultrasound scanners at frequencies ≤20 MHz. To the best of our knowledge, there are no commercially available test phantoms for assessment of the performance of ultrasound scanners employing ultrasound frequencies >20 MHz.

A variety of TMMs are currently produced both commercially and within laboratories. These include: agar-based TMMs (Teirlinck et al. 1998), condensed milk TMMs (Madsen et al. 1998), gelatin TMMs (Culjat et al. 2010), konjac–carrageenan TMMs (Kenwright et al. 2014; Meagher et al. 2007), urethane rubber TMMs (Culjat et al. 2010), poly (vinyl alcohol) cryogel (PVA-C) TMMs (Cournane et al. 2010; Culjat et al. 2010; King et al. 2011) and Zerdine TMMs (CIRS, Norfolk, VA, USA). The International Electrotechnical Commission (IEC) agar-based TMM has become widely used and popular for clinical and pre-clinical test objects (Brewin et al. 2008; Browne et al. 2003; Cannon et al. 2011; Culjat et al. 2010; Inglis et al. 2006; Moran et al. 2011a, 2011b; Rajagopal et al. 2014; Sun et al. 2012; Yang et al. 2013). The acoustical properties of this agar-based TMM are designed to comply with the ultrasound acoustical parameters provided by the IEC (2001) with the recommended SoS and attenuation over the frequency range 2–10 MHz being 1540 ± 15 m/s and 0.5 ± 0.05 dB/cm, respectively.

Moderately high-frequency ultrasound scanners (≤20 MHz) have been manufactured for many years and have been utilised clinically in assessment of the skin (Machet et al. 2009), vascular structures (Rhee 2007) and in retinal imaging (Foster et al. 2000). In recent

Address correspondence to: Adela Rabell Montiel, 47 Little France Crescent, Queen's Medical Research Institute, Centre for Cardiovascular Science, EH16 4 TJ, Edinburgh, UK. E-mail: adela.rabell@ed.ac.uk

years, reliable high-frequency (20–50 MHz) and very high frequency (>40 MHz) ultrasound scanners have become mainstream technology for the imaging of superficial structures in clinical imaging and for pre-clinical imaging applications due to improvements in transducer engineering and software technology (Banchhor et al. 2016; Moran et al. 2011a, 2011b; Schmitt et al. 2010; Sundholm et al. 2015; Xu et al. 2012).

With the increase in high-frequency ultrasound imaging applications, there is a need to develop and acoustically characterise TMMs suitable for high-frequency ultrasound quality assurance and training phantoms. It has been reported that above 10 MHz, the TMMs in the commercial test phantoms do not have optimum acoustic properties, as the attenuation starts to exhibit a non-linear response with increasing frequency (Browne et al. 2003), whereas the IEC guidelines for TMM properties recommend a linear relationship between attenuation and frequency up to 10 MHz.

The agar-based TMM developed under the IEC guidelines and used in this study has previously been found to have a non-linear response when acoustically investigated at frequencies ≤23 MHz by Brewin et al. (2008) and in our own laboratory and in the National Physical Laboratory (Teddington, UK) at frequencies up to 47 MHz (Sun et al. 2012) and 60 MHz (Rajagopal et al. 2014), respectively. In these studies, test cells or TMM samples wrapped with film material (Saran Wrap or Mylar) were employed to preserve the samples during acoustic characterisation when degassed, de-ionised water was used as the reference medium. Moreover, thin slices of TMM ranging in thickness from 2.5 to 30 mm were used, enabling higher ultrasound frequencies to propagate through the TMM slices (Brewin et al. 2008; Rajagopal et al. 2014; Sun et al. 2012). The encasing of the TMM in film is important as, without the film, the TMM will degrade rapidly. This degradation is due to leaching of the glycerol from the TMM into the water reference medium, thus altering the acoustic properties of the TMM (Brewin et al. 2008). A reference water test cell, also encapsulated in Saran Wrap or Mylar film, was used in the reference measurement to account for the effect of the film on measurements (Rajagopal et al. 2014; Sun et al. 2012). However, the production of both the TMM slices wrapped in film and water test cells is time consuming and technically challenging, especially for thin TMM samples. Therefore, the aim of this study was to compare this well-established technique for the measurement and preservation of an IEC agar TMM to a technique in which TMM is characterised and preserved in a preserving fluid. Furthermore, this method was evaluated over a 1-y period to determine the longitudinal stability of the acoustic properties.

METHODS

Acoustical measurements

Data were captured using two different acoustical systems, described briefly here and elsewhere (Sun et al. 2012). First, a Vevo 770 pre-clinical ultrasound scanner (Visualsonics, Toronto, ON, Canada) was used at the University of Edinburgh, and second, a scanning acoustic macroscope (SAM) system developed in-house was used at the Dublin Institute of Technology (Cannon et al. 2011). The SAM system was used to provide additional acoustic data and to extend the lower limit of the bandwidth of the measurements to 4.5 MHz.

Manufacture of FTMM and UTMM samples

A batch of the IEC agar-based TMM was manufactured according to a widely used standard recipe and method (Brewin et al. 2008; Browne et al. 2003; Cannon et al. 2011; Ramnarine et al. 2001; Teirlinck et al. 1998). This mixture was poured at 42°C onto a pre-warmed metal plate. The plate was pre-warmed to ensure that the mixture spread uniformly. The TMM mixture was then left to cool to room temperature. From this batch of TMM, 22 cylindrical slices of TMM

Table 1. Characteristics of Vevo 770 and SAM system transducers*

Transducer model and measurement system	Central frequency (MHz)	Focal length (mm)	Measured 3-dB bandwidth (MHz)	Peak negative pressure (MPa)
Vevo 770				
RMV 704	40	6	18–40	0.52
RMV 707 B	30	12.7	12–32	1.05
RMV 710 B	25	15	12–28	1.06
RMV 711	55	6	25–50	0.23
SAM system				
V320	7.5	95	4.5–9	0.05
V317	20	65	14–25	0.021
V390	50	12	20–40	0.022

SAM = scanning acoustic macroscope.

* The central frequency and focal length are parameters provided by the manufacturer: Vevo 770 (VisualSonics, Toronto, ON, Canada) and SAM system (Olympus Panametrics NDT, Waltham, MA, USA), The 3-dB bandwidth is from measurements, and the peak pressure is from Sun (2012).

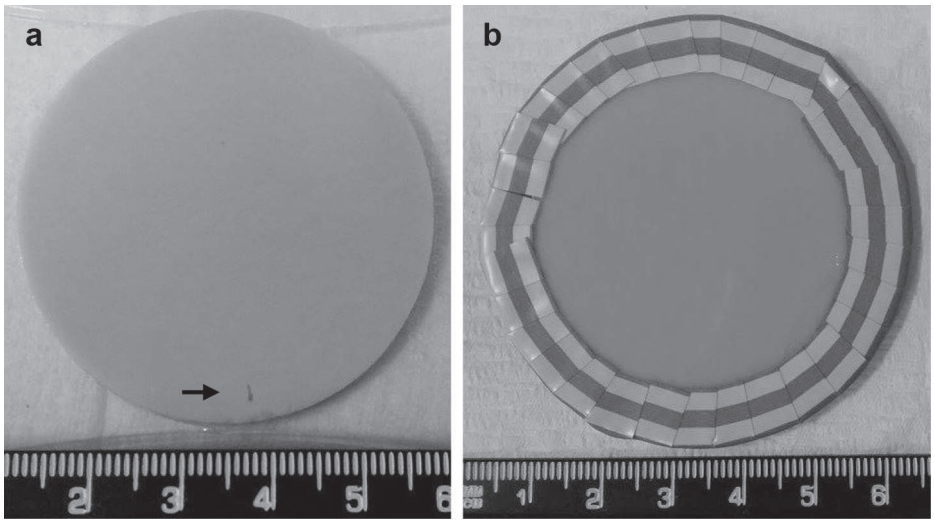

Fig. 1. (a) Unwrapped tissue-mimicking material (UTMM); the *arrow* indicates the identification mark on the sample. (b) Film-wrapped tissue-mimicking material (FTMM).

of diameter 5.5 cm were cut using a thin-walled plastic tube. Due to the short focal lengths associated with high-frequency transducers (Table 1), the thickness of the TMM slices was constrained to <3.2 mm and ranged from 1.8 to 3.2 mm.

After being cut, 11 of these cylindrical TMM samples were left uncovered and placed in a sealed container with TMM preserving fluid. This TMM preserving fluid was manufactured in-house (Brewin et al. 2008; Cannon et al. 2011; Inglis et al. 2006). These samples are referred to as unwrapped TMM (UTMM) (Fig. 1a).

The remaining 11 TMM samples were used to manufacture the samples that were subsequently covered with clear film as follows. Initially, a layer (0.015 mm thick) of Saran Wrap film (SC Johnson, Racine, WI, USA) was stretched over a 10-cm-diameter embroidery ring. A fast-hardening epoxy (Araldite Rapid, Huntsman Advanced Materials, Basel, Switzerland) was then applied to one side of a PVC ring (2 mm thick, 5.8 mm in outer diameter), and the stretched Saran Wrap was lowered onto the PVC ring. This was left to set overnight. The TMM was then manufactured as described above. After setting and being cut, the 11 samples were placed into the PVC rings. Five drops of TMM preserving fluid was added to the surface of the TMM to ensure good acoustic coupling between the film and the TMM, and a second layer of Saran Wrap was glued to the other side of the ring, similar to that described above, such that the TMM slices were "sandwiched" between the two films and thereby film wrapped (FTMMs). These final film-wrapped samples were left to set overnight. Finally, epoxy was used to seal the edges of the film–ring–film to ensure the FTMMs did not leak. This was re-enforced with insulating tape to ensure that the film would not peel off during the 1-y period of investigation (Fig. 1b). These FTMMs were preserved in a box with tissue paper moistened with TMM preserving fluid to create a humid TMM preserving fluid-saturated environment. In a similar manner, a water test cell was manufactured whereby the TMM was replaced by degassed, de-ionised water in the manufacturing process.

Experimental setup of Vevo 770 pre-clinical ultrasound scanner

In this study, the radiofrequency (RF) data were collected and analysed from 11 FTMMs and 11 UTMMs. To measure the acoustic properties, the FTMMs were submerged in a tank filled with degassed, de-ionised

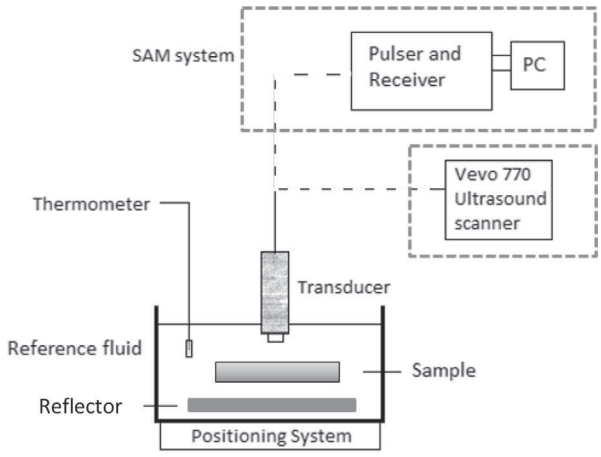

Fig. 2. Experimental setup comprising a high-frequency ultrasound scanner (Vevo 770) used at the University of Edinburgh and scanning acoustic macroscope (SAM) system used at the Dublin Institute of Technology.

water as the reference medium, whereas for the UTMM measurements, the tank was filled with TMM preserving fluid. For both measurements, a polymethylpentene (TPX, Boedeker Plastics, TX, USA) reflector 2.5 cm in diameter and 5 mm thick was located beneath the samples at the focal position of each transducer, as illustrated in Figure 2.

Measurements were made with four transducers (Table 1) at 10% output power, using a high-frequency ultrasound scanner Vevo 770. This power output was considered sufficient signal magnitude to obtain good signal-to-noise data without the generation of significant non-linear effects (Sun et al. 2012). The regions of interest (ROIs) were located at the upper surface of the TPX reflector with and without the sample in place and from the lower and upper surfaces of each sample. For each measurement, the RF data were collected from 10 scan lines within these pre-selected ROIs at four different positions on the FTMMs or UTMMs. The data were analysed off-line using a MATLAB script (MATLAB R2013 The MathWorks, Natick, MA, USA). The calculated angular separation between the RF acquisition lines is approximately 0.15°, so the lines were considered parallel and perpendicular to the TPX reflector. For the FTMMs, identical acoustic measurements were also taken through the water test cell to take into account potential reflections from the Saran Wrap interfaces and to obtain absolute values of attenuation (Cannon et al. 2011; Sun et al. 2012).

The performance of both FTMMs and UTMMs was assessed over a 1-y period at approximately 0, 6 and 12 months time-points.

The 3-dB bandwidth of each transducer (Table 1) was measured from the frequency spectra taken from the TPX reflector in a degassed, de-ionised water tank without the sample in place, where the reflector was placed at the focal length of the transducer.

Analysis of speed of sound, thickness and attenuation data of FTMM and UTMM samples

The analysis of FTMMs was performed based on a broadband pulse-echo substitution technique (American Institute of Ultrasound in Medicine [AIUM] 2014). The pulse-echo return times from the front and rear surfaces of the FTMMs and from the front surface of the TPX reflector were used to determine the thickness and SoS of the samples. The magnitude of these pulse echoes was used to calculate the attenuation. In addition, the echoes from the TPX reflector with the water test cell were acquired. These data were then used to calculate the SoS, thickness and attenuation of the FTMM samples in a manner similar to that described in Sun et al. (2012).

For the SoS and thickness of the UTMMs, the measurement and analysis were carried out as for the FTMMs. However, because the UTMMs were not wrapped in Saran Wrap, no water test cell was required and the reference measurements from the TPX were taken through the bath of TMM preserving fluid. The absence of Saran Wrap meant that the magnitude of the echoes from the boundaries of the TMM was reduced. This necessitated manual selection of the position of the boundaries from the raw RF signals, which was accomplished by selecting the largest pulse echo at each interface of the UTMMs. The criterion for this was that the peak selected was at least 100% greater than the magnitude of the previous peak within a 2-μs time window. This procedure was carried out for each of the 10 lines of raw RF signal inside the ROI of the UTMMs, enabling the thickness of the sample to be determined at each of these positions. In addition, the thickness of the UTMMs was measured manually in five different positions on each UTMM with a digital calliper (DURATOOL, Taiwan, 0–150 mm). Each sample was placed between two plastic plates of known thickness to avoid excessive compression of the UTMMs (Brewin et al. 2008; Rajagopal et al. 2014). This was performed at the initial time point before the acoustic measurements commenced.

The SoS in the UTMMs was calculated using the equation

$$\mathrm{SoS}_{\mathrm{UTMM}} = \left(1+\frac{T_{\mathrm{R}}-T_{TMMR}}{T_{\mathrm{TMMLw}}-T_{\mathrm{TMMUp}}}\right)\mathrm{SoS}_{\mathrm{TMMfluid}} \qquad (1)$$

where T_{R} is the time from the transducer to the TPX in the tank with no sample in the acoustical path; T_{TMMR} is the time from the transducer to the TPX reflector through the sample; T_{TMMLw} and T_{TMMUp} are the times from the transducer to the lower and upper surfaces, respectively, of the sample; and $\mathrm{SoS}_{\mathrm{TMMfluid}}$ is the SoS of the TMM preserving fluid in which the samples were immersed.

Attenuation of the UTMMs was calculated in a manner similar to that for FTMMs, but without the use of the water test cell, to compensate for the interfacial attenuation loss.

Acoustical properties of TMM preserving fluid and degassed, de-ionised water

The acoustic properties of the TMM preserving fluid were measured by the National Physical Laboratory. The SoS was found to be 1538.15 ± 0.22 m/s at 19.3 ± 0.1°C, and a second-degree polynomial function was fitted to the attenuation data (α [dB/cm]) as a function of frequency (f [MHz]) as $\alpha_{\mathrm{TMMfluid}} = 0.00309f^2 - 0.004996f$ ($R^2 = 0.99$) over the frequency range 1–60 MHz.

The acoustic properties of the degassed, de-ionised water have previously been measured and found to have an attenuation proportional to f^2 over the range 7.5–67.5 MHz (Duck 1990; Pinkerton 1949). Furthermore,

the SoS of degassed, de-ionised water varies with temperature (Bilaniuk and Wong 1992; Del Grosso and Mader 1972). In this study, all measurements were undertaken at 22.2 ± 0.5°C with a SoS of 1488.88 m/s.

Experimental setup and data analysis using the SAM system

The SAM system (Dublin Institute of Technology) uses broadband transducers that work as both transmitter and receiver (Olympus NDT, Waltham, MA, USA). The experimental setup was similar to that used with the Vevo 770 (Fig. 2). Three different transducers were used (Table 1), and the 3-dB bandwidth was measured as for the transducers of the Vevo 770.

A pulser-receiver (Model 5052 PR, Panametrics, Waltham, MA, USA) was used to transmit and receive the pulses. The received reflected pulse was digitised and captured using a data acquisition card (PCI-5144: National Instruments, Austin, TX, USA), with the data acquisition controlled by a LabView (National Instruments) program.

The SAM system displayed the RF data in real time during the measurements. Ten lines of data were acquired from each of four different positions on the TPX reflector with and without the sample (FTMM or UTMM) in place.

The calculations of the SoS and attenuation coefficient were also based on the broadband pulse-echo substitution technique. However, here the thickness of the sample was inputted into the calculation of SoS and attenuation coefficient. The thickness value input for each FTMM and UTMM was the mean of the 10 different measurements at each of eight locations calculated using the four transducers of the Vevo 770® ultrasound scanner.

At all time points, measurements taken with the Vevo 770 were performed before measurements with the SAM system.

Unpreserved samples, batch-to-batch variation and repeatability of the UTMMs

The acoustic properties of two UTMM slices were measured identically to the UTMMs described previously using the RMV704 transducer (centre frequency 40 MHz) (Table 1). Measurements were undertaken initially and then approximately once every 24-h over a 96-h period. However, between measurements, the samples were left exposed to the air. These samples will be referred to as unpreserved samples.

An indication of TMM batch-to-batch variability was assessed by measuring the acoustical properties of 6 UTMMs manufactured from a different batch of TMM. These samples will be referred to as UTMM2 and had a mean thickness of 2.01 ± 0.05 mm as measured using the Vevo 770 scanner. The acoustical properties were measured with the Vevo 770 and with the SAM system at the 6 and 12 month time points.

Data analysis was performed as for the 11 UTMMs described above.

To assess the repeatability of the measurement system, the acoustic properties of the 11 UTMMs were measured with one transducer RMV710 with the Vevo 770 at five different times over a 1-month period. The reference medium was TMM preserving fluid. The temperature for these measurements was 22.0 ± 0.4°C.

RESULTS

The mean thicknesses of the FTMMs and UTMMs calculated using the RF ultrasound signals from the Vevo 770 over all the time points had maximum variations of 0.25 and 0.08 mm, respectively. The thicknesses of the 11 UTMMs measured with the digital calliper had a maximum variation of 0.03 mm.

Table 2 lists the mean SoS values of FTMMs and UTMMs at each time point. It can be seen that the SoS of the FTMMs exhibited larger variability than the SoS of the UTMMs. With Student's *t*-test it was found that the mean SoS values of the FTMM and UTMM samples did not statistically differ ($p > 0.5$) at the 0 time point, but did significantly differ ($p < 0.05$) at the remaining time points. The results after 1-y indicated that the SoS of FTMMs decreased 22.1 m/s compared with the first measurement at 0 months, whereas the SoS of the UTMMs decreased 4.1 m/s over the same 12-month period. The SoS of UTMM2 samples calculated over a 6-month period exhibited a decrease from 1558.1 ± 5.3 to 1544.8 ± 3.3 m/s, with a difference of 13.3 m/s.

Table 3 lists the mean SoS values averaged over all time points for each of the measurement systems. It was found that the SoS measurements obtained with the SAM system had smaller variability than SoS measurements obtained with the Vevo 770 for FTMMs and UTMMs. The mean values over all samples over all time points, using both measurement systems, were 1538.2 ± 14.5 m/s for the FTMMs and 1544.0 ± 3.5 m/s for the UTMMs

Table 2. Speed of sound measured with the Vevo 770 and SAM system at each time point for the FTMM and UTMM samples

	Speed of sound (m/s)*		
	0 months	6 months	12 months
FTMM	1547.4 ± 19.2*	1547.2 ± 21.5	1525.5 ± 16.5
UTMM	1545.9 ± 10.4	1544.2 ± 11.0	1541.8 ± 1.6

SAM = scanning acoustic macroscope; FTMM = film-wrapped tissue-mimicking material; UTMM = unwrapped tissue-mimicking material.

* Mean ± standard deviation.

Table 3. Speed of sound over all time points of 11 FTMM and 11 UTMM samples measured with the four transducers of the Vevo 770 and the three transducers of the SAM system

	Speed of sound (m/s)*	
	Vevo 770	SAM system
FTMM	1539.6 ± 17.1*	1536.3 ± 10.3
UTMM	1542.9 ± 3.6	1545.3 ± 3.0

SAM = scanning acoustic macroscope; FTMM = film-wrapped tissue-mimicking material; UTMM = unwrapped tissue-mimicking material.
* Mean ± standard deviation.

(Table 4). The mean SoS for UTMM2 samples was found to be 1551.4 ± 6.2 m/s. Table 4 also outlines the SoS results in comparison with those values published for IEC agar TMM (Brewin et al. 2008; Browne et al. 2003; IEC, 2001; Rajagopal et al. 2014; Sun et al. 2012). The mean SoS values of the FTMMs and UTMMs are within the values specified by the IEC (2001).

Figures 3 and 4 illustrate attenuation as a function of frequency for the FTMMs and UTMMs, respectively, at 0, 6 and at 12 months, measured using the seven different transducers. The variation in mean attenuation values for the UTMMs is small in comparison to the variation observed in mean attenuation values for the FTMMs.

Figures 5 and 6 illustrate the mean attenuation data over the frequency range 4.5–50 MHz, averaged over all 11 FTMMs and over all 11 UTMMs and time points, respectively.

The batch-to-batch variation of TMM was assessed with the UTMM2 samples (2.01 ± 0.05 mm thick). These samples were measured with both the Vevo 770 and SAM system (at 6 and 12 months). The mean SoS of UTMM2 samples was found to be 0.44% higher (7.4 m/s) than the mean SoS of the 11 UTMMs. For attenuation, the UTMM2 samples were found to have a maximum difference of ±1 dB/cm in mean attenuation across the frequency range illustrated in Figure 7.

After 96 h of exposure to air, the unpreserved samples were visibly dehydrated. The mean thickness of the two samples had decreased by 1.22 mm, and the diameter had decreased by 1.5 cm. Additionally, the SoS was found to have increased by 140 m/s for sample 1 and 180 m/s for sample 2 over the entire period. The attenuation was found to have increased by approximately 10 dB/cm per day.

In the assessment of repeatability, the mean SoS over the five measurements for the 11 UTMMs was calculated to be 1543.0 m/s with a range of ±11.0 m/s. The mean SoS was found to be smaller by 1 m/s compared with the mean SoS calculated using all the transducers at all time points (Table 4) of the UTMMs. The variation in attenuation as a function of frequency was ±1 dB/cm over the frequency range of the Vevo770 RMV710 B probe.

Polynomial functions were calculated for attenuation as a function of frequency at each time point for the FTMMs and UTMMs. The best-fit polynomial function was determined over all attenuation-versus-frequency data in the range 4.5–50 MHz as a combination of Vevo 770 and SAM system data over all time points (Fig. 8). The polynomial fits found were $0.4649f + 0.007363f^2$ ($R^2 = 0.80$) for FTMMs and $0.4897f + 0.008366f^2$ ($R^2 = 0.99$) for UTMMs. The goodness of fit (R^2) of the three polynomial fits at each of the three time points for the FTMMs ranged between 0.78 and 0.92, whereas for the UTMMs, R^2 ranged between 0.96 and 0.99. In addition, in Figure 8, for comparison, the attenuation data of the IEC agar TMM from studies already published is included.

DISCUSSION

This aim of this study was to develop a robust and easy-to-use technique for the characterisation and preservation of IEC agar TMM and to compare the acoustic properties obtained using this modified technique with those obtained with the standard technique over a 1-y period.

The thickness used in the calculation of SoS from the SAM system was the mean of thicknesses measured with the Vevo 770 ultrasound scanner at eight different locations on the UTMMs (10 lines at each position).

Table 4. Comparison of speeds of sound measured in this study with the published data

Source	Type of sample	Speed of sound (m/s)*	Frequency range (MHz)
IEC 2001		1540 ± 15	2–10
Browne et al. 2003	UTMM measured in degassed water	1546.5 ± 3	2.25–15
Brewin et al. 2008	UTMM measured in degassed water	1537 ± 2.6	17–23
	FTMM	1540.9 ± 8.7	
Sun et al. 2012	FTMM	1547.8 ± 3.7	10–47
Rajagopal et al. 2014	FTMM	1544 ± 3.1	1–60
This study	FTMM	1538.2 ± 14.5	4.5–50
	UTMM measured in TMM preserving fluid	1544.0 ± 3.5	

FTMM = film-wrapped tissue-mimicking material; UTMM = unwrapped tissue-mimicking material.
*Mean ± standard deviation.

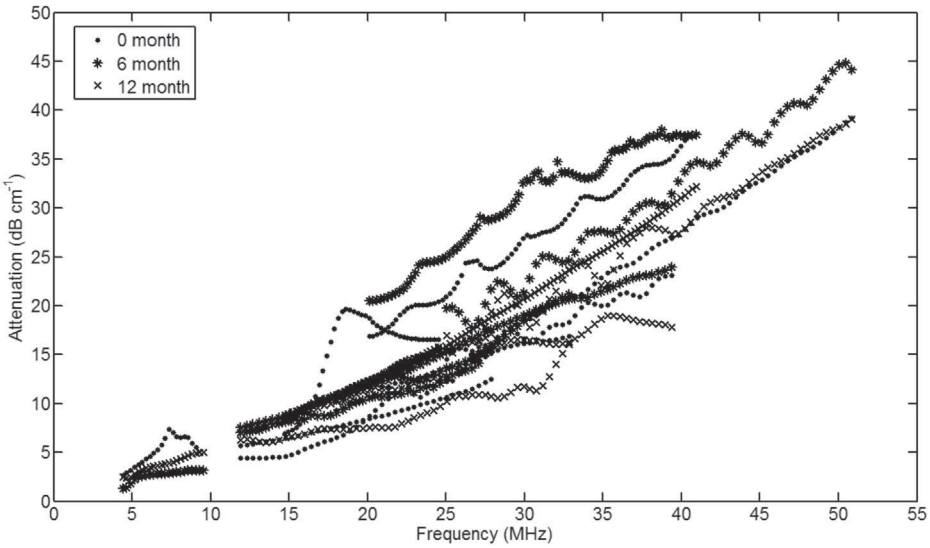

Fig. 3. Attenuation measured with the Vevo 770 and scanning acoustic macroscope (SAM) system of 11 film-wrapped tissue-mimicking material (FTMM) slices at 0, 6 and 12 months as a function of frequency. Each line represents one of the seven different transducers used at each time point: RMV704 (18–40 MHz), RMV707 B (12–32 MHz), RMV710 B (12–28 MHz), RMV711 (25–50 MHz), V320 (4.5–9 MHz), V317 (14–25 MHz), V390 (20–40 MHz).

Although this mean thickness was used, the standard deviations (SD) of the SoS values from the SAM system were smaller than the SD variation calculated using the Vevo 770 (Table 4), which suggests that the use of this mean thickness in the SAM system measurements did not contribute significantly to the experimental error.

The acoustic properties of the UTMMs were measured in TMM preserving fluid whose acoustical properties were assessed by the National Physical Laboratory at 19.3 ± 0.1°C, whereas the UTMMs in this study were measured at 22.2 ± 0.5°C. The TMM preserving fluid is composed of the same fluid as used in the TMM manufacturing process, and Brewin et al. (2008) has previously reported a TMM SoS temperature dependence of 2.1 m/s/°C. Consequently, there is likely to be a maximum variation of 6 m/s in the SoS of the TMM preserving fluid, which could be attributable to the temperature change. Such a change would result in a potential

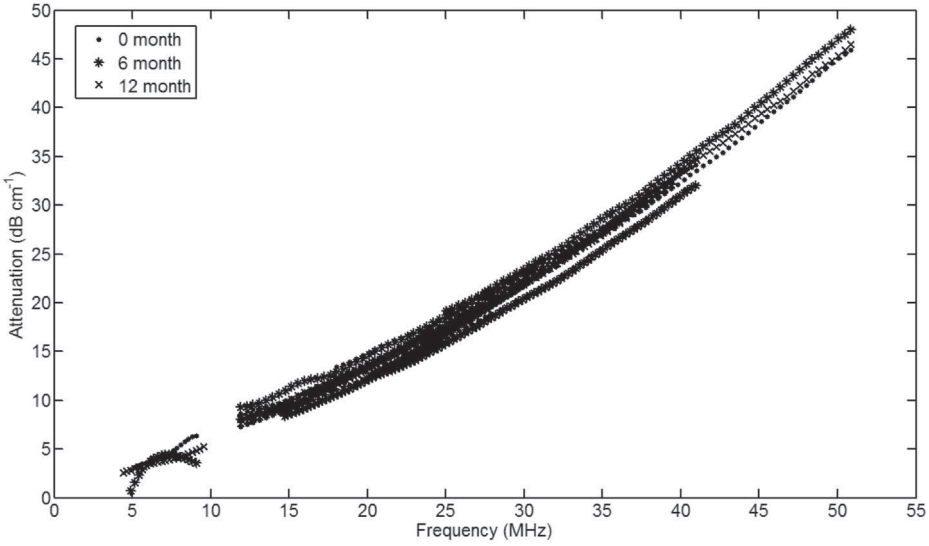

Fig. 4. Attenuation measured with the Vevo 770 and scanning acoustic macroscope (SAM) system of 11 unwrapped tissue-mimicking material (UTMM) slices at 0, 6 and 12 months as a function of frequency. Each line represents one of the seven different transducers used at each time point: RMV704 (18–40 MHz), RMV707 B (12–32 MHz), RMV710 B (12–28 MHz), RMV711 (25–50 MHz), V320 (4.5–9 MHz), V317 (14–25 MHz), V390 (20–40 MHz).

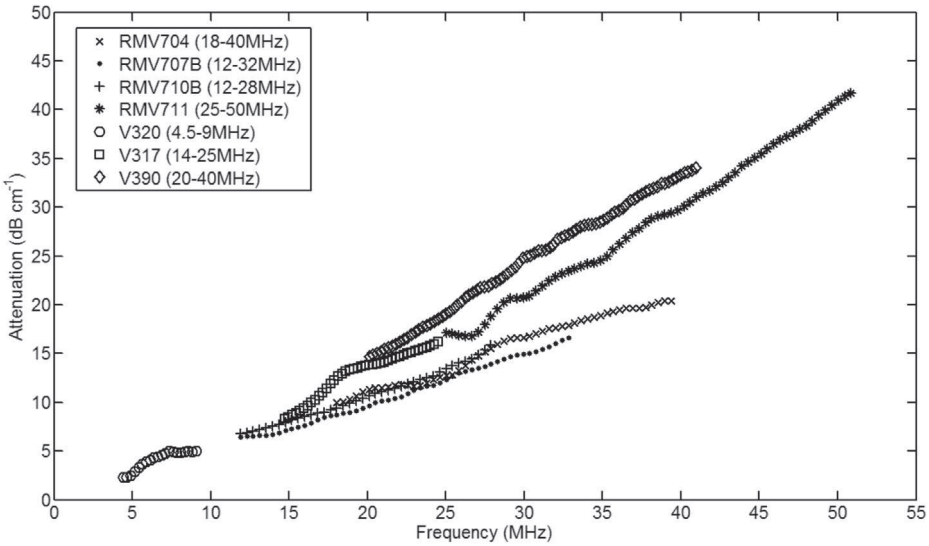

Fig. 5. Attenuation as a function of frequency averaged over all time points. Data set: 11 film-wrapped tissue-mimicking material (FTMM) slices measured in degassed, de-ionised water with the Vevo 770 and scanning acoustic macroscope (SAM) system in the frequency range 4.5–50 MHz.

error of $<$7 m/s in the measured SoS of the UTMMs. Nevertheless, the SoS values of the UTMM were found to be in good agreement with those of Rajagopal et al. (2014), Sun et al. (2012) and Brewin et al. (2008). Furthermore, the SoS of the UTMMs was found to decrease by 4.1 m/s over a 12-months period compared with that of the FTMMs, indicating a decrease in the mean SoS of 22.1 m/s over the same period. Additionally, the standard deviation of the mean SoS values for FTMM samples was larger than that for UTMM samples at all time points. There may be a number of reasons for this increased variation in SoS values for the FTMMs in comparison to the UTMMs. First, although a visual inspection was performed on each of the FTMMs before each acoustical measurement and no evidence of leakage was observed, in several samples, the epoxy securing the film to the rings exhibited signs of ageing and the Saran Wrap film appeared to become less taut over the 1-y period. This could have potentially increased the permeability of the film, allowing the glycerol from the TMM to

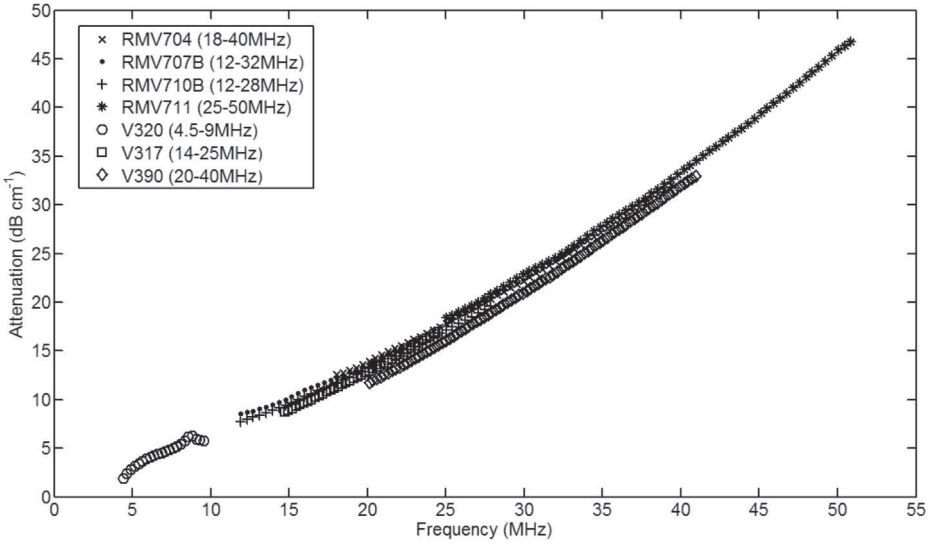

Fig. 6. Attenuation as a function of frequency averaged over all time points. Data set: 11 unwrapped tissue-mimicking material (UTMM) slices preserved and measured in TMM preserving fluid with the Vevo 770 and scanning acoustic macroscope (SAM) system in the frequency range 4.5–50 MHz.

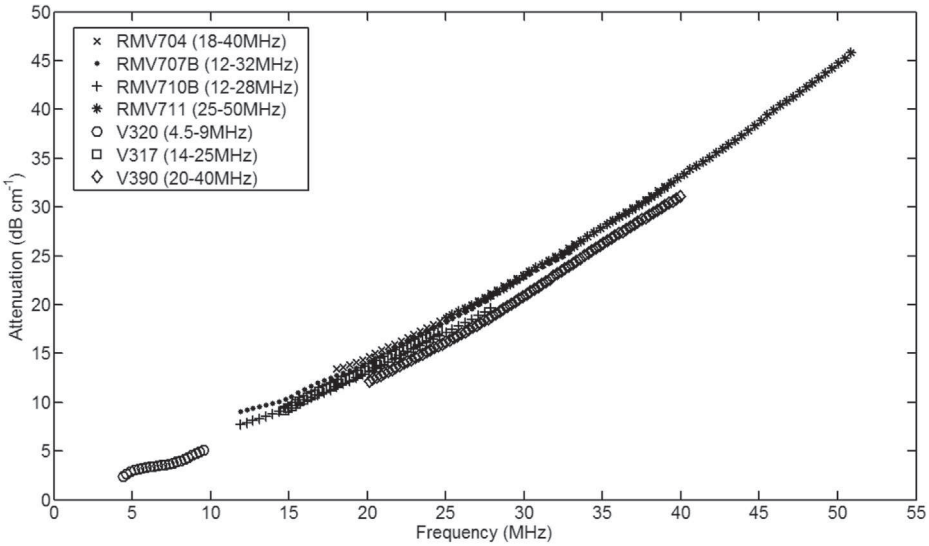

Fig. 7. Attenuation as a function of frequency averaged over all time points for the 6 UTMM slices manufactured from a different batch of TMM (UTMM2). Data set: 6 UTMM2 slices preserved and measured in TMM preserving fluid with the Vevo 770 and scanning acoustic macroscope (SAM) system at 6 and 12 months in the frequency range 4.5–50 MHz.

leach into the water medium, resulting in a decrease in the measured SoS properties of the FTMM. However, although a decrease in SoS in FTMMs was measured between 0 and 12 months, the SoS did not decrease continuously over the 1-y period, which would suggest that the measured variation is not likely to be attributable to glycerol leakage. Second, for the FTMMs, the position of the water–film interfaces was selected using MATLAB code based on identification of the position of the maximum rectified RF signal, and it was assumed that this signal also marked the TMM interface. Although this is a reasonable assumption, if any of the FTMM samples were subject to shrinkage (by drying out) over the 1-y period, this would represent a potential source of error.

The SoS results of both FTMMs and UTMMs in this study were compared with previously published work (Table 4). It is seen that the UTMM mean SoS values are in good agreement with those published, whereas

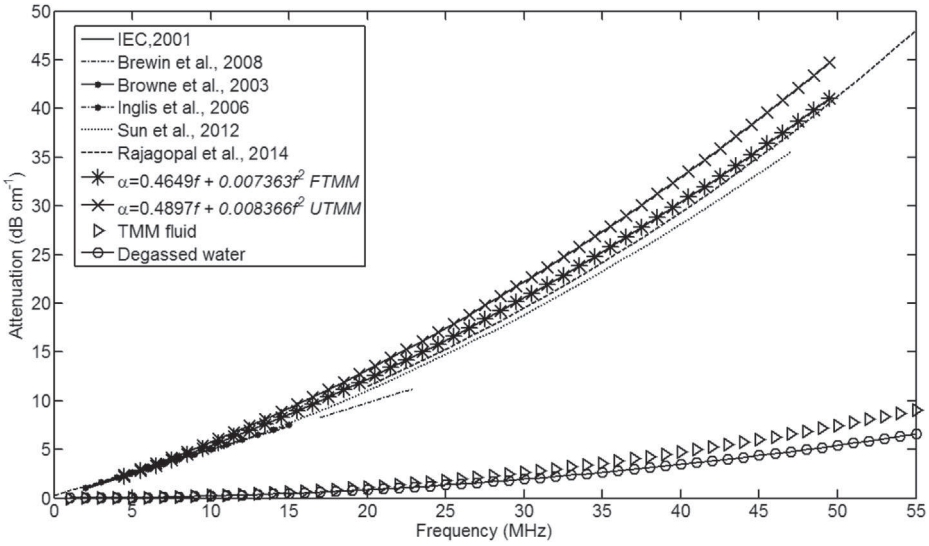

Fig. 8. Polynomial curve fit of all attenuation data as a function of frequency and the attenuation (compensated for the attenuation in water) of tissue-mimicking material (TMM) at 2–10 MHz (IEC 2001), 17–23 MHz (Brewin et al. 2008), 2.25–15 MHz (Browne et al. 2003), 6–15 MHz (Inglis et al. 2006), 10–47 MHz (Sun et al. 2012) and 1–60 MHz (Rajagopal et al. 2014). Attenuation as a function of frequency is also provided for the TMM preserving fluid and degassed, de-ionised water.

the mean FTMM SoS values were 5.8 m/s smaller compared with those of Rajagopal et al. (2014) and up to 9.6 m/s smaller compared with those of Sun et al. (2012). In Rajagopal et al. (2014), the manufacture of FTMM was achieved by sandwiching the TMM slice between two sheets of Mylar (∼12 μm thick) affixed into Perspex frames, whereas in Sun et al. (2012), the manufacture of the FTMM was similar to the method used in this study (referred to as TMM test cells in that study). However, in Rajagopal et al. (2014), even though the acoustic measurement was completed relatively quickly (within seconds), the edges of the TMM were not covered, which is likely to have led to some undefined glycerol leakage and to have potentially affected the measured acoustical properties. Furthermore, in Brewin et al. (2008), the acoustical properties of two different batches of TMM with a thickness ranging from 3 to 12.7 mm were measured over a 3-y period. In Brewin et al. (2008), the first batch consisted of TMM samples not protected by a film and measured in double degassed, de-ionised water. Because glycerol leached from the samples in this batch, the SoS was found to decrease by 2.1 m/s/°C. The second batch consisted of TMM samples protected by Saran Wrap and also measured in water. With this method, thinner samples (3 mm) displayed the largest SoS variation of 13.4 m/s. This value is comparable to the SD found in this study for the FTMMs (Table 4), but considerably higher than that measured for the UTMMs.

Figures 3 and 4 illustrate the attenuation of FTMMs and UTMMs, respectively, at 0, 6 and 12 months. It can be observed that there is a much larger variation in the attenuation measurements obtained from the FTMMs than in those from the UTMMs. In both the lower (4.5–9 MHz) and higher (40–50 MHz) frequency ranges, the data displayed were obtained with a single transducer. Nevertheless, the attenuation versus frequency for the FTMMs would suggest that with increasing frequency, there is an increasing difference in measured mean attenuation values between the 6-month data and 0- and 12-month data. The maximum difference, 7 dB/cm, occurred over the frequency range 30–42 MHz, and the minimum difference occurred in the range 15–19 MHz. For the UTMMs, a maximum variation of 2 dB/cm was observed across the time points, at a frequency of 47 MHz, and a minimum variation was observed from 37 to 47 MHz.

Moreover, the difference in mean attenuation values between the UTMMs and FTMMs would suggest that despite compensation for the effects of the Saran Wrap, some additional acoustic effects were introduced that were not fully compensated using the Saran-wrapped reference water test cell. These effects are unlikely to be due to the difference in non-linear effects between water and TMM preserving fluid as it has previously been reported (Sun 2012) that even in water, at these output powers, the second harmonic component of the ultrasound beam is at least 30 dB smaller in magnitude than the first harmonic (fundamental). Because non-linear effects are easier to generate in water than in the TMM preserving fluid, it is unlikely that non-linearities are significantly greater than the experimental errors identified.

Figures 5 and 6 illustrate the mean attenuation of the 11 FTMMs and 11 UTMMs across the seven different transducers and measured three times during the 1-y period. The FTMMs (Fig. 5) exhibited greater variability (∼15 dB/cm) across samples and transducers. This may be the result of inadequate acoustical correction for the interface layers when using the reference water test cell, leading to an increased uncertainty in the attenuation measurements in addition to the factors previously described. The UTMMs (Fig. 6) exhibited good consistency and little variability in attenuation over the frequency range 4.5–50 MHz.

Polynomial fits from FTMM and UTMMs were in good agreement with previous studies in the frequency ranges of 17–23 MHz (Brewin et al. 2008), 10–47 MHz (Sun et al. 2012) and 1–60 MHz (Rajagopal et al. 2014). The polynomial fits were also in good agreement at lower frequencies, 4.5 to 10 MHz, as reported by the IEC (2001) and other studies (Browne et al. 2003; Inglis et al. 2006), as illustrated in Figure 8. The attenuation from FTMMs and UTMMs does not increase linearly with frequency as indicated by the quadratic terms of the polynomial fit. This quadratic term was found to be 0.0073 for FTMMs and 0.0083 for UTMMs, which are in good agreement with the 0.0076 reported by Sun et al. (2012) and with 0.0081 reported by Rajagopal et al. (2014).

Finally, the unpreserved samples displayed significant visual degradation and changes in SoS and attenuation over the 96 h. These results are consistent with those of Brewin et al. (2008), who also reported shrinking and hardening of TMM samples that were not preserved.

CONCLUSIONS

In this study, we evaluated two different measurement techniques for assessing the temporal stability of the acoustic properties of the IEC agar TMM over the frequency range 4.5–50 MHz. In the first technique, thin slices were wrapped and stored in Saran Wrap and measured in degassed, de-ionised water. In the second technique, thin slices of TMM were preserved and measured in TMM preserving fluid. Measurements were undertaken over a 1-y period. The measured SoS values of an IEC agar TMM calculated with the Vevo 770 and SAM system were found to be 1538.2 ± 14.5 m/s for the FTMMs and 1544.0 ± 3.5 m/s for the UTMMs. For FTMMs the SoS results were <10 m/s lower compared with those

published. The acoustic properties of UTMMs (SoS and attenuation values) were found to be in good agreement with results in earlier studies by Brewin et al. (2008) over the range 17–23 MHz, Sun et al. (2012) over the range 10–47 MHz and Rajagopal et al. (2014) over the range 1–60 MHz. Nevertheless, the results for both FTMMs and UTMMs were consistent at low frequencies (Browne et al. 2003; Inglis et al. 2006) and within the range provided by the IEC (2001). However, the attenuation coefficient was found to be non-linear as a function of frequency. The attenuation was found to increase as $0.4649f + 0.007363f^2$ for FTMMs and as $0.4897f + 0.008366f^2$ for UTMMs with increasing frequency. This second-degree polynomial fit was derived based on the data generated in this study using two different measurement systems and was found to be able to estimate the attenuation of this IEC agar TMM in the frequency range 4.5–50 MHz. The quadratic term was also found to be in good agreement with previous studies.

Finally, this study indicated that using UTMM slices, maintained and measured in TMM preserving fluid, results in approximately four times smaller SD values for the SOS and up to five times smaller variation for the attenuation values compared with the common method using FTMM slices measured in degassed, deionised water. This suggests that despite compensation within the calculation of the attenuation effects of the Saran Wrap, additional acoustic effects are introduced that are not fully compensated using the standard technique (FTMMs). Moreover, this study has also brought into question the validity and subsequent stability of encasing gel TMM QA phantoms in a sealed film-dry environment.

Acknowledgments—We thank Dr. David Kenwright, Mr. Adrian Thomson, Mr. Chris McLeod and Dr. Bakary Diarra for their help during the production of this work and to the National Physical Laboratory for acoustic characterisation of the TMM preserving fluid. This study was funded by a CONACyT (Becas al Extranjero 2014) PhD studentship and a Carnegie Trust Small Research Grant (31921).

REFERENCES

American Institute of Ultrasound in Medicine (AIUM), Technical Standards Committee. Methods for specifying acoustic properties of tissue-mimicking phantoms and objects. 2nd edition. Laurel, MD: Author 2014.

Banchhor SK, Araki T, Londhe ND, Ikeda N, Radeva P, Elbaz A, Saba L, Nicolaides A, Shafique S, Laird JL, Suri JS. Five multiresolution-based calcium volume measurement techniques from coronary IVUS videos: A comparative approach. Comput Methods Programs Biomed 2016;134:237–258.

Bilaniuk N, Wong GSK. Speed of sound in pure water as a function of temperature. J Acoust Soc Am 1992;93:1609–1612.

Brewin M, Pike LC, Rowland DE, Birch MJ. The acoustic properties, centered on 20 MHz, of an IEC agar-based tissue-mimicking material and its temperature, frequency and age dependence. Ultrasound Med Biol 2008;34:1292–1306.

Browne JE, Ramnarine K, Watson AJ, Hoskins PR. Assessment of the acoustic properties of common tissue-mimicking test phantoms. Ultrasound Med Biol 2003;29:1053–1060.

Cannon LM, Fagan AJ, Browne JE. Novel tissue mimicking materials for high frequency breast ultrasound phantoms. Ultrasound Med Biol 2011;37:122–135.

Cournane S, Cannon L, Browne JE, Fagan AJ. Assessment of the accuracy of an ultrasound elastography liver scanning system using a PVA-cryogel phantom with optimal acoustic and mechanical properties. Phys Med Biol 2010;55:5965–5983.

Culjat MO, Goldenberg D, Tewari P, Singh RS. A review of tissue substitutes for ultrasound imaging. Ultrasound Med Biol 2010;36:861–873.

Del Grosso VA, Mader CW. Speed of sound in pure water. J Acoust Soc Am 1972;52:1442–1446.

Duck FA. Physical properties of tissues: A comprehensive reference book. Bath: Academic Press; 1990.

Foster FS, Pavlin CJ, Harasiewicz KA, Christopher DA, Turnbull DH. Advances in ultrasound biomicroscopy. Ultrasound Med Biol 2000;26:1–27.

Inglis S, Ramnarine K, Plevris JN, McDicken WN. An anthropomorphic tissue-mimicking phantom of the oesophagus for endoscopic ultrasound. Ultrasound Med Biol 2006;32:249–259.

International Electrotechnical Commission (IEC). IEC 61685: International Standard. Ultrasonics—Flow measurement systems—Flow test object. Geneva: Author; 2001.

Kenwright DA, Sadhoo N, Rajagopal S, Anderson T, Moran CM, Hadoke PW, Gray GA, Zequiri B, Hoskins PR. Acoustic assessment of a Konjac–carrageenan tissue-mimicking material at 5–60 MHz. Ultrasound Med Biol 2014;40:2895–2902.

King DM, Moran C, McNamara JD, Fagan AJ, Browne J. Development of a vessel-mimicking material for use in anatomically realistic Doppler flow phantoms. Ultrasound Med Biol 2011;37:813–826.

Machet L, Belot V, Naouri M, Boka M, Mourtada Y, Giraudeau B, Laure B, Perrinaud A, Machet MC, Vaillant L. Preoperative measurement of thickness of cutaneous melanoma using high-resolution 20 MHz ultrasound imaging: A monocenter prospective study and systematic review of the literature. Ultrasound Med Biol 2009;35:1411–1420.

Madsen EL, Frank GR, Dong F. Liquid or solid ultrasonically tissue-mimicking materials with very low scatter. Ultrasound Med Biol 1998;24:535–542.

Meagher S, Poepping TL, Ramnarine K, Black RA, Hoskins P. Anatomical flow phantoms of the nonplanar carotid bifurcation: Part II. Experimental validation with Doppler ultrasound. Ultrasound Med Biol 2007;33:303–310.

Moran C, Ellis W, Janeczko A, Bell D, Pye S. The Edinburgh pipe phantom: Characterising ultrasound scanners beyond 50 MHz. J Phys Conf Ser 2011a;279:12008.

Moran C, Pye S, Ellis W, Janeczko A, Morris K, McNeilly AS, Fraser H. A comparison of the imaging performance of high resolution ultrasound scanners for preclinical imaging. Ultrasound Med Biol 2011b;37:493–501.

Pinkerton JMM. The absorption of ultrasonic waves in liquids and its relation to molecular constitution. Proc Phys Soc B 1949;62:129–141.

Rajagopal S, Sadhoo N, Zeqiri B. Reference characterisation of sound speed and attenuation of the IEC agar-based tissue-mimicking material up to a frequency of 60 MHz. Ultrasound Med Biol 2014;41:317–333.

Ramnarine K, Anderson T, Hoskins P. Construction and geometric stability of physiological flow rate wall-less stenosis phantoms. Ultrasound Med Biol 2001;27:245–250.

Rhee S. High frequency (IVUS) ultrasound transducer technology—Applications and challenges. IEEE Int Symp Appl Ferroelectr 2007;856–857.

Schmitt C, Hadj Henni A, Cloutier G. Ultrasound dynamic microelastography applied to the viscoelastic characterization of soft tissues and arterial walls. Ultrasound Med Biol 2010;36:1492–1503.

Sun C. Acoustic characterisation of ultrasound contrast agents at high frequency. PhD University of Edinburgh, Edinburgh, Scotland, UK; 2012.

Sun C, Pye S, Browne J, Janeczko A, Ellis B, Butler M, Sboros V, Thomson AJW, Brewin MP, Earnshaw CH, Moran C. The speed of sound and attenuation of an IEC agar-based tissue-mimicking material for high frequency ultrasound applications. Ultrasound Med Biol 2012;38:1262–1270.

Sundholm JKM, Olander RFW, Ojala TH, Andersson S, Sarkola T. Feasibility and precision of transcutaneous very-high resolution ultrasound for quantification of arterial structures in human neonates: Comparison with conventional high resolution vascular ultrasound imaging. Atherosclerosis 2015; 239:523–527.

Teirlinck CJ, Bezemer RA, Kollmann C, Lubbers J, Hoskins P, Fish P, Fredfeldt KE, Schaarschmidt UG. Development of an example flow test object and comparison of five of these test objects, constructed in various laboratories. Ultrasonics 1998;36:653–660.

Xu J, Tripathy S, Rubin JM, Stidham RW, Johnson LA, Higgins PDR, Kim K. A new nonlinear parameter in the developed strain-to-applied strain of the soft tissues and its application in ultrasound elasticity imaging. Ultrasound Med Biol 2012;38:511–523.

Yang X, Sun C, Anderson T, Moran C, Hadoke PWF, Gray G, Hoskins P. Assessment of spectral Doppler in preclinical ultrasound using a small-size rotating phantom. Ultrasound Med Biol 2013;39:1491–1499.

Ultrasound in Med. & Biol., Vol. 44, No. 3, pp. 702–713, 2018

0301-5629/$ - see front matter

https://doi.org/10.1016/j.ultrasmedbio.2017.11.003

● *Original Contribution*

ACOUSTIC PROPERTIES OF SMALL ANIMAL SOFT TISSUE IN THE FREQUENCY RANGE 12–32 MHZ

Adela Rabell-Montiel,* Adrian J. Thomson,* Tom A. Anderson,* Stephen D. Pye,† and Carmel M. Moran*

* Centre for Cardiovascular Science, University of Edinburgh, Edinburgh, United Kingdom; and † Medical Physics, NHS Lothian, Royal Infirmary of Edinburgh, Edinburgh, United Kingdom

(*Received* 27 *July* 2017; *revised* 16 *October* 2017; *in final form* 7 *November* 2017)

Abstract—Quality assurance phantoms are made of tissue-mimicking materials (TMMs) the acoustic properties of which mimic those of soft tissue. However, the acoustic properties of many soft tissue types have not been measured at ultrasonic frequencies >9 MHz. With the increasing use of high-frequency ultrasound for both clinical and pre-clinical applications, it is of increasing interest to ensure that TMMs accurately reflect the acoustic properties of soft tissue at these higher frequencies. In this study, the acoustic properties of *ex vivo* brain, liver and kidney samples from 50 mice were assessed in the frequency range 12–32 MHz. Measurements were performed within 6 min of euthanasia in a phosphate-buffered saline solution maintained at 37.2 ± 0.2 °C. The measured mean values for the speed of sound for all organs were found to be higher than the International Electrotechnical Commission guideline recommended value for TMMs. The attenuation coefficients measured for brain, liver and kidney samples were compared with the results of previous studies at lower frequencies. Only the measured kidney attenuation coefficient was found to be in good agreement with the International Electrotechnical Commission guideline. The information provided in this study can be used as a baseline on which to manufacture a TMM suitable for high-frequency applications. (E-mail: adela.rabell@ed.ac.uk) **© 2018 World Federation for Ultrasound in Medicine & Biology. All rights reserved.**

Key Words: **Ultrasound, High frequency, Mice, Brain, Liver, Kidney, Speed of sound, Attenuation.**

INTRODUCTION

The purpose of tissue-mimicking materials (TMMs) is to mimic the acoustic properties of soft tissue. Currently, the International Electrotechnical Commission (IEC 2001) guideline recommends standard values for the speed of sound (SoS) (1540 ± 15 m/s) and an attenuation coefficient for TMM of 0.5 ± 0.05 dB/cm at frequencies up to 10 MHz. Also, the International Commission on Radiation Units and Measurements (ICRU 1998) reports that for non-fatty tissues, the attenuation at 1 MHz should be 0.6 dB/cm. With the increasing use of high-frequency ultrasound in both clinical (2–15 MHz) and pre-clinical (>15 MHz) (Banchhor et al. 2016; Cook et al. 2011; Machet et al. 2009; Moran 1995; Rhee 2007; Schmitt et al. 2010; Sundholm et al. 2015; Xu et al. 2012) imaging applications, there is a need to extend the frequency range of these recommended acoustic values. Furthermore, the development of phantoms that incorporate TMMs that realistically mimic the acoustic properties of small animal soft tissue will enable a reduction in the use of small animals to optimize ultrasound imaging techniques.

The acoustic properties of brain, liver and kidney, among other organs, have previously been measured in small animals (Foster et al. 2000; Frizzel and Gindorf 1981; Goss et al. 1979; Gray et al. 2013; Szabo 2014; Tervola et al. 1985), humans (Bamber and Hill 1979; Bamber 1981; Kremkau et al. 1981; Ludwig 1950; Parker 1983; Rajagopalan et al. 1979; Sehgal et al. 1986) chickens (Martínez-Valdez et al. 2015) and mammals (Bamber et al. 1977; Ghoshal et al. 2011; Goss et al. 1979; López-Haro et al. 2010; Martial and Cachard 2007). These studies measured the acoustic properties up to 9 MHz at either room temperature (22 °C–26 °C) or human body temperature (37 °C). Wirtzfeld et al. (2015) measured the extracellular matrix (ECM) attenuation coefficient of murine liver and kidney across the frequency range 15–35 MHz using

Address correspondence to: Adela Rabell-Montiel, Queen's Medical Research Institute, Cardiovascular Science, 47 Little France Crescent, EH16 4 TJ, Edinburgh, UK. E-mail: adela.rabell@ed.ac.uk

a decellularized method and found that the ECM of the organ contributes to the ultrasonic properties. Additionally, Frizzel and Gindorf (1981), O'Brien (1988) and Tervola et al. (1985) performed very high frequency acoustical measurements up to 100 MHz using a scanning laser acoustic microscope (SLAM). Measurements performed at 100 MHz were undertaken at room temperature (20 °C–26 °C).

It has been reported that the SoS and attenuation coefficient of soft tissue increase with increasing temperature (Bamber and Hill 1979; Ghoshal et al. 2011; López-Haro et al. 2010; Rajagopalan et al. 1979; Suomi et al. 2016). However, there is no further increase in the SoS in soft tissue above 50 °C (Duck 2012). Furthermore, it is well known that *ex vivo* soft tissue samples deteriorate with time after excision as gas bubbles form within the tissue, affecting its acoustic properties (Bamber 1981; Duck 2012). To prevent this, soft tissue should be excised and measured as soon as possible after euthanasia or stored at 4 °C (Bamber et al. 1977; Bamber and Nassiri 1985; Foster and Hunt 1979).

The acoustic properties of soft tissue have also been measured *in vitro* or by embedding the organ sample in an ultrasound-compatible acoustic material such as TMM (Bamber and Hill 1979; Bamber et al. 1977; Goss et al. 1979; Martínez-Valdez et al. 2015; Muleki-Seya et al. 2016; Sundholm et al. 2015; Suomi et al. 2016), but very few experiments have been undertaken using *ex vivo* tissue (Kumagai et al. 2014) or *in vivo* tissue (Kagadis et al. 2010; Zderic et al. 2004).

To address the current limited data on the acoustic properties of soft tissue, the study described here sought to measure the acoustic properties of *ex vivo* mouse brain, liver and kidney immersed in phosphate-buffered saline (PBS, Sigma-Aldrich, Saint Louis, MO, USA) at 37 °C, over the frequency range 12–32 MHz.

METHODS

Soft tissue sample preparation

We analyzed 20 brains, 20 livers and 20 kidneys from 50 recently euthanized healthy male C57BL/6 mice, a common inbred laboratory mouse strain. The mice were euthanized by cervical dislocation under the auspices of the Animals (Scientific Procedures) Act 1986 (Schedule 1) approved by the University of Edinburgh Animal Welfare and Ethical Review Board (AWERB). Within 6 min of euthanasia, the organs were extracted and sliced in either the coronal or transverse plane, and their acoustic properties were measured. Excised mouse tissues were sliced using a 1-mm adult rat brain acrylic slicer matrix (Zivic Instruments, Pittsburgh, PA, USA).

Twenty brains were excised and sliced in the frontal plane at the superior colliculus, which included the cerebral cortex (Fig. 1a). For brain tissue, the sample thickness was 3 mm, as thinner samples tended to disintegrate during handling. Acoustical measurements were made in the center of each sample, within the grey matter. Twenty murine left lateral liver lobes were excised and sliced in the coronal plane, to a thickness of 2 mm (Fig. 1b). Twenty kidneys from 10 mice were excised and sliced (2 mm) as follows: the right kidney was sliced in the coronal plane (Fig. 1c), and the left kidney was sliced in the transverse plane (Fig. 1d). Acoustical measurements were undertaken in the center of each sliced kidney sample in an endeavor to ensure location within the *medulla* of the kidney. Only one tissue sample was collected from each organ. The lateral (radial) dimensions of the samples were 0.5 cm for brain, 1 cm for liver and 0.5 cm for both dissection planes in the kidney.

Experimental setup using the high-frequency Vevo 770 ultrasound scanner

A temperature-controlled water-filled reservoir (Grant Instruments, Cambridge, UK) with dimensions of $15 \times 33 \times 19$ cm was used to heat phosphate-buffered saline (PBS; Sigma-Aldrich, Saint Louis, MO, USA) to 37.2 ± 0.2 °C. A smaller glass container ($10 \times 8 \times 7.5$ cm and 0.6 cm thick) was placed inside the water reservoir. A 1-cm layer of acoustic absorber (Aptflex F28, Precision Acoustics, Dorset, UK) was fixed at the bottom of the glass container. A 2.5-cm-diameter, and 5-mm-thick cylindrical acoustic reflector made from polymethylpentene (TPX; Boedeker Plastics, Shiner, TX, USA) was glued to the absorber. A 1-mm-thick, 2.5-mm-inner-diameter, 2.5-cm-outer-diameter circular washer made of the acoustic absorber was attached to the top surface of the TPX reflector, as illustrated in Figure 2. The circular washer acted as a tissue holder and ensured there was a space between the soft tissue sample and the TPX reflector. The aim of this separation was to allow the echoes from the tissue and from the TPX reflector to be differentiated during later analysis.

Acquisition and analysis of the acoustic data

Radiofrequency (RF) data from 60 soft tissue samples were acquired using a single-element, high-frequency probe RMV707 B attached to the Vevo 770 ultrasound scanner (Visualsonics, Toronto, ON, Canada). The RMV707 B probe has a center frequency of 30 MHz, focal depth of 12.7 mm and 3-dB bandwidth from 12 to 32 MHz (Rabell Montiel et al. 2017). The acoustic properties of the soft tissues were measured while immersed in PBS at 37.2 ± 0.2 °C. The TPX reflector was located at the focal point of the probe (Fig. 2). Data were collected at 10% of maximum acoustic output power (peak negative pressure: 1.05 MPa), which gave a satisfactory signal-to-noise ratio while avoiding significant non-linear propagation effects (Sun et al. 2012). By use of a broadband

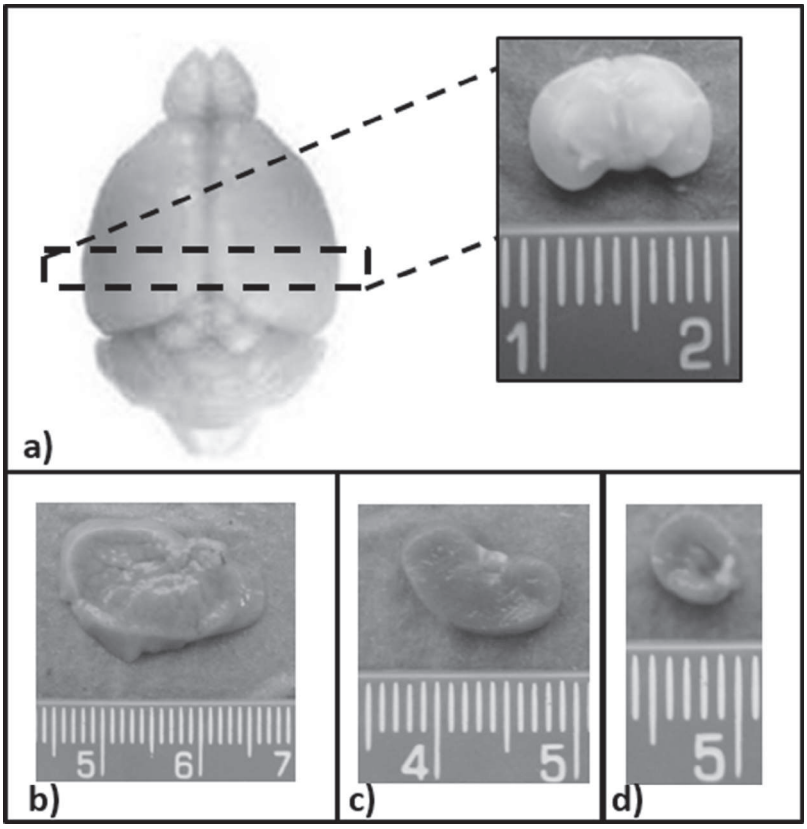

Fig. 1. Examples of how the brain (a), liver (b), and kidney (c and d) were sliced within 6 min after euthanasia.

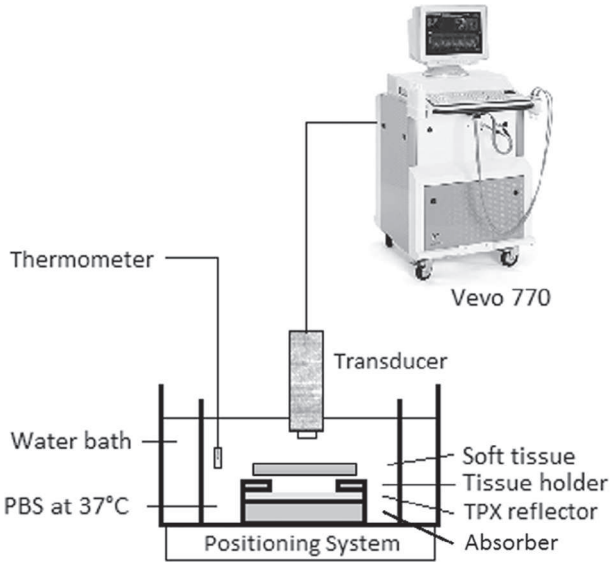

Fig. 2. Experimental setup using the RMV707 B from the preclinical ultrasound scanner Vevo 770 (Visualsonics, Toronto, ON, Canada). The tissue holder (circular washer) was made from an acoustic absorber material (Aptflex F28, Precision Acoustics, Dorset, UK). PBS = phosphate-buffered saline; TPX = polymethylpentene.

pulse-echo substitution technique (American Institute of Ultrasound in Medicine [AIUM] 2014), the data were analyzed based on pre-selected regions of interest (ROIs). These ROIs were located at the front and rear of the sample and at the front surface of the TPX reflector with and without the sample placed in the acoustical path. Acoustic data were acquired from 10 ultrasonic data lines distributed equally across the ROIs, and measurements were undertaken at 37.2 ± 0.2 °C.

After slicing, the sample was immediately immersed and mounted in the tissue holder in the PBS tank, ready for acoustic measurements to be undertaken. Precise thickness measurements were obtained using the timing of the echoes from the front and rear surfaces of the sample. The tissue holder was necessary to enable these measurements to be made accurately and reproducibly.

Three measurements were undertaken for each sample: immediately after immersion in PBS ($t = 0$), after 5 min ($t = 5$) and after 10 min ($t = 10$). The PBS reference fluid was changed daily after each set of measurements. Up to three organ samples were assessed on any given day.

Acoustic properties of PBS

The PBS was prepared according to the manufacturer's recommendations (pH 7.4 at 25 °C; Sigma-Aldrich,

Saint Louis, MO, USA). PBS was chosen as a physiologic fluid to delay tissue deterioration and death and, thus, to minimize physiologic and mechanical changes within the tissue during the measurement period (Bader et al. 2015; Edgeworth et al. 2009; Foster and Hunt 1979; Garcia-Duitama et al. 2016; Lay et al. 2003; Muleki-Seya et al. 2016; Wirtzfeld et al. 2015; Worthington and Sherar 2001).

The SoS of the PBS at 37 °C was calculated using the equation

$$C = 1449.05 + (45.7t) - 5.21t^2 + 0.23t^3 + \left((1.333 - 0.126t + 0.009t^2) * (10S - 35)\right) \quad (1)$$

with a standard deviation (SD) of 0.02 m/s (Coppens 1981), where t is the temperature of the fluid ($t = T/10$, T in °C), and S is the salt concentration (in g/100 cm^3). The salinity of the PBS was calculated as 0.41 g/100 cm^3. At 37 °C, the SoS used in this study was calculated to be 1527.9 m/s.

The attenuation of PBS was measured using a pulse-echo substitution technique (AIUM 2014) with an experimental setup similar to that illustrated in Figure 2, but without the tissue holder in place. Fifty measurements were taken using the RMV707 B and Vevo 770 scanner at 10% of maximum output power. The TPX reflector was placed at the focal depth of the transducer. Degassed, de-ionized water at 37 °C was placed in the glass box to act as a reference fluid. After acoustic measurement, the degassed de-ionized water was replaced with PBS, at the same temperature. Raw RF data were collected from 10 lines within pre-selected ROIs located at the surface of the TPX reflector and analyzed offline using a MATLAB script (MATLAB R2013 a, The MathWorks, Natick, MA, USA).

With D_F as the distance between the transducer and the front surface of the TPX reflector, the attenuation coefficient (α_0 in dB/cm) can be calculated as

$$\alpha_0(f) = -\frac{20}{2D_F} log \frac{A(f)}{A_0(f)} \quad (2)$$

where $A(f)$ and $A_0(f)$ are the magnitudes of the signal spectra from the TPX measured in degassed, de-ionized water and PBS fluid, respectively, and D_F is the distance calculated using the return time intervals of the echoes from the TPX as described above.

This enabled the attenuation coefficient of PBS to be calculated relative to degassed, de-ionized water. The SoS and the attenuation coefficient of degassed, de-ionized water are well documented (Bilaniuk and Wong 1992; Coppens 1981; Del Grosso and Mader 1972; Pinkerton 1949; Rajagopal et al. 2015). The absolute attenuation coefficient of PBS at 37 °C was calculated and fitted using a second-degree polynomial as $\alpha_0 = 0.002127 f^2 + 0.02076 f$ ($R^2 = 0.99$).

Table 1. Speed of sound measured within 6 min post-euthanasia (t = 0) and then at t = 5 and t = 10 min using a Vevo 770 pre-clinical ultrasound scanner over the frequency range 12–32 MHz

	Speed of sound (m/s), mean ± SD		
Organ	$t = 0$	$t = 5$ min	$t = 10$ min
Brain	1565.9 ± 9.6	1566.1 ± 9.5	1566.9 ± 11.2
Liver	1604.4 ± 16.5	1603.8 ± 15.9	1604.7 ± 18.2
Kidney	1575.3 ± 10.8	1574.8 ± 11.9	1574.1 ± 9.5

RESULTS

The mean age of the animal organs used in this study was 8.5 ± 3.1 mo for brains, 6.8 ± 4.9 mo for livers and 5.2 ± 3.6 mo for kidneys. The mean weight across all mice was 34.4 ± 6 g (minimum: 22.6 g, maximum: 45 g).

Table 1 lists the mean SoS values at $t = 0$ and then at the $t = 5$ and $t = 10$ min intervals for brain, liver and kidney tissue samples. It can be seen that the variation in SoS as a function of time was less than 1.5 m/s across the soft tissue samples. Although the SD of the mean SoS values increased for the brain and the liver samples in the last measurement (approximately 16 min after euthanasia), Student's t-test did not reveal that these values were statistically different ($p > 0.5$) at $t = 0$, $t = 5$ or t = 10.

The mean and SD of the SoS values of the 20 soft tissue samples from brain, liver and kidney are listed in Table 2.

The difference in SoS between the centers of the left and right kidney samples (different dissection planes) was 0.97 ± 0.69 m/s.

Figures 3, 4 and 5 illustrate the mean attenuation versus frequency at each time point for brain, liver and kidney respectively. The displayed SD was calculated from the mean attenuation data averaged over all time points. A second-degree polynomial fit was calculated to be the best fit over all the mean attenuation-versus-frequency data. The goodness of fit (R^2) for the mean attenuation-versus-frequency data over all time points varied between 0.70 and 0.85 for the small animal soft tissue. The best fits were found to be for the attenuation-versus-frequency data of brain tissue ($R^2 = 0.85$) and kidney tissue ($R^2 = 0.83$). Figures 3, 4 and 5 also illustrate the polynomial fit calculated from the data of 20 brains, 20 livers and 20 kidneys, respectively. The polynomial fit was found to be

Table 2. Speed of sound of small animal soft tissue samples measured using the Vevo 770 pre-clinical ultrasound scanner over the frequency range 12–32 MHz

Organ	Speed of sound (m/s), mean ± SD
Brain	1566.33 ± 9.9
Liver	1604.7 ± 16.8
Kidney	1574.9 ± 10.8

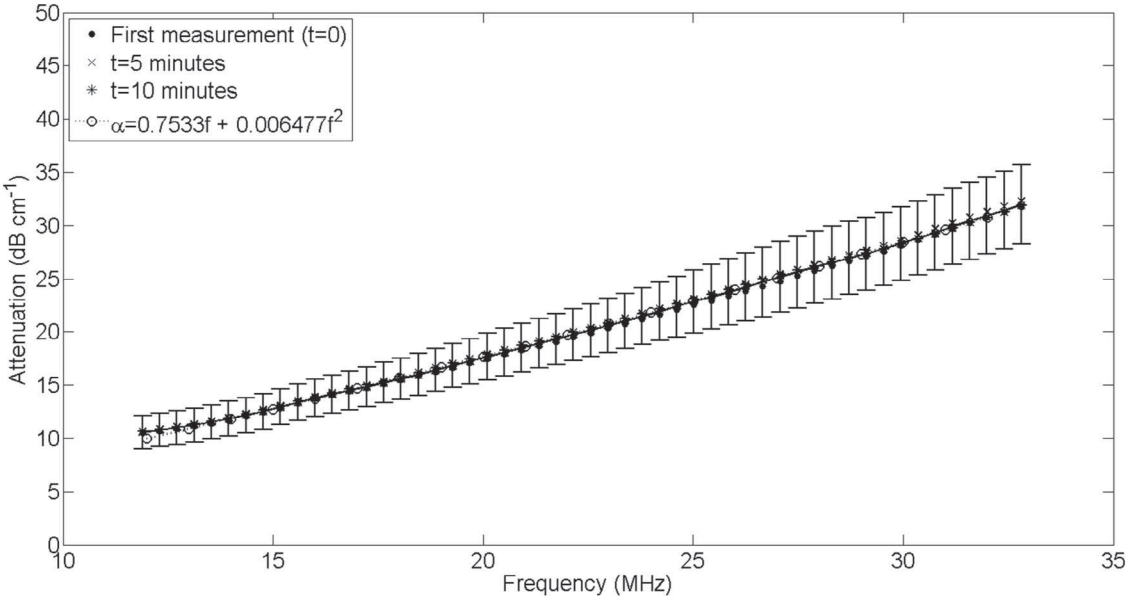

Fig. 3. Attenuation as a function of frequency for brain tissue measured the first time ($t = 0$) and then at $t = 5$ min and $t = 10$ min after initial measurement. The standard deviation shown is calculated from the mean attenuation across all time points. The second-degree polynomial fit calculated in this study is also shown. Data from 20 brain tissue samples.

$0.7533f + 0.006477f^2$ ($R^2 = 0.85$) for brain, $0.7252f + 0.01414f^2$ ($R^2 = 0.70$) for liver and $0.5771f + 0.006322f^2$ ($R^2 = 0.83$) for kidney in the frequency range 12–32 MHz.

Figures 6, 7 and 8 illustrate the polynomial fit previously calculated, from the mean attenuation across all time points, with other published studies for each organ. The polynomial fit found in this study has been extended to lower frequencies for comparison purposes. Figure 9 illustrates the three polynomial fits calculated for each organ in this study in comparison with the attenuation coefficient of the IEC agar-TMM (Rabell Montiel et al. 2017) in the frequency range 4.5–50 MHz and the IEC guideline (IEC 2001). The IEC recommended values are the most widely used; therefore, in this study the

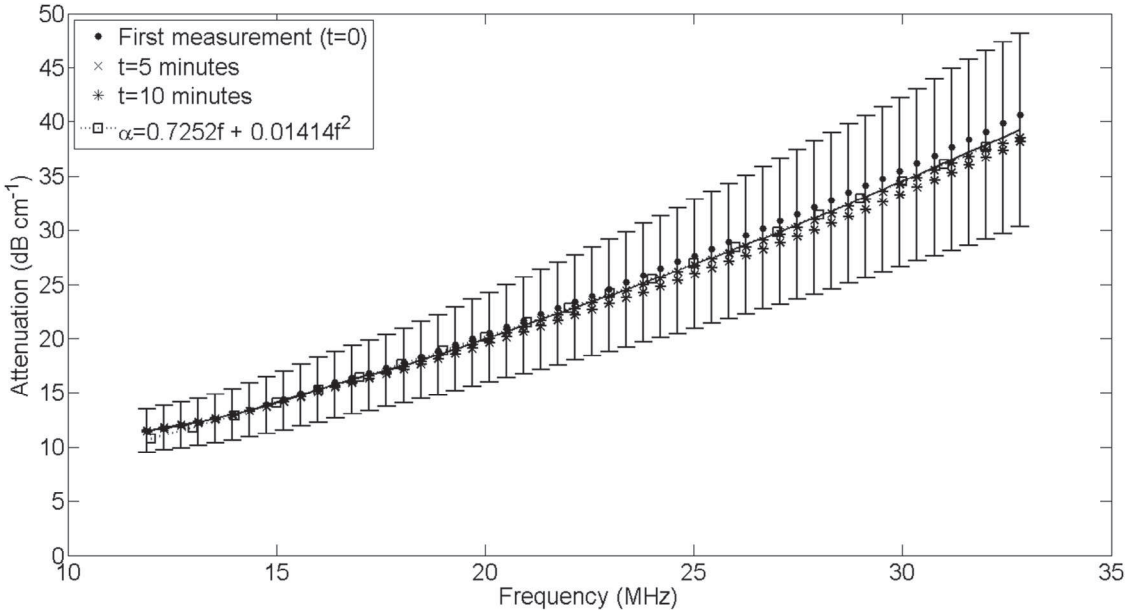

Fig. 4. Attenuation as a function of frequency for liver tissue measured the first time ($t = 0$) and then at $t = 5$ min and $t = 10$ min after initial measurement. The standard deviation shown is calculated from the mean attenuation across all time points. The second-degree polynomial fit calculated in this study is also shown. Data from 20 liver tissue samples.

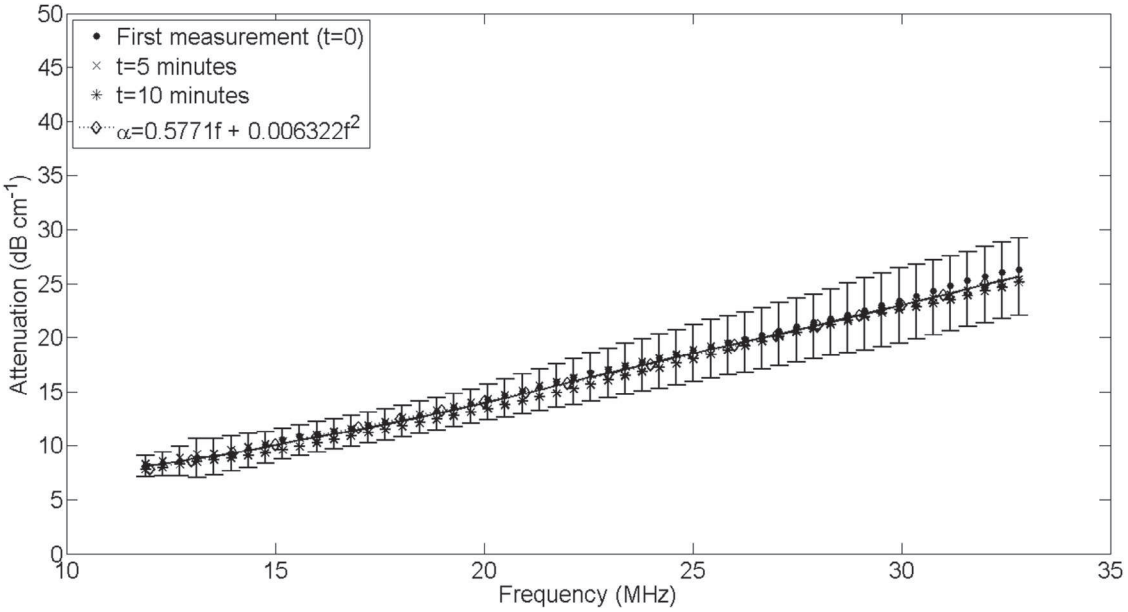

Fig. 5. Attenuation as a function of frequency for kidney tissue measured the first time ($t = 0$) and then at $t = 5$ min and $t = 10$ min after initial measurement. The standard deviation shown is calculated from the mean attenuation across all time points. The second-degree polynomial fit calculated in this study is also shown. Data from 20 kidney samples (10 left and 10 right kidneys).

acoustic properties of soft tissues were compared with these values.

DISCUSSION

The aim of this study was to measure the acoustic properties of *ex vivo* small animal soft tissue. Twenty brains, 20 kidneys (10 left and 10 right kidneys) and 20 livers were extracted from 50 mice and sliced, and their acoustic properties measured using a pre-clinical ultrasound scanner within 6 min post-euthanasia. Table 3 lists the SoS values of published studies of the acoustic properties of brain, liver and kidney from various sources at room and body temperature.

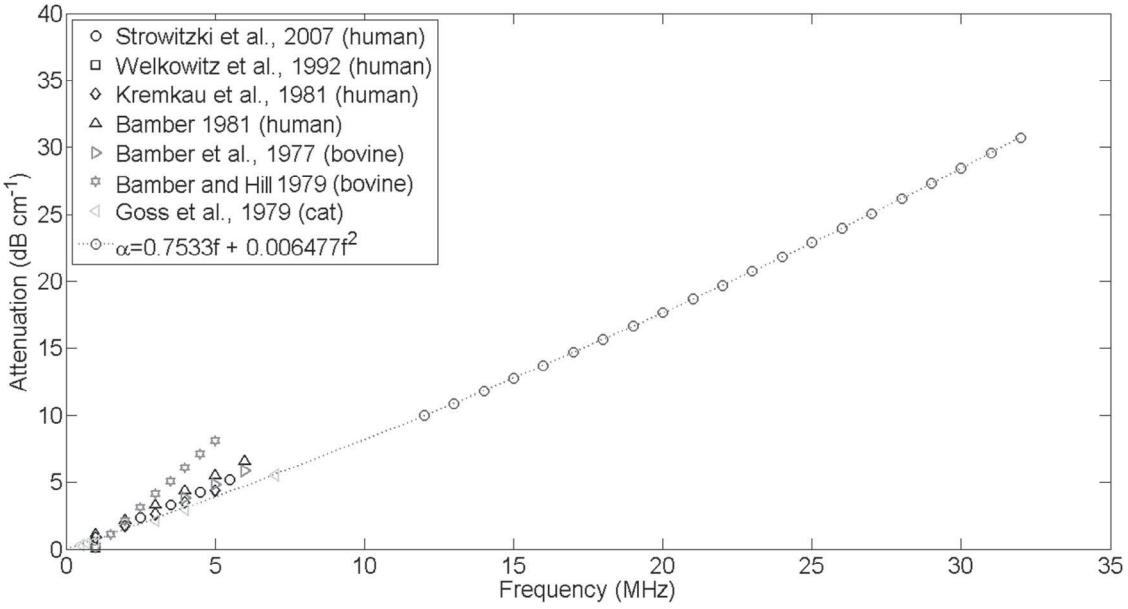

Fig. 6. Attenuation versus frequency of brain soft tissue data published in the literature and the second-degree polynomial fit calculated in this study. The polynomial fit was calculated from the acoustical data collected from 20 mouse brains and was extended to low frequencies (*dotted line*) for comparison purposes.

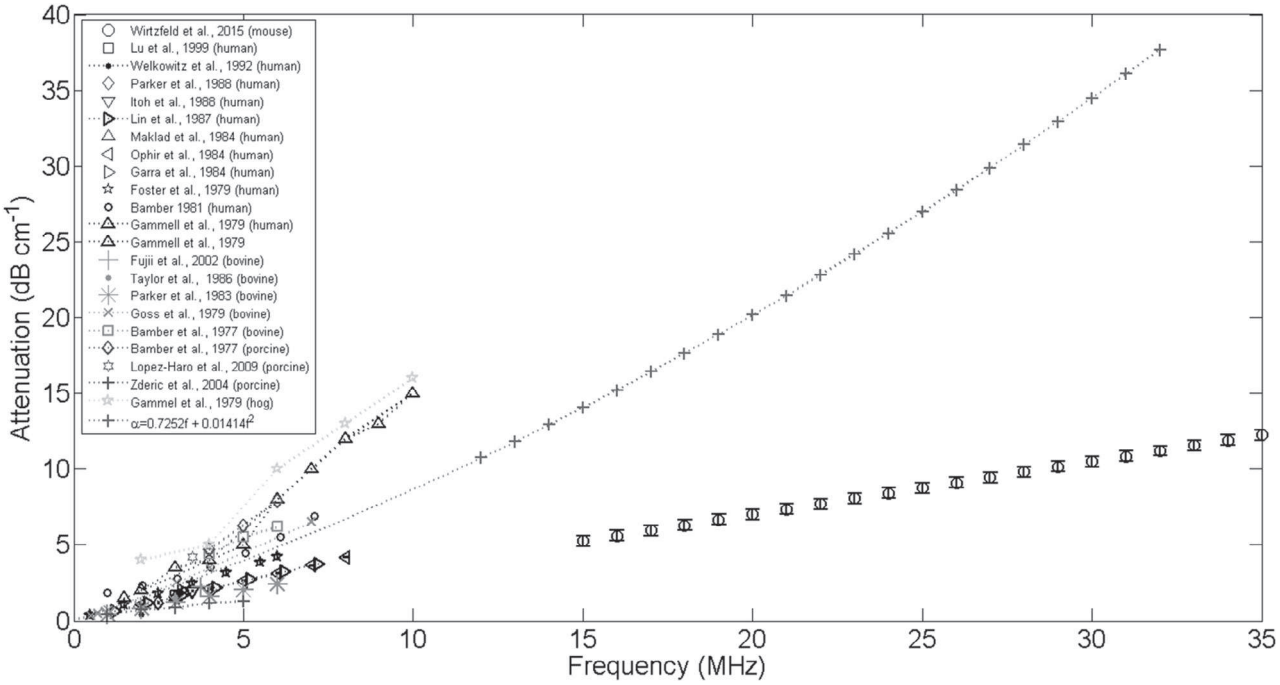

Fig. 7. Attenuation versus frequency of liver soft tissue data published in the literature and the second-degree polynomial fit calculated in this study. The polynomial fit was calculated from the acoustical data collected from 20 mouse livers and was extended to low frequencies (*dotted line*) for comparison purposes..

An increase in either water or fat content results in a decreased velocity of ultrasound in soft tissue (Duck 2012). For the brain and liver samples, SoS and attenuation were analyzed against the weight and age of the animal and against the measured thickness of the sample (data not shown). Also, the SoS and attenuation coefficient of the soft tissue samples were analyzed as a function of time after excision, up to 15 min. None of these variables were

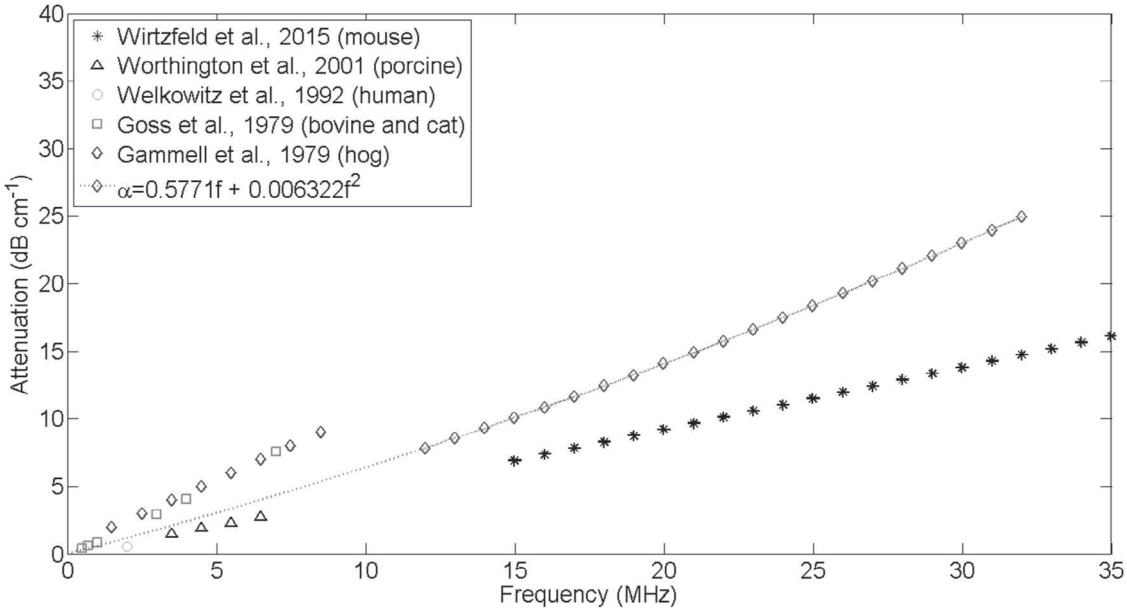

Fig. 8. Attenuation versus frequency of the kidney soft tissue data published in the literature and the second-degree polynomial fit calculated in this study. The polynomial fit was calculated from the acoustical data collected from 20 mouse kidneys (10 left and 10 right) and was extended to low frequencies (*dotted line*) for comparison purposes.

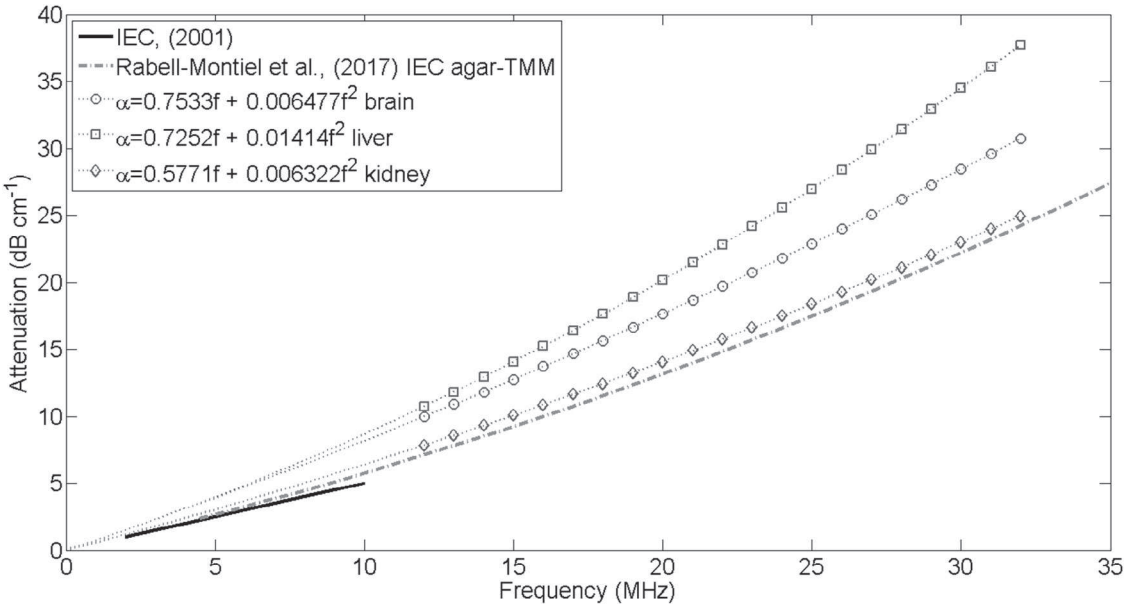

Fig. 9. Attenuation versus frequency of polynomial fit found in this study, comparison with the attenuation data for International Electrotechnical Commission (IEC) agar tissue-mimicking material (IEC 2001; Rabell Montiel et al. 2017).

found to have a relationship with the measured acoustic properties.

Acoustic properties of PBS

In other studies, the acoustic properties of PBS were considered similar to those of degassed, de-ionized water at the same temperature (Muleki-Seya et al. 2016). In addition, some studies used saline (9% salinity) as their acoustic reference fluid (Kumagai et al. 2014) and obtained a SoS of 1536 m/s at 36 °C. However, saline has higher salinity than PBS (4%).

The calculated SoS for PBS at 37 °C used in this study was 1527.9 m/s. This SoS value was found to be 8.14 m/s less than the SoS for saline (Kumagai et al. 2014) and up to 4.5 m/s greater than the SoS for pure water (Bilaniuk and Wong 1992; Del Grosso and Mader 1972).

Table 3. Speed of sound (SoS) of the small animal soft tissue samples, brain, liver and kidney from published studies. The values measured in this study has been added for comparison purposes only. Blank spaces indicate that no information is available

Organ	Temperature (°C)	Frequency (MHz)	SoS (m/s), mean ± SD	Source of tissue	Reference
Brain	37	1–5	1562 ± 1.2	Human	Kremkau et al. 1981
		1	1510		Welkowitz et al. 1992
		12–32	**1566.33 ± 9.9**	**Mouse**	**This study**
Liver	22	100	1570 ± 10	Rat	O'Brien 1988
	Room	100	1550		Tervola et al. 1985
	36.3		1596 ± 4.8	Human	Kumagai et al. 2014
		2	1510		Welkowitz et al. 1992
	37	3	1578.3 ± 5.4		Chen et al. 1987
	37.2		1578.1 ± 2.9		Sehgal et al. 1986
	20	1–6	1577 ± 11		Bamber and Hill 1980
	37	1–7	1607		Bamber and Hill 1979
		1–7	1597–1639	Bovine	Bamber and Hill 1979
		3.5	1579	Pig	Lopez-Haro et al. 2010
	23–26	100	1565 ± 7.8	Sheep/cat	Frizzel and Gindorf 1981
			1567 ± 13.2		
	21.8	5	1588.2	Chicken	Martinez-Valdez et al. 2015
	46	5	1609.8		
	37.2	**12–32**	**1604.7 ± 16.8**	**Mouse**	**This study**
Kidney		2	1560	Human	Welkowitz et al. 1992
	37.2	100	1560.2 ± 1.8		Rajagopalan et al. 1979
	37	3.5–7	1571	Pig	Worthington and Sherar 2001
	23–26	100	1586 ± 10.7	Mouse	Frizzel and Gindorf 1981
	37.2	**12–32**	**1574.9 ± 10.8**	**Mouse**	**This study**

Additionally, Worthington and Sherar (2001) measured a SoS for PBS at 37 °C of 1541 m/s, but using a salinity of 0.9% in Coppens's (1981) formula. This results in a SoS value of 13.1 m/s higher than the SoS value used in this study. The difference in the calculated SoS values between saline and PBS is likely due to the different salt concentrations.

The attenuation data for PBS at 37 °C calculated in this study was found to be similar to that of degassed, deionized water, and was proportional to f^2 over the frequency range 12–32 MHz. Previous published studies (Muleki-Seya et al. 2016; Worthington and Sherar 2001) that used PBS as a reference fluid assumed the attenuation coefficient to be the same as that of water (2.17×10^{-3} dB/cm/MHz^2 at 20 °C) (Duck 2012). At 32 MHz, the difference in attenuation coefficient between pure water at 20 °C and PBS at 37 °C was found to be 0.67 dB/cm.

Brain

The SoS measured in the brain samples is in good agreement with Kremkau et al. (1981) where measurements were taken from human brain samples over the frequency range 1–5 MHz and measured at 37 °C. However, the SoS measured in this study was 56 m/s higher than that of human brain tissue samples measured by Welkowitz et al. (1992).

For brain attenuation, the largest inter-sample difference of 13.2 dB/cm was found at 26 MHz. By extending the second-degree polynomial fit calculated in this study to lower frequencies, we found that the attenuation from this study agrees at 1 MHz with a 0.5 dB/cm difference with the values of Bamber (1981), Goss et al. (1979), Kremkau et al. (1981) and Welkowitz et al. (1992). Compared with the extended polynomial fit at lower frequencies, the maximum difference was found to be 5 dB/cm at 5 MHz (Foster and Hunt 1979; Gammell et al. 1979). Moreover, the attenuation-versus-frequency data measured in this study were re-expressed and extended to lower frequencies as a power law of the form af^b, where f is the frequency (MHz) and a and b are the coefficients of the fit. The power law fit calculated for the brain was 0.91 dB/cm/MHz ($R^2 = 0.84$). Kremkau et al. (1981) reported an attenuation of 1.08 dB/cm/MHz, Bamber (1981) reported 1.1 dB/cm/MHz and Strowitzki and Brand (2007) reported 0.94 ± 0.13 dB/cm/MHz. The maximum difference in the attenuation power law fit was with Bamber and Hill (1979) by 4.2 dB/cm at 5 MHz (Fig. 6).

Liver

There have been extensive publications of the acoustical properties of liver at low frequencies, yielding a wide range of SoS and attenuation coefficient values. Based on those studies published for mammalian livers, at ultrasound frequencies ranging from 1 to 9 MHz at different temperatures (22 °C and 37 °C), the SoS varied between 1545 and 1639 m/s (Bamber and Hill 1979, 1980; Chen et al. 1987; Frizzel and Gindorf 1981; Kumagai et al. 2014; Martínez-Valdez et al. 2015; Welkowitz et al. 1992). The attenuation coefficient from those published studies (Fig. 7) varied between 0.35 and 1.3 dB/cm/MHz (Bamber et al. 1977; Fujii et al. 2002; Garra et al. 1984; Goss et al. 1979; Itoh et al. 1988; López-Haro et al. 2010; Lu et al. 1999; O'Brien 1988; Ophir et al. 1984; Parker 1983; Parker et al. 1988; Taylor et al. 1986; Welkowitz et al. 1992).

The SoS of liver measured in this study was found to be within 5 m/s of the values in the studies by Bamber and Hill (1979) and Martínez-Valdez et al. (2015) and was up to 33 m/s higher than those of Bamber and Hill (1980), Chen et al. (1987), Kumagai et al. (2014), Martínez-Valdez et al. (2015), López-Haro et al. (2010), O'Brien (1988) and Sehgal et al. (1986). The largest difference was found to be with Welkowitz et al. (1992), who reported a SoS of 1510 m/s at 2 MHz.

It is known that during excision, gas is more likely to be introduced into the liver than into any other organ because of its highly vascular structure and its tendency to produce gas during autolytic decay. The presence of gas in specimens is reported to be the greatest problem in the preparation of soft tissue samples for acoustical measurements (Bamber 1981). Measurements in this study were initiated within 6 min post-euthanasia, and during measurement sequences, the samples were kept in PBS at 37 °C. Therefore, it is not believed that the high variability (18 dB/cm at 32 MHz, see Fig. 4) of the attenuation coefficient in this study derives from the production of gas by autolytic decay.

Previous studies obtained attenuation coefficients ranging between 0.44 and 0.65 dB/cm/MHz (Fujii et al. 2002; Itoh et al. 1988; Lu et al. 1999; Parker et al. 1988). Even though the attenuation of liver has been studied extensively in various publications, there is an 8.8 dB/cm variability in the attenuation coefficients at 9 MHz (Garra et al. 1984; Itoh et al. 1988; Lu et al. 1999; Maklad et al. 1984; Parker et al. 1988; Taylor et al. 1986). The attenuation of the liver has also been studied at frequencies similar to those used in this study. Wirtzfeld et al. (2015) found a difference of 26.5 dB/cm at 32 MHz compared with the results of this study. This difference could be due to the decellularized method used by Wirtzfeld et al. (2015) versus the fresh tissue *ex vivo* method used in this study. Furthermore, by extending the second-degree polynomial fit found in this study to lower frequencies (Fig. 7), the data from this study were found to be in good agreement with the data published for bovine and human liver at 37 °C up to 9 MHz (Foster and Hunt 1979; Fujii et al. 2002; Gammell et al. 1979; Goss et al. 1979; Lu et al. 1999). Also, the second-degree polynomial fit calculated in this study was found to be in agreement within ±6 dB/cm with

those for pig, rat and human livers measured up to 9 MHz by López-Haro et al. (2010), O'Brien (1988), Lu et al. (1999) and Gammell et al. (1979).

The attenuation-versus-frequency data for liver samples calculated in this study can also be expressed as a power law of the form 1.08 dB/cm/MHz ($R^2 = 0.66$). This power law was found to be in good agreement (±0.42 dB/cm/MHz) with those power laws reported for pig (1.2 dB/cm/MHz (López-Haro et al. 2010)), rat (1.3 ± 0.09 dB/cm/MHz (O'Brien 1988)) and human (1.6 ± 0.21 dB/cm/MHz (Lu et al. 1999), 1.5 dB/cm/MHz (Gammell et al. 1979)) livers.

Kidney

The difference in SoS values between the left and right kidneys, using different dissection planes, was 0.97 m/s. Based on the second polynomial fit, the difference in attenuation coefficient was found to be a maximum of 1.31 dB/cm between the planes across the frequency range 12–32 MHz. Despite measurement of the acoustic properties from different dissection planes, the mean attenuation values did not exhibit a consistent variation. Previous work has indicated that the variations in acoustic properties of the kidney are associated with five sections across the longitudinal axis in canine renal anatomy (Sarvazyan and Klemin 1983). In that study, the SoS exhibited a difference of 5 m/s and a difference of 0.5 dB/cm at 8.8 MHz in dog kidney (from the *cortex* through to the *renal veins*).

In this study, an endeavor was made to ensure measurements were undertaken within the medulla in both dissection planes. The limited variation in our measurements would suggest that this has been achieved. The acoustic properties found for both the left and right kidneys were combined by taking the mean value and comparing the means with those in the literature. The mean magnitude of the SoS values from the kidney was found to lie within the range of values obtained from studies published on human and mouse kidneys at different temperatures (Table 3). Inter-sample attenuation as a function of frequency was found to vary up to 5 dB/cm at 30–32 MHz, and the smallest difference, 1 dB/cm, was seen at 3 MHz. In Figure 8, the polynomial fit calculated in this study is compared with those in published studies. The magnitude of the attenuation data calculated using the second-degree polynomial fit calculated in this study fall within the magnitude of attenuation found in the published studies. This polynomial fit was found to be smaller by 2.7 dB/cm compared with data from Gammell et al. (1979), Goss et al. (1979) and Welkowitz et al. (1992), and higher by up to 1.6 dB/cm compared with data reported by Worthington and Sherar (2001) in the frequency range 1–9 MHz. The attenuation-versus-frequency data for kidney can be fitted to a power-law curve. The power-law fit obtained was 0.73 dB/cm/MHz ($R^2 = 0.81$). This fit gave values of attenuation as much as 0.33 dB/cm/MHz higher than the attenuation measured for bovine and porcine kidney at 37 °C and 45 °C (Goss et al. 1979; Worthington and Sherar 2001). These differences could be attributable to differences in animal kidneys or to the difference in temperatures at which the studies were undertaken up to 65 °C (Worthington and Sherar 2001). The kidney has been studied up to 35 MHz by Wirtzfeld et al. (2015), the difference in the attenuation coefficient with this study was found to be up to 10.2 dB/cm at 32 MHz.

Comparison with TMM

The frequency range used in this study (12–32 MHz) falls out-with the range over which the IEC guidelines give recommended values (2–10 MHz). However, assuming that dispersion is insignificant, the biggest difference in the SoS from recommended TMM SoS values was found in liver tissue (64 m/s).

For the attenuation coefficient, the polynomial fits calculated from the brain, liver and kidney tissue data were compared with previously published acoustical measurements for the IEC agar-TMM (Fig. 9) up to 50 MHz. The attenuation of kidney matched that of the IEC agar-TMM with a consistent difference of 0.5 dB/cm in the frequency range 12 to 32 MHz. This difference falls within the 2 dB/cm SD specified for IEC agar-TMM attenuation (Rabell Montiel et al. 2017). The largest difference in the attenuation coefficient was found to be that for liver tissue, 14 dB/cm at 32 MHz, compared with IEC agar-TMM (Rabell Montiel et al. 2017).

CONCLUSIONS

The acoustical properties of mouse soft tissue samples (brain, liver and kidney) were measured over the frequency range 12–32 MHz while immersed in PBS at 37 °C. The samples were obtained from recently euthanized C57BL/6 healthy male mice with a mean age of 6.9 ± 3.9 mo. Measurements were undertaken within 6 min after euthanasia and then at 5 and 10 min after the first measurement.

The measured SoS values of the brain, liver and kidney were found to be 1566.3 ± 9.9, 1604.7 ± 16.8 and 1574.9 ± 10.8 m/s, respectively. For all the small animal soft tissues, the SoS results were comparable to those published at lower ultrasound frequencies (1–9 MHz).

The attenuation of the small animal soft tissue samples was seen to increase with increasing frequency. The attenuation coefficient was found to be non-linear as a function of frequency and was modelled as second-degree polynomials: $0.7533f + 0.006477f^2$ ($R^2 = 0.85$) for brain, $0.7252f + 0.01414f^2$ ($R^2 = 0.70$) for liver and $0.5771f + 0.006322f^2$ ($R^2 = 0.83$) for kidney.

Research into the acoustical properties of soft tissue based on the structure of the organ during normal and abnormal function is vitally important (Sarvazyan and Klemin 1983) as this information is useful for diagnosis (Kumagai et al. 2014).

Finally, quality phantoms are made of TMM that mimics the acoustic properties of soft tissue. The use of high-frequency ultrasound for both clinical and preclinical applications has increased in recent years, resulting in a need to develop a relevant TMM suitable for use at these high frequencies. The acoustic properties of soft tissue have been previously assessed up to 9 MHz and at 15–35 MHz. Establishing the acoustic properties of soft tissue at high frequency is a required first step in the development of a suitable TMM quality assurance phantom. Currently, the IEC guideline does not provide the necessary guidance data to develop a TMM suitable for frequencies above 10 MHz. Furthermore, to reproduce the acoustic properties of small animal soft tissue using the IEC agar-TMM as a base, a modification in the IEC agar-TMM recipe must be generated to match the SoS of the brain, liver and kidney at these higher frequencies. Therefore, the data provided in this study can be used as a basis for a recipe for TMM that is representative of tissue properties at high frequencies.

Acknowledgments—We thank Dr. Julie McNairn for her help during the production of this work. This study was funded by a CONACyT (Becas al Extranjero 2014) Ph.D. studentship.

REFERENCES

American Institute for Ultrasound in Medicine (AIUM), Technical Standards Committee Methods for specifying acoustic properties of tissue-mimicking phantoms and objects. Laurel, MD: Author, 2014.

Bader KB, Crowe MJ, Raymond JL, Holland CK. Effect of frequency-dependent attenuation on predicted histotripsy waveforms in tissue-mimicking phantoms. Ultrasound Med Biol 2015;42:1701–1705.

Bamber JC. Ultrasonic attenuation in fress human tissues [Letter to the Editor]. Ultrasonics 1981;19:187–188.

Bamber JC, Fry MJ, Hill CR, Dunn F. Ultrasonic attenuation and backscattering by mammalian organs as a function of time after excision. Ultrasound Med Biol 1977;3:15–20.

Bamber JC, Hill CR. Ultrasonic attenuation and propagation speed in mammalian tissues as a function of temperature. Ultrasound Med Biol 1979;5:149–157.

Bamber JC, Hill CR. Acoustic properties of normal and cancerous human liver: I. Dependence on pathological condition. Ultrasound Med Biol 1980;7:121–133.

Bamber JC, Nassiri DK. Effect of gaseous inclusions on the frequency dependence of ultrasonic attenuation in liver. Ultrasound Med Biol 1985;11:293–298.

Banchhor SK, Araki T, Londhe ND, Ikeda N, Radeva P, Elbaz A, Saba L, Nicolaides A, Shafique S, Laird JR, Suri JS. Five multiresolution-based calcium volume measurement techniques from coronary IVUS videos: A comparative approach. Comput Methods Programs Biomed 2016;134:237–258.

Bilaniuk N, Wong GSK. Speed of sound in pure water as a function of temperature. J Acoustic Soc Am 1992;93:1609–1612.

Chen CF, Robinson DE, Wilson LS, Griffiths KA, Manoharan A, Doust BD. Clinical sound speed measurement in liver and spleen in vivo. Ultrason Imaging 1987;9:221–235.

Cook JR, Bouchard RR, Emelianov SY. Tissue-mimicking phantoms for photoacoustic and ultrasonic imaging. Biomed Opt Express 2011;2:3193–3206.

Coppens AB. Simple equations for the speed of sound Neptunin waters. J Acoust Soc Am 1981;69:862–863.

Del Grosso VA, Mader CW. Speed of sound in pure water. J Acoust Soc Am 1972;52:1442–1446.

Duck FA. Physical properties of tissues. A comprehensive reference book. Bath: Academic Press; 2012.

Edgeworth AL, Anderson T, Ross JA, Ansell IF, Butler M, Norrie L, McDicken WN, Moran C. Strength of attachment of an in-house, microbubble, ultrasound contrast agent. Proc 2009 IEEE Int Ultrason Symp; 2009:1262–1265.

Foster FS, Hunt W. Transmission of ultrasound beams through human tissue—Focussing and attenuation studies. Ultrasound Med Biol 1979;5:257–268.

Foster FS, Pavlin CJ, Harasiewicz KA, Christopher DA, Turnbull DH. Advances in ultrasound biomicroscopy. Ultrasound Med Biol 2000;26:1–27.

Frizzel LA, Gindorf JD. Measurement of ultrasonic velocity in several biological tissues. Ultrasound Med Biol 1981;7:385–387.

Fujii Y, Taniguchi N, Itoh K, Shigeta K, Wang Y, Tsao J, Kimasaki K, Itoh T. A new method for attenuation coefficient measurement in the liver. J Ultrasound Med 2002;21:783–788.

Gammell PM, Croissette DHLE, Heyser RC. Temperature and frequency dependence of ultrasonic attenaution in selected tissues. Ultrasound Med Biol 1979;5:269–277.

Garcia-Duitama J, Chayer B, Goussard Y, Cloutier G. Segmentation of blood layers with particle image velocimetry (PIV) for reproducible in vivo characterization of erythrocyte aggregation. Proc 2016 IEEE Int Ultrason Symp Proc; 2016:1–4.

Garra BS, Shawker TH, Nassi M, Russell MA. Ultrasound attenuation measurements of the liver in vivo using a commercial sector scanner. Ultrason Imaging 1984;6:396–407.

Ghoshal G, Luchies AC, Blue JP, Oelze ML. Temperature dependent ultrasonic characterization of biological media. J Acoust Soc Am 2011;130:2203–2211.

Goss SA, Frizzell LA, Dunn F. Ultrasonic absorption and attenuation in mammalian tissues. Ultrasound Med Biol 1979;5:181–186.

Gray G, White CI, Thomson A, Kozak A, Moran C, Jansen M. Imaging the healing murine myocardial infarct in vivo: Ultrasound, magnetic resonance imaging and fluorescence molecular tomography. Exp Physiol 2013;98:606–613.

International Commission on Radiation Units and Measurements (ICRU). ICRU Report 61: Tissue substitutes, phantoms, and computational modelling in medical ultrasound. Bethesda, MD: Author; 1998.

International Electrotechnical Commission (IEC). International Standard IEC 61685. Ultrasonics—Flow measurement systems—Flow test object. Geneva: Author, 2001.

Itoh ST, Jing-wen ST, Konishi ST. Studies on frequency-dependent attenuation in the normal liver and spleen and in liver diseases, using the spectral-shift zero-crossing method. J Clin Ultrasound 1988;16:553–562.

Kagadis GC, Loudos G, Langer SG, Nikiforidis GC. In vivo small animal imaging: Current status and future prospects. Med Phys 2010;37:6421–6442.

Kremkau FW, Barnes RW, McGraw CP. Ultrasonic attenuation and propagation speed in normal human brain. J Acoust Soc Am 1981;70:29–38.

Kumagai H, Yokoyama K, Katsuyama K, Hara S, Yamamoto H, Yamagata T, Taniguchi N, Hirota N, Itoh K. A new method for measuring the speed of sound in rat liver ex vivo using an ultrasound system: Correlation of sound speed with fat deposition. Ultrasound Med Biol 2014;40:2499–2507.

Lay H, Cox B, Sunoqrot M, Demore CEM, Näthke I, Gomez T, Cochran S. Microultrasound characterisation of ex vivo porcine tissue for ultrasound capsule endoscopy. J Phys Conf Ser 2003;797:Conference 1.

López-Haro SA, Leija L, Favari L, Vera A. Measurement of ultrasonic properties into biological tissues in the hyperthermia temperature range. Phys Proc 2010;3:551–558.

Lu ZF, Zagzebski JA, Lee FT. Ultrasound backscatter and attenuation in human liver with diffuse disease. Ultrasound Med Biol 1999;25: 1047–1054.

Ludwig GD. The velocity of sound through tissues and the acoustic impedance of tissues. J Acoust Soc Am 1950;22:862–866.

Machet L, Belot V, Naouri M, Boka M, Mourtada Y, Giraudeau B, Laure B, Perrinaud A, Machet M, Vaillant L. Preoperative measurement of thickness of cutaneous melanoma using high-resolution 20 MHz ultrasound imaging: A monocenter prospective study and systematic review of the literature. Ultrasound Med Biol 2009;35:1411–1420.

Maklad NF, Ophir JVH, Balsara V. Attenuation of ultrasound in normal liver and diffuse liver disease *in vivo*. Ultrason Imaging 1984;6:117–125.

Martínez-Valdez R, Contreras MVH, Vera A, Leija L. Sound speed measurement of chicken liver from 22°C to 60°C. Phys Proc 2015;70: 1260–1263.

Martial J, Cachard C. Acquire real-time RF digital ultrasound data from a commercial scanner. Electron J Tech Accoust 2007;3:1–16.

Moran C. Ultrasonic propagation properties of excised human skin. Ultrasound Med Biol 1995;21:1177–1190.

Muleki-Seya P, Guillermin R, Guglielmi J, Chen J, Pourcher T, Konofagou E, Franceschini E. High frequency quantitative ultrasound spectroscopy of excised canine livers and mouse tumors using the structure factor model. IEEE Trans Ultrason Ferroelectr Freq Control 2016; 63:1335–1350, 3010.

O'Brien WD. Ultrasonic propagation properties (@100 MHz) in excessively fatty rat liver. J Acoust Soc Am 1988;83:1159–1166.

Ophir J, Shawker TH, Maklad NF, Miller JG, Flax SW, Narayana PA, Jones JP. Attenuation estimation in reflection: Progress and prospects. Ultrason Imaging 1984;6:349–395.

Parker KJ. Ultrasonic attenuation and absorption in liver tissue. Ultrasound Med Biol 1983;9:363–369.

Parker KJ, Asztely MS, Lerner RM, Schenk EAH, Waag RC. In-vivo measurements of ultrasound attenuation in normal or diseased liver. Ultrasound Med Biol 1988;14:127–136.

Pinkerton JMM. The absorption of ultrasonic waves in liquids and its relation to molecular constitution. Proc Phys Soc B 1949;129–141.

Rabell Montiel A, Browne JE, Pye SD, Anderson TA, Moran CM. Broadband acoustic measurement of an agar-based tissue mimicking material: A longitudinal study. Ultrasound Med Biol 2017;43:1494–1505.

Rajagopal S, Sadhoo N, Zeqiri B. Reference characterisation of sound speed and attenuation of the IEC agar-based tissue-mimicking material up to a frequency of 60 MHz. Ultrasound Med Biol 2015;41: 317–333.

Rajagopalan B, Greenleaf JF, Thomas PJ, Johnson SA, Bahn RC. Variation of acoustic speed with temperature in various excised human tissues studied by ultrasound computerized tomography. In: Linzer M, ed. Ultrasonic tissue characterization II. Special Pub. 525. Washington, DC: U.S. Government Printing Office, 1979:227–233.

Rhee S. High frequency (IVUS) ultrasound transducer technology—Applications and challenges. In: Proceedings, Sixteenth IEEE International Symposium on the Applications of Ferroelectrics (ISAF), Nara, Japan, May 27–31, 2007. New York: IEEE, 2007: 856–857.

Sarvazyan AP, Klemin VA. Study of ultrasonic topography of the kidney. In: Millner R, Rosenfeld E, Cobet U, (eds). Ultrasound interactions in biology and medicine. New York: Plenum; 1983.

Schmitt C, Hadj Henni A, Cloutier G. Ultrasound dynamic microelastography applied to the viscoelastic characterization of soft tissues and arterial walls. Ultrasound Med Biol 2010;36:1492–1503.

Sehgal CM, Brown GM, Bahn RC, Greenleaf JF. Measurement and use of acoustic nonlinearity and sound speed to estimate composition of excised livers. Ultrasound Med Biol 1986;12:865–874.

Strowitzki M, Brand S. Jenderka KV. Ultrasonic radio-frequency spectrum analysis of normal brain tissue. Ultrasound Med Biol 2007; 33:522–529.

Sun C, Pye S, Browne J, Janeczko A, Ellis B, Butler M, Sboros V, Thomson AJW, Brewin M, Earnshaw CH, Moran C. The speed of sound and attenuation of an IEC agar-based tissue-mimicking material for high frequency ultrasound applications. Ultrasound Med Biol 2012;38:1262–1270.

Sundholm JKM, Olander RFW, Ojala TH, Andersson S, Sarkola T. Feasibility and precision of transcutaneous very-high resolution ultrasound for quantification of arterial structures in human neonates: Comparison with conventional high resolution vascular ultrasound imaging. Atherosclerosis 2015;239:523–527.

Suomi V, Han Y, Konofagou E, Cleveland RO. The effect of temperature dependent tissue parameters on acoustic radiation force induced displacements. Phys Med Biol 2016;61:7427–7447.

Szabo TL. Scattering From Tissue and Tissue Characterization. In: Diagnostic Ultrasoind Imaging: Inside Out, 2nd ed. Boston, MA, USA: Academic Press; 2014. p. 295–363.

Taylor KJW, Riely CA, Hammers L, Flax S, Garcia-Tsao G, Conn HO, Kuc R, Barwick KW. Quantitative US attenuation in normal liver and in patients with diffuse liver disease: Importance of fat. Radiology 1986;66:65–71.

Tervola KMU, Foster SG, O'Brien WD. Attenuation coefficient measurement technique at 100 MHz with the scanning laser acoustic microscope. IEEE Trans Sonics Ultrason 1985;32:259–265.

Welkowitz W, Deutsch S, Akay M. Biomedical instruments: Theory and design, 2nd ed. New York: Academic Press; 1992.

Wirtzfeld LA, Berndl ESL, Kolios MC. Ultrasonic characterization of extra-cellular matrix in decellularized murine kidney and liver. Proc 2015 IEEE Intl Ultrason Symp; 2015:1–4.

Worthington AE, Sherar MD. Changes in ultrasound properties of porcine kidney tissue during heating. Ultrasound Med Biol 2001;27:673–682.

Xu J, Tripathy S, Rubin JM, Stidham RW, Johnson LA, Higgins PDR, Kim K. A new nonlinear parameter in the developed strain-to-applied strain of the soft tissues and its application in ultrasound elasticity imaging. Ultrasound Med Biol 2012;38:511–523.

Zderic V, Keshavarzi A, Andrew MA, Vaezy S, Martin RW. Attenuation of porcine tissues in vivo after high-intensity ultrasound treatment. Ultrasound Med Biol 2004;30:61–66.